Automatic Glycemia Regulation of Type I Diabetes

Taghreed Mohammadridha

Thèse de Doctorat

Taghreed MOHAMMADRIDHA

Mémoire présenté en vue de l'obtention
du grade de Docteur de l'École Centrale de Nantes
sous le sceau de l'Université Bretagne Loire.

École doctorale : **Sciences et Technologies de l'Information et Mathématiques.**

Discipline : **Automatique, Productique et Robotique.**
Unité de recherche : **Laboratoire des Sciences du Numérique de Nantes.**

Soutenue le 10 Mai 2017

Automatic Glycemia Regulation of Type I Diabetes

JURY

Président :	**DAROUACH Mohamed**, Professeur des universités, IUT Henry Poincaré de Longwy.
Rapporteurs :	**MOUNIER Hugues,** Professeur des universités, Université Paris-Sud, Paris.
	TARBOURIECH Sophie, Directrice de Recherche CNRS, LAAS, Toulouse.
Examinateurs:	**CHAILOUS Lucy,** Docteur, CHU Hôpital Nord Laennec - Nantes.
	LEFEBVRE Marie-Anne, Maître de Conférences, Centrale Supélec, Rennes.
Directeur de thèse :	**MOOG Claude,** Directeur de Recherche CNRS, Ecole Centrale de Nantes.

Automatic Glycemia Regulation of Type I Diabetes

Taghreed MohammadRidha

Supervised by: Claude MOOG

Ecole **C**entrale de **N**antes

Laboratoire des **S**ciences du **N**umérique de **N**antes

This dissertation is submitted for the degree of

Doctor of Philosophy

Doctoral School: STIM July 2017

I would like to dedicate this humble work to the gracious souls of our beloved Prophet of mercy Mohammad, his cousin Ali and his daughter Fatima.
Peace be upon Mohammad and his holy Family.

I also dedicate this work to the brave Iraqi army who took the noble mission of fighting and defeating terrorism for Iraq and for the world peace.

Acknowledgements

All praises to Allah for His blessing in completing this thesis. I would like to ask him to make this work as another useful tool for type 1 diabetes treatment.

I would like to express my sincere gratitude to my advisor Prof. C. H. Moog for the continuous support of my Ph.D study, for his patience, motivation, and immense knowledge.

I also thank my fellow labmates and the visiting researchers for the stimulating and valuable discussions.

Last but not the least, I would like to thank my family: my parents and to my sister and brothers for supporting me spiritually throughout writing this thesis and my life in general.

Abstract

The Problem Pancreas secretes two main hormones: insulin and glucagon, to regulate the main source of energy "glucose" to body cells in blood stream. Insulin stimulates the uptake of glucose in the blood stream to cells and muscles for energy. On the contrary, glucagon stimulates the liver to break down stored glycogen to release glucose when blood glucose (BG) levels are under 70 mg/dL during fasting or exercises and while insulin is suppressed. Type 1 Diabetes Mellitus (T1DM), or *insulin-dependent diabetes*, is a chronic disease that mainly results from the autoimmune destruction of the insulin-producing β cells in the pancreas. The result is an absolute lack of endogenous insulin production. Without insulin stimulating the uptake of glucose to cells and muscles, blood glucose remains in the blood stream and grows into hyperglycemia (above 180 mg/dl). The disease was fatal before the discovery of insulin in 1921.

Available (Open-loop) Solution To survive, daily exogenous insulin injections/infusions is the only solution to regulate blood glucose. The patient injects the adequate amount of insulin calculated according to the glucose amount in a meal. These doses known as boluses are associated to a background steady insulin infusion rate called the basal level. The latter is responsible for maintaining blood glucose constant during fasting conditions. The patient must also consider, in this stressful daily self-treatment process, the perturbations like stress, sickness and physical activities etc. Poor treatment causes long term complications like renal failure and peripheral vascular complications.

Engineering (closed-loop) Solution From the sixties till today, the research objective, in the engineering field, is to take the burden off T1DM patients by replacing the stressful (open-loop) programmed basal/bolus insulin doses known as the *Functional Insulin Therapy or Treatment)* (FIT) by the automatic infusion device. Therefore, an Artificial Pancreas (AP) appeared to be the ultimate goal of glycemia regulation of T1DM. This long standing project has the aim to close the loop between an automated insulin pump and a continuous glucose measurement (CGM) sensor to approach natural regulation of glycemia. With the rapid growth of technology this topic has received a worldwide interest and it witnesses a

great ongoing development. Though it is a long standing problem, so far, there is no fully automated viable device available for diabetic patients. As will be detailed in the literature survey of Chapter 2, different control strategies have been tested *in silico* and *in vivo* for this purpose.

Contributions To close the loop between an insulin pump and a blood glucose sensor, two main types of control algorithms have been used: non-model-based and model based controllers. These are Model-free Control (MFC), positive Sliding Mode Control (SMC)and positive state feedback control. The controllers have been tested on T1DM simulators to evaluate their performances. In addition, an important open-loop result is obtained that is, hypoglycemia prediction under basal injection during fasting phase. The following points summarize the work done in this thesis in a chronological order:

1. First application of MFC (intelligent Proportional (iP) and intelligent Proportional-Integral-Derivative (iPID) controllers) for glycemia regulation of T1DM.

2. A Positive SMC is designed for the first time for glycemia regulation respecting the positivity constraint of the insulin pump. The controller is positive everywhere inside the largest invariant set of plasma insulin.

3. The theory of positively invariant sets of linear systems is employed for the first time on a T1DM model. The major outcome is glycemia regulation, hypoglycemia prevention and prediction.

4. The largest positively invariant set under constant basal insulin injection (open-loop) in fasting phase is found. It is used to predict and prevent from future hypoglycemia.

5. The input/state positivity analyses are considered for the first time to design a positive state feedback controller to regulate glycemia. Inside the closed-loop largest positively invariant set glycemia is regulated and hypoglycemia is prevented. Future hypoglycemia is predicted when the system initial condition is outside the largest Positively Invariant Set (PIS).

Publication List

1. **International Journals**

   - T. MohammadRidha, C.H. Moog, M. Aït-Ahmed, L. Chaillous, M. Krempf, I. Guilhem and J.Y. Poirier, "Model Free iPID Control for Glycemia Regulation of Type-1 Diabetes", IEEE Transactions on Biomedical Engineering, accepted.
   - K. Menani, T. MohammadRidha, N. Magdelaine, M. Abdelaziz and C. H. Moog, " Positive Sliding Mode Control for Glycemia Regulation", submitted to International Journal of Systems Science (under second revision).
   - T. MohammadRidha, P.S. Rivadeneira, M. Cardelli, N. Magedelaine and C.H. Moog, "Positively Invariant Sets of a T1DM Model: Hypoglycemia Prediction and Avoidance", submitted to Automatica.
   - N. Magdelaine, P. S. Rivadeneira, L. Chaillous, Anne-Laure Fournier-Guilloux, M. Krempf, T. Mohammadridha, M. Ait-Ahmed, C. H. Moog "Hypo-Free Hyper-Minimizer for the Artificial Pancreas", submitted to Control Engineering Practice.

2. **International Conferences (with proceedings)**

   - T. MohammadRidha, and C.H. Moog, "Model Free Control for Type-1 Diabetes: A Fasting-Phase Study", 9th IFAC Symposium on Biological and Medical Systems, Berlin, Germany, Volume 48, Issue 20, 2015, Pages 76–81. dx.doi.org/10.1016/j.ifacol.2015.10.118
   - T. MohammadRidha, C.H. Moog, E. Delaleau, M. Fliess and C. Join, "A Variable Reference Trajectory for Model-Free Glycemia Regulation", SIAM Conf. on Control and its Applications, July 2015, Paris, France, pp. 60-67.
   - T. MohammadRidha, P.S. Rivadeneira, M. Cardelli, N. Magedelaine and C.H. Moog,"Toward Hypoglycemia Prediction and Avoidance for Type 1 Diabetic Patients", accepted in the 56th IEEE Conference on Decision and Control, December, 2017, Melbourne, Australia.

3. **International Conferences (without proceedings)**

   T. MohammadRidha, P.S. Rivadeneira, J.E. Sereno, M. Cardelli and C.H. Moog, "Description of the Positively Invariant Sets of a Type 1 Diabetic Patient Model", IFAC XVII CLCA 2016, Medellin, Colombia, October 2016.

Contents

List of Figures

Glossary

AP Artificial Pancreas

BG Blood Glucose

CGM Continuous Glucose Monitor

CSII Continuous Subcutaneous Insulin Infusion

CIPII Continuous Intraperitoneal Insulin Infusion

CHO Carbohydrate

DIA Duration of Insulin Action

FDA Food and Drugs Administration

FIT Functional Insulin Therapy

HSMC Higher order Sliding Mode Control

iP intelligent Proportional controller

iPvref intelligent Proportional with variable reference

iPID intelligent Proportional Integral Derivative controller

IP Intraperitoneal

IV Intravenous glucose sensor

IVGTT Intravenous Glucose Tolerance Test

IFB Insulin FeedBack

IOB Insulin On Board

MAGE Mean Amplitude of Glycemic Excursion

MFC Model-free Control

MPC Model Predictive Control

MSII Multiple Subcutaneous Insulin Injections

OGTT Oral Glucose Tolerance Test

PD Proportional Derivative controller

PDs Pharmacodynamics: is the relationship between the drug concentration in the body and its intended and antagonistic effects achieved with time.

PK Pharmacokinetics: is defined as the relation between the drug input (e.g. insulin) and its produced concentration in the body with time.

PID Proportional Integral Derivative controller

PIS Positively Invariant Set

T1DM Type 1 Diabetes Mellitus

T2DM Type 2 Diabetes Mellitus

TDD Total Daily Dose

SC Subcutaneous injection route

SMC Sliding Mode Control

Chapter 1

General Introduction

1.1 Chapter Introduction in French

1.1.1 Le problème

Le pancréas sécrète deux hormones principales : l'insuline et le glucagon. Elles régulent la source principale de l'énergie «le glucose» des cellules du corps dans la circulation sanguine. L'insuline stimule l'absorption de glucose par les cellules et les muscles. Au contraire, le glucagon stimule le foie pour décomposer le glycogène stocké et libérer du glucose lorsque le taux de glucose sanguin (BG) est inférieur à 70 mg/dl pendant le jeûne ou lors des efforts physiques et que l'insuline est supprimée. Le diabète de type 1 (DT1), ou diabète insulinodépendant, est une maladie chronique qui résulte principalement de la destruction auto-immune des cellules *beta* produisant de l'insuline dans le pancréas. Il en résulte un manque absolu de production endogène d'insuline. Sans insuline stimulant l'absorption de glucose aux cellules et aux muscles, la glycémie n'est pas visible et donc elle s'accumule (au-dessus de 180 mg/dl) dans la circulation sanguine conduisant à des complications à long terme. La maladie était fatale avant la découverte de l'insuline en 1921.

1.1.2 Solution disponible (boucle ouverte)

Pour survivre, les injections/infusions quotidiennes d'insuline exogène sont la seule solution pour réguler la glycémie. Le patient injecte la quantité adéquate d'insuline calculée en fonction de la quantité de glucose absorbée dans un repas. Ces doses, connues sous le nom de bolus, sont associées à un taux de perfusion régulière d'insuline de fond appelé niveau basal. Ce dernier est responsable de maintenir la glycémie constante pendant les conditions de jeûne. Le patient doit également considérer, dans ce processus d'auto-traitement quotidien

qui peut être une source de stress, les perturbations comme le stress, la maladie et les activités physiques, etc.

1.1.3 Solution d'ingénierie (boucle fermée)

Depuis les années soixante jusqu'à nos jours, l'objectif de la recherche, dans le domaine de l'ingénierie, est de prendre le fardeau des patients T1DM en remplaçant les doses stressantes d'insuline basale / bolus (boucle ouverte) connues sous le nom d'insulinothérapie fonctionnelle (ITF) par un dispositif automatique. Par conséquent, un pancréas artificiel (PA) est le but ultime de la régulation de la glycémie DT1. Ce projet de longue date a pour but de fermer la boucle entre une pompe à insuline automatisée et un capteur de mesure continue du glucose (MCG) pour reproduire la régulation naturelle de la glycémie. Avec la croissance rapide de la technologie ce sujet a reçu un intérêt mondial et il est l'objet d'un grand développement en cours. Bien qu'il s'agisse d'un problème ancien, jusqu'à présent, il n'existe pas de dispositif viable entièrement automatisé disponible pour les patients diabétiques. Comme on le verra plus en détail dans la littérature du chapitre 2, différentes stratégies de contrôle ont été testées *in silico* et *in vivo* dans ce but.

1.1.4 Notre contribution

Pour fermer la boucle entre une pompe à insuline et un capteur de glucose sanguin, deux principaux types d'algorithmes de contrôle ont été utilisés : des commandes basées sur des modèles et des commandes non basées sur des modèles. Il s'agit de la commande sans modèle (CSM), de la commande *positive* par modes glissants (CMG) et d'une commande *positive* par retour d'état. Les contrôleurs ont été testés sur des simulateurs T1DM pour évaluer leurs performances. En outre, on obtient des résultats importants en boucle ouverte, c'est-à-dire une prédiction d'hypoglycémie sous injection basale pendant la phase de jeûne. De manière exhaustive, nous listons l'ensemble de nos contributions :

1. Première application de CSM (contrôleurs proportionnels et Proportionel-Intégral-Dérivé intelligents) pour la régulation de glycémie de T1DM.

2. Une CMG positive est conçue pour la première fois pour la régulation de la glycémie en respectant la contrainte de positivité de la pompe à insuline. La commande est positive partout à l'intérieur du plus grand ensemble invariant d'insuline dans le plasma.

3. La théorie des ensembles invariants positifs de systèmes linéaires est employée pour la première fois sur un modèle T1DM. Le principal résultat est la régulation de la glycémie, la prévention et la prédiction de l'hypoglycémie.

4. Le plus grand ensemble positivement invariant sous injection basale constante d'insuline (boucle ouverte) en phase de jeûne est trouvé. Il est utilisé pour prédire et prévenir une future hypoglycémie.

5. Les analyses de positivité d'entrée / d'état sont considérées pour la première fois pour concevoir un retour d'état positif pour réguler la glycémie. En boucle fermée, la glycémie est réglée tout en restant positive et l'hypoglycémie est évitée. L'hypoglycémie future est prédite lorsque la condition initiale du système est en dehors du plus grand ensemble positivement invariant.

1.2 General Introduction

The problem of regulating glycemia of Type-1 Diabetes Mellitus (T1DM) is investigated in this work. T1DM is a chronic autoimmune disease affecting approximately 25 million individuals in the world. A T1DM patient suffers from an absolute lack of insulin due to autoimmune destruction of pancreatic β-cells. Insulin stimulates the uptake of glucose in the blood stream to cells and muscles for energy. Without insulin stimulating the uptake of glucose to cells and muscles, blood glucose remains in the blood stream and grows into hyperglycemia. To survive, exogenous insulin injections is the only solution to regulate glycemia. The disease was fatal before the discovery of insulin in 1921.

Current treatment requires programmed injections. These are either multiple daily insulin injections or continuous subcutaneous insulin infusion (CSII) delivered *via* a pump. While calculating insulin doses, the patient must consider many factors like carbohydrates in every meal and physical activities. Poor treatment causes long term complications like renal failure and peripheral vascular complications. As a result, automatic control of these injections has received a wide interest especially with the rapid development of sensing technologies and insulin pumps. For more than 50 years, the idea of an Artificial Pancreas (AP) device was envisioned. The core of the device is the control algorithm that closes the loop between blood glucose measurements and insulin injections of T1DM patients. The objective is to replace the manual injections and to enhance the stressful everyday life of T1DM patients. The main challenge is hypoglycemia that is an acute complication in the life of a T1DM subject especially in nocturnal time. It is a major open problem which stood against the realization of AP device.

In general the focus of any research on AP is to design a control algorithm adaptable to different patient insulin sensitivity and robust enough to deal with non modeled dynamics, uncertainties and measurement noise. An important factor that affects controllers performance

is to achieve the trade-off between reducing hyperglycemia and avoiding hypoglycemia. Moreover, the positivity of the control input (insulin infusion) must be taken into account in the design.

The mainstream of control algorithms, that was used previously in different clinical tests, is the Proportional-Integral-Derivative (PID) controller and the Model Predictive Control (MPC). MPC is popular in this field as it handles the system constraints in the design. Its main drawback is the cumbersome optimization process. PID was also frequently tested as it was observed that it mimics pancreatic β-cells behavior. Moreover, its design does not require a precise model of the system.

In this work two main controller types are employed: model-based and non-model based controllers. To asses their efficiency, both types are tested *in silico* on two T1DM simulators. The first simulator is a long-term model that is derived from clinical data of T1DM subjects and developed in LS2N laboratory in France. The second simulator is the Uva/Padova T1DM simulator that is approved by the Food and Drugs Administration (FDA) for closed-loop control validations. All controllers designed and tested hereafter are fully automatic without meal announcements nor supplementary insulin doses.

In this work, Model-free control (MFC) is designed for glycemia regulation for the first time. In its control, poorly known dynamics and perturbations are estimated on line via the unique knowledge of the input/output measurements. The estimation is employed in the control law to compensate for perturbations and the loop is closed via a simple PID controller. MFC with PID in the feedback is called intelligent PID (iPID). It offers the simple features of a PID control in the frame of a model free design. In opposition to previous PID studies, the control algorithm developed hereafter is fully automated without any feed-forward or supplementary insulin doses. Intelligent proportional (iP) is firstly tested employing a variable reference trajectory to circumvent the poor postprandial behavior of constant reference iP. Variable reference iP produced an impulsive control of fast reaction to meals that yielded a reduced postprandial hyperglycemia. To further enhance postprandial response, additional closed loop terms are added and an iPID is designed using a constant glycemia reference. *In silico* results comparison showed a better postprandial glycemia regulation with constant reference iPID over iP employing a variable reference. iPID is also compared to a classic PID on the well known Uva/Padova T1DM simulator. The results showed that the postprandial response was improved with iPID reducing hyperglycemic excursions with minimal hypoglycemic events. Moreover, the results showed that iPID, who has the classic PID structure with new adaptive feature, emulated insulin delivery of pancreatic β-cell. MFC showed a good robustness level. The system is considered as a black box and MFC parameters are tuned empirically based on the input/output measurements.

Another robust controller is designed and tested in this thesis, that is Sliding Mode Control (SMC). A *positive* SMC is designed for the first time for glycemia regulation. The controller is positive everywhere in the largest closed-loop Positively Invariant Set (PIS) of plasma insulin subsystem. Two-stage SMC is designed, the second stage SMC2 block uses the glycemia error (with respect to the desired level) to design the desired insulin trajectory. Then the plasma insulin state is forced to track the reference via first stage control SMC1. The switching variable of SMC1 is the first order polynomial of the insulin error. Sliding mode of SMC1 guarantees insulin reference tracking. The resulting desired insulin trajectory is the required virtual control input of the glycemia system to eliminate glycemia error. Glycemia error is the switching variable of SMC2. Glycemia is steered to the normal set point during sliding mode of SMC2. *In silico* trial is performed to validate the theoretical results on the nominal system during fasting phase. Robustness of SMC against parameter change, meal perturbations and sensor noise is considered as a perspective.

Due to the discontinuity of the control law, designing a positive SMC everywhere in the largest PIS such that glycemia remains invariant within the desired level is much more complex. The positive SMC is a proof of concept and the design can be extended to include hypoglycemia constraint. In other words, the future problem maybe to design a positive SMC in the largest PIS where glycemia is above hypoglycemic threshold (70 mg/dL).

The problem of finding the largest PIS where glycemia remains *invariant* within or above the desired threshold is addressed via a simple continuous control law. In other words, to design a positive controller that takes hypoglycemia constraint into account and establishes a tight control. The loop is closed via a *positive* state feedback controller. First of all, the control law is simple and continuous. Thus, the design of a positive state feedback in the largest PIS such all system states are positive, is less complex than that with SMC. Moreover, the theory of invariant polyhedra for continuous linear systems is directly applied to find a positive state feedback controller. The largest PIS of the open-loop system (where only a basal insulin rate is infused) is firstly obtained. Secondly, the largest PIS of the closed-loop system under a stabilizing positive state feedback control is found. Inside the PIS, glycemia is regulated to its desired level without hypoglycemia risk. The main outcome of the largest open and closed-loop PIS for glycemia system is the *hypoglycemia prediction*. A solution to avoid the life-threatening barrier to the optimal diabetic treatment. Hypoglycemia is predicted here based on the system initial conditions. The prediction is established when the initial conditions are outside the largest closed-loop PIS (BG<70 mg/dL). In this case, the loop is opened to either administrate basal insulin only, or to switch the pump off. If the initial condition belongs to the open-loop (basal) PIS then the loop is opened to inject basal insulin only. Otherwise, if future hypoglycemia is also predicted under basal injection, then

the pump is switched off signaling severe hypoglycemia. In this manner, positivity analysis is shown to be very useful for tight glycemia regulation and also for hypoglycemia prediction.

1.3 Thesis Overview

The next chapter is an introductory chapter that presents the problem of glycemia regulation in humans from healthy to diabetic subjects. The disease is introduced in its two types reviewing the available programmed insulin therapy. The state of the of AP studies and the related clinical trials is reviewed in the end of Chapter 2.

In Chapter 3, a review of the main mathematical models and T1DM simulators that describe glucose-insulin dynamics of T1DM is given. A new long-term glycemia-insulinemia model that was derived from real T1DM clinical data is presented. The existence of an equilibrium point of a T1DM model in fasting conditions is discussed from the physiological point of view. On these bases, the presented mathematical models are assessed to find out whether they give a good description of glycemia-insulinemia dynamics T1DM.

In Chapter 4, MFC design theory is recalled and a brief stability study of iP controller is presented. A counter academic example of an unstable linear system is given showing that it can not be stabilized by an iP. Thereafter, iP controller is tested for glycemia regulation employing a constant reference and a variable reference trajectory. The iP behavior is compared to a constant reference iPID. Model-free iPID performance is also compared to a classic PID and the *in silico* results showed a better postprandial response with the iPID. The overall MFC results are discussed and a general conclusion is given.

In Chapter 5, SMC is designed for glycemia regulation. The largest PIS of insulin system is firstly found in open and closed-loop. Then, the parameters of SMC are designed to yield a positive control everywhere in the closed-loop PIS. The desired insulin trajectory is designed to steer glycemia error to its desired level via a second SMC. The design steps of the second SMC control are detailed.

In Chapter 6, positivity and invariance of overall system in $\mathbb{R}^3$ is presented in open-loop (under constant basal insulin injection) and under positive state feedback control. In the first part of the chapter, the largest open-loop PIS is firstly found such that glycemia error is nonnegative. At first the polyhedral PIS is characterized. This is followed by characterizing the surface that bounds the largest PIS. The result is used to predict hypoglycemia under basal injection. In the second part of Chapter 6, a positive state feedback controller is designed such that glycemia state remains invariant above hypoglycemia threshold. The resulting largest polyhedral PIS is presented. The limiting surfaces of the largest PIS are then found. Open and closed-loop PIS results are used to implement a general hypoglycemia prediction

algorithm. The resulting positive state feedback controller is tested *in silico* to validate the theoretical results.

Finally, a general conclusion is given **in Chapter 7** followed by the planned future work of this thesis. Each chapter begins with a French introduction and the overall thesis resume in French is presented directly after Chapter 7.

Chapter 2

Glycemia Regulation: from natural to artificial

2.1 Chapter Introduction in French

Il s'agit d'un chapitre introductif sur la régulation de la glycémie pancréatique chez l'homme sain et diabétique. Tout d'abord, la production de glucose sanguin endogène est brièvement revue suivie de l'introduction des principaux organes qui consomment le glucose comme une source d'énergie majeure. Les hormones pancréatiques principales sont l'insuline et le glucagon. Leurs rôles principaux sont définis. Le diabète dans ses deux types est présenté ainsi que le traitement quotidien de chacun mettant le focus sur DT1. La description commence par le traitement manuel jusqu'à la solution artificielle, c'est-à-dire la régulation de la glycémie en boucle fermée dans la cadre d'un PA. L'état de l'art des études de PA est revu et l'accent est mis sur les courants principaux des algorithmes de commande utilisés. L'état de l'art des études AP commence avec le régulateur PID dans les essais *in silico* et *in vivo*. Ceci est suivi par la commande industrielle plus avancée, le CP et les réalisations principales de cette commande à ce jour. Une étude de CMG conçue pour la régulation de la glycémie, en tant que commande robuste, est ensuite présentée. Finalement, certaines études de la commande par retour d'état sont revues. Une conclusion générale de ces algorithmes de commande et leur contribution au projet AP global est présentée. Leurs principaux problèmes ouverts sont également soulignés donnant les solutions de cette thèse pour chacun.

2.2 Introduction

This is an introductory chapter for pancreatic glycemia regulation in humans from healthy to diabetic. Firstly, endogenous blood glucose production is briefly reviewed followed by introducing the main organs that consume blood glucose as a major energy source. the key pancreatic hormones: insulin and glucagon and their principal roles are defined. Diabetes mellitus in its two types is introduced presenting the daily treatment of each putting the focus on T1DM. The passage turn from manual self treatment to artificial solution i.e. glycemia regulation via closed-loop control under AP project. The state of the art of AP studies are reviewed and the focus is on the mainstream of the employed control algorithms.

2.3 Blood glucose: The ubiquitous fuel in biology

Glucose: a name given to the grape sugar by the committee of the French Académie des Sciences in its report on July 1838. The name is contrived from the Greek *glukus*, "*sweet to the taste*" and the suffix *-ose*, derived from the Latin *-osus*, became biochemical suffix indicating a carbohydrate [1]. Carbohydrates (CHO) are the body's primary energy source and glucose is their basic unit which is absorbed quickly as a single component.

2.3.1 Glucose Production

- The liver: it plays a central role to balance glucose uptake and storage. In absorptive state it stocks the elevated postprandial glucose (around two-thirds of blood glucose (BG)[2]) as glycogen. Conversely, in post-absorptive or fasting phase glucose release is activated to maintain glucose homeostasis.

- The kidneys: during fasting state, kidneys participate to glucose production of about $20 \sim 25\%$ of glucose release in this condition [3].

- Intestine: recently a novel function of intestinal endogenous glucose production was described [4]. It contributes to $20 \sim 25\%$ of total fasting endogenous glucose production.

2.3.2 Glucose Consumption

A steady glucose supply, transported by the blood stream, is needed by most of tissues and organs:

- The brain is the major consumer of about 120g of glucose daily, which corresponds to 60% of the utilization of glucose by the whole body in the resting state [2]. Glucose is the only fuel for the brain except for starvation where liver breaks down fatty acids into ketone bodies to partly replace glucose.

- Muscles: In addition to glucose, they consume fatty acids and ketone bodies. In resting state, fatty acids covers 85% of their energy needs [2].

- Kidneys: their glucose consumption, filtration, and re-absorption play an important role in glucose homeostasis. They contribute to about 20% of the total glucose removed from the circulation [3].

Blood glucose concentration or *glycemia*[1] is measured in terms of either molar concentration (mmol/L) or mass concentration (mg/dL) and the over night or fasting normoglycemia, is within 70-100 mg/dL for a non-diabetic. This tight control is mainly achieved through the balance between glucose consumption and production. The process of preserving glucose in its narrow normal limits is called *Glucose homeostasis* [5].

2.4 Glycemia Regulation: Glucose homeostasis

The property of a system to maintain its variables relatively constant (in their normal levels) to keep a stable internal environment is called *homeostasis*. The term originally referred to the processes within living organisms like the internal body temperature and glycemia regulation. The principle is also found in automatic control such as the classic examples of thermostat and autopilot. Glucose homeostasis is a natural control mechanism that regulates glycemia based on the interaction and balance between two main pancreatic hormones: insulin and glucagon. They have antagonistic effects to maintain normoglycemia, insulin promotes glucose transport to cells to reduce elevated glycemia, while glucagon stimulates endogenous glucose production to rise low glycemia (see Fig. 2.1)[2]. From automatic control point of view glucose homeostasis represents a negative feedback control.

It is maintained by a variety of cellular mechanisms. Important mechanisms are carried out by hormones and the pancreas plays the fundamental role.

[1] first recognized by the French physiologist François Magendie in the early 19th century [1]

[2] image taken from https://zhiyaobme.wordpress.com/2014/10/17/balance-mattars

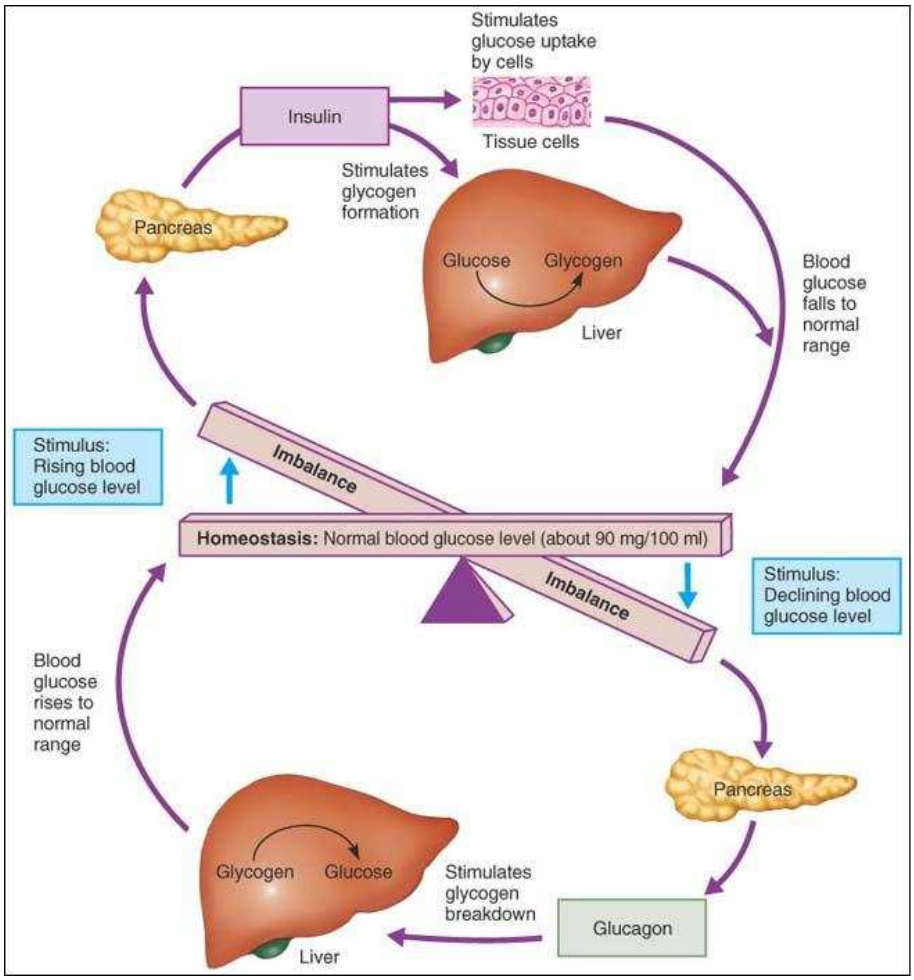

Figure 2.1 Glucose Homeostasis

2.5 Pancreatic secretion

The pancreas represents the control center of glucose homeostasis via its endocrine function of secreting the glycemia regulating hormones into the blood stream. Its major glucoregulators are:

1. Insulin: secreted by β Langerhans cells in response to glucose and nervous stimuli. It is the key hormone in glucose metabolism. It promotes
    - glucose transport to most cells: like in resting skeletal muscles and adipose tissue. Some tissues do not rely on insulin for efficient glucose uptake like in the brain who uses non insulin-sensitive transporters [6], [7].
    - glucose storage by the liver and the muscles in the form of glycogen.
    - inhibits endogenous glucose production.

2. Glucagon: secreted by α Langerhans cells in response to low blood glucose concentrations as in fasting state. It promotes the breakdown of glycogen in the liver to release glucose and stimulates the conversion of fatty and amino acids into glucose.

Insulin is secreted in the following phases:

- Basal rate: a steady background rate secreted during post-absorptive state *i.e.* overnight or during fasting, that balances the endogenous glucose production to maintain normoglycemia.
- Cephalic phase: is stimulated by the sight, smell and taste of food before any nutrient intestinal absorption.
- First phase: the initial rapid acute pulse of insulin 5-10 min after β cells are signaled that glycemia is abruptly elevated. It promotes peripheral utilization of the nutrient and suppresses endogenous glucose production [8], [9].
- Second phase: prolonged insulin secretion following the first phase which is related to the degree and stimulus duration and sustained until normoglycemia is attained.

In addition to the endocrine system, the pancreas function is also controlled by the autonomic nervous system. For example, during stressful situations and physical exercise alpha cells are stimulated to release glucagon into the blood stream to fulfill the energy needs [10].

2.6 Defect of Glucose homeostasis: Diabetes

Any metabolic abnormality involving organs or hormones breaks the continuous balance between glucose transport, storage and metabolism which causes impaired glucose homeostasis. Deficiency of insulin secretion and/or action leads to elevated glucose concentrations or *Hyperglycemia*. Prolonged hyperglycemia cause serious long-term complications like renal failure, blindness, cardiac diseases and peripheral vascular complications that represent the main cause of mortality in diabetics [5]. Recurrent hyperglycemia condition indicates diabetes if it is greater than 126 mg/dL [3] after 8-hours fasting or greater than 200 mg/dL for a 2-hours postprandial measurement after 75g oral glucose load. Dawn hyperglycemia or *dawn phenomenon* is observed in diabetics which is defined as the early morning abrupt rise in glycemia above fasting levels without antecedent hypoglycemia. It occurs due to increased nocturnal secretion of cortisol and the growth hormones that stimulates hepatic

[3] According to American Diabetes Association (ADA).

glucose production.
The two main forms of Diabetes mellitus are the insulin-independent or Type II (T2DM)and insulin-dependent Type I (T1DM) diabetes. In the early stage of T2DM, the impaired first- phase insulin secretion contributes to postprandial hyperglycemia (as illustrated in Fig. 2.2). This is compensated by a prolonged second-phase secretion to restore normoglycemia but for the price of eventual late-phase hyperinsulinemia. Over time, cells, and primarily skeletal muscles, do not respond properly to insulin and thus glucose absorption is reduced which develops insulin resistance condition. In addition, the vicious cycle of chronic hyperglycemia/insulinemia may lead to the exhaustion and damage of β cells [8] and thus develops T2DM. Treatment is carried out by improving lifestyle like weight control, diets and regular physical activities added to oral medication associated in some cases with insulin injection. Major concern for T2DM is cardiovascular complications.

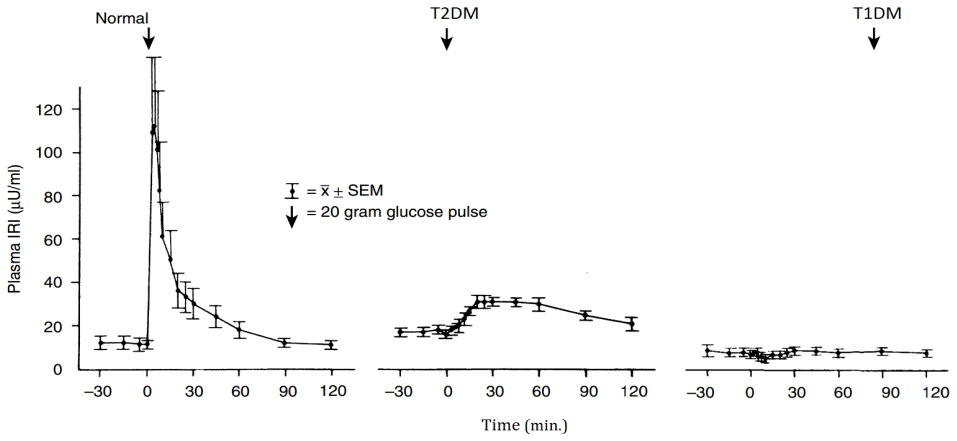

Figure 2.2 First phase insulin in response to intravenous glucose in normal and diabetic subjects. Mean fasting glycemia in normal 83± 3mg/dL versus 160 ± 10 in T2DM and 325± 33 mg/dL in T1DM. Note the lack of first phase insulin in T2DM and a total lack of insulin response to glucose load. (Data from [11]).

2.7 T1DM

T1DM is known as juvenile diabetes since it usually develops in children and adolescents. It occurs due to the progressive autoimmune destruction of β cells until eventually insulin

(*): ImmunoReactive Insulin: insulin levels in blood measured using radioimmunoassay methods.

is no more produced. By the time of diagnosis, more than 80-90% of the β cells have been destroyed due to the large gap between the autoimmunity onset and diabetes onset. However, recent studies showed that they never reach zero in some established T1D patients [12]. Main symptoms of T1DM are increased thirst, fatigue and frequent urination. The only treatment is the exogenous insulin therapy.

2.7.1 Complications

- Acute complications

  1. Hypoglycemia: a fall of blood glucose below normal levels. Mainly frequent hypoglycemia in T1DM is related to three reasons [13] : i) unregulated insulin injection and sustained hyperinsulinemia. ii) impaired glucagon response to hypoglycemia which begins within 5 years of disease diagnosis. iii) defect in the autonomic counterregulatory response of nervous system and reduced awareness of hypoglycemia. The latter impairment results from hypoglycemia *per se* (i.e. the patient has a history of hypoglycemia) during intensive insulin therapy. The average T1DM patient suffers from two episodes of common hypoglycemia per weak and one severe (often with seizure and coma) per year. Severe hypoglycemia leads to cerebral damage (at plasma glucose levels of 30-35 mg/dL) or even death to 2-4% of patients. (see[5] and the references therein).
     Overnight hypoglycemia is more frequent and attributes to nocturnal sudden death "dead-in -bed" syndrome which is a more serious concern for young patients.
  2. Ketoacidosis: It occurs during hyperglycemia due to a lack or reduce effective insulin against increased hepatic and renal glucose production. It is a life-threatening complication that indicates increased level of ketone bodies and acidity in the blood. It develops when the body starts to break down fats to release energy to compensate for faulty glucose metabolism. This metabolic state is sometimes the first sign of diabetes. Its treatment necessitates immediate hospitalization, re-hydration and insulin replacement.

- Chronic complications
  Management of diabetes during childhood have implications of the future development of the long-term complications. These include micro-vascular and macro-vascular complications. The latter cover circulatory and cardiovascular such as stroke and myocardial infraction (heart attack). Whereas the micro-vascular complications include nephropathy (kidney damage), neuropathy (usually starts with feet) and retinopathy [14].

2.8 The survival: insulin therapy

Before the discovery of insulin by Banting, Best Macloed and Collip in 1921, T1DM was a fatal disease. To survive, the patients were under severe diets to limit glycemia growth which did not much to their life span. According to International Diabetes Federation (IDF) diabetes atlas - 7th edition, there are 415 million diabetics world wide and it estimates 642 million incidences in 2040 among people aged 20-79 [4]. It estimates 0.5 million of T1DM among children only in 2015. For the no-cure disease, exogenous insulin therapy is the only treatment for survival. According to the ADA, insulin can be found in the following types:

1. Rapid-acting: 15 min onset [5], peaks time of about one hour and a total duration of 2-4 hours.
2. Short-acting (regular): 30 min onset, peak time within 2-3 hours and total effective duration 3-6 hours.
3. intermediate-acting: 2-4 hours, peaks within 4-12 hours and is effective in 12-18 hours.
4. long-acting: several hours onset, and regulates glycemia evenly (peakless) and effective over 24-hour period.
5. inhaled insulin [6]: 12-15 min onset peaks by 30 min and cleared out after 180 min.

2.8.1 Insulin delivery

Insulin is delivered mostly by subcutaneous (SC) injection using an insulin syringe. At increased cost, an insulin pen is more accurate and more convenient. Continuous Subcutaneous Insulin Infusion (CSII) using a electromechanical pump administers insulin even more accurately. However, it has a higher risk of ketoacidosis resulting from some pump infusion-related issues as pipe clogs or insulin leak[16].

Two main forms of treatments: conventional and functional or intensive. Those regimens are to control blood glucose in the normal bounds by mimicking the normal insulin secretion. Dose size and frequency is based on the insulin type, meal (size, composition and timing) and exercise throughout the day.

- Conventional: A standard fixed insulin administration that requires fixed daily meals to be taken at set times corresponding to 1 to 3 injections per day. Short and regular

[4] includes diagnosed and non-diagnosed subjects
[5] the time taken by insulin to reach blood stream and starts acting.
[6] recently approved by Food and Drugs Administration (FDA) [15].

insulin accompanied with intermediate-acting are usually used. The dietary and activity regimens are set to match the fixed insulin doses. The physician modifies and updates the regimen based on major changes in life-style like illness. This regimen is more affordable to diabetics than the intensive therapy.

- Functional (or Flexible) Insulin Therapy/Treatment (FIT): in this regimen insulin is infused in two separate rates: continuous basal rate (long-acting insulin) and insulin boluses[7] to account for meals (short-acting). The dosing is adjusted according to glycemia reading, meal size (carbohydrate intake) and physical activities. It is a self-management therapy where BG is monitored 3-5 times a day and insulin doses are calculated following a predefined program. FIT provides a good glycemic control in a more flexible life-style but requires a higher financial budget and an experienced assisting team. This basal-bolus regime can be given by either Multiple Subcutaneous Insulin Injections (MSII) or by CSII [15].

- Intraperitoneal (IP) administration: Insulin delivery using Continuous Intraperitoneal Insulin Infusion (CIPII) through implantable IP pumps (see Fig. 2.3). Insulin delivered through the IP route is absorbed rapidly into the portal vein and thus is a more physiologic mode of insulin as compared to SC delivery [17]. IP implanted pumps last years and they are refilled with transcutaneous insulin which has 1 min onset, 20-25 min peak time, and 1-2 h as total duration [18]. CIPII is emerging as a valuable treatment option for closed-loop BG control.

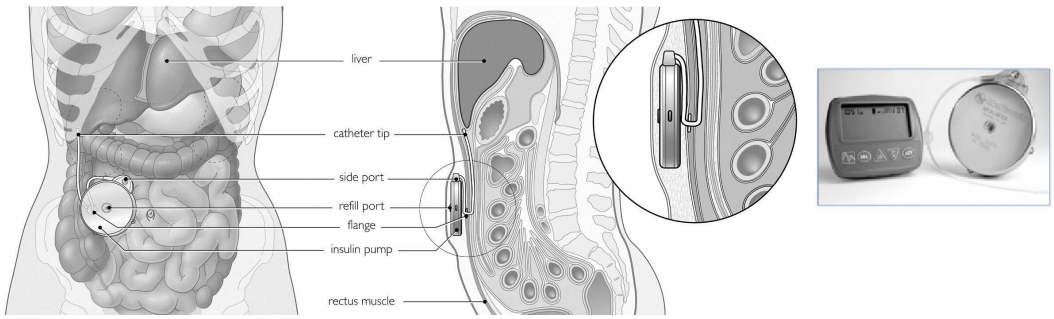

Figure 2.3 Illustration of IP implantable pump. Right image modified from [19] and left image IP pump and its insulin delivery communicator: MIP 2007C, Medtronic/Minimed, Northridge, CA, USA.

[7] from Latin which means the administration of discrete dose of a substance like drug to rapidly achieve an effective therapeutic concentration in the blood stream. Insulin bolus is injected (or infused) intravenously or subcutaneously in an amount to account for the upcoming meal load

2.8.2 FIT: how to

A general common algorithm to calculate FIT for T1DM subject is described as follows [20]:

1. Total Daily Dose (TDD) is calculated roughly as: TDI=0.55* body weight [kg].
2. Daily basal injection is usually 40-50% of TDD.
3. Insulin to CHO ratio I:CHO is defined as how many grams of CHO are covered by one unit of insulin. If the 500 rule[8] is used then I:CHO=500 ÷ TDD.
4. Insulin Sensitivity (correction) Factor (ISF) estimates the point drop of glycemia in mg/dL for every unit of insulin. If rapid or short-acting insulin is used then ISF is obtained by 1800[9] rule ISF=1800÷TDD.

N.B. The subject sensitivity to insulin is not a fixed value and it potentially varies during the day, due to sickness, physical activities or stress. Therefore, this calculation serves as basic start-up value that may be adjusted by the individual during the day.

Before meal intake, the patient weighs its CHO and according to his I/CHO ratio he deduces the necessary meal bolus to be injected. Then, he measures his BG and if the reading is above the desired target the subject should inject a pre-meal correction dose:

$$\text{Correction dose} = \frac{\text{BG target - BG reading}}{\text{ISF}} \tag{2.1}$$

Then the subject injects the prandial bolus of rapid-acting insulin 20 min prior to the meal [10].

2.8.3 Insulin on Board (IOB)

Bolus calculation (BC) in CSII regimen can be found as a feature of modern insulin pumps. Beside taking into account the right hand side of (2.1), bolus calculators take another important aspect into consideration: the approximation of the insulin decay curve [23]. This curve estimates the remaining amount of insulin in the body from previous insulin bolus which is defined as the insulin on board (IOB). IOB must be taken into account correctly to

[8] The 500 CHO rule assumes that the subject consumption+endogenous production of glucose is about 500g per day. This rule is applied when rapid or short-acting insulin is used otherwise, with regular type a 450g rule is applied.

[9] Dr. Paul Davidson proposed the first the insulin management system of 1500 formula for the ISF and 450 for I:CHO in the mid 1980s and it was later modified to 1800 for ISF and 500 for I: CHO [21]

[10] a 20 min bolus prior to a meal is shown to significantly lower BG better than 20 min post-meal bolus or immediate pre-meal injection [22]

reduce the size of future bolus to avoid insulin stacking that leads to later hypoglycemia [24]. The BC pump setting that critically affects IOB correct calculation is the Duration of Insulin Action (DIA). As detailed in [24], the widespread confusion in accurate DIA setting has lead to more common insulin stacking which has a direct impact on hypoglycemia. Among the authors recommendations, insulin manufacturers verify actual DIA for their short-acting insulins. Based on a generic insulin sensitivity variation curve, [23] developed a dynamic IOB estimator to be used in CSII or closed-loop treatments that showed better simulation results than the current static pump IOB approximations.

2.9 Artificial Pancreas

In diabetic patients the physiological closed-loop system of the glucose homeostasis is broken due to the deficiency or lack of beta cells response to glycemia elevation. Therefore the patient needs to self-monitor his blood glucose using a glucometer and inject insulin accordingly taking into account the external perturbations like meals and exercise. Blood glucose sensing technology has evolved rapidly providing a feedback tool for diabetic patients. The two main sensors used by diabetic individuals are finger-stick glucose meters and Continuous Glucose Monitor (CGM). The former reads blood glucose levels by taking blood samples obtained by pricking the finger. CGM measures glucose levels in the interstitial fluid providing real time readings. CGMs are mainly accompanied with insulin pumps in CSII of FIT as illustrated in Fig. 2.4.

Figure 2.4 Insulin delivery system *MiniMed®640G system^*, insulin pump in black and a CGM in white.

In this manner, insulin administration is not automated as the subject himself closes the loop between the CGM and the insulin pump and controls his BG following the algorithm of FIT. FIT + CSII provide a more flexible life style since it adapts to external loads like variable

meal amounts and timings. However, the self BG regulation is cumbersome and T1DM subjects still have a stressful everyday life maintaining tight BG control while reducing the frequency and severity of hypoglycemia. Mimicking normal pancreas through different therapeutic strategies is surely not an easy task and thus the alternative solution is the development of artificial pancreas. Different approaches have been evaluated:

1. Bio-artificial pancreas: β cells or islet encapsulation in an immunoisolating semi-permeable membrane. The concept is to surgically implant the islet tissue to artificially function as a pancreas. The membrane should allow nutrient, insulin, glucose and waste exchange with surrounding environment. Islet encapsulating can avoid *foreign body* response and thus avoiding immunosuppressive medications. The approach is quite promising but the research field is still on development to address the current challenges such as materials used to create the tissue with the required properties and its lifetime and the sufficiency of donor islets[25].

2. Insulin gene therapy: the transfer of a foreign gene into body cells to produce insulin. Insulin gene could be injected to no-β cells [26]. This approach is applied to the treatment of T1DM either by preventing the autoimmune destruction of β cells for the new diabetics, or by engineering a β cell replacement [27]. The research is ongoing and advancing to develop a therapy with a more precisely regulated insulin production and secretion.

3. Artificial pancreas (the device): a closed-loop system composed of a control algorithm device that administers insulin delivery of the pump depending on the real time reading of the CGM.

Artificial Pancreas (AP) studies and tests have been evolving rapidly in parallel with the technological advances. Automation of BG regulation has received a world-wide attention and clinical trials of different control algorithms have been conducted and showed satisfactory results that meet their own objectives. Yet, challenges are facing the realization of a commercialized AP. Those range from technical like CGM performance (calibration and delay), insulin delays, safety and reliability and robust communication between components [29]. Others are physiological like insulin sensitivity and the positive irreversible insulin injection as it can not be removed from the body once it is injected. Those challenges give rise to increased hypoglycemic events and thus less efficient BG control.

Figure 2.5 A smart-phone based portable artificial pancreas: Diabetes Assistant system (Dias) as presented in [28] where it was used in clinical trials.

2.10 Literature Survey: Closing the loop

The early efforts to develop AP started more than 50 years ago by the work of [30] who developed an on-off feedback controller to regulate BG between 50-150 mg/dL. In the study, a pair of servo-operated syringe pumps (glucagon and insulin) assemblies and a continuous BG sampler are used to intravenously inject glucose and insulin. This promising initiation was followed by the development of another AP in early 1970 called a Biostator ^{TM} approved by FDA for treating hospitalized T1DM patients [31]. It used a nonlinear Proportional-Derivative controller implemented in a digital computer unit deriving dual infusion pumps (insulin and glucose) based on sampled Intravenous (IV) BG . Although the device marked a step toward a commercialized AP, it was never adopted as a clinical device due to its high cost, large dimensions (about the size of a console television set), technological complexity (e.g. unreliable BG sensor and the need for blood withdrawal) [31, 32].

In the following years Biostator studies continued with IV BG sensing which is considered as a practical obstacle. The authors of [32] were motivated by the fact that this device has been the most clinically validated algorithm, for hospitalized T1DM subjects, to develop a recent version of the device Biostator II optimized to be used with subcutaneous BG sensor. The device test on virtual T1DM subjects, using an emulated continuous glucose sensor, have shown a good control of 93% of time in normoglycemia.

The core of the AP design is the control algorithm and the ongoing research in this application tries to find the best controller that mimics glucose homeostasis control mechanism. The widely applied controllers especially in closed-loop trials are Proportional-Derivative-Integral (PID) and Model Predictive Control (MPC) [29].

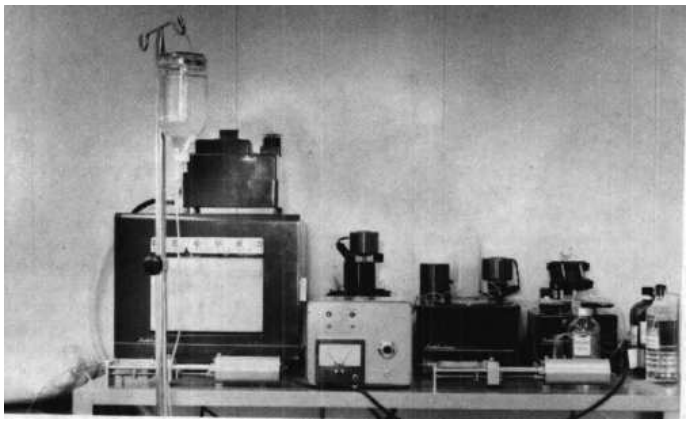

Figure 2.6 Photograph of overall equipment including BG autoanalyzer, control cabinet and servo-syringes which connected to injection sites. Photo taken from [30]

2.10.1 PID

The well-known industrial PID control has a grand share in the literature of AP studies. BG of intensive care unit patients is regulated using expert sliding-table-based PID [33]. The gain scheduled Proportional and Integral terms are updated hourly. The expert method allows insulin rate to be decreased if BG falls below (180 mg/dL) and integral part is activated if BG$>$ 180mg/dL to increase insulin rate. In this same condition the control by rate of change D term contributes by giving a bolus when BG rate crosses certain barriers. The clinical results are shown to be comparable to the manual routine treatment but the closed-loop control was sensitive to sensor errors which required manual intervention.

Some studies modeled PID algorithm as an artificial β cell. Starting from the principal idea that any closed-loop system should mimic β cells, G. Steil used PID to emulate the multiphasic insulin response of β cells [34] in different clinical trials. The D term produces the first phase insulin and the integral term produces the steady basal rate added to the Proportional that increases the insulin delivery if BG is above target and vice versa. The author applied it in a clinical trial [35] on 10 subjects and results showed a comparable closed-loop performance to that of conventional CSII and a stable nocturnal response. Despite that, the trial marked some elevated postprandial BG as compared to no-diabetics under the same conditions with hypoglycemic events. In the following clinical study on adolescents, the authors of [36] enhanced PID performance by incorporating a manual bolus of 25-50 % of the insulin bolus. It was given 15 min. prior to the meal. The added bolus is to compensate the delay of subcutaneous insulin absorption and to reduce postprandial BG excursions. The P gain is set as a proportion of TDD and I and D gains are adjusted between two values during the day. The algorithm was later modified to include the estimated plasma insulin

concentration as a feedback term. The authors of [37] added estimated plasma Insulin in the Feedback loop (IFB) of the PID control law. IFB works to attenuate insulin delivery from the feedback loop over the increase in estimated plasma insulin levels to prevent overdosing.

The aim is to reduce postprandial hypoglycemia. The modified PID control was tested on 8 adults and results revealed a good estimation of plasma insulin but with postprandial hypoglycemia episodes. A similar approach was tested on human subjects [38] which compared the two iterations of PID with and without IFB. The authors considered the perspective of [37] and constructed IFB as a linear combination of subcutaneous, plasma and the interstitial/effective insulin concentrations. The authors considered IFB as a "brake" on the insulin infusion in the feedback loop to prevent postprandial hypoglycemia. Results came up without postprandial hypoglycemia. A subsequent study conducted on diabetic dogs [39] marked an improvement of postprandial BG without undershoot hypoglycemia. It was shown that the addition of IFB is equivalent to the placement of the poles of the insulin compartmental model to the desired locations by choosing the IFB gain. PID+ IFB has also shown a reduced risk of nocturnal hypoglycemia regardless of the preceding afternoon level of physical activity as compared to conventional CSII regimen [40] in an inpatient study. A recent PID study [18] utilized IFB in a fully implantable AP system with intraperitoneal (IP) insulin delivery and glucose sensors. Their AP incorporated an anti-reset windup [11] method to limit the integral rate of change and prevent postprandial hypoglycemia. It was shown in the *in silico* test that the IP route for AP is promising as it provided a faster behavior. Since the insulin injection is a positive input, thus PID is followed by a saturation function to block any negative input. Thus, PID designers usually incorporate some anti-windup protection for the integrator, or even remove the integral and replace it by the patient specific basal rate in a PD+Basal control [41]. The authors compared PID and PD+Basal on Uva/Padova simulator and concluded that the latter reduced postprandial hyperglycemia, but and conversely to PID, it failed to respond appropriately to changes in insulin sensitivity.

As an overall view, frequent PID employment for glycemia regulation shows its merits as a simple and efficient control algorithm. In this thesis, *model-free control* is chosen as it offers the simple features of a PID control in the frame of a model free design. In opposition to previous PID studies, the control algorithm designed hereafter (in Chapter 4) is fully automated without any feed-forward or IFB terms.

[11] Integral wind-up occurs when the integral term builds up (in response to the error signal) and accumulates beyond the actuator saturation limit. It takes significantly long time to recover to get back to be within the actuator operating range. It causes excessive overshoot, sustained oscillations and long settling time.

2.10.2 MPC

Model Predictive Control (MPC) is the advanced industrial counterpart of PID. The main idea of MPC is that a mathematical model of the plant is used to predict the future behavior of the process output during a sliding time window or the *prediction horizon*. The prediction is used to optimize the control signal during a *control horizon*. The prediction and then the optimization are updated using feedback measurements of the controlled variable. MPC is widely known in the industry as an advanced algorithm that can handle process constraints. Its predictive nature and constraint handling pushed MPC to the top of the list of controllers used in AP application. Numerous publications have shown its potentials in both *in silico* and *in vivo* test studies.

Of the early *in silico* studies of MPC is that of a nonlinear auto regressive model identified off-line using artificial neural network [42]. They showed the feasibility of SC route in closed-loop AP when compared to Biostator II with IV route. The authors of [43] designed MPC tested on a nineteen-order compartmental model. Two MPC of two internal models are compared: a linear identified step response model of the original nonlinear system, and a linearised model of the patient with Kalman state estimation with improved results. A clinical proof of the concept is realized in a 15 clinical trials study of nonlinear MPC in [44]. The experiments were performed during fasting conditions on 10 subjects using IV BG sampling and SC insulin delivery . Hovorka's nonlinear model [45] is employed as an internal model with time-varying parameters that are estimated at each control step. Linear MPC acknowledged by the meal announcement (meal information is given to the controller) is tested *in silico* in[46] and compared to PID under same conditions. A linearised internal model of a nonlinear system and its parameters are obtained from the average values of the population. For both PID and MPC, one parameter is tuned per individual, K_p for the former and the output prediction weighting parameter for MPC. Although both showed deteriorated performance with imperfect meal knowledge amount, the effect on MPC was marginal. To avoid postprandial hyperglycemia, [47] presented a meal detection algorithm to notify MPC by an upcoming meal. It was shown that a meal is flagged 30 min before meal onset to notify MPC to switch the desired BG level from constant to a variable trajectory that mimics a generic BG absorption profile for different meal loads using a meal library. Another comprehensive *in silico* study [48] used MPC associated with meal size estimation, IOB and a pump shut-off procedure to avoid hypoglycemia. The meal estimation provided a feed-forward tool to automatically give priming meal boluses. IOB is computed based on

fitting *Pharmacodynamics PDs* [12] curves to two compartmental models. IOB is used as an additional constraint to avoid hypoglycemia. The test is accomplished on the Uva/Padova T1DM simulator [50]. MPC was also tested under dynamic IOB (dIOB) constraint in [23]. In this study dIOB took into account diurnal insulin sensitivity variation and used it to adjust the static available IOB (sIOB) estimations. The authors used a technique to superimpose diurnal insulin sensitivity (depending on the time of the day) on the sIOB to personalize it. The purpose was similar to that of IFB, to avoid insulin stacking to prevent hypoglycemia. Improved hypoglycemia prevention was noticed employing dIOB as a constraint in the study that was conducted on 100 patients of Uva/Padova simulator.

An outpatient study was performed in [51] of a wearable AP(DiAs) device of a smart phone core on 20 patients under 42 hours of 28h of AP. This proof of concept encouraged future trials. A bihormonal (Glucagon and insulin) AP outpatient study was performed in [52] using MPC control for insulin delivery and Proportional-Derivative control for glucagon (the gains were chosen to be functions of BG level for better control). Meal size information is forwarded to the controller to trigger a small automatic priming bolus. The *bionic* wearable device consisted of a smart phone and SC pumps and a 5 min CGM. They performed two studies: 5 days under open-loop control and another 5 days under AP for 20 adults and 38 adolescents. Under AP, the only given information to initialize the controller is the patient's weight. As compared with open-loop, the device showed improved mean BG with less hypoglycemia.

2.10.3 Sliding Mode Control (SMC)

Sliding mode Control has been employed for glycemia regulation due to its known robustness properties against model parameters uncertainties and external disturbances [53]. This can be established by directing the state trajectory of the system toward a pre-designed surface (during reaching phase) along which the trajectory slides to reach the desired reference value. Classic SMC is a discontinuous controller that yields high frequency chattering in the control action. In modern SMC theory, Higher Order SMC (HOSMC) is presented as a solution to this problem, it provided a continuous controller when designed in [53] for glycemia regulation of T1DM. The *in silico* test was performed on Bergman T1DM model and robustness was checked testing the controller on three virtual subjects under meal intake as an external disturbance. Finite time convergence was achieved for the switching variable but asymptotic convergence for the glucose error was yielded. To reduce persistent error

[12] Pharmacodynamics (*PDs*): is the relationship between the drug concentration in the body and its intended and antagonistic effects achieved with time. *Pharmacokinetics (PK)*: is defined as the relation between the drug input (e.g. insulin) and its produced concentration in the body with time [49] (see Fig. 3.1 in Chapter 3).

and improve SMC performance against meals, meal announcement scheme was used in [54]. Moreover, to alleviate the system's time delay problem, the authors designed SMC in a Smith predictor [13] structure. SMC design was based on an internal model that was identified on Hovorka's T1DM model (see §3.5 for Hovorka model details). Sigmoid-like function was used to avoid chattering. The design was tested *in silico* on six patients in nominal conditions and also under modeling errors and parametric uncertainties like variation in insulin sensitivity of the patient.

For glycemia regulation, SMC was usually used as a model-based control mainly employing Bergman minimal T1DM model (see §3.4.1 for details on the model) e.g. in [53], [55] and [56]. The authors of [55] designed HOSMC to regulate glycemia based on Bergman minimal model and on Sorensen complex model [57]. The controller was validated *in silico* on six virtual patients of Hovorka T1DM simulator and *in vivo* on laboratory rats. During the validation, the same controller with exactly the same parameters was tested that showed a good robustness level. However, as far as the author knows, SMC studies, concerning glycemia regulation, have never considered the positive input constraint. In other words, insulin injection/infusion is a nonnegative input and thus the only admissible SMC is the *nonnegative* SMC. For that reason, a positive SMC for BG regulation of T1DM will be presented in Chapter 5. Moreover, for a model-based control design, like MPC or SMC, the system model plays a capital role in the overall controller performance. Therefore, an appropriate model that provides a good description of glycemia-insulinemia dynamics for a T1DM must be chosen. Unfortunately, the historical models like Bergman have non-natural equilibria that are not consistent with T1DM glycemic behavior in real life. As explained in [58], those equilibria imply a set of basal insulin that keeps BG level constant. Whereas a T1DM patient has a unique basal insulin level (independent from BG) that stabilizes BG at any value, namely a critically stable system and not asymptotic as the historical models present. For theses reasons, the employed model in this thesis is the recently developed long-term T1DM model [58]. This model has shown a good description of glycemia-insulinema dynamics of T1DM as compared to other models (see Chapter 3 for more details). It is used to design a nonnegative SMC in Chapter 5 for glycemia regulation. The model parameters were identified on T1DM clinical data supported by university hospital center of Nantes and Rennes.

[13] The basic idea of Smith Predictor is to use the system model to predict the pure time delay for the controller [54].

2.10.4 Positivity and state feedback Control

As stated earlier and according to the literature of AP studies, input/output constraints of T1DM closed-loop system is mainly taken into account by MPC. Recently, positivity of the closed-loop controller is considered in the design by [59]. The authors treated glycemia-insulinemia system as a class of internally positive systems where the input response is slower than that of the disturbance. To achieve a trade-off between hyper and hypoglycemia peaks under positive control, they used a model-based control design where the controller is the result of a minimization of the output response of two time instants. State feedback is also employed for glycemia regulation. However, positivity of the controller has not been considered. Take for instance two recent state feedback design based on Bergman model [60] and [61]. The feedback gains of the controller designed in [60] are the solution of an optimization program that uses some uncertainty bounds on the model parameters. Robustness and simplicity of the linear controller were the main achievements of this work. Other researchers [61] used observer-based state feedback controller. The feedback gains are designed using pole placement method based on Bergman linearized model. The controller results are compared to an adaptive PID and the simulations showed comparable performance. The authors considered the fixed design state feedback controller as simpler and less complex to implement compared to the adaptation technique of th PID. Two important remarks are highlighted from these two publications:

1. Bergman model for *non-diabetic* subject was used: both publications keep the internal insulin regulatory function in the model. This function does not exist for T1DM subjects (See § 3.4.1 and Remark 1). The result is that when the controller is off, endogenous basal plasma insulin is yielded! see Fig. 2 in [60].

2. Positivity of the state feedback controller is not considered in the design.

2.11 Conclusions

Researchers are working for decades to find the optimal continuous insulin delivery to regulate glycemia for a T1DM either via biological solutions or using engineering techniques and closed-loop control. The ultimate goal for the latter solution is the realization of a reliable AP device. A brief history of the main AP control algorithms is presented. As an overall overview, the following points are worth noting:

PID benefits

- It was shown that PID mimics the pancreatic β-cell insulin secretion. This behavior was observed in response to a step change in BG [37]. The derivative term produces the first phase insulin and compensates for the delay in Pharmacokinetic/Pharmacodynamic (PK/PDs) curve. The integral term produces the steady basal rate added to the Proportional term that increases the insulin delivery if BG is above target and vice versa.

- Tuning a PID controller does not require precise mathematical model in its design. However, optimal tuning may not be a straightforward matter especially under external disturbances like meals.

PID drawbacks

- It was shown that fully automatic PID is not sufficient to achieve the trade-off between hyperglycemia reduction and hypoglycemia prevention. It was either supported by IFB or by supplementary meal boluses.

- Another PID drawback is its degraded performance due to the actuator saturation (nonnegative insulin infusion). The saturation to zero, whenever PID goes negative (to compensate for negative error), means that the loop is broken. In this case, the system is no more under control. Another consequence is the integral windup which forced many researchers to replace the integral term by the insulin basal rate.

MPC features and drawbacks

- MPC is an advanced industrial counterpart of the PID. MPC main advantage is its capability in handling system constraints: hypoglycemia for the output and positivity constraint for the input.

- The main drawback of MPC is its cumbersome optimization procedures.

- This model-based controller requires sometimes model linearization (if nonlinear models are used) and parameter identification to cope with changes in system parameters. This complicates the parameter tuning process per individual.

- According to the meta-analysis provided by [62], MPC performance is not superior to that of a PID, bearing in mind that the latter's parameters are derived empirically or are based on a model which may not be the optimal choice.

This thesis solution In this thesis, Model-free PID or intelligent PID (iPID) is used for the first time for glycemia regulation of T1DM. It has the nice properties of a simple PID with some adaptive features. Model-free control has already been successfully applied in many concrete and diverse situations (see [63] and the references therein). Fully automatic iPID is tested and compared to the model-free intelligent Proportional or iP controller and also to classic PID control. The test was conducted *in silico* on two simulators as detailed in Chapter4.

SMC main features

- SMC is a variable structure controller which has its share in the literature of AP being a robust controller.
- Robustness of SMC is exhibited from being a variable structure control. It uses a discontinuous function to steer the state trajectory to a pre-specified path toward the equilibrium.
- The sliding surface is reached in finite time.
- SMC robustness properties has been shown in several closed-loop studies via *in silico* tests and an *in vivo* one on laboratory rats.

SMC drawback and open problem

- The major side effect of the discontinuity in the control law is the high frequency chattering. Several solutions are available in the literature to alleviate this problem, one of which is via HOSMC.
- None of SMC studies considered the nonnegative constraint on the control action.

Our solution Therefore, in Chapter 5, nonnegative SMC is designed for glycemia regulation for the first time. SMC is designed to be nonnegative everywhere in the largest closed-loop positively invariant set of the insulin subsystem of the T1DM model in [58]. Two stage SMC is designed, the last stage SMC2 block uses the glycemia error to design the desired insulin trajectory. Then the plasma insulin state is forced to track the reference via SMC1. The switching variable of SMC1 is the first order polynomial of the insulin error. Sliding mode of SMC1 guarantees insulin reference tracking. The resulting desired insulin trajectory is the required virtual control input of the glycemia system to eliminate BG error. BG error is the switching variable of SMC2. BG is steered to the normal set point during

sliding mode of SMC2. *In silico* trial is performed to validate the theoretical results on the nominal system.

Concerning the available T1DM models

- Model-based controllers, like SMC and MPC, require an internal model that provides a good description of glycemia-insulinemia dynamics for a T1DM. Otherwise, a poor closed-loop response is yielded.
- Historical T1DM models that are widely used in closed-loop studies, like Bergman, have strange equilibria that are not consistent with T1DM glycemic behavior in real life (more details are found in §3.8).

More details about mathematical modeling of this biological system, especially concerning the widely employed models, are presented in Chapter 3. Equilibrium of these models and a recently developed long-term model [58] are discussed in this chapter as well.

Positivity and positive state feedback in this thesis To the best of our knowledge, positivity analyses and invariance of glycemia-insulinemia system were not considered previously for the control design purposes. This motivated open and closed-loop input/output positivity analyses of the linear affine model in [58] in Chapter 6. It is shown that glycemia output does not remain positive for any positive input. Therefore, the largest positively invariant set in open-loop and under positive state feedback control are found.

The main issues of the previous state feedback designs in the literature (in subsection 2.10.4) are taken into account in the design of a *positive* state feedback controller in Chapter 6. The result is a stable closed-loop system under positive controller that regulates BG and prevents hypoglycemia. Another important achievement is that hypoglycemia is predicted in case the initial condition is outside the invariant set. Future hypoglycemia episodes are predicted in both open-loop and closed-loop cases. It is the main result of the computation of the largest positively invariant sets.

Chapter 3

Glucose-insulin Dynamics: Mathematical modeling

3.1 Chapter Introduction in French

Dans ce chapitre, nous présentons une revue des modèles mathématiques qui décrivent la dynamique glucose-insuline du DT1. La modélisation mathématique en biologie est utilisée comme un outil utile pour décrire et simuler des systèmes physiologiques et leurs variables à des fins différentes. Le système glucose-insuline a gagné beaucoup d'intérêt dans la littérature de ce domaine. Il permet de simuler et de tester l'administration d'insuline pour le DT1 en particulier des algorithmes de commande en boucle fermée pour préparer la voie à un AP fiable.

Le focus, dans ce chapitre, est mis sur les modèles bien connus et largement utilisés dans la littérature et plus spécifiquement dans les études de PA. Ils sont principalement utilisés pour construire des simulateurs DT1 et des commandes basées sur des modèles pour des tests en boucle fermée. Ils vont des modèles non linéaires minimaux aux modèles à ordre élevé et certains modèles linéaires récemment présentés. Deux des modèles historiques largement connus sont considérés et validés en tant que modèles à court terme et un nouveau modèle linéaire à long terme est présenté dans ce chapitre qui sera utilisé dans le reste de la thèse. L'existence du point d'équilibre d'un modèle DT1 dans des conditions de jeûne est discutée du point de vue physiologique.

3.2 Introduction

In this chapter a review of the mathematical models that describe glucose-insulin dynamics of T1DM is presented. The focus will be on the well known widely used models in the literature and more specifically in AP studies. They are mainly used to build up T1DM simulators and model-based controllers for closed-loop tests. They range from minimal to high order nonlinear models and some recently presented linear models. Two of the widely known historical models are reviewed as short-term models and a new long-term linear model is presented in this chapter which will be used in the rest of the thesis. The existence of an equilibrium point of a T1DM model in fasting conditions is discussed from the physiological point of view.

3.3 Compartmental Modeling of Biological Systems

Compartmental models are used to describe the transport process of materials between interconnected volumes (e.g. drugs) in a biological system. They can be seen as systems composed of interconnected chambers or stirred tanks of well mixed materials. The compartments exchange materials which are concentrations or molar amounts of chemical species which represent the system states variables [64]. For instance, for T1DM subject, injected insulin enters first the subcutaneous tissue (first compartment) before its transfer to the plasma compartment. The flow rate between compartments is described usually by ordinary differential equations following mass conservation law. It states that the difference between the flow in and flow out determines the amount of the material in the compartment [65]. Compartmental models are widely used in pharmacokinetics (PK), for illustrating the concentration-time curves of a drug after administration. PK describes thus the availability duration of the drug in the body and defines the dosage and route of administration; whereas, pharmacodynamics (PDs) is the physiological response of the drug and its effect on the biological system with time [64]. The mathematical description between the drug delivery to the response mechanisms comprise the combination PK/PDs. For instance, [66] presented a three-differential equation insulin system: a two compartmental model for PK response for subcutaneous to plasma insulin and a third for PDs response called the *effective* (or active) insulin in compartments remote from plasma that interacts directly on glycemia level.

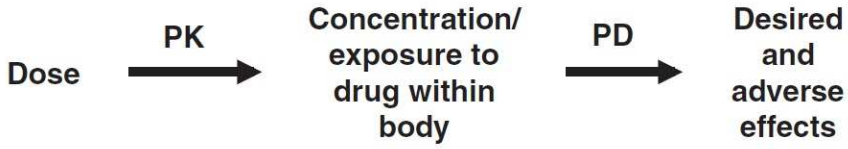

Figure 3.1 Relationship between pharmacokinetics PK and pharmacodynamics PD [49].

3.4 Historical Models

Several Mathematical models are available in the literature to describe the glucose-insulin dynamics. The modeling process usually starts with the interpretation of plasma glucose and insulin concentrations during glucose tolerance tests. These are either intravenous glucose tolerance test (IVGTT) or an Oral route (OGTT). Those models range from minimal models starting by the 1961's Bolie model [67], Bergman's [68] to other more complex like Sorensen's model 19 equations model [57]. Here the three models that are widely used in AP *in silico* tests will be reviewed.

3.4.1 Bergman minimal model

It is a well known classical model that is first developed in 1979 and then insulin sensitivity is evaluated using a clinical study on 18 hospitalized healthy subjects [68]. The standard formulation of the model is a system of three differential equations [69]:

$$\dot{G}(t) = -p_1.(G(t) - G_b) - X(t).G(t) \tag{3.1}$$

$$\dot{X}(t) = -p_2.X(t) + p_3.(I(t) - I_b) \tag{3.2}$$

$$\dot{I}(t) = p_4.(G(t) - p_5)^+.t - p_6(I(t) - I_b) \tag{3.3}$$

Where $G(t)$ [mg/dL]:plasma glucose concentration, $I(t)$ [μU/mL] plasma insulin concentration, $X(t)$ [min^{-1}] interstitial/active insulin in remote compartment. The suffix b refers to basal state. Parameters p_5 [mg/dL] is a pancreatic "glycemia threshold" above which the pancreas starts secreting insulin. p_1, p_2, p_6 [min^{-1}], p_3 [min^{-2} /μU/mL] and p_4 [μU/mL/(mg.min/dL)] are rate coefficients, for more details see [69] and [68]. The plus sign in (3.3) means:

$$(G(t) - p_5)^+ = \begin{cases} 0 & if \quad G \leq p_5 \\ (G - p_5) & if \quad G > p_5 \end{cases} \tag{3.4}$$

This model was developed on healthy subjects and this fact can be seen from the term $p_4.(G(t)-p_5)^+$ which represents pancreatic insulin secretion when BG exceeds certain threshold.

Remark 1. *It is good to mention that several T1DM closed-loop glycemia regulation studies considered $p_4(G(t)-p_5)^+$ as an internal insulin regulatory function that does not exist for T1DM cases. The parameter p_1 has been also argued to be reduced to zero for a diabetic patient (see [55] and the references therein). Thus p_1 and p_4 are set to zero in* (3.1) *and* (3.3) *when Bergman model was employed for closed-loop glycemia regulation as in [53] and [55].*

3.5 Hovorka's model

This model, which was developed on healthy subjects [45], describes the input/output relationship between subcutaneous insulin infusion as input and intravenous glucose concentration as output. It has also meal ingestion and intravenous (IV) glucose infusion as exogenous glucose inputs [1] [44].

The glucose kinetics parameters values are determined using glucose tracers on normal subjects during overnight fasting phase and during IVGTT. This model consists of:

1. Glucose subsystem: absorption, distribution and disposal.
2. Insulin subsystem: absorption, distribution and disposal.
3. Insulin-action subsystem: its action on glucose transport, disposal and endogenous production.

3.5.1 Glucose subsystem

$$\begin{cases} \dot{Q}_1(t) = -\left[\frac{F_{01}^c}{V_G G(t)} + x_1(t)\right] Q_1(t) + k_{12} Q_2(t) - F_R + U_G(t) + EGP_0[1 - x_3(t)] \\ \dot{Q}_2(t) = x_1(t).Q_1(t) - [k_{12} + x_2(t)] Q_2(t) \\ G(t) = \frac{Q_1(t)}{V_G} \end{cases} \tag{3.5}$$

where Q_1, Q_2 [mmol] glucose masses in the accessible [2] (plasma) and non-accessible compartments (e.g. interstitial and intracellular distribution space [45]). k_{12} transfer-rate constant from non-accessible to accessible compartment. V_G [L] distribution volume of the accessible

[1] Glucose is infused intravenously during clinical studies when hypoglycemia is detected.

[2] represents plasma and tissues that equilibrate quickly with plasma [45]

compartment. G [mmol/L] is the measurable glucose concentration. EGP_0 [mmol/min] Endogenous Glucose Production extrapolated at zero insulin concentration which is a constant value [44]. $U_G(t)$ [mmol/L] is the is the gut absorption which is a function of digested CHO. In general a two compartmental model (D_1, D_2) is used to simulate oral meal (CHO) digestion for AP tests (e.g. see [70]). F_{01}^c [mmol/min] is the total non-insulin-dependent glucose flux corrected for the ambient glucose concentration.

$$F_{01}^c = \begin{cases} F_{01} & \text{if} \quad G(t) \geq 4.5 \\ \frac{F_{01}.G(t)}{4.5} & \text{otherwise} \end{cases} \tag{3.6}$$

and F_R [mmol/L] is the renal glucose clearance above 9 mmol/L (162 mg/dL)

$$F_R = \begin{cases} 0.003(G(t)-9)V_G & \text{if} \quad G(t) \geq 9 \\ 0 & \textit{otherwise} \end{cases} \tag{3.7}$$

F_{01} is a constant [44].

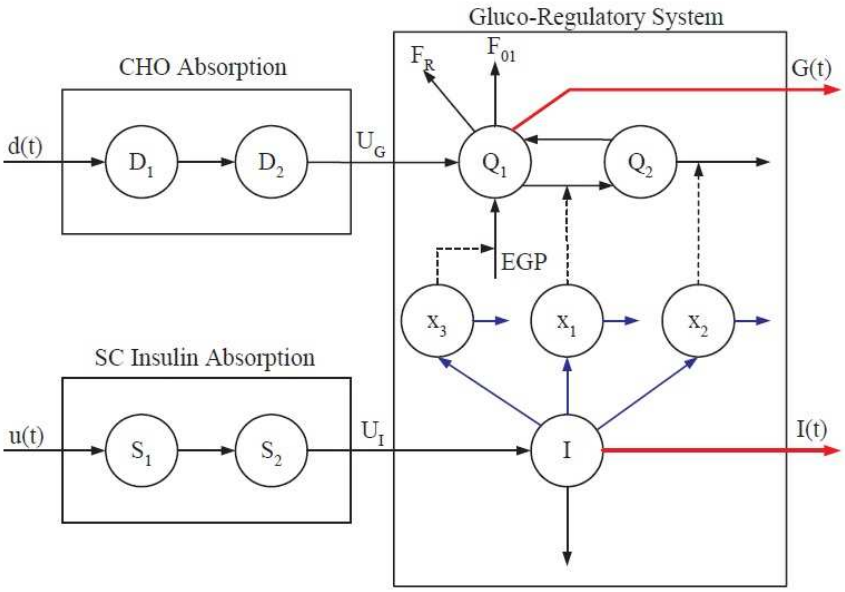

Figure 3.2 Hovorka's compartmental model with meal subsystem. d(t) [g/min] is the CHO input rate [70].

3.5.2 Insulin subsystem

- Absorption model [44]:

$$\begin{cases} \dot{S}_1(t) = u(t) - \frac{S_1(t)}{t_{max,I}} \\ \dot{S}_2(t) = \frac{S_1(t) - S_2(t)}{t_{max,I}} \end{cases} \tag{3.8}$$

where $S_1(t), S_2(t)$[mmol] two-compartment chain representing absorption of subcutaneously administered short-acting insulin. $u(t)$ [mmol/min] insulin infusion rate and $t_{max,I}$ [min] time-to-maximum insulin absorption.

- The plasma insulin concentration $I(t)$

$$\dot{I}(t) = \frac{U_I}{V_I} - k_e I(t) \tag{3.9}$$

where k_e[min^{-1}] is the fractional elimination rate, U_I [mU]$= \frac{S_2(t)}{t_{max,I}}$ is the appearance of insulin in plasma and V_I [L] is the distribution volume.

3.5.3 Insulin action subsystem

It is of three actions on glucose kinetics

$$\dot{x}_i(t) = -k_{ai} x_i(t) + k_{bi} I(t), \qquad i = 1,2,3. \tag{3.10}$$

where $x_i(t)$ [min^{-1}] the remote effects of insulin on glucose for $i = 1$ distribution/transport, $i = 2$ disposal and $i = 3$ on endogenous glucose production. k_{ai} [min^{-1}] are the deactivation rate constants, and k_{bi} [min^{-1}] are the activation rate constants. $S_{IT} = \frac{k_{b1}}{k_{a1}}$ represents insulin sensitivity of distribution/transport, $S_{ID} = \frac{k_{b2}}{k_{a2}}$ insulin sensitivity of disposal and $S_{IE} = \frac{k_{b3}}{k_{a3}}$ is insulin sensitivity of EGP. Model parameters and constants values can be found in [44]. A T1DM simulator is realized from this model known as *APCam* for (Artificial Pancreas project at Cambridge) of 18 virtual patients. It is developed by the University of Cambridge for closed-loop control test studies.

3.6 Dalla Man model: Uva/Padova Simulator

This model is developed based on OGTT rather than the intravenous perturbations to develop a meal simulator [71]. Meal data set of 204 normal individuals is used to validate a model

of glucose ingestion and absorption. The identification process is also realized on smaller database of 14 T2DM subjects. This compartmental model is composed of two main subsystems: glucose and insulin. It describes also the relationship between the plasma measurements of glucose and glucose rate of appearance in plasma due to:

- the glucose rate of appearance in plasma (meal intake) R_a [mg/kg/min],
- the liver's $EGP(t)$ [mg/kg/min],
- dependent and independent utilization of glucose $U_{id}(t)$ and $U_{ii}(t)$ [mg/kg/min]respectively,
- renal excretion $E(t)$,
- insulin secretion and degradation.

3.6.1 Glucose subsystem

A two compartmental subsystem that is shown in the first panel of Fig. 3.3 consisting of plasma glucose mass $G_p(t)$ and tissues $G_t(t)$ [mg/kg]

$$\begin{cases} \dot{G}_p(t) = EGP(t) + R_a(t) - U_{ii}(t) - E(t) - k_1.G_p(t) + k_2.G_t(t), & G_p(0) = G_{pb} \\ \dot{G}_t(t) = -U_{id}(t) + k_1.G_p(t) - k_2.G_t(t), & G_t(0) = G_{tb} \\ G(t) = \frac{G_p}{V_G}, & G(0) = G_b \end{cases} \tag{3.11}$$

where V_G [dL/kg] is the glucose distribution volume, $G(t)$ [mg/dL] is the plasma glucose concentration and k_1, k_2 [min^{-1}] are the rate parameters, the suffix b refers to basal state.

Note that intestinal glucose absorption subsystem whose output is $R_a(t)$ and insulin dependent glucose utilization $U_{id}(t)$ unit model are nonlinear models (see [71]for more details). Description of these unit models and the rest like $EGP(t)$ and $E(t)$ are detailed in [71].

3.6.2 Insulin subsystem

As illustrated in the second panel of Fig. 3.3, it is also a two compartmental model of insulin mass in plasma $I_p(t)$ [pmol/kg] and insulin mass in the liver $I_l(t)$ [pmol/kg]

$$\begin{cases} \dot{I}_l(t) = -(m_1 + m_3(t)).I_l(t) + m_2.I_p(t) + S(t), & I_l(0) = I_{lb} \\ \dot{I}_p(t) = -(m_2 + m_4).I_p(t) + m_1.I_l(t), & I_p(0) = I_{pb} \\ I(t) = \frac{I_p}{V_I}, & I(0) = I_b \end{cases} \tag{3.12}$$

where $S(t)$ [pmol/kg/min] is insulin secretion, m_1, m_2 [min^{-1}] are transport rates, m_4, [min^{-1}] m_5 [min.kg/pmol] are the degradation rate parameters and m_6 [dimensionless] is a constant. In summary this T1DM model consists of 13 differential equations and 35 parameters per subject. Despite the fact that the model is validated on non-diabetic and T2DM subjects, it is realized to be a T1DM simulator that is known as *Uva/Padova T1DM Metabolic Simulator*. To simulate a T1DM, the above insulin secretion model was replaced by the exogenous insulin infusion model in [72]:

$$\begin{cases} \dot{I}_{sc1}(t) = -(k_d + k_{a1}).I_{sc1}(t) + u(t), & I_{sc1}(0) = I_{sc1b} \\ \dot{I}_{sc2}(t) = k_d.I_{sc1}(t) - k_{a2}.I_{sc2}(t), & I_{sc2}(0) = I_{sc2b} \end{cases} \tag{3.13}$$

Where I_{sc1}, I_{sc2} [pmol/kg] are the insulin masses in the subcutaneous space, k_{a1}, k_{a2} [min^{-1}] are their rate constants. k_d [min^{-1}] is the insulin rate constant of dissociation and $u(t)$ [pmol/kg/min] is the exogenous insulin infusion rate. In addition to this change, a higher EGP (vs normal) is introduced in [72] to account for higher basal rates for T1DM subjects. The remaining parameters are kept as they were for non-diabetic. Uva/Padova T1DM simulator is approved by the FDA to test and validate any closed-loop control algorithms for the artificial pancreas studies. It is considered now as a mandatory validation step that precedes any clinical trials as detailed earlier in the bibliography of Chapter 2.

3.7 A long-term model of glucose-insulin dynamics of T1DM

This model is developed based on the clinical data of the University Hospital Centers of Nantes and Rennes [58]. It has the following advantages over other existing models in the literature:

1. The parameters are identified on standard clinical diary [3] (in- or outpatient data) for a time span up to two days.

2. Unlike the existing models, its glycemic stability property is consistent with T1DM glycemic behavior (see [58] for more details).

3. It permits calculating FIT tools such as ISF and basal rate of insulin.

[3] Mainly consists of CGM record, insulin injection history and estimated CHO intake.

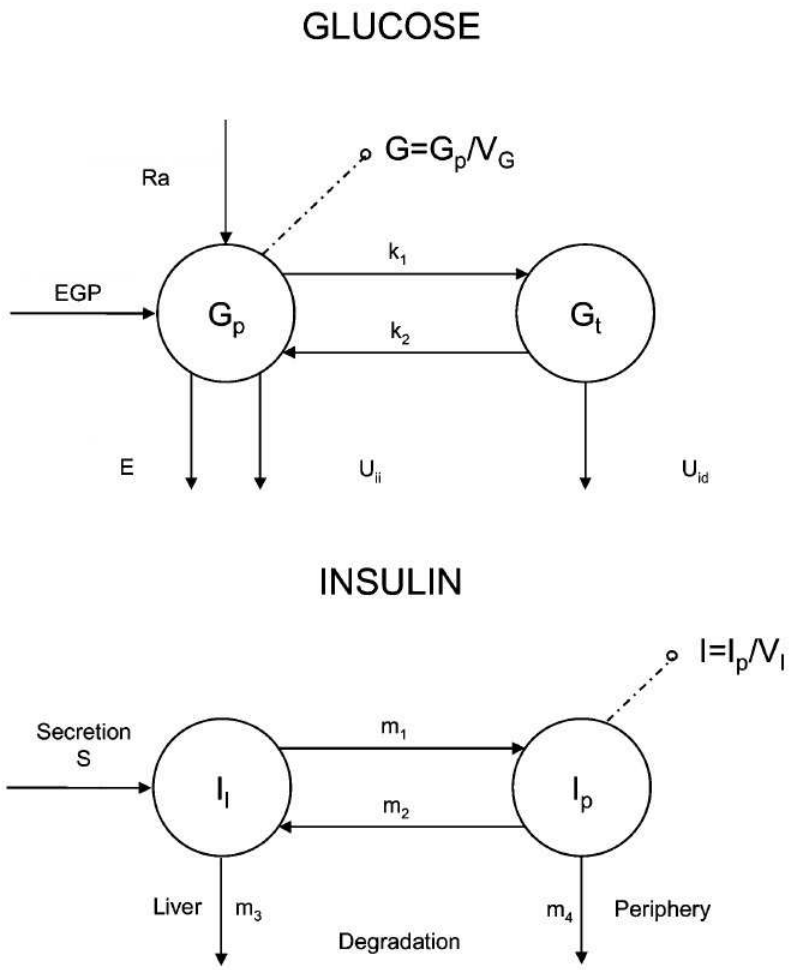

Figure 3.3 Dalla Man compartmental model of insulin-glucose system [71].

As the third point is useful in the usual self insulin administration for T1DM patients (open-loop control), the other points are significant in the T1DM virtual simulation for any control algorithm test (closed-loop control).

The model comprises the three main dynamics of glucose-insulin system: glucose, insulin and digestion subsystem.

3.7.1 Glucose subsystem

$$\dot{G}(t) = -k_{si}.I(t) + k_l - k_b + D(t) \tag{3.14}$$

where $G(t)$ [mg/dL] is glucose concentration, $I(t)$ [U/dL] insulin in plasma. On one hand, glycemia decrease is either related to insulin in a constant rate defined by the parameter k_{si} [mg/(U.min)], or by the fixed brain consumption that is anti proportional to the body mass

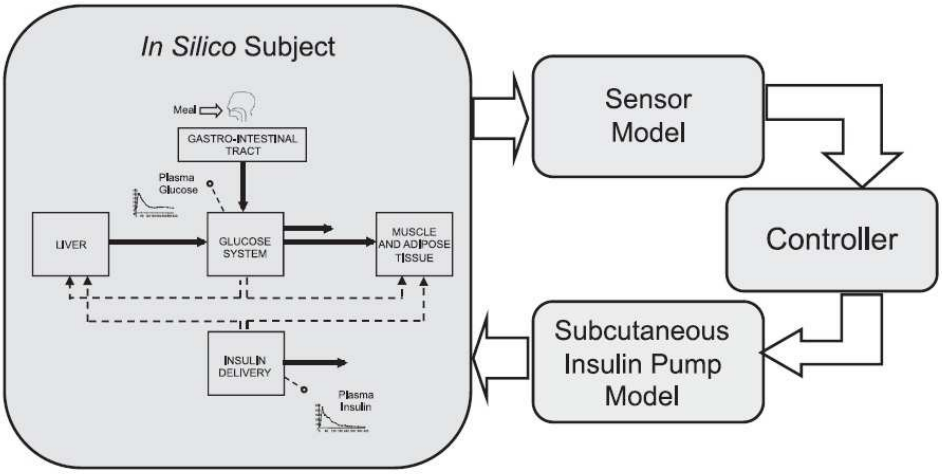

Figure 3.4 Principal component of Uva/Padova T1DM simulator [73].

M $k_b = \frac{128}{M}$ [mg/(dL.min)]. On the other hand, glycemia rate increases either endogenously represented here by the liver constant production rate k_l [mg/(dL.min)] or through an exogenous rate $D(t)$ [mg/(dL.min)] which is the glucose appearance rate in the plasma due to CHO digestion. The term $k_l - k_b$ represents the net balance between the endogenous glucose production and insulin-independent consumption. As explained in [58] for average hepatic glucose production during fasting for $M > 40$ kg then $k_l - k_b > 0$. The PDs of insulin on glycemia in is found in the term $-k_{si}I(t)$ of (3.14).

3.7.2 Insulin subsystem

It is a second order model of a single time constant T_u [min] that describes insulin PK [58]:

$$\ddot{I}(t) = -\frac{I(t)}{T_u^2} - \frac{2\dot{I}(t)}{T_u} + \frac{k_u}{V_I.T_u^2}u(t) \tag{3.15}$$

k_u [min] is a static gain, V_I [dL]$= 2.5M$ is insulin distribution volume and $u(t)$ [U/min] is the exogenous insulin injection/infusion rate.

3.7.3 Digestion subsystem

A similar second order model of a single time lag T_r [min]

$$\ddot{D}(t) = -\frac{D(t)}{T_r^2} - \frac{2\dot{D}(t)}{T_r} + \frac{k_r}{V_B.T_r^2}r(t) \tag{3.16}$$

k_r [unitless] is a static gain, V_B [dL]$= 0.65M$ is the blood volume and $r(t)$ [mg/min] is the CHO amount rate. As detailed in [58], five clinical diaries of T1DM subjects are used to identify the model parameters. The same injection/meal scenario is applied i.e. $u(t), r(t)$ are taken from the diary of the patient to create a glycemia output to be fitted on the CGM curve from the diary using data fitting and least square method.

3.7.4 Overall model

The state space representation of the overall T1DM system is written as follows considering the glucose rise due meals $D(t)$ as a perturbation:

$$\begin{pmatrix} \dot{G}(t) \\ \dot{I}(t) \\ \ddot{I}(t) \end{pmatrix} = \begin{pmatrix} 0 & -k_{si} & 0 \\ 0 & 0 & 1 \\ 0 & -\frac{1}{T_u^2} & -\frac{2}{T_u} \end{pmatrix} \begin{pmatrix} G(t) \\ I(t) \\ \dot{I}(t) \end{pmatrix} + \begin{pmatrix} 0 \\ 0 \\ \frac{k_u}{V_I.T_u^2} \end{pmatrix} u(t) + \begin{pmatrix} k_l - k_b \\ 0 \\ 0 \end{pmatrix} + \begin{pmatrix} 1 \\ 0 \\ 0 \end{pmatrix} D(t) \quad (3.17)$$

The perturbation $D(t)$ will be considered as external unknown input which is zero during

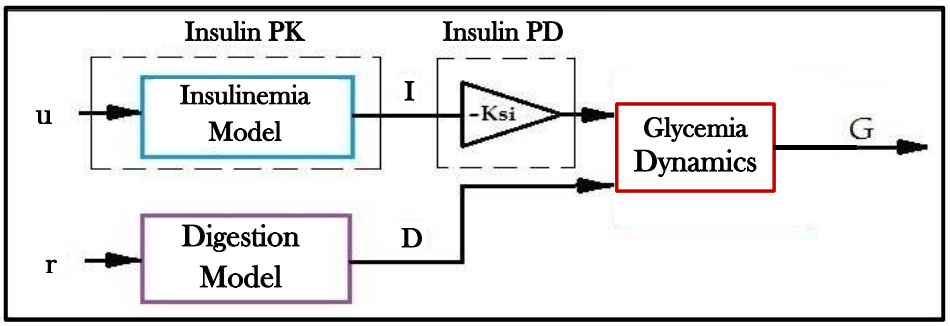

Figure 3.5 Magdelaine's T1DM simulator.

fasting times. In addition, it is not affected by the change of variables in the following section.

3.7.5 A more physiological representation of Magdelaine's model

The model (3.17) has one state as the derivative of plasma insulin. Since this variable does not have a physiological meaning, and based on [66], a new state variable is introduced the subcutaneous insulin $I_{sc} = T_u\dot{I} + I$ [U/min]. In this manner, PK/PDs insulin model includes subcutaneous and plasma insulin compartments. To simplify the change of variables let $x_1 = I, x_2 = \dot{I}$ and:

$$x_{sc} = \theta_3 x_2 - x_1 \quad (3.18)$$

This leads to:

$$\begin{pmatrix} \dot{G} \\ \dot{x}_1 \\ \dot{x}_{sc} \end{pmatrix} = \begin{pmatrix} 0 & -k_{si} & 0 \\ 0 & -\frac{1}{T_u} & \frac{1}{T_u} \\ 0 & 0 & -\frac{1}{T_u} \end{pmatrix} \begin{pmatrix} G \\ x_1 \\ x_{sc} \end{pmatrix} + \begin{pmatrix} 0 \\ 0 \\ \frac{k_u}{V_I.T_u} \end{pmatrix} u + \begin{pmatrix} k_l - k_b \\ 0 \\ 0 \end{pmatrix} + \begin{pmatrix} 1 \\ 0 \\ 0 \end{pmatrix} D(t) \tag{3.19}$$

The state variables in this representation of the system are concentration variables. Moreover, it will be shown in Chapter 5 and 6 that insulin subsystem of (3.19) is an *internally positive* system i.e. if $x_1(0), x_{sc}(0) \geq 0$ then $x_1(t)$[U/dL], $x_{sc}(t)$[U/dL]$\geq 0 \; \forall t \in \mathbb{R}^+$.

A new version of the model is currently developed where the parameters are reduced to 5 instead of 6:

$$\theta_1 = k_l - k_b, \;\; \theta_2 = \frac{k_{si}k_u}{V_I}, \;\; \theta_3 = T_u, \;\; \theta_4 = T_r, \;\; \theta_5 = \frac{k_r}{V_B} \tag{3.20}$$

Consider the following change of variables:

$$x_{n_1} = \frac{V_I}{k_u} x_1 \tag{3.21}$$

$$x_{n_2} = \frac{V_I}{k_u} x_{sc} \tag{3.22}$$

where x_{n_1} [U/min] plasma insulin rate and x_{n_2} [U/min] is the subcutaneous insulin rate. In this case the system model (3.19) becomes as follows:

$$\begin{pmatrix} \dot{G} \\ \dot{x}_{n_1} \\ \dot{x}_{n_2} \end{pmatrix} = \begin{pmatrix} 0 & -\theta_2 & 0 \\ 0 & -\frac{1}{\theta_3} & \frac{1}{\theta_3} \\ 0 & 0 & -\frac{1}{\theta_3} \end{pmatrix} \begin{pmatrix} G \\ x_{n_1} \\ x_{n_2} \end{pmatrix} + \begin{pmatrix} 0 \\ 0 \\ \frac{1}{\theta_3} \end{pmatrix} u + \begin{pmatrix} \theta_1 \\ 0 \\ 0 \end{pmatrix} + \begin{pmatrix} 1 \\ 0 \\ 0 \end{pmatrix} D(t) \tag{3.23}$$

3.8 Stability and equilibrium of T1DM models

It is worth noting that historical T1DM models has an equilibrium point of glycemia even though insulin injection is zero. This observation contradicts the physiological fact that for a T1DM subject in fasting conditions (zero CHO intake) and if insulin is not injected at all, glycemia diverges (becomes huge). As stated earlier in Chapter 1, this occurs as the zero insulin concentration stimulates hepatic endogenous glucose production and the lack of insulin secretion leads to hyperglycemia. This stability property is remarked in [58] and the authors took, as an example, a T1DM model presented in [69] and studied its equilibrium state. It was shown that, for that model, glycemia reaches the equilibrium for different insulin concentrations even for $I(t) = 0$.

Here, the equilibrium state of Hovorka's and Magdelaine's models are further investigated. These analyses are followed by a simulation example of Uva/Padova simulator that shows the non-natural set of equilibria during fasting phase.

3.8.1 Hovorka's model: equilibrium

3.8.2 Autonomous system

The equilibrium point is analyzed first for the autonomous system i.e. in fasting conditions: $U_G(t) = 0$, and zero insulin injection: $u(t) = 0$. Starting with the insulin absorption subsystem (3.8) $\dot{S}_{1,2} = 0$ yields :

$$S_1 = 0, S_2 = 0 \tag{3.24}$$

and from (3.9) plasma insulin concentration in its equilibrium ($\dot{I} = 0$) yields $I_{eq} = 0$ and thus from (3.10) $\dot{x}_i = 0$ implies $x_{i_{eq}} = 0$. Applying this result in the glucose model (3.5) leads to:

$$-F_{01}^c + k_{12}Q_2(t) - F_R + EGP_0 = 0 \tag{3.25}$$

$$Q_2(t) = 0 \tag{3.26}$$

In the region where $G < 4.5$mmol/L where $F_{01}^c = F_{01}\frac{G}{4.5}, F_R = 0$:

$$G_{eq} = 4.5\frac{EGP_0}{F_{01}} \tag{3.27}$$

$G_{eq} = 7.4$ mmol/L higher than the given operating threshold 4.5 mmol/L, i.e. there is no equilibrium in this region. Similarly, in the region $4.5 \leq G < 9$ mmol/L one has $F_{01}^c = F_{01}$ and $F_R = 0$ substituting in (3.5) leads to:

$$\dot{Q}_1(t) = EGP_0 - F_{01} \quad \neq 0 \tag{3.28}$$

As $EGP_0 - F_{01} > 0$ [44], and as $G = \frac{Q_1}{V_G}$, this results in a diverging glycemia and thus there is no equilibrium in the region $4.5 \leq G < 9$ for the autonomous system. Conversely, when $G(t) \geq 9$ mmol/L, according to (3.6) and (3.7) this leads to $F_{01}^c = F_{01}$ mmol which is a constant, and $F_R = 0.003(G(t) - 9)V_G$ and from (3.26) yields:

$$G_{eq} = 9 + \frac{EGP_0 - F_{01}}{0.003(V_G)} \tag{3.29}$$

which is according to the parameters of [44] $G_{eq} = 22.333$ mmol/L (≈ 399 mg/dL). This result $I_{eq} = 0$ and $G_{eq} =$ constant is not consistent with the physiological fact that if a T1DM subject did not inject insulin at all then his glycemia diverges.

3.8.3 Fasting phase

This time equilibrium state for a constant basal insulin injection is considered during the fasting phase with $U_G(t) = 0$ and $u(t) = u_b$ a steady injection rate. The objective is to find, I_b the value under which glycemia is stabilized at an equilibrium state. It is expected, as the physiological fact implies, that there exists a unique basal rate I_b for this purpose. Starting again from the equilibrium of (3.8):

$$S_{1_{eq}} = u_c.t_{max,I} \tag{3.30}$$

$$S_{2_{eq}} = S_{1_{eq}} \tag{3.31}$$

equation (3.9) yields

$$I_{eq} = \frac{S_{1_{eq}}}{t_{max,I}.V_I.k_e} \tag{3.32}$$

substituting (3.31) in (3.32):

$$I_{eq} = \frac{u_c}{V_I.k_e} \tag{3.33}$$

and thus

$$x_{i_{eq}} = \frac{k_{bi}.I_{eq}}{k_{ai}}, \qquad i = 1,2,3. \tag{3.34}$$

Take for instance $4.5 \leq G_{eq} < 9$ mmol/L and according to (3.6) and (3.7) this leads to $F_{01}^c = F_{01}, F_R = 0$ and substituting (3.34) in (3.5) and sensitivity parametrization (S_{IT}, S_{ID}, S_{IE}) in section 3.5.3 yields:

$$G_{eq} = \frac{(EGP_0.(1 - S_{IE}) - F_{01}).(k_{12} + S_{ID}.I_{eq})}{I_{eq}^2.S_{IT}.S_{ID}} \tag{3.35}$$

First, notice that from (3.33) the basal insulin concentration I_{eq} depends on the injection rate u_c and does not have a unique value as expected. Moreover, there are infinite number of equilibrium points depending on an infinite constant input points u_b.

3.8.4 Magdelaine's Model: equilibrium

3.8.5 Autonomous system: $D(t), u(t) = 0$

As stated in section 3.7, in fasting phase equation(3.17) reveals that when $u = 0$ then $I = 0$ and thus glycemia diverges ($\dot{G} > 0$). This is due to the continuous liver glucose production, i.e. $k_l - k_b > 0$. In other words, for a T1DM during fasting phase, a zero insulin injection leads to fasting hyperglycemia and thus there is no equilibrium for glycemia in this case.

3.8.6 Fasting phase

The equilibrium point in this case for fasting conditions $D(t) = 0$ and constant delivery rate $u(t) = u_b$ according to (3.17) this leads to:

$$G = G_{eq}, \qquad I_{eq} = \frac{k_l - k_b}{k_{si}} \equiv \frac{\theta_1}{K_{si}} \tag{3.36}$$

The basal constant basal rate I_{eq} is thus unique and does not depend on the delivery rate u_c. Moreover, this implies a unique constant basal infusion rate u_b:

$$u_b = \frac{V_I}{k_u}.\frac{k_l - k_b}{k_{si}} \equiv \frac{\theta_1}{\theta_2} \tag{3.37}$$

3.8.7 Uva/Padova Equilibria: A fasting test

Like the main historical models, Uva/Padova simulator exhibits also non-natural equilibria. An illustrative simulation test is performed to demonstrate this fact. An open-loop fasting test scenario is performed (no meal intake) under three different constant insulin injection rates: $u(t)$= 2 U/h, 0 U/h (no insulin) and $u(t) = u_b$ the subject's specific basal rate as provided by the simulator. The resulting glycemia of Adult5 is depicted in Fig. 3.6. Three different BG equilibria are yielded in response to the three different insulin rates. This is inconsistent with real life basal-bolus therapy where steady-state glycemia can only be obtained under a unique basal injection value u_b[58]. Another important observation is that although the scenario starts with hyperglycemia, BG=350 mg/dL, and no boluses are injected, BG settles to some constant value. Take for instance the lower panel of Fig. 3.6, when the basal is injected, BG is steered to 120 mg/dL. In other words, the simulator's open-loop BG can be regulated from hyperglycemia without the need of a bolus! This contradicts the well known T1DM basal-bolus therapy as stated in [74] that confirms the fact that the role of basal insulin is not to normalize BG, but to stabilize it during 24 hours within a tolerance of $\pm$30 mg/dL.

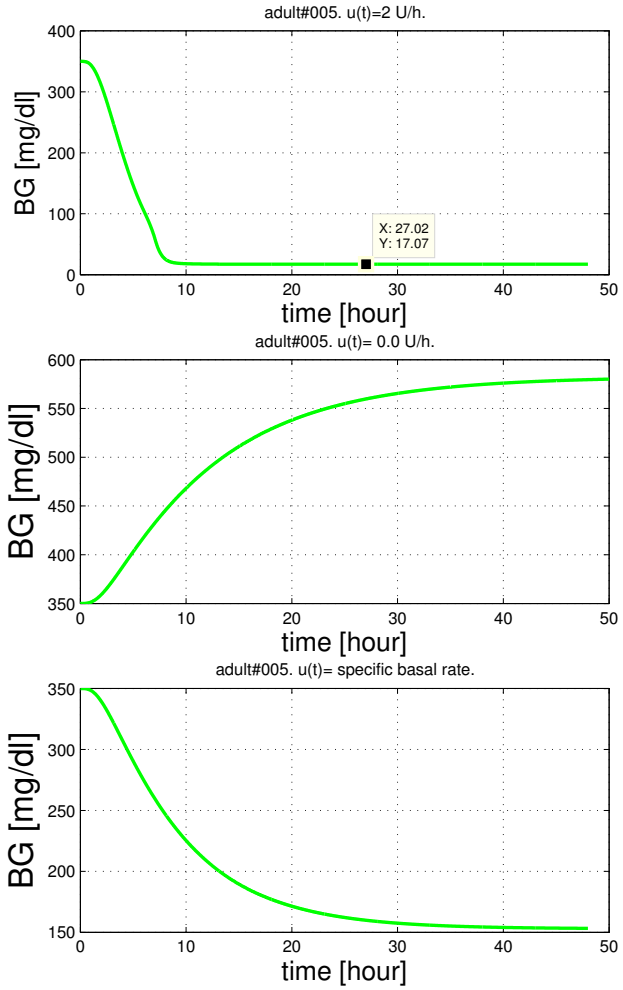

Figure 3.6 Glycemia behavior during fasting scenario for adult5 of Uva/Padova simulator. upper panel for u(t)=2U/h and middle panel for u=0 U/h and lower panel for u(t)= the basal rate provided by the simulator.

3.9 Conclusion

Mathematical modeling in biology is used as a useful tool to describe and simulate physiological systems and their variables for different purposes. Glucose-insulin system has gained lot of interest in the literature of this field. It permits to simulate and test insulin administration of T1DM therapies especially closed-loop control algorithms to pave the way for a reliable AP. Most existing models introduce some apparent equilibria which are not consistent with real life. Equation (3.17), though it is linear, or, more exactly, affine, appears to be a significant scientific alternative as it displays a long-term fit with clinical data. A good mathematical representation of the system is crucial for any control algorithm of AP, not only to test its performance *in silico*, it is also essential in the design process of model-based controllers.

Thus, the simulation results based on poor models are misleading and may lead to a poor closed-loop behavior during a real clinical trial. In this thesis, model-based controllers, SMC and state feedback, are designed employing the long-term model (3.17). Our early work of positivity analyses, presented in Chapter 5, for sliding mode control was established on the standard model (3.17). After observing the new model representation of insulin dynamics in Section 3.7.5, it is employed in the positive invariance analyses in Chapter 6. Insulin subsystem in this case represents an internally positive system as will be shown later.

Chapter 4

Fully automatic Model-free Control for Glycemia Regulation

4.1 Chapter Introduction in French

Dans ce chapitre, la théorie et la conception de la commande sans modèle (CSM) sont présentées. Il est présenté ici comme un algorithme de commande du PA pour la première fois. La commande CSM est choisie car elle offre les fonctions simples d'une commande PID en s'affranchissant de tout modèle mathématique. Contrairement aux études PID précédentes, l'algorithme de commande développé ci-après est entièrement automatique sans aucune dose d'insuline complémentaire. La commande proportionnelle sans modèle où les résultats de la commande proportionnelle intelligente iP sont d'abord présentés et analysés avec des systèmes linéaires stables et instables. Le focus est mis sur la stabilisation du régulateur iP via ses paramètres de réglage, en particulier pour le cas instable. Ensuite, on présente les résultats préliminaires du régulateur iP avec une trajectoire de référence constante, puis une trajectoire de référence variable pour la régulation de la glycémie. Le correcteur iP est testé en utilisant une trajectoire de référence variable pour contrecarrer le mauvais comportement postprandial avec la référence constante. Le iP avec référence variable produit une commande impulsive et une réaction rapide aux repas engendrant une hyperglycémie postprandiale réduite. Pour améliorer encore la réponse postprandiale, des termes de boucle fermée supplémentaires sont ajoutés et un PID intelligent (iPID) est conçu en utilisant une référence de glycémie constante. De plus, la boucle de CSM est fermée *via* un PID car on a observé que le PID classique émulait le comportement des cellules *beta* déficientes du pancréas chez un patient DT1 (voir l'étude de la littérature sur le PID au Chapitre 2). La comparaison des résultats *in silico* montre une meilleure régulation de la glycémie postprandiale avec le iPID et une référence

constante par rapport au iP en utilisant une référence variable. iPID est également comparé à un PID classique sur le simulateur Uva / Padova. Les résultats ont montré que la réponse postprandiale était améliorée avec l'iPID réduisant les excursions hyperglycémiques avec des événements hypoglycémiques minimes. En outre, iPID imite mieux le comportement postprandial des cellules *beta* du pancréas qu'un PID avec une réponse plus rapide.

4.2 Introduction

In this chapter, the theory and design of Model-free Control (MFC) are presented. It is presented here as an AP control algorithm for the first time. MFC is chosen as it offers the simple features of a PID control in the frame of a model free design. In opposition to previous PID studies, the control algorithm developed hereafter is fully automated without any feed-forward or supplementary insulin doses. Model-free proportional control or intelligent Proportional iP control results are first presented and analyzed with stable and unstable linear systems. The focus is on the stabilizability of iP controller via its design parameters especially for the unstable case. Thereafter, the preliminary results of constant and variable reference trajectory iP controller for glycemia regulation are presented. iP is tested employing a variable reference trajectory to circumvent the poor postprandial behavior of constant reference iP. Variable reference iP produced an impulsive control of fast reaction to meals that yielded a reduced postprandial hyperglycemia. To further enhance postprandial response, additional closed loop terms are added and an intelligent PID (iPID) is designed using a constant glycemia reference. Moreover, MFC loop is closed *via* PID as classic PID was observed to emulate the behavior of the missing pancreatic β-cell in T1DM (see the literature survey of PID in Chapter2). *In silico* results comparison showed a better postprandial glycemia regulation with constant reference iPID over iP employing a variable reference. iPID is also compared to a classic PID on the well known Uva/Padova T1DM simulator. iPID is compared to a standard PID controller in two cases: i) each controller parameters were tuned independently on a case study and then the design is applied on other subjects adapting one weighting parameter to avoid hypoglycemia and results are compared. ii) A reference PD+basal control previously designed to reduce BG risk index is compared to iPD+basal blocking the integral term to the basal rate of the patient. The superiority of the intelligent part of iPD over the classic is shown in this case by setting the same feedback gains. The results showed that the postprandial response was improved with iPID reducing hyperglycemic excursions with minimal hypoglycemic events. Moreover, the results showed that iPID, who has the classic PID structure with new adaptive feature, emulated insulin delivery of pancreatic β-cell.

4.3 Model-free control: Recalls

Model-free control consists in controlling a given unknown plant as a first order, second or eventually higher order [1] linear system, the so-called ultra-local model. The latter is estimated online.

4.3.1 Ultra-local Model

Model-free control is designed based on an ultra-local model of order ν [63], for a Single Input Single Output (SISO) system:

$$y^{(\nu)} = F + \alpha u \tag{4.1}$$

where:

- u, y are the input and output signals respectively. These are the only signals required to be known for the design.
- $\alpha \in \mathbb{R}$ is a non-physical design parameter, which is chosen so that αu and $y^{(\nu)}$ have the same magnitude.
- The order of differentiation ν may in general be chosen 1 or 2 and has no connection with the order of the system which is unknown [63].
- F stands for unknown system dynamics and perturbations. It is estimated and approximated by a piece-wise constant function during a quite short time lapse. It is estimated based on the knowledge of the input u and the estimate of the derivative of output measurement $y_e^{(\nu)}$ [76]:

$$F_e = y_e^{(\nu)} - \alpha u(t-h) \tag{4.2}$$

where $u(t-h)$ is a delayed version of the control, taken as a crude a crude approximation of $u(t)$ and h is a non-zero small delay (might be one sampling instant) to avoid any algebraic loop [77, 75]. The role of h will be further discussed in the sequel. The computation of F_e necessitates a good estimation of the νth-order derivative of the output signal $y_e^{(\nu)}$ that may be noisy.

Remark 2. *In (4.2), a numerical differentiator is required to estimate $y^{(\nu)}$. This is a major feature for the performance of Model Free Control. At this stage, a trade off exists between the value of ν and the accuracy of F_e: the higher the integer ν is, the richer is the controller in the*

[1] In the literature of MFC it was never taken higher than two [75, 63].

sense that is involves a large number of tuning parameters, and control actions. Unfortunately, in practice this is challenged by the increasing difficulty to achieve an accurate estimate of the higher order derivative $y^{(\nu)}$.

4.4 Intelligent Proportional iP

Let $y^*(t)$ denote a reference trajectory to be tracked, considering a first order ultra-local model $\nu = 1$, closing the loop with a proportional control yields the following intelligent proportional iP controller [63]:

$$u = \frac{-F_e + \dot{y^*} + K_p e}{\alpha} \tag{4.3}$$

where y^* is the reference input, $e = y^* - y$ and K_p is the proportional gain. Combining Equations (4.2) with $\nu = 1$ and (4.3) yields:

$$\dot{e} + K_P e = 0 \tag{4.4}$$

F does not appear anymore with the assumption that $F_e \approx F$. However, as a simple counter example, and as will be shown in section 4.5.2, the following linear second order system can not be stabilized using iP controller

$$\ddot{y}(t) - \dot{y}(t) = u(t) \tag{4.5}$$

Ideally the closed-loop system always leads to the error polynomial equation (4.4) and it is stable for any $K_P > 0$. However, in practice, even if the derivative in (4.2) was perfectly estimated it remains a small delay h in $u(t-h)$

$$F_e(t) = \dot{y}(t) - \alpha u(t-h) \tag{4.6}$$

thus the latter influences on the stability of closed-loop iP as will be discussed in the following section.

4.5 Effect of $u(t-h)$

The goal in this section is to show that some non obvious necessary conditions have to be completed for the doability of an iP controller. Those conditions are shown to be just independent form the quality of the estimation of $\dot{y}_e(t)$. So, assume at this stage that ideally

the derivative of the output is perfectly estimated, that is $\dot{y}_e(t) = \dot{y}(t)$. Substituting (4.2) in (4.3) with $\nu = 1$ yields

$$u(t) = u(t-h) + \frac{\dot{e}(t) + K_p e(t)}{\alpha} \tag{4.7}$$

The effect of the delay h on the stability of the closed-loop system will be investigated next. Stability is studied in the light of neutral delay system in a brief review.

4.5.1 Neutral Delay Systems

Whenever the delay h introduced in eq. (4.2) is not small enough, then the above approximation of the time derivative of the control input is no more valid. Still it is possible to analyze the closed-loop system, under the assumption that $\dot{y}(t)$ is perfectly estimated/known, to arrive at the same conclusion. So, in this section, it is shown that the iP control (4.7) yields a neutral closed-loop system. The byproduct is again that a necessary condition for the stability of the MFC closed-loop system is the stability of this neutral system. Consider the special case of a linear SISO system:

$$\dot{x}(t) = A_{n\times n}x(t) + B_{n\times 1}u(t) \tag{4.8}$$

$$y(t) = Cx(t) \tag{4.9}$$

A copy of the delayed dynamics (4.9) reads:

$$\dot{x}(t-h) = Ax(t-h) + Bu(t-h) \tag{4.10}$$

For simplicity assume $C_{1\times n} = [1\ 0 \ldots 0]$ and $B_{n\times 1} = [0\ 0 \ldots 1]^T$ and let $y^* = 0$. Subtracting (4.10) from (4.9) and substituting (4.7) yields:

$$\dot{x}(t) - \dot{x}(t-h) = A[x(t) - x(t-h)] - B[\frac{C\dot{x}(t) + K_p Cx(t)}{\alpha}] \tag{4.11}$$

the latter leads to:

$$[I_{n\times n} + \frac{1}{\alpha}BC]\dot{x}(t) - \dot{x}(t-h) = [A - \frac{K_p}{\alpha}BC]x(t) - Ax(t-h) \tag{4.12}$$

Denote $A_0 = [I_{n\times n} + \frac{1}{\alpha}BC]$, $A_1 = [A - \frac{K_p}{\alpha}BC]$ and the characteristic equation of (4.12) in Laplace domain:

$$q_o(s, e^{-hs}) = \det\Big(s[A_0 - I_{n\times n}e^{-hs}] - A_1 + Ae^{-hs}\Big), \qquad s \in \mathbb{C} \tag{4.13}$$

where det(.) denotes the determinant of a matrix. The stability of (4.13) is necessary for a stable closed-loop system under iP controller. Thus, iP controller is not a universal controller and its stability is not simply defined by (4.4) as presented in the literature of MFC.

A sufficient stability condition for (4.12) is that the system is asymptotically stable if its characteristic equation satisfies[78]:

$$\sup\{Re(s) : \det\Big(s[A_0 - I_{n\times n}e^{-hs}] - A_1 + Ae^{-hs}\Big) = 0\} < 0 \tag{4.14}$$

The stability of system (4.11) for any delay h can be studied using the literature of neutral-delay systems. If the latter polynomial is of the form $q_o(s,e^{hs}) = p(s) + q(s)e^{-hs}$ then the sufficient stability conditions of Theorem 2.1 of [79] can be applied as will be shown in the following example in 4.5.2.

The purpose, so far, was just to show the possibility of examining stability of iP controller via neutral delay systems. To go further, it is suggested to seek the necessary stability conditions of neutral systems (if any) for the iP controlled system (4.12) to give a hint on the choice h, K_p and α.

4.5.2 Academic example: iP control

In this section a counter example is presented to show that stability can not be always guaranteed with iP controller. Consider the following linear system:

$$\begin{cases} \dot{x}_1(t) = x_2(t) \\ \dot{x}_2(t) = -ax_2(t) + u(t) \\ y(t) = x_1(t) \end{cases} \tag{4.15}$$

In the unstable case $a < 0$. The stability of the closed-loop system under iP control with a zero reference $y^* = 0$ is investigated. The following computations are obtained from [80]. Suppose $\dot{y}_e = \dot{y}$. For this system $F = -\frac{\ddot{y}}{a}$ and $\alpha = \frac{1}{a}$. Combining (4.6) and (4.7) yields the following controller:

$$u(t) = -\frac{\dot{y}(t) + K_p y(t)}{\alpha(1-\delta_h)} \tag{4.16}$$

where δ_h is the delay operator of amplitude h: $f(t) - f(t-h) = (1-\delta_h)f(t)$. The closed-loop system is thus:

$$\ddot{y}(t) = -a\dot{y}(t) - \frac{\dot{y}(t) + K_p y(t)}{\alpha(1-\delta_h)} \tag{4.17}$$

Rearranging the above equation yields

$$\Big[\frac{\mathrm{d}}{\mathrm{d}t}(\frac{\mathrm{d}}{\mathrm{d}t}+a)(1-\delta_h)+a(\frac{\mathrm{d}}{\mathrm{d}t}+K_p)\Big]y(t)=0 \tag{4.18}$$

Taking Laplace transform to the above equation yields[2]

$$s(s+a)(1-e^{-hs})+a(s+K_p) \tag{4.19}$$

rearranging yields the following characteristic polynomial of the form:

$$s^2+2as+aK_p-e^{-hs}(s^2+as)=0 \tag{4.20}$$

the stability of the above polynomial is studied via its roots. Use Theorem 2.1 of [79] on the system whose transfer function $G(s)=\frac{r(s)}{p(s)+q(s)e^{-hs}}$. Note that deg $p(s)$ = deg $q(s)$ as required in [81]. The characteristic polynomial (4.20) is of the form $p(s)+q(s)e^{-hs}$ with

$$\frac{p(s)}{q(s)}=-\Big(1+a\frac{s+K_p}{(s^2+as)}\Big) \tag{4.21}$$

or

$$\frac{p(s)}{q(s)}=-1-\frac{1}{\alpha s}-a\frac{K_p-a}{s^2}+O(\frac{1}{s^3}) \tag{4.22}$$

According to [79], the roots s_n of $p(s)+q(s)e^{-hs}$ satisfy

$$s^n=\frac{\lambda_n}{h}-\frac{1}{\alpha\lambda_n}+\frac{h}{\alpha_n^2}\Big(\frac{a^2}{2}-a(K_p-a)\Big)+o(\frac{1}{n^2}) \tag{4.23}$$

for sufficiently large integer n. Equation (4.22) leads to $\lambda_n=2\pi n\mathrm{i}$. For stability, we have the following situations:

$$\text{if } a(K_p-\frac{3a}{2})>0, \quad \text{then (4.15) has infinite number of unstable poles} \tag{4.24}$$

$$\text{if } a(K_p-\frac{3a}{2})<0, \quad \text{then (4.15) has infinite number of stable poles} \tag{4.25}$$

Obviously, the following two conditions must be satisfied for the stability of (4.15) and (4.16):

1. Satisfying (4.25).
2. There is no further unstable root of (4.20).

[2] note that $\mathscr{L}\{f(t-h)\}=F(s)e^{-hs}$.

The second condition is verified numerically using Quasi-Polynomial Mapping Based Rootfinder [82] as suggested in [81]. For the special case $a = -1$ with K_p satisfying condition 1 above, the quasi characteristic polynomial (4.20) has always an unstable root for different values of h (e.g. $h = 0.001, 0.01$ and 1) according to the numerical application of qpmr function of [82]. Thus, even though condition 1 is satisfied, no stabilizing h is found to yield zero number of unstable roots of (4.20). It is good to notice that these analyses are valid under the assumption that $\dot{y}_e = \dot{y}$ which is never the case in practice. If the estimate includes approximations for $\dot{y}_e$ and $u(t)$ (other than $u(t-h)$), and if these have regulatory effect, then a stabilizing controller may well be obtained.

In the following section the estimator of F in (4.1) with $\nu = 1$ for iP controller will be derived according to [63].

4.6 Estimation of F

Equation (4.1) for an iP controller becomes:

$$\dot{y} = F + \alpha u \tag{4.26}$$

F may be assumed to be approximated by a piecewise constant function F_e. Rewrite then Equation (4.26) in the operational domain [63]:

$$sY(s) = \frac{F_e}{s} + \alpha U(s) + y(0) \tag{4.27}$$

where F_e is a constant. Differentiate both sides w.r.t. s to eliminate the initial condition $y(0)$:

$$Y(s) + \frac{\mathrm{d}Y(s)}{\mathrm{d}s}s = -\frac{F_e}{s^2} + \alpha\frac{\mathrm{d}U(s)}{\mathrm{d}s} \tag{4.28}$$

To filter the output multiply both sides by s^{-2}

$$\frac{Y(s)}{s^2} + \frac{\mathrm{d}Y(s)}{\mathrm{d}s}\cdot\frac{1}{s} = -\frac{F_e}{s^4} + \frac{\alpha}{s^2}\cdot\frac{\mathrm{d}U(s)}{\mathrm{d}s} \tag{4.29}$$

Take the inverse of Laplace transform of (4.29) and using the following properties:

$$\mathscr{L}^{-1}\{G_1(s)G_2(s)\} = \int_0^t g_1(t-\tau)g_2(\tau)\mathrm{d}\tau \tag{4.30}$$

$$\mathscr{L}^{-1}\{\frac{d^iG(s)}{ds^i}\} = (-t)^i g(t) \tag{4.31}$$

then we have the estimation F_e in the time interval $t \in [0,\ T]$

$$F_e(0) = -\frac{6}{T^3}\int_0^T \Big((T-2\tau)y(\tau) + \alpha\tau(T-\tau)u(\tau)\Big)\mathrm{d}\tau \tag{4.32}$$

where T is a small estimation time window which depends on sampling period and the noise intensity [63].

To obtain $F_e(t)$ at any time instant t, shift the functions $y(\tau)$ and $u(\tau)$ into $y(t+\tau)$ and $u(t+\tau)$ (if $y(T)$ by $y(t+T)$) respectively keeping the interval width $\tau \in [0,T]$, i.e. sliding the time window for the functions y, u and F_e without changing the variables.

$$F_e(t) = -\frac{6}{T^3}\int_0^T \Big((T-2\tau)y(t+\tau) + \alpha\tau(T-\tau)u(t+\tau)\Big)\mathrm{d}\tau \tag{4.33}$$

The above equation allows to estimate the $F_e(t)$ in the interval $[t,\ t+T]$ as $\tau \in [0,\ T]$.

To make the estimation causal in time, invert the time intervals i.e. T to $-T$ and τ to $-\tau$. First change T to $-T$ in (4.33):

$$F_e(t) = \frac{6}{T^3}\int_0^{-T} \Big((-T-2\tau)y(t+\tau) + \alpha\tau(-T-\tau)u(t+\tau)\Big)\mathrm{d}\tau \tag{4.34}$$

or

$$F_e(t) = \frac{6}{T^3}\int_{-T}^0 \Big((T+2\tau)y(t+\tau) + \alpha\tau(T+\tau)u(t+\tau)\Big)\mathrm{d}\tau \tag{4.35}$$

Then change the variable τ to τ', $\tau' = -\tau$, $\mathrm{d}\tau = -\mathrm{d}\tau'$, $\tau \in [-T,0]$ implies $\tau' \in [T,0]$:

$$F_e(t) = -\frac{6}{T^3}\int_T^0 \Big((T-2\tau')y(t-\tau') - \alpha\tau'(T-\tau')u(t-\tau')\Big)\mathrm{d}\tau' \tag{4.36}$$

Now to simplify the writing of the above equation change the integral limits into $(t-T,\ t)$ using the following change of variables $\sigma = t-\tau'$, $\mathrm{d}\tau' = -\mathrm{d}\sigma$ and $\tau' \in [T,0]$ leads to $\sigma \in [t-T,t]$:

$$F_e(t) = \frac{6}{T^3}\int_{t-T}^t \Big((T-2t+2\sigma)y(\sigma) - \alpha(t-\sigma)(T-t+\sigma)u(\sigma)\Big)\mathrm{d}\sigma \tag{4.37}$$

For numerical implementation, the following F_e is preferred:

$$F_e(t) = -\frac{6}{T^3}\int_0^T \Big((T-2\sigma')y(\sigma'+t-T) + \alpha\sigma'(T-\sigma')u(\sigma'+t-T)\Big)\mathrm{d}\sigma' \tag{4.38}$$

where $\sigma' = T-\tau'$

Remark 3. *The estimator equation as appeared in section 3.4.1 of [63] (first estimator formula) seems to be valid only when the integral limits are* $[0,\ T]$ *and thus it estimates only in the first time window* $F_e(0)$*. To support this claim, suppose that* $u(t) = 0$ *in* (4.26) *thus* $F_e(t) = \dot{y}(t)$ *(see Appendix A.1 for demonstration) i.e. the first term of* F_e *in* (4.37) *represents an estimation of the first derivative of* $y(t)$ *(as stated in the first MFC publications as in [83]). An illustrative example to compute* $F_e = \dot{y}(t)$ *for some function* $y(t)$ *in Appendix A.1 is presented to compare* (4.37) *(*$u(t) = 0$*) to the estimator equation in section 3.4.1 of [63] with* $u(t) = 0$*.*

Remark 4. *The second term of* F_e *in* (4.37) *buffers the input signal* $u(t)$ *and adds a delay of* $h = \frac{T}{2}$ *to the buffered signal* $u(t-h)$ *as demonstrated by some illustrative examples in A.2.*

Remark 5. *There are two forms of the estimators of* F_e*: the standard* (4.6) *and the one in* (4.37)*. The latter assumes* F_e *is constant whereas this is not the case in the standard form. The methods are numerically quite different which led to quite different results. Thus, the following question arises: what is the best form of estimation of* F_e*? Another question is that does the choice of the estimation window* T *has an infleunce on the stability of the closed-loop system?*

For some applications more control actions may be needed in the control law for stability, like the case in Section 4.5.2 when $a = -1$, or for faster convergence of the error signal. This motivates to close the loop via a PID to yield an *intelligent PID*, or *iPID*.

4.7 iPID

iPID is designed by setting $\nu = 2$ in (4.1). The local model becomes:

$$\ddot{y} = F + \alpha u \tag{4.39}$$

The iPID control law is:

$$u = \frac{-F_e + \ddot{y}^* + K_p(e + K_i \int e\mathrm{d}t + K_d \dot{e})}{\alpha} \tag{4.40}$$

where y^* is the reference input, $e = y^* - y$ and the usual feedback gains are K_p, K_i, K_d. The estimation equation (4.2) of F becomes:

$$F_e = \ddot{y}_e - \alpha u(t-h) \tag{4.41}$$

As stated earlier $u(t-h)$ is a delayed version of u(t). Assuming a perfect estimation in (4.41), applying the control law in (4.40) into (4.39), F will be canceled out and the following error dynamics is obtained:

$$\ddot{e} + +K_p(K_d\dot{e} + e + K_i \int e\mathrm{d}t) = 0 \tag{4.42}$$

The system in Section 4.5.2 can now be stabilized for both $a = \pm 1$ using iPID as more control parameters: K_d, K_i are available.
Concerning glycemia regulation, two MFC designs will be presented next:

- iP control: even though the system (3.17) is stable (critically), employing a constant reference, iP performance is poor. Thus, a variable reference iP is presented as a solution to enhance the closed-loop performance.
- iPID: constant reference is employed with iPID which is compared to iP and standard PID controllers.

The statistical parameters showed that iPID outperforms its classic PID counterpart and its performance also dominates iP controller.

4.8 Variable reference iP for Glycemia regulation

The control design of an artificial pancreas, is tackled via the newly introduced model-free control and its corresponding iP. The purpose is to show the efficiency of this non-model based controller, which has already been successfully applied in many concrete and diverse situations (see [63] and the references therein), as an artificial pancreas control algorithm. It results in an insulin injection for T1DM which displays via constant references an acceptable nocturnal/fasting response, but unfortunately a poor postprandial behavior due to long hyperglycemia. When a variable reference is introduced, that switches between a constant one, when glycemia is more or less normal or moderate, and an exponential decay reference path, when a high glycemia rate indicates a meal intake, the *in silico* postprandial response is enhanced.

In the following section the main constraints and limitations of the system to be controlled are presented which hold for any control algorithm.

4.9 Constraints and limitations

As detailed in Section 3.8.5, during fasting/nocturnal conditions if a very low constant insulin rate ($u < u_{eq}$) is injected to a T1DM then glycemia diverges. Whereas, the case $u > u_{eq}$ leads

to hypoglycemia. The objective is to inject the adequate amount of insulin to compensate for meal disturbance without late hypoglycemia. Therefore, the challenge is to maintain the trade-off between hyper and hypoglycemia in both postprandial and fasting phases.

Thus, for an insulin-dependent diabetic, the control objective is to steer G from hyperglycemia into the normal interval $[70, 120]$ mg/dL relatively fast. Two main constraints are emphasized:

- hypoglycemic limit of 70 mg/dL,
- the input is nonnegative ($u \geq 0$).

The latter point means that insulin infusion rate cannot be reversed once it is spread out in the blood stream. If BG drops into hypoglycemia, the only possible control is to shut off the insulin pump temporarily and to have some carbohydrates to raise BG back to normal level.

4.10 iP Control implementation

4.10.1 Constant Reference

The iP control law as presented in (4.3) is applied where F_e is estimated according to (4.38). The parameters are specified as follows:

- $T = nT_s$, where T_s is the sampling time, and $n \geq 1$ is an integer,
- $T_s = 1$ min, $n = 3$, $T = 3$ min,
- since BG responds inversely to the control variable, α is negative and adjusted per patient.
- $K_P = 0.01$.
- The constant set point is $G_r = 120$ mg/dL.

iP design in [84] is modified and corrected here where T is reduced to be as small as $T = 3$ min. (as recommended in the MFC literature) and α is the only parameter adjusted per patient (instead of K_p) for an optimal performance. This constant reference iP is tested *in silico* on five virtual patients of the T1DM simulator presented in (3.17). It has a poor postprandial performance with persisting hyperglycemia as shown in Fig. 4.1. To enhance its performance during postprandial phase and to circumvent the lack of a standard insulin bolus a more aggressive action is required. For this purpose, a meal detection scheme is introduced to obtain faster controlled infusion rate via a variable reference iP control designed in the next subsection.

4.10.2 Variable Reference iP

The iP designed in the previous section is applied here with the same design parameters. The remaining step in this design is to define the variable reference input to the controller. The time-varying reference trajectory which was introduced in [85] for the purpose of PID switching control, is modified in order to be utilized here:

$$G_{\text{ref}}(t) = \begin{cases} (G(t^s) - G_r)\exp^{-\frac{t-t^s}{\tau_{\text{ref}}}} + G_r & \text{if } G(t) \geq G^s \\ \\ G_r & \text{if } G(t) < G^s \end{cases} \tag{4.43}$$

- t^s is the switching time,
- $\tau_{\text{ref}} = 3$min. is a design parameter,
- $G_r = 120$ is the previous constant set point, G^s is the switching threshold.

The following properties hold:

1. The time-varying trajectory starts decaying directly at $G(t^s)$.
2. The switching threshold G^s is set to 140 mg/dL while $G_r = 120$ mg/dL to avoid hypoglycemia.
3. t^s is the switching/reset time: to re-start the trajectory if $(t - t^s) > 45$ min and $\dot{G} > 0$ (if BG is still increasing). In other words, a meal is detected if the rate of BG change is non negative and BG is growing above 140 mg/dL.

When G is above the postprandial hyperglycemia level ($G \geq 140$mg/dL)[3], the controller switches from a constant reference $G_r = 120$ mg/dL to an exponential-decay trajectory initiated at $G_{\text{ref}}(t) = G(t_s)$. It settles eventually at G_r. The resulting discontinuity produces an impulsive control due to $\dot{e}$ that appears in the iP control law. This bolus-shaped insulin rate permits to have a fast response in order to regulate G towards the normal level and to avoid extended postprandial hyperglycemia.

iP test results on patients IF9 and LR which were not included in [84] are included here as well. Once they are designed, the parameters T, τ_{ref}, K_p are kept constant. The closed-loop design, with constant or variable reference, will be compared to the open-loop therapy with the same meal protocol. The control will first be designed and tested on IF2 subject, variable reference iP will be denoted as iPvref in the sequel.

[3] 140 mg/dL is defined as the *2 hours postprandial hyperglycemia*, [86].

4.11 Simulation results

4.11.1 Simulator 1: clinical data

Five patient profiles are considered, based on Magdelaine T1DM model in Section 3.7. The model has been identified on the clinical data of five patients by data fitting (see for more details [58]). In what follows, the same meal scenario logged in the clinical diary of those subjects is used. Each clinical diary includes:

- A time window during which the diary is registered.
- Meal intake: amount of carbohydrates taken by the patient at time t,
- Open-loop insulin dosing at time t: basal and meal boluses,
- CGM data.

Among the five considered patients, one is an outpatient and four are hospitalized. They are tagged as IF2, IF3 IF9, BE and LR. Two of the hospitalized patients start with a one-day fasting.

The *in silico* trial is based on the following facts:

- Open and closed-loop simulations have the same time window.
- The meal protocol is fixed from each patient's clinical diary .
- Open-loop insulin administration, closed-loop MFC algorithms are tested and compared.

4.11.2 *In silico* Test

A mathematical model of the system is not required in the model-free design process, it is used to test the design *in silico*. F_e in (4.38) is employed in the iP control law. The T1DM simulator given in (3.17) is employed to test iP and iPvref performances for T1DM glycemia regulation. Figure 4.1 displays the difference between iP and iPvref strategies in the postprandial phase. IF2 has a one-day fasting phase during which both iP controllers have a much better performance than the open-loop control with a fasting hyperglycemia time lapse greater than 11 hours (see Fig. 4.1-a). The maximum postprandial glycemia peak with iP is reduced by 46 mg/dL applying iPvref according to Table 4-1. This design is tested on the two other virtual patients IF3, BE, IF9 and LR as shown in Figures 4.2, 4.3,

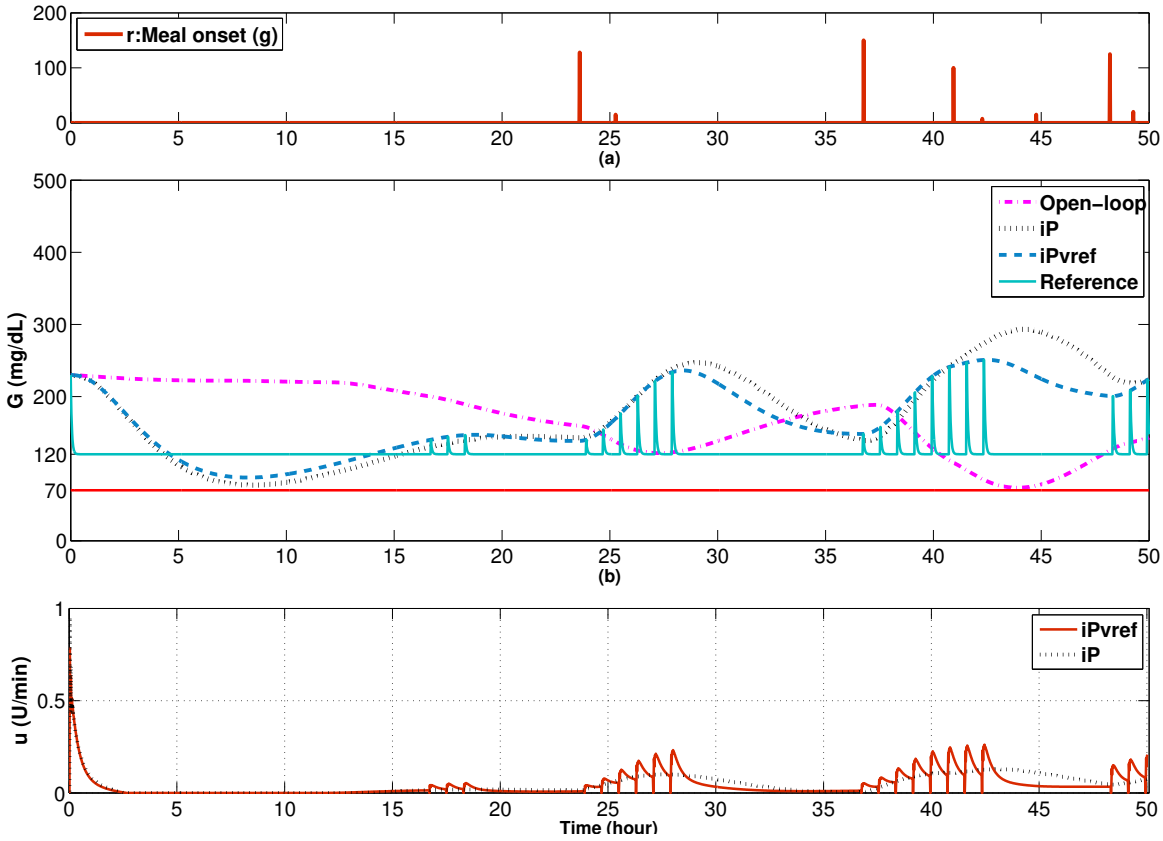

Figure 4.1 IF2 response for open-loop, iP with $\alpha = -139$ and iPvref $\alpha^{-1} = -198$. (a): Meal intake. (b): BG behavior. (c): iP and iPvref insulin infusion rates.

4.4 and 4.5. The simulator is considered as a black box where the model parameters and meals are all unknown and only α is adapted per patient to obtain minimum hypoglycemic episodes during the simulated period. $-\alpha = 174, 101, 483$ and 675 for IF3, BE, IF9 and LR respectively for variable-reference control while $-\alpha = 129, 101, 340$ and 540 for IF3, BE, IF9 and LR respectively using iP control. Some statistical parameters are calculated for each patient under open and closed-loop control and illustrated in Table 4-1. The frequent initialization of the exponential decay reference path appeared as a series of consecutive impulsive insulin rates (e.g. see Fig. 4.3-c). These bolus-shaped rapid pulses are infused only when a postprandial phase is detected i.e. BG $\geq$ 140 mg/dL in a positive rate of change. These pulses enhanced the iPvref over the poor iP performance. They added the needed postprandial impact that reduced glycemic excursions in time and amplitude as illustrated in Table 4-1. In Appendix A.3 results of iP and iPvref under some output noise are illustrated.

The postprandial peaks under closed-loop insulin administration are higher than that of open-loop control. This is actually due to the fact that the manual boluses are injected before meals (see open-loop injections [58] for more details). For the fully automatic control, meals

Table 4-1: Time performance indicators for open and closed-loop iP controllers.

Patient	%Time in target [70-180] - [70-140]			%Time in hypo. [<70]			%Time in hyper. [180-250]|[>250]			Mean ± std			Min:Max(BG)		
	Open-loop	iP	iP_{vref}	Open-loop	iP	iP_{vref}	Open-loop	iP	iP_{vref}	Open-loop	iP	iP_{vref}	Open-loop	iP	iP_{vref}
IF2	55|30	56|29	59|30	0	0	0	45|0	31|13	40|2	169±47	176±63	168±49	74|230	80|297	88|251
IF3	78|77	68|17	80|36	22	5	0	0|0	17|10	13|8	91±23	168±55	155±50	46|142	56|317	72 | 298
BE	82|48	73|44	70|83	0	0	0	14|4	21|6	17|0	155±39	153±52	128±44	84|260	73|269	73 | 230
IF9	70|65	69|26	72|27	37	0	0	8|6	4|19	4|18	108±62	180±108	174±104	49|320	85|499	80 | 495
LR	57|32	35|17	50|22	2	3	6	33|8	33|30	21|23	171±54	209±82	185± 80	63|300	60|408	59 | 409

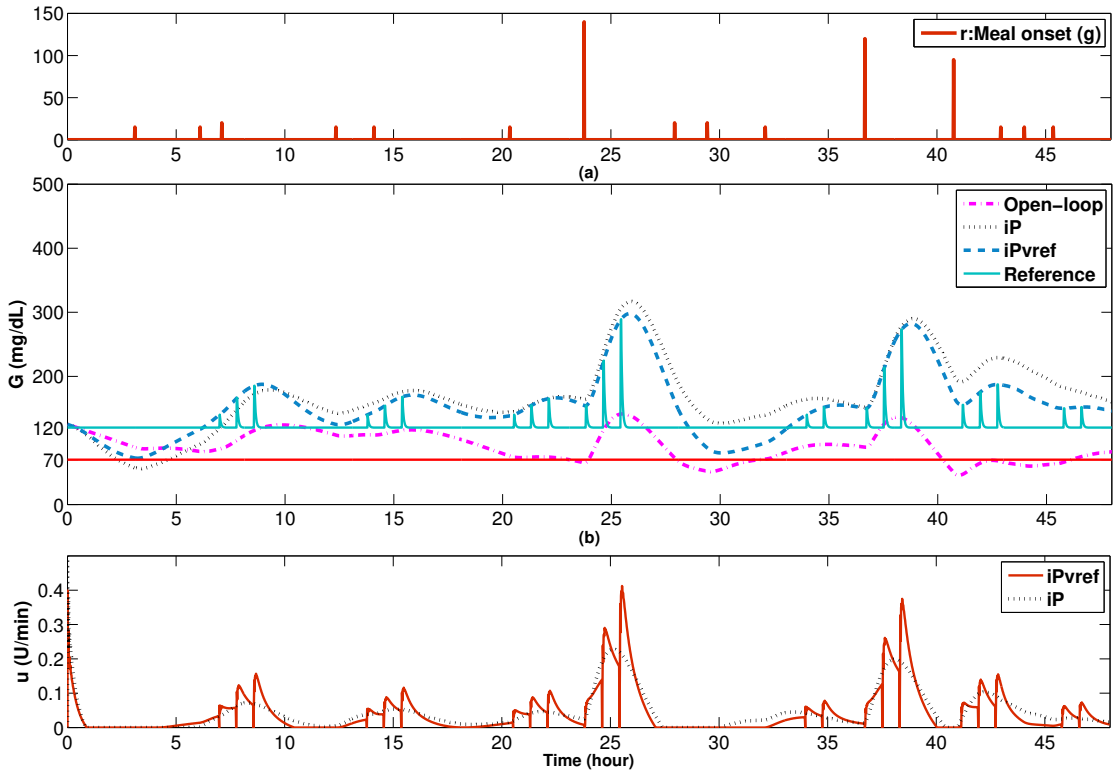

Figure 4.2 IF3 response for open-loop, iP with $\alpha = -129$ and iPvref $\alpha^{-1} = -174$. (a): Meal intake. (b): BG behavior. (c): iP and iPvref insulin infusion rates.

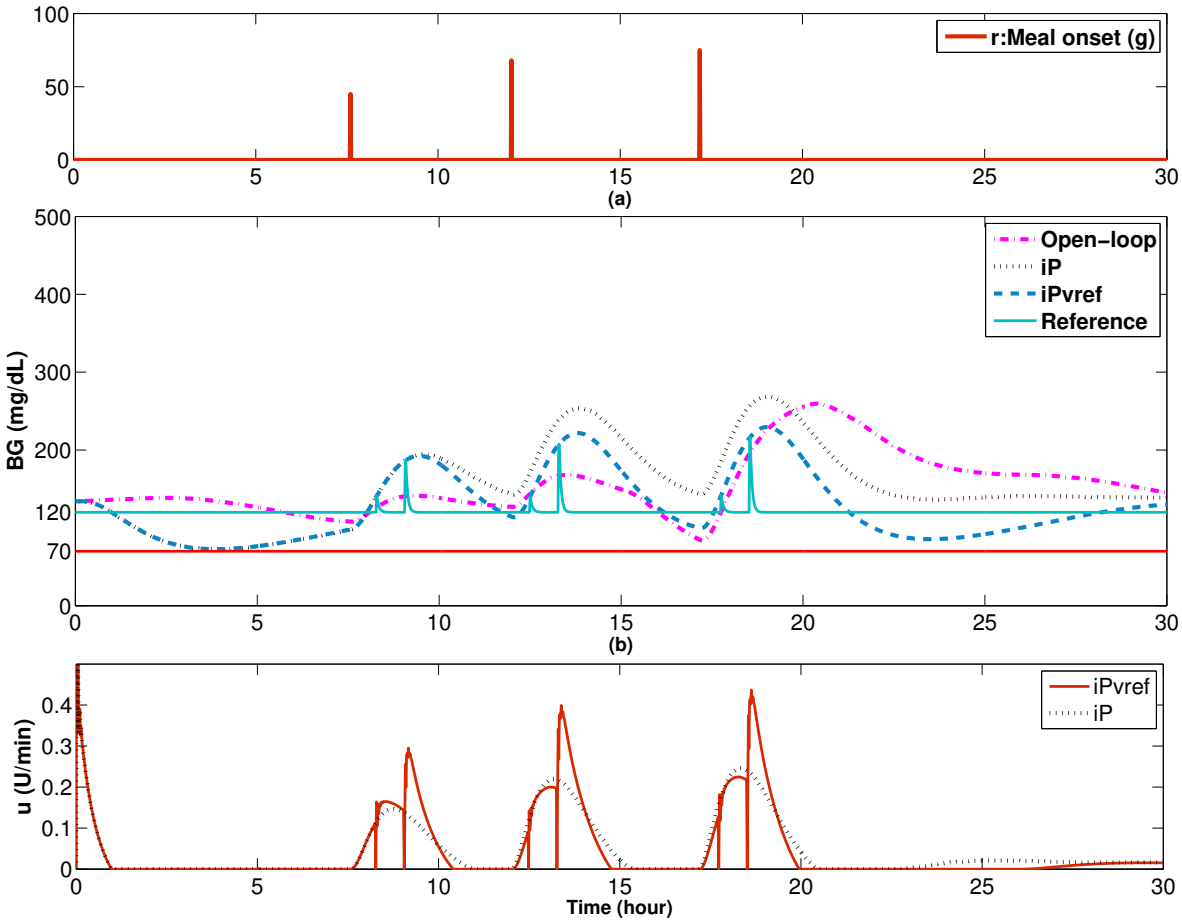

Figure 4.3 BE response for open-loop, iP and iPvref (a): Meal intake. (b): BG behavior. (c): iP and iPvref insulin infusion rates.

are unknown disturbances. In addition, the insulin absorption rate is slow (see Table 1 in [58] for insulin dynamics parameters). According to the ADA, the minimum insulin onset[4] is 15 minutes. It takes about 60 minutes to reach its peak with a minimum overall duration of 2-4 hours.

Results showed that certain cases, like IF9 and LR, have severe hyperglycemia with a rapid BG drop rate which is a result of its high insulin sensitivity (see Table 1 in [58]). These cases have a noticeable high glycemic variability that necessitated a further investigation and whether the type of control therapy can affect their diabetic stability. To have a better understanding of this issue, an important diabetic statistical parameter is calculated in Appendix A.5.

[4]It is the time lapse before insulin reaches the bloodstream and begins lowering blood glucose.

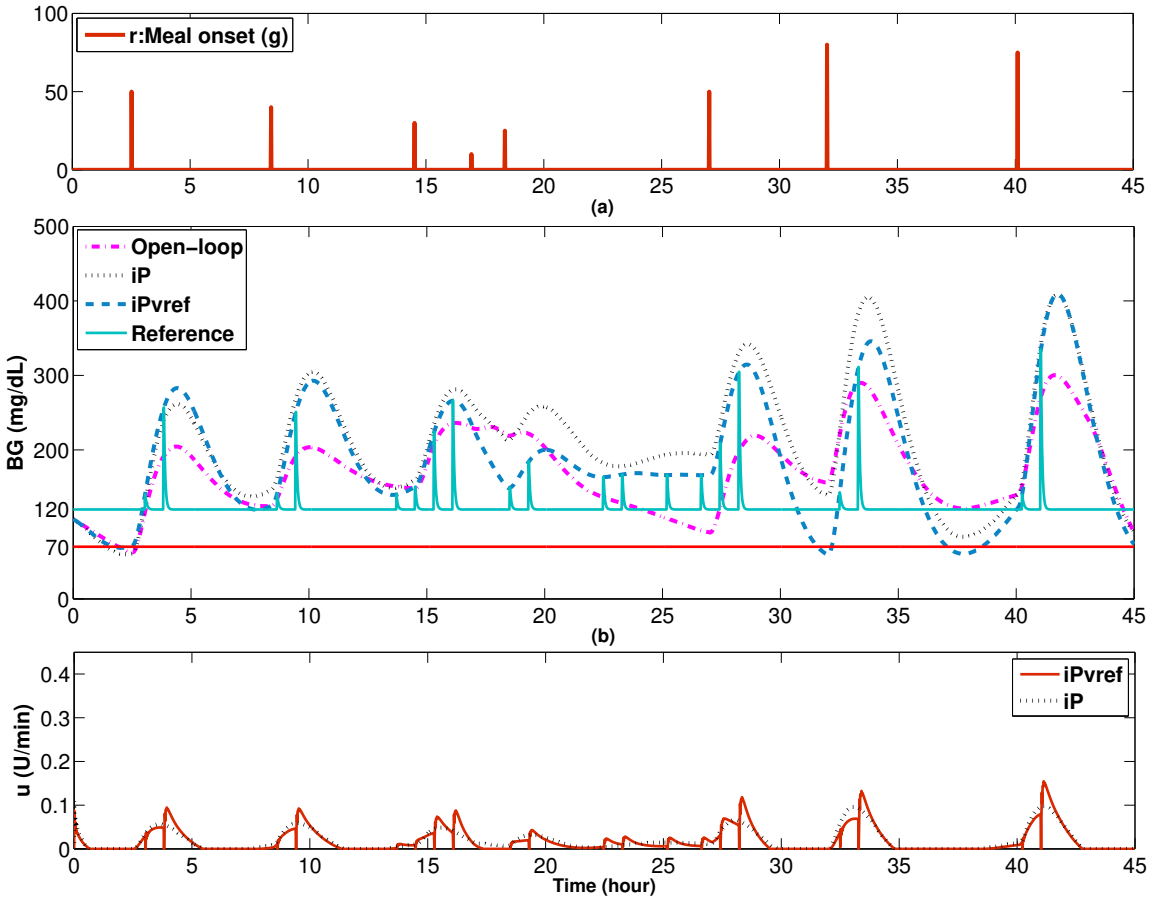

Figure 4.4 LR response for open-loop, iP and iPvref (a): Meal intake. (b): BG behavior. (c): iP and iPvref insulin infusion rates.

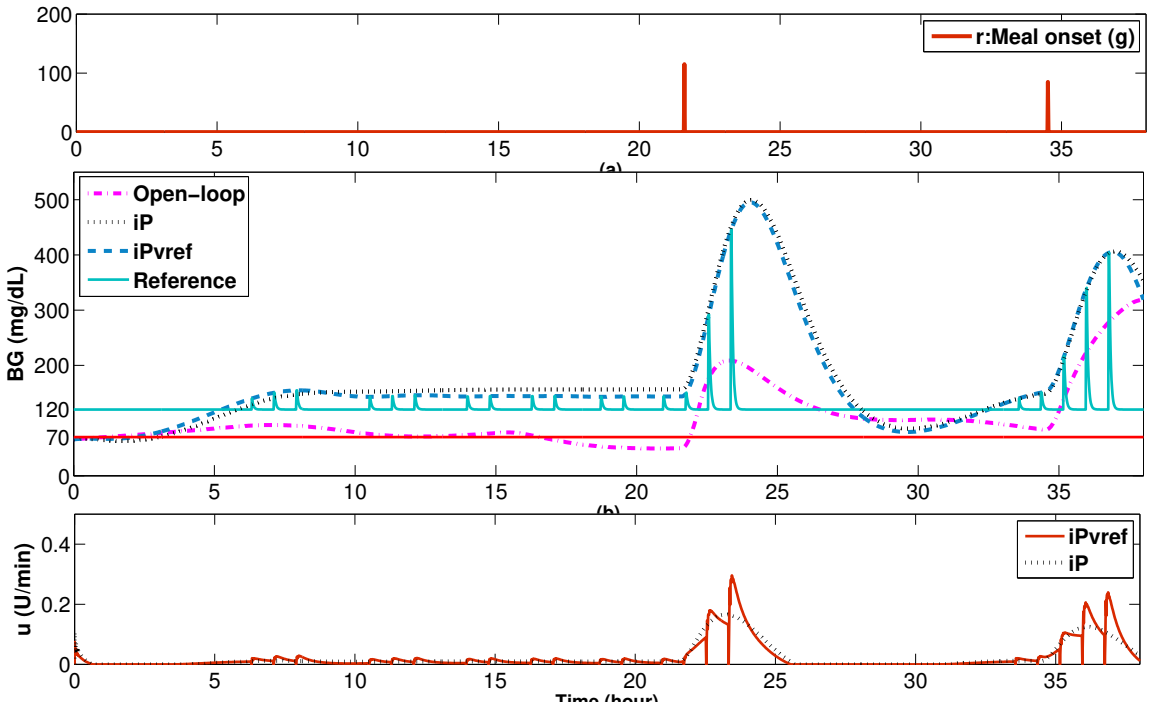

Figure 4.5 IF9 response for open-loop, iP and iPvref (a): Meal intake. (b): BG behavior. (c): iP and iPvref insulin infusion rates.

As an overall overview, iP performance was enhanced when a variable reference was used to create the auto-bolus that reduced postprandial hypoglycemia. However, it was noticed that for both iP and iPvref, to reduce or eliminate the static error during fasting phase for instance, it is required to increase the overall gain (reduce α), a value that might be too high in postprandial phase that leads to higher hypoglycemia risk. Therefore, even though iP performance was enhanced to some extent, via creating auto-boluses when a meal is detected, still, the steady-state error elimination, especially during fasting phase (if same gain is used), is not ensured (see Fig. 4.5). This is mainly related to the system constraints (as seen in Section 4.9) i.e. the input is positive and iP can only be saturated to zero whenever BG<120. One solution is to use multiple gain iP i.e. a fasting α value and another value for postprandial phase for each patient. Another alternative is to incorporate derivative and integral terms i.e. to employ an iPID control instead as will be shown in the next section. iPvref numerical results are compared to classic PID and also to iPID and the comparison are illustrated in Tables 4-3 and 4-4.

4.12 iPID Control

In this section the feasibility of iPID for glycemia regulation is tested *in silico*. This section and the following sections results are extracted from and based on the publication [87]. Firstly, iPID is compared to iPvref performance. Secondly, iPID is compared to a standard PID on two T1DM simulators with and without measurement noise. The first simulator is the long-term linear time-invariant model (3.17). The controller is also validated on the UVa/Padova metabolic simulator on 10 adults under 25 runs/subject for noise robustness test.

iPID previously designed and tested for fasting conditions [88] is corrected and tested in [87] including postprandial phase on a larger cohort of T1DM patients from the Uva/Padova simulator. The parameter α is tuned here such that $\ddot{y}$ and αu_f have the same order of magnitude as suggested in [63], for a better estimation of F. This is an advantageous robustness property of the intelligent controller as α can be used to individualize the controller for each subject. Moreover, the tuning of α is based on the output and previously applied input that are already available for the controller. As BG responds inversely to the control variable, α is negative. The PID parameters of (4.40) are $K_p = 3 \times 10^{-5}, K_i = 0.001$ and $K_d = 250$ tuned and tested on patient tagged as IF2.

Remark 6. *In silico tests of iPID are obtained with and without CGM measurement noise. To test the feasibility of the iPID control, it is tested on Simulator 1 in a noise-free environment in order to have a perfect estimation of F_e and thus to test the performance of an ideal iPID. Using Simulator 2 or the Uva/Padova simulator, the robustness of iPID against CGM noise was tested.*

A Luenberger observer is used to estimate $\dot{y}(t)$ (see Appendix A.4 for the design). The input to the observer is the pure blood glucose output of the model in Simulator 1. For simulator 2, the noisy sensor signal of the simulator is differentiated to obtain $\dot{y}(t)$ using the algebraic derivative estimator in Appendix A.1 that has a filtering properties (see [83] and the references therein).

To estimate $\ddot{y}(t)$ for both simulators, a two-stage differentiation is done: a Dormand-Prince ode45 numerical differentiator method is utilized followed by Luenberger first order derivative estimator for Simulator 1 and the algebraic differentiator for Simulator 2 respectively.

F_e is estimated according to (4.41), with $\ddot{y}_e(t)$ is estimated as explained previously. The delay buffer in (A.22) of Appendix A.2 is useful to obtain a delayed signal like $u(t-h)$, thus eq. (4.41) becomes:

$$F_e(t) = \ddot{y}_e(t) - \frac{6}{T^3}\int_{t-T}^{t} \alpha(t-\sigma)(T-t+\sigma)u(\sigma)\mathrm{d}\sigma \tag{4.44}$$

For simulator 1, the controller is sent every 5 minutes and the integration time window is $T = 20$ min. (recall that $h = T/2$). For the Uva/Padova simulator, the built-in sampling time is one minute and $T = 5$ min.

4.13 Standard PID

A standard PID controller is designed and compared to the iPID performance [87]. The classic PID parameters are tuned on IF2 subject to yield a tight BG control, with a performance comparable to that of iPID, with maximum time percentage in euoglycemia and minimum hypoglycemic episodes. For this purpose, the two-day meal scenario is used as logged in the clinical diary. The controller parameters are $K_{pc} = 0.0005, K_{dc} = 250$ and $K_{ic} = 0.001$.

For comparison, this standard PID will be also scaled by a constant parameter p when applied on different patients. It will be tuned per individual to minimize hypoglycemic events during the simulation period. Individualizing only one control parameter per subject is employed previously by [46] in an *in silico* trial for both PID and MPC, K_{pc} for the former and the output prediction weighting parameter for MPC.

Remark 7. *The integral term is limited to limit the integral windup due to control saturation resulting from the inherent large and slow error dynamics especially during postprandial phase. As time grows, the integral action excessively builds up to cope with postprandial hyperglycemia yielding severe BG oscillations. For this system there is no negative action to compensate for negative error excursions. Insulin injection is a positive input, i.e. insulin can not be removed in case of over dosing, thus the input is saturated to zero. The result is input saturation, on one hand, and oscillatory behavior and hypoglycemia in the output channel on the other hand. For this reason, PID users usually incorporate some anti-windup protection for the integrator, or even replace the integral by the patient optimal basal rate in PD+Basal control [41]. The authors compared PID and PD+Basal on Uva/Padova simulator. They concluded that the latter outperformed in reducing postprandial hyperglycemia, but and conversely to PID, it failed to respond appropriately to changes in insulin sensitivity.*

In this work and as will be shown in the next section, iPID is tested in two cases:
i) an anti wind-up scheme is employed for the integral action, for both PID and iPID, to avoid the long-term accumulation. It discharges when hyperglycemia is attained (BG $\geq$ 180 mg/dL).
ii) The integral action is turned off and replaced by the subject's specific basal rate, i.e. iPD+basal.

4.14 Methods

iPID controller is tested *in silico* on two different simulators. The first is the long-term model identified on clinical data of five T1DM subjects (see § 3.7). The same meal scenario logged in the clinical diary of those subjects is used. The second trial is performed on the well known Uva/Padova metabolic simulator that is approved by FDA (see §3.6). The second trial is performed on ten adults using a meal scenario of other published results of PID and MPC controllers. For both tests, all simulator parameters are unknown to the controller and meals are unannounced disturbances.

4.14.1 Simulator 1

The *in silico* tests will be performed on simulator 1 on five T1DM subjects using the clinical diary as explained in Section 4.11.1. The open-loop basal-bolus injections of each diary will be compared here to the closed-loop algorithms PID and iPID. The details of the simulation results are presented in Section 4.15.

4.14.2 Simulator 2: UVa/Padova T1DM simulator

The PID designed in [89] that was compared to MPC performance, will be re-simulated here under the same meal scenario and compared to iPID performance. The PID was actually a (PD+basal rate) where the integral term is replaced by the subject's specific basal rate. The authors optimized PD weights to minimize average BG risk. This design is employed here for the iPID i.e. turning the integral term off and replace it by the subject's specific basal. The purpose is to study the effect of the intelligent part of the iPID over a classic PID. The PID as appeared in [89], sampled every 5 minutes is described as follows changing only the set point to 120 mg/dL :

$$u_n = 6.375 \times 10^{-5} P_n + basal + 0.0046 D_n, \tag{4.45}$$

$$P_n = y_n - 120 \tag{4.46}$$

$$D_n = y_n - y_{n-1} \tag{4.47}$$

Where P_n, D_n are the proportional and derivative gains respectively. y_n is BG at instant n. The Uva/Padova built in basal rate will be used for each subject in the current study. The desired set point for both controllers is set to 120 instead of the previously chosen 140 mg/dL in [89]. The meal scenario is a 36 hours of six unannounced 20 min. duration meals. The meal amount and timing are given in Table 4-2.

Table 4-2: Meal Scenario for Simulator 2.

Time	09:00h	13:00h	17:30h	20:00h	09:00h	13:00h
Meal	50g	70g	90g	25g	50g	70g

iPID will be tested in three different tests each start with a closed-loop fasting day:

1. IV sensor test (noise-free measurement): iPID performance will be compared to standard PID designed in (4.45) applying the same meal scenario on five adults. The subject's specific basal rate is injected in both cases i.e. the integral term of iPID is turned off. The same proportional and derivative gains in (4.45) are used for both controllers. The remaining MFC structure in Section 4.12 is kept unchanged (like derivative estimators and sampling time). The comparison is thus between iPD+basal versus PD+basal. The objective is to perform a noise-free measurement test equivalent to what is done in Simulator 1 and show the prandial adaptive feature of iPD+basal over PD+basal controller.

2. CGM (noisy measurements):
   I) iPD+basal versus PD+basal test: this comparison is performed now employing CGM sensor on ten adults and the test is repeated 25 times for each subject to check robustness against measurement noise.
   II) iPID in a heavy meal test: it is performed on three subjects (5 runs for each) to show the iPID performance in such challenge. The previous iPID designed for Simulator 1 is tested in this case adding the integral term back initialized at the basal level and with $\alpha = -7, T = 15$min. A scenario of meals=[20 120 90 100]g at time=[18:00h 20:00h 09:00h 13:00h].

The authors of [89] found that one of the patients (adult 9) was an outlier and not representative of a normal T1D. They studied his behavior and it was shown that even with an optimal bolus correction this patient suffers from hypoglycemia due to the powerful and slow suppression of endogenous glucose production. Thus, this patient was excluded from the averaged results of [89] and also in [90]. In this study all 10 virtual adults are considered including adult 9. Details on the simulation results are presented in 4.15.3.

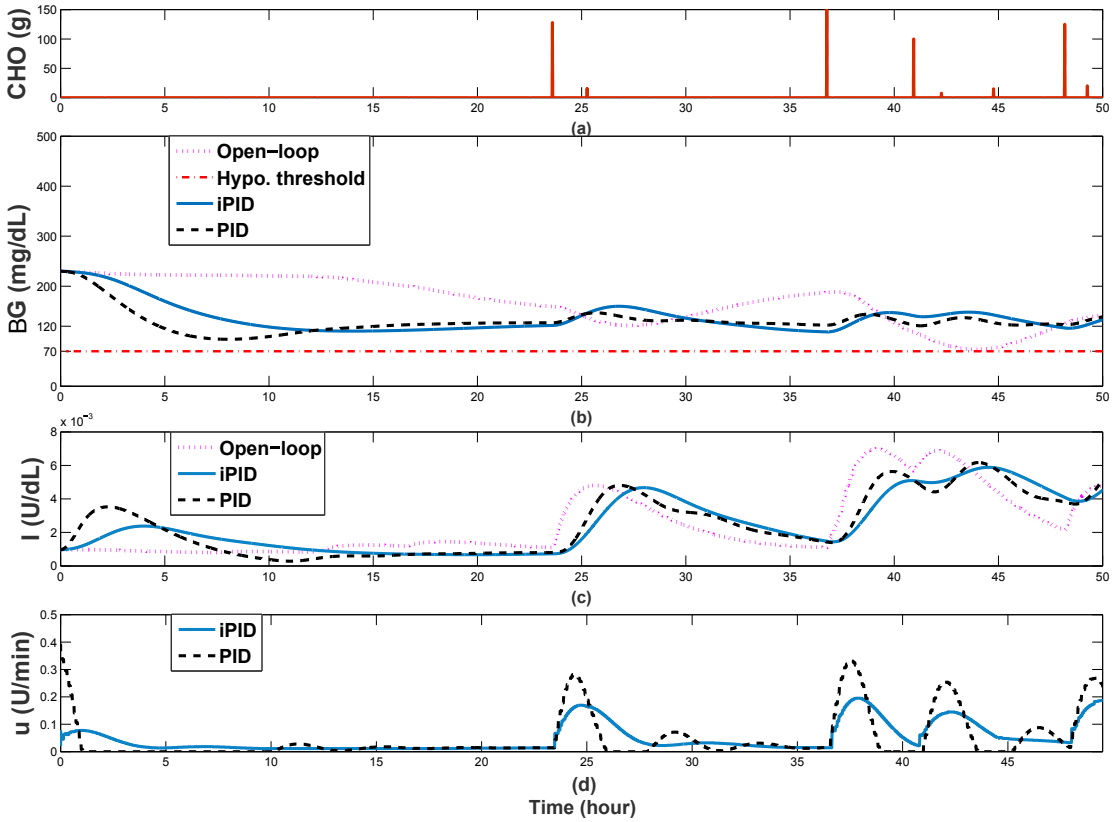

Figure 4.6 IF2 response for open-loop, PID and iPID ($p = -0.14, \alpha = -0.16$) (a): Meal intake. (b): BG behavior. (c): Insulinemia. (d): PID and iPID insulin infusion rates.

4.15 In silico results and statistics

4.15.1 Simulator 1, without measurement noise

Applied on IF2 of 2-day clinical data of both fasting and postprandial phases, classic and intelligent PID controlled BG behavior compared to FIT therapy are shown in Fig. 4.6-(b). Each control signal is applied every 5 min.

Fig. 4.6-(a) displays meal intakes. iPID and PID yielded euglycemia during fasting day while open-loop control persisted in hyperglycemia for over eleven hours. As Tables 4-3 and 4-4 read, mean values and time in target are improved for both controllers as compared to open-loop therapy. The major difference between iPID and PID performance is that iPID has a nice continuous smooth basal rate in the first fasting day and high rate during postprandial phase as illustrated in Fig. 4.6-(d). Conversely, PID was off (saturated) most of the fasting day and during 25 % of the overall time. Insulinemia behavior for the three therapies is illustrated in Fig. 4.6-(c).

iPID: a three-phase control

Both controllers are tested on the four other subjects tagged as IF3, IF9, BE and LR changing $-\alpha = 0.32, 0.43, 0.18, 1.6$ and $-p = 0.65, 1.3, 0.45, 3.5$ for iPID and PID respectively as designed in Section 4.13. α may have a range of acceptable values per individual that verify the order of magnitude of the estimators terms. This is an interesting feature of iPID as it permits to detect and respond to the varying insulin sensitivity. The *in silico* test is conducted applying meal scenarios as logged in the clinical diary (see [58] for more details).

As illustrated in Table 4-3 and 4-4, satisfactory BG behavior is achieved under both controls with high percentage of time in target and mean values without severe hypoglycemic events. The first three subjects are assessed in [87] as stable diabetics according to the Mean Amplitude of Glycemic Excursion (MAGE) index while IF9 and LR are brittle diabetics (see Appendix A.3).

Although meals are unannouned for both controls, iPID produced a faster bolus-shaped infusion and thus a reduced postprandial BG excursion without the risk of late hypoglycemia (see Fig. 4.8-(b)and 4.7 (b)). This improvement of iPID over its classic counterpart can be observed also by the time percentage in hyperglycemia and the maximum peak as shown in Table 4-4. The overall average percentage of BG in [180, 250] is 12.6% versus 14.6% and BG $>$250 is 1.6% versus 4.8% for iPID and PID respectively. iPID control has a better mean and time-in-target values with less hyperglycemia in amplitude and duration as compared to PID control. The average over all percentage of BG in [70, 180] is 85.6% versus 80.4% with overall mean 141$\pm$ 37 versus 147 $\pm$ 42 for iPID and PID respectively. As illustrated in Tables 4-3 and 4-4, PID and iPID control performances dominated those of iPvref control.

4.15.2 Simulator 2, with measurement noise: Uva/Padova

4.15.3 IV sensor

In this test a scenario of 33 hours of fasting followed by the meal scenario mentioned earlier in Section 4.14.2 tested on five patients (adults 1, 3, 7, 8, 10). The objective is to test the superiority of the intelligent part of iPD+basal over standard PD+basal performance in (4.45) employing the same feedback gains with $\alpha = -7$. As detailed in Section 4.14.2, the integral term is turned off and the subjects specific basal rate is injected in both algorithms. As illustrated in Fig. 4.9, although both controllers reacted fast to meal perturbations, iPD+basal was more aggressive which had a higher impact on postprandial hyperglycemia without a risk of late hypoglycemia. As a result, iPD+basal achieved a better trade-off between hyper and hypoglycemia with average overall mean of 138 versus 155 mg/dL for PD+basal.

Table 4-3: Time performance indicators for open and closed-loop controls.

Patient	%Time in target [70-180] - [70-140]				%Time in hypo. [<70]				%Time in hyper. [180-250]|[>250]			
	Open-loop	iP_{vref}	PID	iPID	Open-loop	iP_{vref}	PID	iPID	Open-loop	iP_{vref}	PID	iPID
IF2	55|30	59|30	95|85	91|69	0	0	0	0	45|0	40|02	5|0	09|0
IF3	78|77	80|36	90|46	91|59	22	0	0	0	0 | 0	13|08	10|0	10|0
BE	82|48	70|83	92|75	100|80	0	0	0	0	14|4	17|0	8|0	0|0
IF9	70|65	72|27	82|46	86|65	37	0	0	0	08|06	04|18	8|09	12|0
LR	57|32	50|22	43|26	60|31	2	6	0	0	33|08	21|23	42|15	32|8

4.15.4 CGM sensor

In this test, $\alpha = -5, -5, -10$ for subjects 6, 8 and 7 and $\alpha = -9$ for 4,5 and 9 and $\alpha = -7$ for all other patients. Table 4-5 and 4-6 provide a performance comparison between iPID and PID algorithms. HBGI and LBGI refer to high and low BG index respectively. They are measures of the frequency and extent of high and low BG readings and are calculated according to the formula is given in [91]. As indicated in the user guide of the Uva/Padova Simulator, HBGI is considered Minimal if HBGI$<$ 5.0, Low if 5.0 $\leq$ HBGI $<$ 10.0, while LBGI<1.1 is considered Minimal and Low when 1.1$\leq$LBGI $<$2.5. According to Table 4-6, LBGI is minimal for PID and iPID while HBGI is minimal for iPID and low for PID.

A reduced mean of time percent in hyperglycemia $BG \in [180, 250]$ for iPID of 21.2% versus 30.32% for PID. The average mean and standard deviation curves are depicted in Fig. 4.10.

The heavy meal scenario is depicted in Fig. 4.11 using iPID designed in Section 4.12. The test is repeated five times for each of the three subjects 5, 7 and 9 taking a set point of 140 mg/dL. This test includes patient 7 that had the highest hyper/ hypoglycemic events and highest HBGI as illustrated in Tables 4-5 and 4-6. The resulting overall mean is 151$\pm$21 mg/dL, the average time percent of BG in [70, 180] is 71% , the average time percent of BG$<$ 50 is 0.53% and time percent in hyperglycemia BG$>$ 250 is 11.83%. HBGI and LBGI are found to be 6.77 and 1.49 respectively. Despite the elevated glycemia excursions, late hypoglycemia events and risk remained low.

Table 4-4: Performance indicators for open and closed-loop controls.

Patient	Mean ± std				Min:Max(BG)				% Time Off control		
	Open-loop	iP_{vref}	PID	iPID	Open-loop	iP_{vref}	PID	iPID	iP_{vref}	PID	iPID
IF2	169±47	168±49	130±22	136±29	74|230	88|251	103|230	110|230	20	25	0
IF3	91±23	155±50	145±33	140±31	46|142	72 | 298	74|244	74|237	24	22	18
BE	155±39	128±44	128±31	123±27	84|260	73 | 230	76|195	75|177	57	44	44
IF9	108±62	174± 104	145±56	133±39	49|320	80 | 495	74|317	75|245	23	23	22
LR	171±54	185± 80	188±67	171±52	63|300	59 | 409	69|363	82|312	36	43	36

4.16 Discussion

iPID control was shown to be appealing for glycemia regulation with the preferred PID features. It was tested *in silico* on 15 T1DM adults on two different T1DM simulators. iPID is compared to a standard PID controller in two cases:
i) each controller parameters were tuned independently on a case study and then the design is applied on other subjects adapting one weighting parameter to avoid hypoglycemia and results are compared.
ii) A PD+basal control previously designed to reduce the average BG risk index was compared to iPD+basal blocking the integral term to the basal rate of the patient. The superiority of the intelligent part of iPD over the classic is shown in this case by setting the same feedback gains. The results showed that the postprandial response was improved with iPID reducing hyperglycemic excursions with minimal hypoglycemic events. Moreover, the results showed that iPID, who has the classic PID structure with new adaptive feature, emulated insulin delivery of pancreatic β-cell. The major problem open for further research is about a numerical differentiator which is able to cope with the typical glycemia measurement noise, as any improvement will impact the performance of iPID. A perspective of this work is to consider variation in insulin sensitivity, due to physical activities or sickness, in the *in silico* test.

Table 4-5: Main Objective Performance Measures.

ID	Mean ± SD*		%BG 70-180		%BG < 50 (n)**		%BG >250		%BG 50-70	
	PID	iPID	PID	iPID	PID	iPID	PID	iPID	PID	iPID
Adult 1	167±06	136±10	68	84	0	0	04.38	0.02	0	1.13
Adult 2	153±07	131±09	81	90	0	0	01.64	0	0.08	0.21
Adult 3	183±05	153±07	46	73	0	0	07.00	0	0	0.16
Adult 4	169±05	147±07	63	75	0	0	03.48	0	0	0.29
Adult 5	197±06	164±07	42	57	0	0	19.25	8.21	0	1.15
Adult 6	180±04	145±07	58	78	0	0	13.36	2.97	0	0.09
Adult 7	177±11	156±14	66	69	0	0.57(4)	14.79	9.75	0	1.02
Adult 8	208±04	151±10	36	65	0	0.46(3)	24.19	1.15	0	2.16
Adult 9	159±07	139±09	72	79	0	0	05.97	0.54	0	0.36
Adult 10	161±04	140±06	70	87	0	0	01.14	0	0	0
Average	175±06	146±09	60.2	75.7	0	0.10	09.50	2.26	0.008	0.66

* Standard deviation.

** n is the number of tests (over 25) where min(BG)<50.

Table 4-6: Performance Measures (Quality Indicators).

ID	LBGI		HBGI		Premeal Mean		Postmeal Mean	
	PID	iPID	PID	iPID	PID	iPID	PID	iPID
Adult 1	0.0002	0.4053	06.64	02.88	159	133	225	188
Adult 2	0.0100	0.1551	04.33	01.95	142	126	202	170
Adult 3	0.0005	0.1528	09.37	05.06	177	154	226	200
Adult 4	0.0005	0.3836	06.89	04.51	164	149	216	200
Adult 5	0.0010	0.5511	12.28	07.77	187	165	254	228
Adult 6	0.0003	0.1514	09.43	04.31	173	139	254	215
Adult 7	0.0115	0.7806	09.32	06.75	159	152	275	245
Adult 8	0.0000	0.8261	14.42	05.59	201	152	268	213
Adult 9	0.0112	0.3946	05.85	03.80	149	136	224	203
Adult 10	0.0007	0.2469	05.75	03.18	158	141	208	185
Average	0.0036	0.4047	08.43	04.58	166.9	144.7	235.2	204.7

4.17 Conclusions

Model-free control is employed for the first time as a control algorithm to close the loop of the artificial pancreas. The feasibility of iP and iPID to regulate glycemia for T1DM is tested and the conclusions are summarized as follows:

1. iP

    - Constant reference iP has shown a poor postprandial response. Under a small estimation time window, the proportional gains α and K_p were not sufficient to reduce hyperglycemia peaks without late hypoglycemia.
    - iP postprandial performance was enhanced by introducing a variable reference trajectory for the controller. Whenever meals were detected, the controller switched between a constant set point, to an exponential decay reference path. This variable reference yielded a postprandial bolus-shaped injection rate which was more effective in handling hyperglycemia peaks.
    - *In silico* tests: the fully automatic model-free iPvref has shown a better postprandial performance with respect to conventional iP.
    - A good fasting-postprandial compromise can not be yielded using fixed design.
    - To further improve the fully automatic controller, a two-phases gain scheduling is proposed: α for fasting phase, and another for postprandial phase. Another possibility, that was realized here, is to increase the degree of control complexity to close the loop with iPID.

2. iPID

    - Constant reference iPID performance indicators dominated those of iPvref *in silico* control.
    - iPID was compared to classic PID behavior that were optimally designed for a T1DM subject of Simulator 1. iPID showed a better glycemia response according to some statistical parameters. It was shown that iPID better emulated β cells behavior than PID control by infusing a faster postprandial (first phase) insulin pulse.
    - iPID was tested on Uva/Padova T1DM simulator on three adults under CGM sensor noise. The fully automatic iPID response to a relatively heavy meal scenario was satisfactory avoiding late hypoglycemia. The same design parameters were used for the three subjects.
    - iPD+basal was compared to an existing PD+basal control from a previous study. For a clear comparison, both controllers are compared employing the same gain parameters.
    - *in silico* Uva/Padova test results, under CGM noise, on 10 adults $\times$25 runs have shown the superiority of the intelligent controller over its classic counterpart. The

intelligent controller detected meals and reacted faster to meal perturbations as compared to a classic PD without neglecting safety.

Diabetic stability is studied through the MAGE index (in Appendix A.5) to explain the excessive glycemic variability in some subjects. They are found to be brittle patients, rare cases that usually need extensive care and of BG fluctuations that are difficult to predict and regulate. For the MAGE-stable patients, the new design yielded a satisfactory glycemic response under the fully automatic MFC.

As a general overview, a better postprandial BG response was obtained with iPID as compared to classic PID and to iPvref. A good robustness level was shown tuning only one parameter from one patient to another. It was tuned empirically to reduce hyperglycemia with least hypoglycemic episodes during the simulation time. The controller was fully automatic without any meal announcement nor supplementary boluses. iPID combines the classic PID nice properties with new adaptive features. However, the following remarks are worth noting:

1. System constraints are not taken into account in the design, namely, hypoglycemia threshold and the positivity of the controller. The controller was saturated to zero which is the lower admissible bound.

2. When the controller saturates to zero, the loop is broken and glycemia is not under iPID control.

3. Integral windup is another known defect for PID-like controllers.

4. Hypoglycemia avoidance is not ensured.

Thus, maintaining a tight BG control, especially during postprandial phase is also not an easy task for this fully automatic iPID.

Regarding MFC in general, some questions were raised concerning the stability of the controller and iP was taken as a case study. It was shown that closed-loop stability, for iP controller, is not simply related to the first order error dynamics resulting form the ultra-local model. Via a second-order academic example, it was shown that closing the loop with iP does not guarantee stability. Stability analyses related to the delay on the control law probably worth further investigation. Other questions regarding the choice of the estimation function of the ultra-local model are underlined. During the design of iPID, for instance, it was found that a problem open for further research is about a numerical second order differentiator which is able to cope with the typical glycemia measurement noise, as any improvement will impact the performance of iPID.

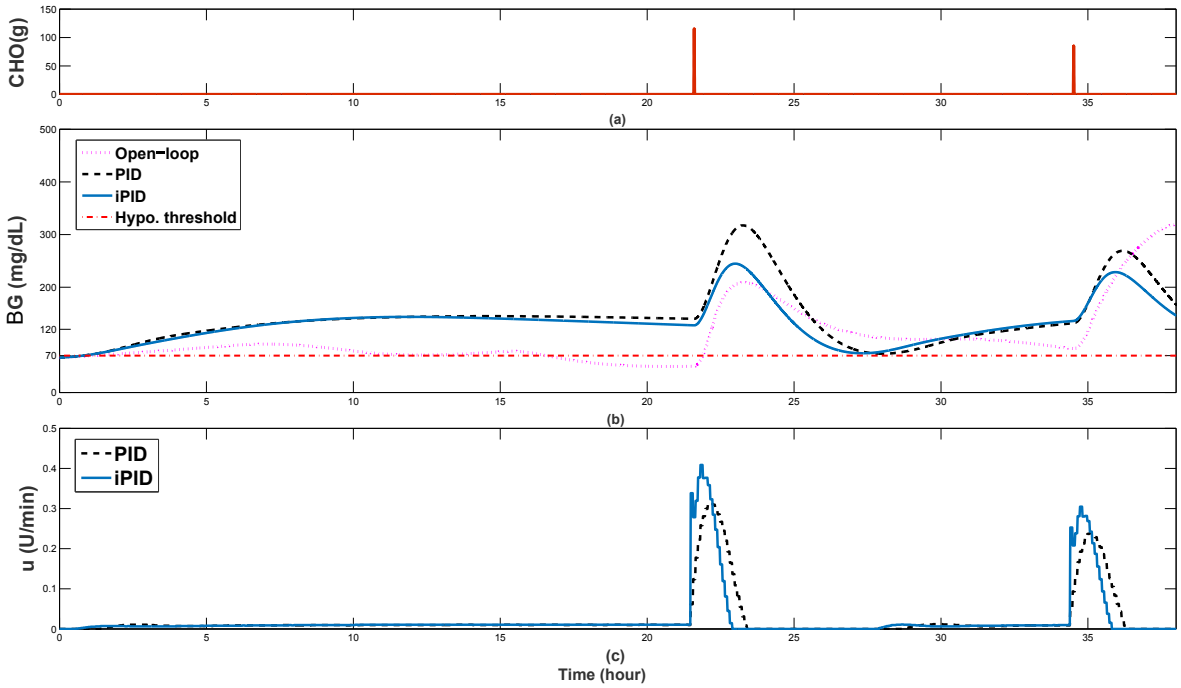

Figure 4.7 IF9 response for open-loop, PID and iPID. (a): CHO amount in meals. (b) BG behavior. (c): PID versus iPID insulin infusion rates.

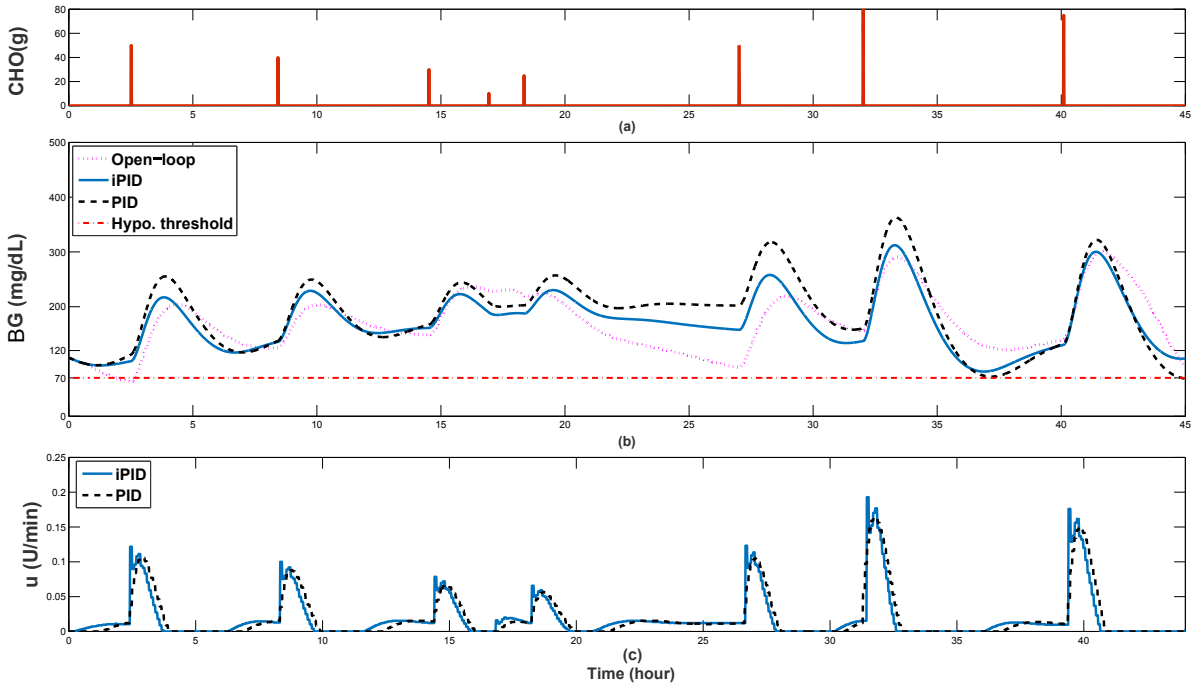

Figure 4.8 LR response for open-loop, PID and iPID. (a):CHO amount in meals. (b): BG behavior. (c): PID versus iPID insulin infusion rates.

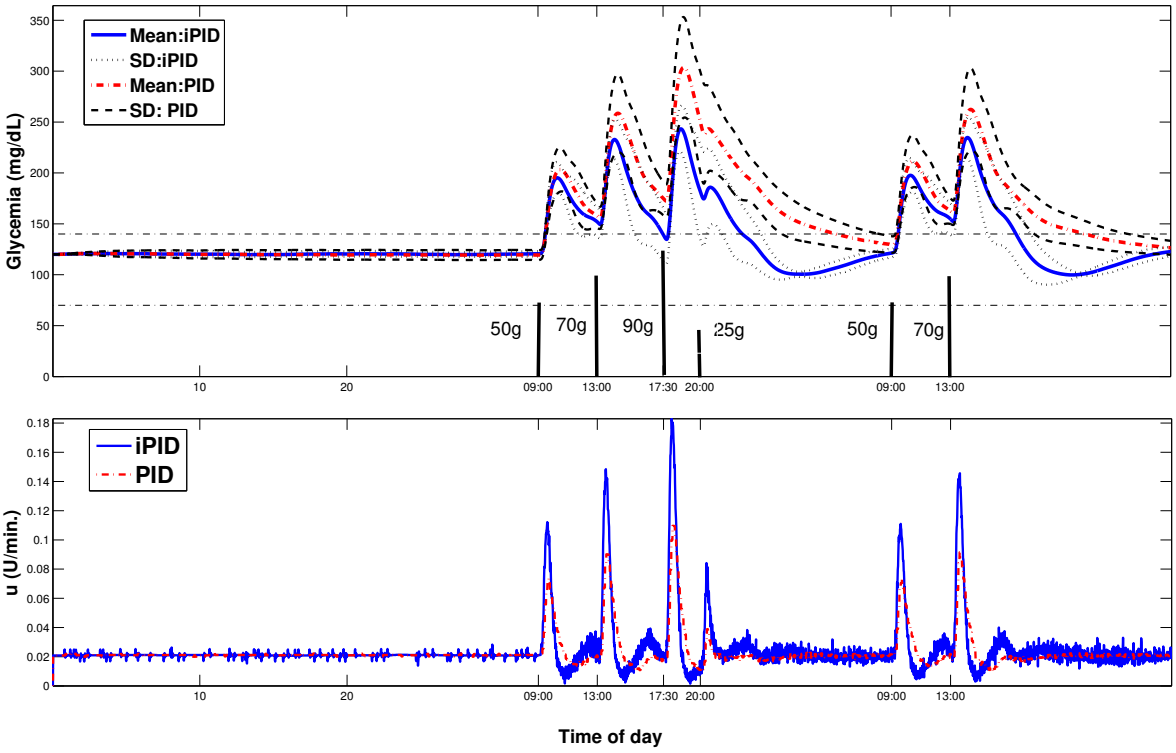

Figure 4.9 BG behavior of Uva/Padova simulator under iPID and PID control employing IV sensor. The bars represents CHO amounts in each meal in grams. Upper Panel is BG behavior and the lower panel is the insulin infusions by each controller.

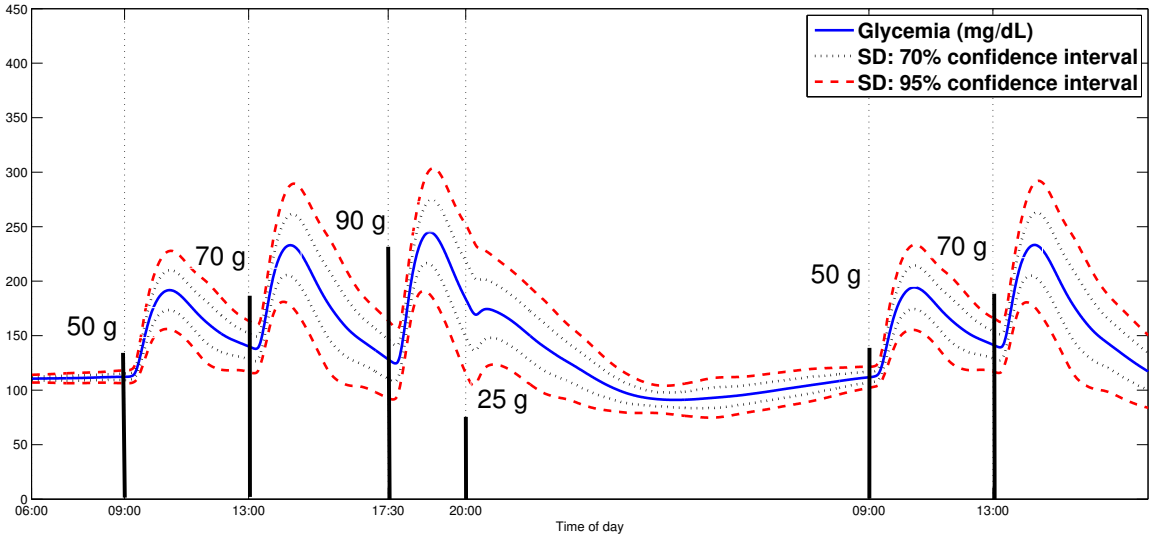

Figure 4.10 Average BG of the (10 adults $\times$25 runs) of Uva/Padova simulator under iPID control: solid line represents the mean and the dashed is the standard deviation (SD). 70% confidence interval is yielded with mean BG $\pm$ SD, and 95% confidence interval is with mean BG $\pm$ 1.96SD.

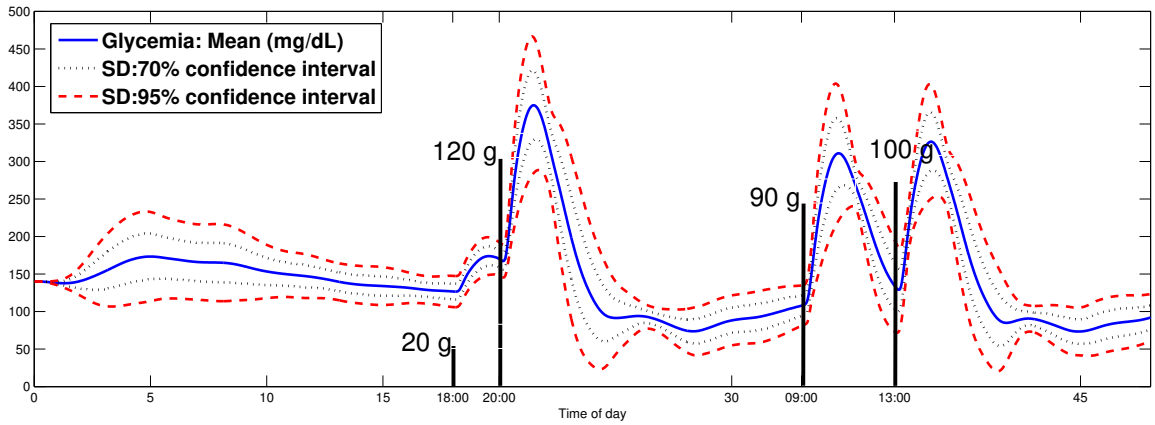

Figure 4.11 Average BG behavior under iPID for heavy meal scenario of adults 5, 7 an 9 (5 runs each) of Uva/Padova simulator. The bars represent CHO amounts in each meal in grams.

Chapter 5

Positive Sliding Mode Control for Glycemia Regulation

5.1 Chapter Introduction in French

Dans les études de PA, deux catégories principales d'algorithmes de commande ont été employées : les commandes basées sur des modèles et les commandes non basées sur des modèles (sans modèle). Chaque catégorie a ses propres avantages et inconvénients. Au chapitre 4, le réglateur iPID (sans modèle) fut conçu et testé. La conception était basée sur l'historique de l'entrée de commande et les mesures de sortie. Le régulateur révèle un bon niveau de robustesse lorsqu'il est appliqué sur différents patients virtuels. Dans ce chapitre, on utilise la commande par modes glissants (CMG), connue pour sa robustesse vis à vis des perturbations et la dynamique non modélisée. Dans le chapitre 4, une saturation a été ajoutée pour contraindre le contrôleur à être non négatif. La commande CMG est conçue ici pour être positive sans la nécessité d'une saturation. Selon la littérature du PA au chapitre 2, la positivité de la commande n'a pas été prise en compte. Alors, l'existence d'une commande CMG positive est obtenue ici pour la régulation de la glycémie pour la première fois. Les propriétés des ensembles positivement invariants sont utilisées à cette fin. On trouve le plus grand ensemble positivement invariant en boucle fermée pour le sous système d'insuline sous CMG. L'insuline contrôlée est l'entrée (variable de commande) du compartiment glycémique pour réguler sa concentration. La trajectoire de référence d'insuline est conçue pour être l'insuline plasmatique nécessaire pour réguler la glycémie. L'erreur de glycémie (par rapport à la normoglycémie) est utilisée pour concevoir la trajectoire de référence de l'insuline pour éliminer cette erreur. La trajectoire de référence de l'insuline est conçue via une seconde commande par modes glissants et est renvoyée, en tant qu'entrée de référence, à la commande

par modes glissants de la première étape. Ainsi, une fois que l'état d'insuline est piloté vers sa référence souhaitée, la glycémie est elle-même pilotée vers son niveau normal.

5.2 Introduction

In AP studies, two main categories of control algorithms were employed: model-based and non-model based (model-free) controllers. Each category had its own advantages and drawbacks. In Chapter 4, model-free PID controller was designed and tested. The design was based on the history of the control input and the output measurements. The controller showed a good level of robustness when applied on different virtual patients. In this chapter sliding model control, that is known for its robustness against perturbations and non-modeled dynamics, is employed. In Chapter 4, a saturation was added to constrain the controller to be nonnegative. The model-based SMC is designed herein to be positive without the need of a saturation. According to the AP literature in Chapter 2, positive SMC has not been considered. Thus, the existence of a positive SMC for glycemia regulation is shown here for the first time. The properties of positively invariant sets are utilized for this purpose. The largest closed-loop positively invariant set of insulin system under sliding mode control is found. SMC is designed to be positive everywhere in the largest closed-loop positively invariant set. The controlled insulin is the input (control variable) to the glycemia compartment to regulate its concentration. The desired insulin trajectory is designed to be the required plasma insulin to regulate glycemia. The error of glycemia (from its desired level) is used to design the insulin reference trajectory to eliminate this error (see Fig. 5.9). The insulin reference trajectory is designed via a second sliding mode control and it is fed back, as a reference input, to the first stage sliding mode control. Thus, once the insulin state is steered toward its desired reference, glycemia is directed toward its normal level. Lyapunov stability and reachability conditions are verified for both controllers.

The work in this chapter is submitted to be published and under revision [92].

5.3 Positivity and Positive Invariance for Linear Systems

In the next subsection, the main motivations behind studying positivity and positive invariance properties of system (3.17), in this chapter and the following chapter, are presented.

5.3.1 Motivation

The glucose-insulin interaction as a physiological process relates positive variables like concentrations or molar amounts. Thus, the input/output positive constraints of the long-term T1DM model in § 3.7 is taken into account in the controller design in the current and the following chapter. In addition, the realization of the mentioned T1DM model is not positive. In other words, not all the positive initial conditions lead to a positive state trajectories for any $t \geq 0$ for insulin and glycemia state variables. Therefore, the largest open-loop Positive Invariant Set (PIS) for the insulin dynamics is identified. It is the set where the plasma insulin variable remains positive. Thereafter, the largest closed-loop PIS under SMC is found. The result is a positive control everywhere in the largest closed-loop PIS of insulin system. The theory of linear positive systems and positively invariant sets is employed for this purpose. The PIS theory is involved in different control problems like: constrained control, robustness analysis and optimization [93]. Moreover, to the best of our knowledge, the existence and characterization of PIS to design a positive control of glycemia-insulinemia models have not been considered previously. A part from MPC which takes constraints inherently in the optimization process, saturation (to zero) is the basic solution to stop the negative control. For these reasons, closed-loop PIS is found and employed to design a positive SMC (in this chapter) and positive state feedback controller later in Chapter 6.

The following subsection gives a brief introduction of positive systems and positively invariant sets. It will be used and applied on the T1DM model (3.17) to study the positivity of its state variables: insulin, in this chapter and glycemia in the next chapter.

5.3.2 Preliminaries

Some useful definitions and theorems of positive systems and positively invariant sets are now recalled from [94, 95]. They will be used throughout this chapter and the following chapters.

In the following, any matrix $E \in \mathbb{R}^{n\times m}$ is said to be nonnegative, denoted by $E \geq 0$ or $E \in \mathbb{R}_{+}^{n\times m}$, if its entries $e_{ij} \geqslant 0 \quad \forall (i,j)$.

5.3.3 Externally Positive Systems

Definition 1. *[94] The following linear system:*

$$\begin{cases} \dot{x}(t) = Ax(t) + Bu(t) \\ y(t) = Cx(t) \end{cases} \tag{5.1}$$

where $x \in \mathbb{R}^n, A \in \mathbb{R}^{n\times n}, B \in \mathbb{R}^{n\times m}, C \in \mathbb{R}^{p\times n}$, is said to be an externally positive system if for any nonnegative input $u(t) \geq 0$ and zero initial conditions, the output is nonnegative $y(t) \geq 0$ for any $t \geq 0$.

External positivity is characterized as follows.

Theorem 1. *[94] System* (5.1) *is externally positive if and only if its impulse response $h(t)$ is nonnegative:*

$$h(t) = Ce^{At}B \in \mathbb{R}_+^{p\times m}, t \geq 0 \tag{5.2}$$

Obviously, the property of external positivity is inherent to the system and does not depend on the special state coordinates used to describe the dynamics (5.1).

The stronger notion of internal positivity is recalled next, and shown to be useful to analyze the insulinemia subsystem in Section 6.3.2.

5.3.4 Internally Positive Systems

Definition 2. *[94] System* (5.1) *is positive or internally positive if for any $x(0) \in \mathbb{R}_+^n$ and $u(t) \in \mathbb{R}_+^m$ the state trajectory $x(t) \in \mathbb{R}_+^n$ and the output $y(t) \in \mathbb{R}_+^p$.*

Internal positivity is easily characterized thanks to the so-called Metzler matrices whose off-diagonal elements have to be nonnegative.

Definition 3. *A matrix $H = [h_{ij}] \in \mathbb{R}^{n\times m}$ is Metzler if $h_{ij} \geqslant 0$ for $i \neq j$.*

Theorem 2. *[94] The system* (5.1) *is internally positive if and only if*
i) A is a Metzler matrix,
ii) $B \in \mathbb{R}_+^{n\times m}, C \in \mathbb{R}_+^{p\times n}$

Surprisingly, in opposition to external positivity, the property of internal positivity is state coordinates dependent. It is not invariant under a change of state coordinates as it is easily shown by the following example.

Example 1. *The system*

$$\begin{cases} \dot{z}(t) = \begin{pmatrix} 0 & 0 & -1 \\ 0 & 0 & 1 \\ 0 & -1 & -2 \end{pmatrix} z + \begin{pmatrix} 0 \\ 0 \\ 1 \end{pmatrix} u \\ y(t) = z_2 \end{cases} \tag{5.3}$$

is not internally positive in the z coordinates since the A matrix is not Metzler.

However, the following change of state variables:

$$\begin{cases} \tilde{z}_1 = -z_1 \\ \tilde{z}_2 = z_2 \\ \tilde{z}_3 = z_2 + z_3 \end{cases} \tag{5.4}$$

yields

$$\begin{cases} \dot{\tilde{z}} = \begin{pmatrix} 0 & 0 & 1 \\ 0 & -1 & 1 \\ 0 & 0 & -1 \end{pmatrix} \tilde{z} + \begin{pmatrix} 0 \\ 0 \\ 1 \end{pmatrix} u \\ y(t) = \tilde{z}_2 \end{cases} \tag{5.5}$$

which fulfills the conditions of Theorem 2 and is thus internally positive.

Remark 8. *Internal positivity implies external positivity and this can be shown using the output time response of system* (5.1) *in the light of the impulse response:*

$$y(t) = Ce^{At}x(0) + \int_0^t h(t-\tau)u(\tau)\mathrm{d}\tau \tag{5.6}$$

To yield $y(t) \geq 0$, Theorem 1 requires only $h(t) \geq 0$ for $x(0) = 0$, while Theorem 2 requires also $x(0) \geq 0, C \geq 0$ and $B \geqslant 0$ for internal positivity. The converse is not true, i.e. an externally positive system is not necessarily internally positive e.g. system (5.3)*. Despite the fact that this system is not positive according to Theorem 2, it is externally positive with $h(t) = te^{-t} \geqslant 0$.*

The following definitions and theorems are useful to study positivity and set invariance especially for the systems that are neither internally nor externally positive.

Definition 4. *A nonempty set $M \subseteq \mathbb{R}^n$ is a Positively Invariant Set (PIS) of* (5.1) *if $\forall x_o \in M \implies x(t,x_o) \in M \quad \forall t \geq 0$.*

Definition 5. *For any $G \in \mathbb{R}^{r\times n}$, $\rho \in \mathbb{R}^r$, $\Omega(G)$ denotes the polyhedron*

$$\Omega(G) = \{x \in \mathbb{R}^n | Gx \geq \rho\}. \tag{5.7}$$

In what follows, the vector $\rho = [0]_{r\times 1}$if not specified otherwise.

Proposition 1. *[95] The polyhedral set $\Omega(G)$ is a positively invariant set for system (5.1) if and only if there exists a Metzler matrix H such that:*

$$GA - HG = 0. \tag{5.8}$$

$$H\rho \geqslant 0 \tag{5.9}$$

Corollary 1. *The positive orthant $\Omega(I) = \mathbb{R}^n_+$ is PIS, if and only if A is Metzler.*

Proof. It follows from Proposition 1 where $H = A$. □

Corollary 2. *The positive orthant $\mathbb{R}^n_+$ of an internally positive system is a PIS.*

Proof. It follows from Theorem 2 and Corollary 1. □

As will be discussed in more details in Chapter 6, the T1DM model (3.17) is not positive neither internally nor externally according to Theorems 2 and 1. This is true for both the original realization in (3.17) and transformed one (3.23). This fact triggered the search to find the largest set where the state variables remain positive at all times i.e. the largest PIS. Invariance analyses were initially discussed for the original state representation (3.17) and specifically on the second order insulin subsystem as a start. Those analyses, as will be presented in this chapter, were undertaken in open and closed-loop control.

The next section investigates invariance properties of the open-loop insulin subsystem.

5.4 PIS of Insulin Subsystem: Open-loop

Consider the insulin subsystem (3.15) which is equivalent to:

$$\begin{cases} \dot{x}(t) = Ax(t) + Bu(t) \\ y(t) = Cx(t) \end{cases} \tag{5.10}$$

$x(t) = [x_1(t) \qquad x_2(t)]^T$

where $y(t)$ is the output and $x_1 = I, x_2 = \dot{I}$ are the system states with: $A = \begin{pmatrix} 0 & 1 \\ -\lambda_m^2 & -2\lambda_m \end{pmatrix}$,

$B = \begin{pmatrix} 0 \\ b \end{pmatrix}, C = \begin{bmatrix} 1 & 0 \end{bmatrix}$

$\lambda_m = \frac{1}{T_u}$, $b = \frac{K_u \lambda_m^2}{V_i}$, $b > 0$. The plasma insulin is nonnegative in the following set $\Omega(C)$, however, this set is not a PIS according to Proposition 1. In the following theorem the largest PIS in $\Omega(C)$ for the open-loop insulin subsystem is presented.

Theorem 3. *The largest PIS in* $\Omega(C)$*of the open loop system* (5.10) *is* $\Omega(G)$*, with* $G = \begin{pmatrix} 1 & 0 \\ \lambda_m & 1 \end{pmatrix}$.

Proof. Firstly, it will be shown that $\Omega(G)$ is the largest polyhedral PIS. Secondly, it will be shown that $\Omega(G)$ is the largest PIS in $\Omega(C)$. As $\Omega(C)$ is not PIS according to Proposition 1, consider $G = \begin{pmatrix} C \\ a \quad b \end{pmatrix}$ and $\Omega(G)$ is just a generic polyhedron contained in $\Omega(C)$. Find a, b such that $\Omega(G)$ is PIS or $H = GAG^{-1}$ is Metzler according to Proposition 1. The unique H is

$$H = \begin{pmatrix} -\frac{a}{b} & \frac{1}{b} \\ -\frac{(a-b\lambda_m)^2}{b} & \frac{(a-2b\lambda_m)}{b} \end{pmatrix} \tag{5.11}$$

and the definition of a Metzler matrix implies $b > 0$ and $a = b\lambda_m$ and hence $G = \begin{pmatrix} 1 & 0 \\ \lambda_m & 1 \end{pmatrix}$. As H is unique that satisfies Proposition1 then $\Omega(G)$ is the largest PIS in $\Omega(C)$ as illustrated in Fig. 5.1. Note, that for any $x(0) \in \Omega(C) \setminus \Omega(G)$, there exists $t > 0$ such that $x(t) \notin \Omega(C)$. Therefore, $\Omega(G)$ is the largest PIS in $\Omega(C)$. □

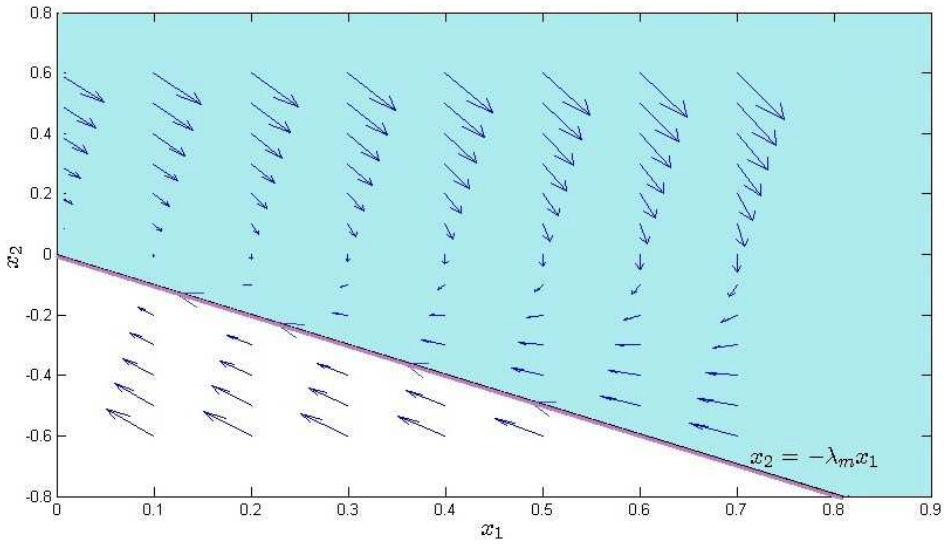

Figure 5.1 The blue region represents $\Omega(G)$ the largest PIS for the insulinemia autonomous subsystem. The arrows represent the vector fields.

In the next section a standard SMC is designed for system (5.10) to obtain the largest closed-loop PIS in $\Omega(C)$ under this control. Positivity constraints of the controller is also considered thereafter.

5.5 Introduction to Sliding Mode Control

Sliding mode control is a particular type of Variable Structure Control (VSC) systems which evolved in Russia. It appeared outside of Russia in the mid of 1970's when a survey paper by Utkin (1977) was published in English. SMC has now a solid position in the field of linear and non-linear control theory [96]. VSC system utilizes a set of continuous subsystems (structures) and a switching function. The switching among different functions is determined by the plant states. The discontinuous manner goes on so that the desired performance is achieved. SMC uses the high-frequency discontinuous control action to derive the state trajectories into a specified and user-defined surface in state space (called sliding or switching surface) and to maintain them on this surface or within its neighborhood while moving toward the equilibrium. During sliding mode the desired performance is maintained even in the presence of disturbances/uncertainties.

5.6 SMC Design of insulinemia subsystem

Since the overall glucose-insulin system is a cascade of the second order insulinemia subsystem and the first order glycemia subsystem, the glycemia regulation problem may be split into the stabilization of the two subsystems. The objective of the first control problem is to stabilize the error $e(t)$ between the insulinemia and its desired value x_d:

$$e(t) = x_1 - x_d$$

$x_d \geq 0$ is assumed to be a constant reference value for the insulinemia at this stage.

The sliding surface is defined by :

$$s(x) = \dot{e} + \lambda e \tag{5.12}$$

where λ is a positive real parameter so that $e(t) \to 0$ when $s = 0$.

5.6.1 Reachability Condition

The aim is to achieve asymptotic convergence of the error e to zero using the control u that drives the sliding variable s to zero in finite time. This task is achieved by using the following Lyapunov function:

$$V = \frac{1}{2}s^2 \tag{5.13}$$

The adequate control is computed as a solution to $\dot{V} \leq 0$, or equivalently $s\dot{s} < 0$ with $s \neq 0$ which is termed as the *the reachability condition*.

$$s\dot{s} = s(-\lambda_m^2 x_1 + (\lambda - 2\lambda_m)x_2 + bu) \tag{5.14}$$

The standard sliding mode control law consists of the sum of a continuous equivalent control $u_{eq}(t)$ and a discontinuous control $u_{dis}(t)$:

$$u = u_{eq} + u_{dis} \tag{5.15}$$

where the continuous part u_{eq} is the solution of $\dot{s} = 0$:

$$u_{eq}(t) = \frac{1}{b}[\lambda_m^2 x_1 + (2\lambda_m - \lambda)x_2] \tag{5.16}$$

while

$$u_{dis}(t) = -k\,\mathrm{sign}(s) \tag{5.17}$$

and $\dot{V}$ is then:

$$s\dot{s} = -kb|s| < 0 \tag{5.18}$$

thus, $s\dot{s} < 0$ is guaranteed whenever $k > 0$.

5.6.2 Reaching Time

Definition 6. *Denote t_r the time instant when the sliding manifold is reached $s(t_r) = 0$.*

t_r can be calculated using

$$\dot{s}(t) = -bk\,\mathrm{sign}(s(t)) \tag{5.19}$$

with $u = u_{eq} - k\,\mathrm{sign}(s)$, integrating both sides of (5.19) in the interval $[0,t]$ yields

$$\int_0^t \frac{\mathrm{d}s(t)}{\mathrm{sign}(s(t))} = -bk \int_0^t \mathrm{d}t \tag{5.20}$$

yields

$$|s(t)| - |s(0)| = -bkt \tag{5.21}$$

and at $t = t_r$ sliding occurs and $s(t_r) = 0$ thus:

$$t_r = \frac{|s(0)|}{bk} \tag{5.22}$$

where $s(0) = s(x(0))$.

In the next sections, output/control positivity and invariance conditions will be investigated. In order to find the largest closed-loop PIS in $\Omega(C)$, and later under nonnegative SMC, the set $\Omega(C)$ will be divided into three regions:

$$\text{i) on the surface } s = 0: \quad S = \{x \in \Omega(C) | s(x) = 0\} \tag{5.23}$$

$$\text{ii) in the region } s \leq 0: \quad S_- = \{x \in \Omega(C) | x_2 \leq -\lambda(x_1 - x_d)\} \tag{5.24}$$

$$\text{iii) in the region } s \geq 0: \quad S_+ = \{x \in \Omega(C) | x_2 \geq -\lambda(x_1 - x_d)\}. \tag{5.25}$$

5.7 Invariance of the Surface S

In ideal sliding mode, the sliding surface represents an invariant manifold of the system [97].

Once this manifold is reached, the state trajectories remain on it for all future times. The invariance condition of $s = 0$ is thus

$$\begin{cases} s = 0 \\ \dot{s} = 0 \end{cases} \tag{5.26}$$

Since the sliding manifold is shown to be PIS, the invariance of the following subsets will be investigated during the reaching phase when $t < t_r$.

Using Lyapunov attractivity condition (5.18) the following sets are PIS:

$$S_R^+ = \{x \in \mathbb{R}^2 | s \geq 0\} \tag{5.27}$$

$$S_R^- = \{x \in \mathbb{R}^2 | s \leq 0\} \tag{5.28}$$

Thus $S_+ \subset S_R^+$, $S_- \subset S_R^-$. In words, if $x(0) \in S_R^+$ ($\in S_R^-$ respectively) then $x(t) \in S_R^+$ (S_R^- respectively) $\forall t \in \mathbb{R}^+$ thanks to Lyapunov condition (5.18). This can be shown using $\dot{s}(t)$ in (5.19) and its solution in (5.21) as follows:

$$\left(\left|s(t)\right| - \left|s(0)\right|\right) \leq 0, \ \forall t \geqslant 0 \tag{5.29}$$

or equivalently

$$\begin{cases} 0 \geq s(t) > s(0) & \text{if } s < 0 \\ 0 \leq s(t) < s(0) & \text{if } s > 0 \end{cases} \tag{5.30}$$

and this implies that if $s(0) \in S_R^+$ (S_R^- respectively) then $s(t) \in S_R^+$ (S_R^- respectively) for any $t > 0$. As a result, any state trajectory initiated in S_R^+(S_R^- respectively) will remain there for all future times. However, our interest in the following sections is to find the largest closed-loop PIS in S_+ and S_- and then the largest overall PIS in $\Omega(C)$.

Remark 9. *As stated earlier S_R^+, S_R^- are PIS, however since $S_+ \equiv \Omega(C) \cap S_R^+, S_- \equiv \Omega(C) \cap S_R^-$ and $\Omega(C)$ is not PIS then S_-, S_+ are not necessarily PIS. Therefore the largest PIS in S_+(S_-respectively) is found such that $x_1(t) \geq 0$ for any $t > 0$ and positive invariance of each set is ensured via the Lyapunov reachability condition. As $S \subset S_+$(S_-respectivlely) is a PIS as shown earlier, therefore, the invariance of S_+(S_- respectively) is analyzed during the reaching phase $s(x) \neq 0$ in S_+ and S_- respectively.*

5.8 Positive invariance in S_-

In the reaching phase of S_- *i.e.* $s(x) < 0$, the closed-loop system is

$$\begin{cases} \dot{x}_1 = x_2 \\ \dot{x}_2 = -\lambda x_2 + bk \end{cases} \tag{5.31}$$

with state variables time solution

$$\begin{cases} x_1(t) = x_{10} + \frac{x_{20} - x_2(t) + bkt}{\lambda} \\ x_2(t) = \frac{bk}{\lambda} + (x_{20} - \frac{bk}{\lambda})e^{-\lambda t} \end{cases} \tag{5.32}$$

Theorem 4. *Assuming ideal sliding mode, the largest PIS in S_- is*

$$M_{s_-} := M_* \cup \{x_0 \in S_- | x_{20} > 0\} \tag{5.33}$$

as illustrated in Fig. 5.2, where

$$M_* := \left\{ x_0 \in S_- | x_{10} \geq \bar{x}_{10},\ x_{20} \leq 0 \right\} \tag{5.34}$$

$$\bar{x}_{10} = -\Big(\frac{bk}{\lambda^2}\ln\Big(\frac{bk-\lambda x_{20}}{bk}\Big)+\frac{x_{20}}{\lambda}\Big) \tag{5.35}$$

Proof. • Case 1: $x_{20} > 0$. According to the second equation of (5.32) and (5.24):

$$x_1(t) = x_{10} + \frac{x_{20}}{\lambda}(1-e^{-\lambda t}) + \frac{bk}{\lambda^2}\Big(\lambda t - (1-e^{-\lambda t})\Big) \tag{5.36}$$

$x_{10} \geq 0, x_{20} > 0$, the first and second terms are nonnegative, hence, it suffices to verify that:

$$\frac{bk}{\lambda^2}\Big(\lambda t - (1-e^{-\lambda t})\Big) \geqslant 0 \tag{5.37}$$

or

$$\lambda t \geq (1-e^{-\lambda t}) \tag{5.38}$$

which is true for any $\lambda > 0$ and $t \geq 0$. Thus, the set $\{x(0) \in S_- | x_{20} > 0\}$ is a PIS.

• Case 2: $x_{20} \leq 0$
In this case, $x_1(t) \in S_-$ is not guaranteed for any t as it decreases until $\dot{x}_1(t^*) = x_2(t^*) = 0$. Thus, define the critical time $t^* < t_r$ which is the solution of $\dot{x}_1(t^*) = 0$:

$$t^* = \frac{1}{\lambda}\ln\Big(\frac{bk-\lambda x_{20}}{bk}\Big) \tag{5.39}$$

Note that (5.39) is well defined in Case 2. The test of the critical point $x(t^*)$ reveals a minimum since $\ddot{x}_1(t^*) > 0$. For a given $x(0)$ substituting $t = t^*$ in (5.32) yields a point of the trajectory in the phase plane $(x_1(t^*), 0)$ where $x_1(t^*) = \min(x_1(t))$. To find the largest PIS in S_- such that $x_1(t) \geqslant 0$, it is required that $\min(x_1) = 0$ i.e. the global minimum at $x_1(t^*) = 0$ such that $x_1(t) \in S_-$ for any t. The largest PIS in S_- must have the global minimum of its state trajectories at the origin. Thus, the substitution of (5.39) into (5.32), to have $x_1(t^*) = 0$ yields

$$x_{10} = -\Big(\frac{bk}{\lambda^2}\ln\Big(\frac{bk-\lambda x_{20}}{bk}\Big)+\frac{x_{20}}{\lambda}\Big) \tag{5.40}$$

and hence (5.35) and the set M_* characterizes the set of points whose trajectories have a nonnegative minimum. To verify that $\bar{x}_{10} \geqslant 0$ in (5.40), taking into account that the current case $x_{20} = -|x_{20}|$, the right-hand side of (5.35) is nonnegative or:

$$\frac{\lambda}{bk}|x_{20}| \geqslant \ln\Big(1+\frac{\lambda|x_{20}|}{bk}\Big) \tag{5.41}$$

which is true as it as (5.41) is equivalent to $t \geq \ln(1+t)$.
If $x(0) \in M_*$ and $\{s(x) = 0\} \subset M_*$ ($t_r \geq t^*$) then $x \in M_* \forall t > 0$. However, M_* is not

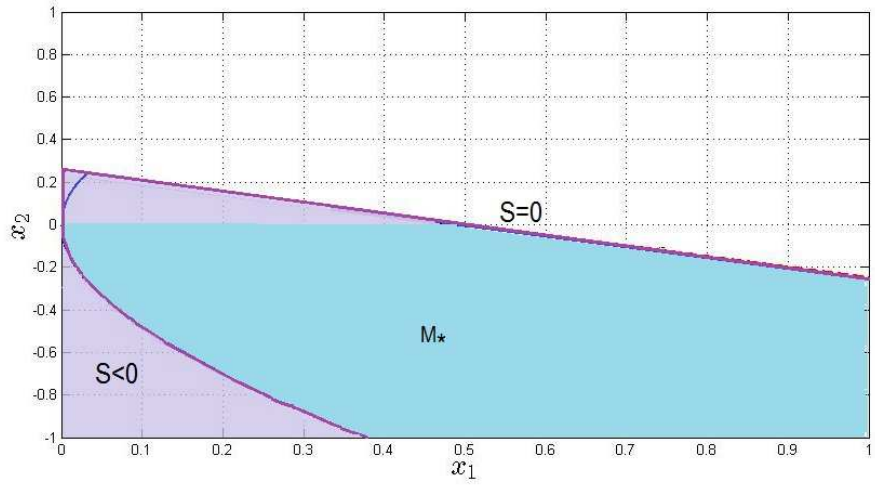

Figure 5.2 Largest PIS in S_- for $bk = 1, \lambda = 0.5, x(0) = (\bar{x}_{10}, -1), \bar{x}_{10} = 0.378$. S_- is in light violet area, M_* is in blue and M_s is bounded by the solid violet line.

entirely a PIS as only $x_1(t) \geqslant 0$ is ensured in it. This is due to the fact that $s = 0$ is not entirely included in M_*. For instance, $x(t^*) \in M_*$ and $t_r < t^*$ then the trajectory leaves M_* (when the coordinate $x_2(t) > 0, t > t^*$) to reach $S \subset S_-$ of Case 1.

The largest PIS in S_- is thus the union of the set in Case 1 and M_* in Case 2 or (5.33) as demonstrated in Fig. 5.2. □

5.9 Positive Invariance in S_+

In this region the closed-loop system during the reaching phase $s(x) > 0$ is

$$\begin{cases} \dot{x}_1 = x_2 \\ \dot{x}_2 = -\lambda x_2 - bk \end{cases} \tag{5.42}$$

with state variables time solution

$$\begin{cases} x_1(t) = x_{10} + \frac{x_{20} - x_2(t) - bkt}{\lambda} \\ x_2(t) = \frac{-bk}{\lambda} + (x_{20} + \frac{bk}{\lambda}) e^{-\lambda t} \end{cases} \tag{5.43}$$

Theorem 5. *Assuming an ideal sliding mode, the largest PIS in S_+ is S_+*

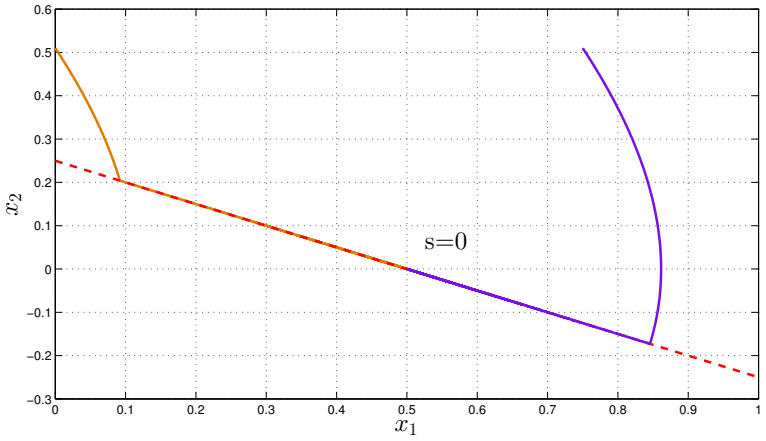

Figure 5.3 Invariance of S_+.

Proof. Following a similar procedure as in Theorem 4, from (5.43) equation $\dot{x}_1(t^{**}) = 0$ is solved at t^{**}:

$$t^{**} = \frac{1}{\lambda} \ln\left(\frac{bk + \lambda x_{20}}{bk}\right) \tag{5.44}$$

The condition for this time to be nonnegative is $x_{20} \geq 0$. This test of the point reveals a maximum i.e. $\ddot{x}_1(t^{**}) < 0$. Here, from (5.42) and (5.43) we have two scenarios in the reaching phase following the initial condition x_{20}:

1. Case1: $x_{20} > 0$ then x_1 will be increasing till x hits the sliding surface to converge to $(x_d, 0)$ at $t \geq t_r$; or the trajectory reaches the maximum before the surface *i.e.* $\dot{x}_1(t^{**}) = 0$ with $t^{**} < t_r$ then the trajectory follows the scenario of case 2.

2. Case2: $x_{20} \leq 0$: this implies that $x_2(t) \leq 0$ according to (5.43). From (5.25) one has $x_1 = 0$ at $x_2 = \lambda x_d > 0$, hence $x_1 \neq 0$ in the region where $x_2 < 0$. As a result, x_1 will decrease (according to (5.42)) but to some strictly positive value and not to zero. Hence, $x_1(t) > 0 \; \forall t < t_r$ and at $t = t_r$ sliding mode occurs.

Therefore $x_1(t) \geq 0$ everywhere in S_+ thus, and according to the reachability condition (5.18), the entire S_+ is a PIS (see Fig. 5.3). □

Using the reachability condition and the fact that S that separates S_+ and S_- is a PIS, the largest closed-loop PIS in $\Omega(C)$ is thus

$$M_+ = M_{s_-} \cup S_+ \tag{5.45}$$

as illustrated in Fig. 5.4. In the following section, λ, k will be designed to yield the largest PIS such that $u \geq 0$ in M_+.

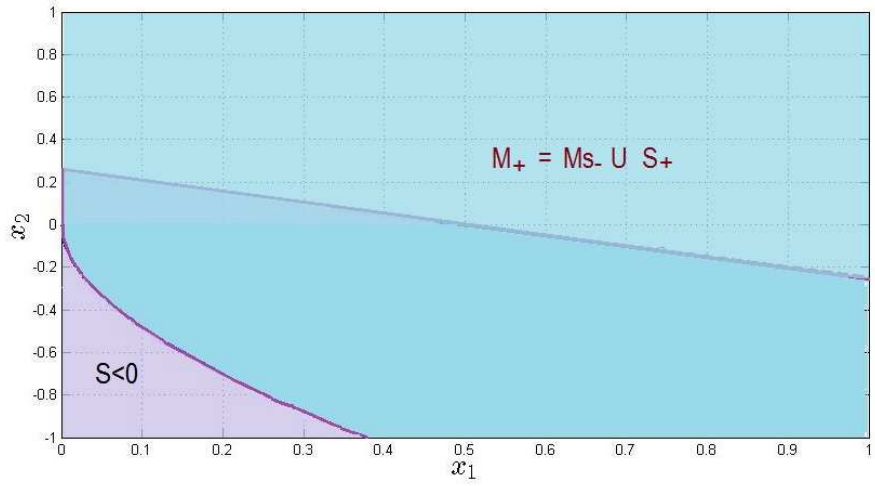

Figure 5.4 The largest PIS: M_+.

5.10 Positive Invariance Under Positive SMC

5.10.1 On the surface S

Firstly, the applied control on S is the equivalent control, that is

$$\dot{s} = 0 \implies u = u_{eq} \tag{5.46}$$

where

$$u_{eq} = \frac{x_2(2\lambda_m - \lambda) + \lambda_m^2 x_1}{b} \tag{5.47}$$

Knowing that during sliding mode $u = u_{eq}$ and thus substituting $s = 0$ in (5.47) yields:

$$u_{eq} = \frac{x_1(\lambda_m - \lambda)^2 + x_d\lambda(2\lambda_m - \lambda)}{b} \tag{5.48}$$

From the above equation it is clear that in the interval $0 < \lambda \leq 2\lambda_m$ is a sufficient condition such that the control action is nonnegative $u = u_{eq} \geq 0$ during sliding mode in the subset S.

Remark 10. *In what follows the sliding surface is designed such that* $0 < \lambda \leq 2\lambda_m$ *to guarantee a positive control in S independently of the point* $x \in M_+$*. This choice leads to the slope* $(-\lambda)$ *of the line* $s = 0$ *is larger than the slope* $(-\frac{\lambda_m^2}{(2\lambda_m - \lambda)})$ *of the line* $u = u_{eq} = 0$*.*

So far, the output/control are nonnegative during sliding mode, next is to investigate the design conditions to ensure the positivity of the control in the reaching phase of the PIS of

S_+ and S_-. Define the following sets where $u \geq 0$ in S_- and S_+ respectively:
• In $S_- \setminus S \quad u = u_{eq} + k$:

$$M_{+k} = \{x \in \{S_- \setminus S\} | x_2 \geq \frac{-bk - \lambda_m^2 x_1}{2\lambda_m - \lambda}\} \tag{5.49}$$

• In $S_+ \setminus S \quad u = u_{eq} - k$:

$$M_{-k} = \{x \in \{S_+ \setminus S\} | x_2 \geq \frac{bk - \lambda_m^2 x_1}{2\lambda_m - \lambda}\} \tag{5.50}$$

With the choice of λ according to Remark 10, SMC is nonnegative on the sliding surface, in M_{+k} and in M_{-k}.

However, whether $M_{+k} \subset S_+$, $M_{-k} \subset M_{s_-}$ or in other words $u \geq 0$ everywhere in the PIS of S_+, S_- respectively is not ensured. Therefore, in the following subsections, the design conditions of the pair (λ, k) are found to yield the largest PIS in S_+, M_{s_-} respectively such that $u \geq 0$.

5.10.2 In the subset S_+

As stated earlier in Theorem 5, the subset S_+ is a PIS. The control is non-negative in the set M_{-k} , but not everywhere in S_+. The following theorem will give necessary conditions such that $u \geq 0$ everywhere in $S_+ \setminus S$ or to have $\{S_+ \setminus S\} \subset M_{-k}$.

Theorem 6. *Assuming* $(0 \leq \lambda \leq 2\lambda_m)$*, the following statements are equivalent:*

1. $\{S_+ \setminus S\} \subset M_{-k}$.
2. $u \geq 0$ *everywhere in* S_+.
3.

$$\lambda_m - \sqrt{\lambda_m^2 - \frac{bk}{x_d}} \leq \lambda \leq \lambda_m + \sqrt{\lambda_m^2 - \frac{bk}{x_d}} \quad , \quad 0 < k \leq \frac{\lambda_m^2 x_d}{b}. \tag{5.51}$$

Proof. According to Remark 10, during sliding mode $u = u_{eq} > 0$ in S and hence it remains to show that $u = (u_{eq} - k) \geq 0$ in $\{S_+ \setminus S\}$. From Remark 10 the slope (-λ) of the line $s = 0$ is larger than the slope $-\frac{\lambda_m^2}{(2\lambda_m - \lambda)}$ of the line $u = 0$ i.e. $\lambda < \frac{\lambda_m^2}{(2\lambda_m - \lambda)}$. Thus, if the following holds

$$(u_{eq} - k)\Big|_{x_1=0} \leq s\Big|_{x_1=0} \tag{5.52}$$

then $\{S_+ \setminus S\} \subset M_{-k}$ or $u \geq 0$ everywhere in S_+ as illustrated in Fig. 5.5.

(5.52) means that the point of intersection of the line $s = 0$ with the x_2-axis is higher than the point of intersection of $u_{eq} - k = 0$ with x_2-axis i.e.:

$$\frac{bk}{2\lambda_m - \lambda} \leq \lambda x_d \tag{5.53}$$

this yields the quadratic polynomial

$$P(\lambda) = \lambda^2 - 2\lambda\lambda_m + \frac{bk}{x_d} \leq 0 \tag{5.54}$$

for real λ then the discriminant is nonnegative: $\Delta = \lambda_m^2 - \frac{bk}{x_d} \geq 0$ or

$$k \leq \frac{\lambda_m^2 x_d}{b} \tag{5.55}$$

also $P(\lambda)$ has the following roots

$$\lambda_{1,2} = \lambda_m \pm \sqrt{\lambda_m^2 - \frac{bk}{x_d}} \tag{5.56}$$

and as $P(\lambda) = 0$ at $\lambda = \lambda_1$ or $\lambda = \lambda_2$, then $P(\lambda) \leq 0$ or (5.53) holds if and only if

$$\lambda_m - \sqrt{\lambda_m^2 - \frac{bk}{x_d}} \ \leq \lambda \leq \ \lambda_m + \sqrt{\lambda_m^2 - \frac{bk}{x_d}} \tag{5.57}$$

therefore, the pair (k, λ) satisfying (5.51) leads to a nonegative control everywhere in S_+.

□

For graphical illustration, see Fig. 5.7. The set M_{-k} is everywhere above the line $u_{eq} - k = 0$.

5.10.3 In the subset S_-

The largest PIS in M_{s_-} such that $u \geq 0$ will be found here using the results of (5.51). It will be shown that the previous design constraints on λ in (5.51) do provide a nonnegative control everywhere in M_{s_-} with additional constraint on the gain k.

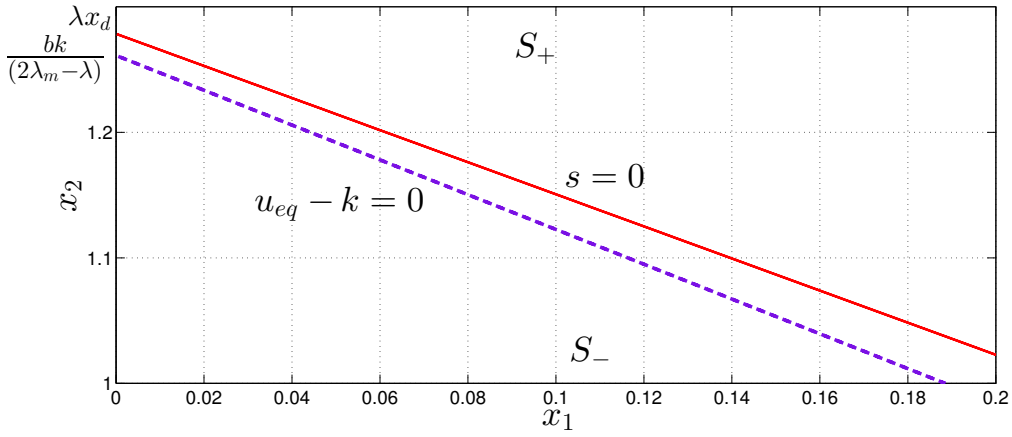

Figure 5.5 The lines $u_{eq}-k=0$ (u=0 in S_+) with respect to the line $s=0$ for a nonnegative control in S_+, with $\lambda_m=1, \lambda=1.2785$ and $k=0.91$.

Theorem 7. *Assuming* (5.51) *then* $u \geq 0$ *everywhere in* M_{s-} *if and only if*

$$1.2785\lambda_m < \lambda \leq \lambda_m + \sqrt{\lambda_m^2 - \frac{bk}{x_d}}, \quad 0 < k \leq 0.9224\frac{x_d\lambda_m^2}{b} \tag{5.58}$$

Proof. As stated earlier $u = u_{eq} > 0$ in S. Thus, in what follows the positivity of the control during the reaching phase is considered i.e.when $u = u_{eq} + k$.

- Case 1: $x \in M_{s_-}, x_2 > 0$
  In this case $u_{eq} \geq 0$ hence, $u = (u_{eq} + k) \geq 0$.

- Case 2: $x \in M_{s_-}, x_2 \leq 0$
  Here, to yield $u \geq 0$ everywhere in M_{s_-} i.e. $M_{+k} \subset M_{s_-}$, design k and λ, satisfying (5.51), such that the line $u = u_{eq} + k = 0$ and the trajectory limiting the set M_* in (5.34) do not intersect. For this purpose, from (5.34) define $f_1(x_2) = -\left(\frac{bk}{\lambda^2}\ln(\frac{bk-\lambda x_2}{bk}) + \frac{x_2}{\lambda}\right)$ and using (5.49) define $f_2(x_2) = \frac{\lambda-2\lambda_m}{\lambda_m^2}x_2 - \frac{bk}{\lambda_m^2}$ and then $F(x_2) \triangleq f_1(x_2) - f_2(x_2) = 0$.

$$F(x_2) = -\frac{bk}{\lambda^2}\ln(\frac{bk-\lambda x_2}{bk}) - x_2\left(\frac{1}{\lambda} + \frac{\lambda-2\lambda_m}{\lambda_m^2}\right) + \frac{bk}{\lambda_m^2} \tag{5.59}$$

  If an intersection exists then $F(x_2) = 0$ has a solution, thus find $x_2 \leq 0$ solving $F(x_2) = 0$. To simplify the search of the solution (if any), note that $F(0) = \frac{bk}{\lambda_m^2} > 0$,

$\lim_{x_2\to-\infty} F(x_2) = +\infty$ and also note that

$$\frac{\mathrm{d}F(x_2)}{\mathrm{d}x_2} = \frac{bk}{\lambda(bk-\lambda x_2)} - \frac{1}{\lambda} + \frac{2\lambda_m-\lambda}{\lambda_m^2} \tag{5.60}$$

$\frac{\mathrm{d}F(x_2)}{\mathrm{d}x_2}|_{x_2=0} = \frac{2\lambda_m-\lambda}{\lambda_m^2} > 0$, $\lim_{x_2\to-\infty} \frac{\mathrm{d}F(x_2)}{\mathrm{d}x_2} = -\frac{(\lambda-\lambda_m)^2}{\lambda\lambda_m^2} < 0$. This reads that $F(x_2)$ has a minimum point and as the initial and final values of $F(x_2)$ are both positive, then if $\min_{x_2\leq 0}(F(x_2)) > 0$ the intersection between f_1, f_2 does not exist. This means that as $u \geq 0$ everywhere in M_{s_-}, thus the aim now is not to find a solution $x_2 \leq 0$ such that $F(x_2) = 0$, but rather to ensure $\min_{x_2\leq 0}(F(x_2)) > 0$. At the minimum point $\frac{\mathrm{d}F(x_2)}{\mathrm{d}x_2} = 0$, one has:

$$x_2 = bk\frac{\lambda-2\lambda_m}{(\lambda-\lambda_m)^2} \tag{5.61}$$

which is a unique solution i.e. the minimum point is global. In order to verify whether $\min(F(x_2)) > 0$ substitute (5.61) in (5.59) which yields:

$$\min(F(x_2)) = -\frac{bk}{\lambda^2}\ln\Big(1-\frac{\lambda^2-2\lambda\lambda_m}{(\lambda-\lambda_m)^2}\Big) - bk\frac{(\lambda-2\lambda_m)}{\lambda\lambda_m^2} + \frac{bk}{\lambda_m^2} \tag{5.62}$$

$$\min(F(x_2)) > 0 \iff -\frac{(\lambda-2\lambda_m)}{\lambda\lambda_m^2} + \frac{1}{\lambda_m^2} > \frac{1}{\lambda^2}\ln\Big(\frac{\lambda_m^2}{(\lambda-\lambda_m)^2}\Big) \tag{5.63}$$

using the property $\ln(\frac{a}{b})^n = n\ln(\frac{a}{b})$:

$$\frac{\lambda}{\lambda_m} > \ln\Big|\frac{\lambda_m}{\lambda-\lambda_m}\Big| \tag{5.64}$$

which can be rewritten as

$$\frac{\lambda}{\lambda_m} > \ln\Big|\frac{1}{\frac{\lambda}{\lambda_m}-1}\Big| \tag{5.65}$$

or

$$\Big|\frac{\lambda}{\lambda_m}-1\Big| e^{\frac{\lambda}{\lambda_m}} > 1 \tag{5.66}$$

As illustrated in Fig. 5.6, equation (5.66) is satisfied only when $\frac{\lambda}{\lambda_m} > 1.2785$ and comparing this new constraint with (5.51):

$$\frac{\lambda}{\lambda_m} > 1.2785 \text{ and } 1-\frac{\sqrt{\lambda_m^2-\frac{bk}{x_d}}}{\lambda_m} \leq \frac{\lambda}{\lambda_m} \leq 1+\frac{\sqrt{\lambda_m^2-\frac{bk}{x_d}}}{\lambda_m} \tag{5.67}$$

and as $1-\frac{\sqrt{\lambda_m^2-\frac{bk}{x_d}}}{\lambda_m} < 1.2785$ then

$$1.2785 < \frac{\lambda}{\lambda_m} \leq 1+\frac{\sqrt{\lambda_m^2-\frac{bk}{x_d}}}{\lambda_m} \tag{5.68}$$

which implies $1.2785 \leq 1+\frac{\sqrt{\lambda_m^2-\frac{bk}{x_d}}}{\lambda_m}$ and hence $k \leq 0.9224\frac{x_d\lambda_m^2}{b}$ yielding (5.58).

□

Using the results of Theorems 6 and 7, SMC designed in (5.58) is nonnegative everywhere in M_+.

See Fig. 5.8 for a graphical illustrative example. The region above the lines $u_{eq}+k=0$ and $u_{eq}-k=0$ represents M_{+k} and M_{-k} respectively. The trajectory in orange passing through the subset S_- is the one that characterizes the PIS M_{s-}. As shown, λ satisfies (5.58) ensures a positive control everywhere in M_+. Whereas, as shown in Fig. 5.7, the value of λ satisfies only (5.51) thus ensures a nonnegtaive control everywhere in S_+ but not in M_{s-} as the red region represents $x \in M_{s\_}$ and $u<0$. The parameters λ_m, b, x_d in the figures are taken to simplify the example and its illustrations.

Remark 11. *The admissible λ that satisfies the positivity constraints in* (5.58) *is within the interval* $1.2785\lambda_m < \lambda \leq \lambda_m+\sqrt{\lambda_m^2-\frac{bk}{x_d}} < 2\lambda_m$. *As a result, the closed-loop eigenvalue is larger than that of the open-loop yielding a relatively faster time response.*

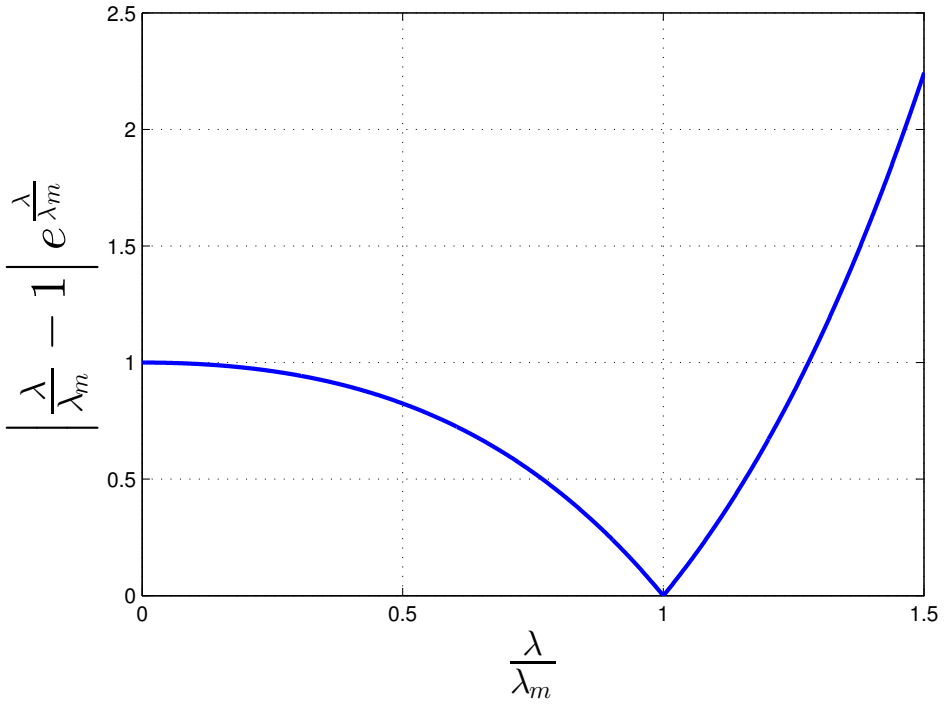

Figure 5.6 $\left|\frac{\lambda}{\lambda_m} - 1\right| e^{\frac{\lambda}{\lambda_m}} > 1$ only when $\frac{\lambda}{\lambda_m} > 1.2785$.

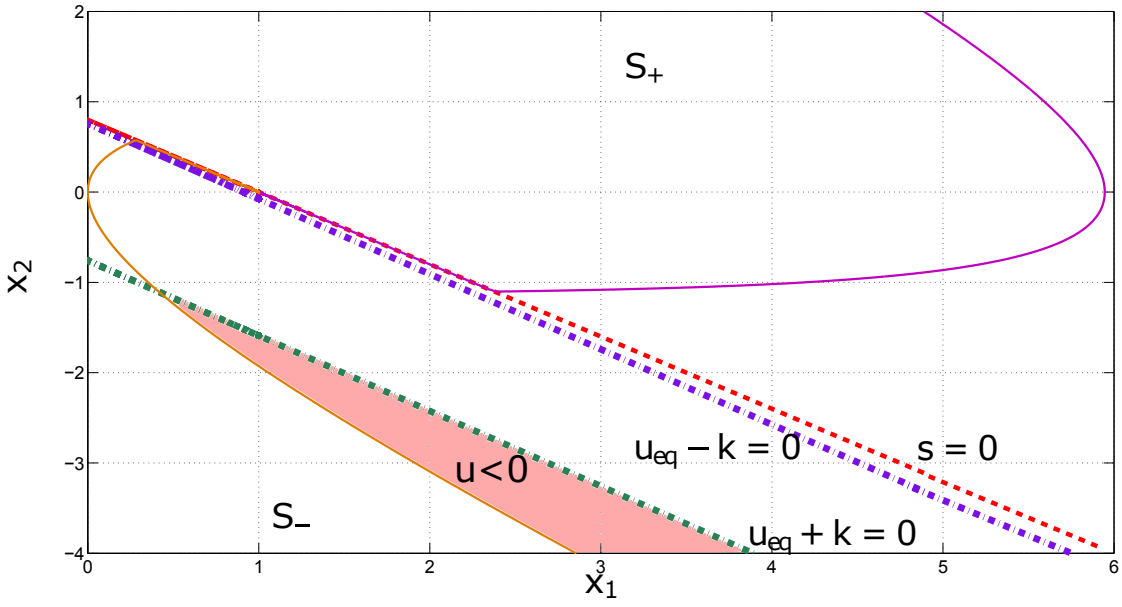

Figure 5.7 Phase plane plot: with $\lambda = 0.8$ satisfying (5.51) i.e. $0.7 < \lambda < 1.3$ but not satisfying (5.58), with $k = 0.91$, $x(0) = (\bar{x}_{10}, -6), \bar{x}_{10} = 4.8887$ for the (bounding) trajectory in S_-. $x(0) = (4.8887, 2)$ for the trajectory in S_+.

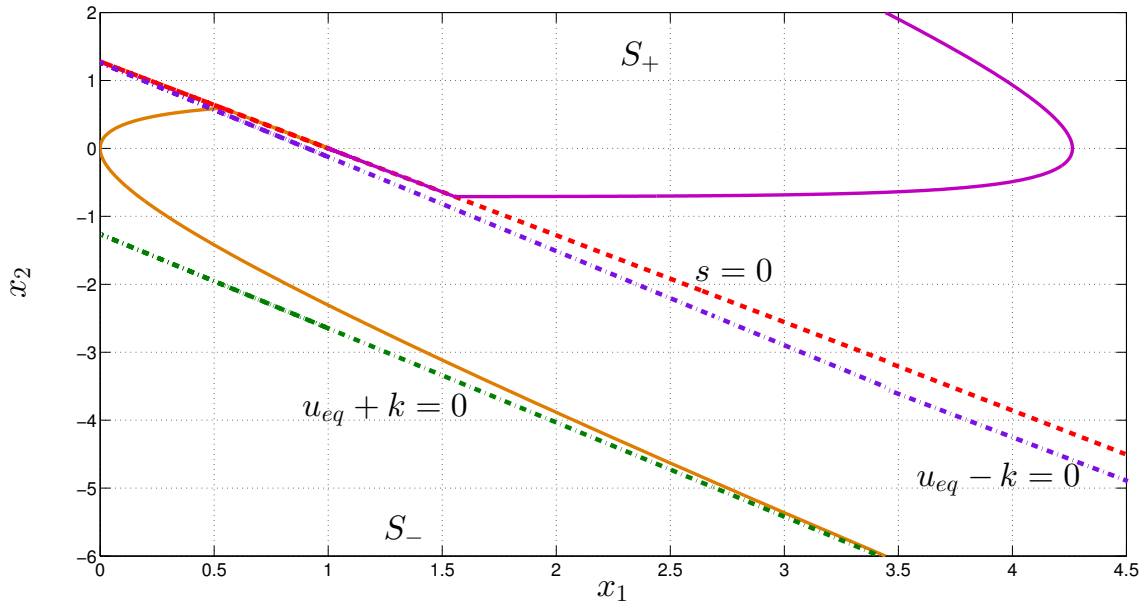

Figure 5.8 Phase plane plot: with $\lambda = 1.2785$ satisfying (5.58), with $k = 0.91$, $x_(0) = (\bar{x}_{10}, -6), \bar{x}_{10} = 3.4438$ for the (bounding) trajectory in S_- , and $x(0) = (3.4438, 2)$ for the trajectory in S_+.

Remark 12. *SMC is a discontinuous controller with high frequency switching frequency in the neighborhood of $s = 0$ known as the chattering phenomenon. To reduce the high frequency chattering, the sharp discontinuous sign function will be replaced by the following smoother sigmoid-like function as suggested often in the literature of SMC (see for instance [98])*

$$\sigma(s) = \frac{s}{\varepsilon + |s|} \tag{5.69}$$

where ε is a small positive scalar and $\lim_{\varepsilon \to 0} \sigma(s) = sign(s)$.

5.11 Glycemia System

The overall system glycemia-insulinemia system (3.17) is a cascade of the second order insulinemia subsystem and the first order glycemia subsystem (see Fig. 3.5). In this manner, the glycemia regulation problem may be split into the decoupled stabilization problems of the two subsystems. As detailed in the previous sections, the first control problem was to stabilize the error $e(t)$ between the insulinemia x_1 and its desired value x_d via positive SMC under positive insulin constraint. The controlled plasma insulin is applied to regulate blood

glucose $G(t)$. In fasting phase glycemia dynamics is described in (3.17) as:

$$\dot{G}(t) = -k_{si}x_1(t) + \theta_1 \tag{5.70}$$

θ_1 as defined in (3.20). In this section a second sliding mode control (SMC2) is designed to choose the insulin level $x_1(t) = x_d$ such that

$$s_1(t) \triangleq G(t) - G_r = 0 \tag{5.71}$$

where s_1 is the new sliding variable and G_r is the desired glycemia level which is often taken to be G_r =120 mg/dL. In other words, the objective of SMC2 is to design x_d as the new sliding mode virtual controller such that $s_1 = 0$ i.e.

$$\dot{s}_1 = -k_{si}x_d + \theta_1 \tag{5.72}$$

Hence, following the classic SMC design procedure and using a Lyapunov function $V_1 = \frac{1}{2}s_1\dot{s}_1$, design a suitable positive $x_d > 0$ such that $s_1\dot{s}_1 < 0$. x_d is then the reference input for SMC1 to control insulin subsystem as illustrated in Fig. 5.9.

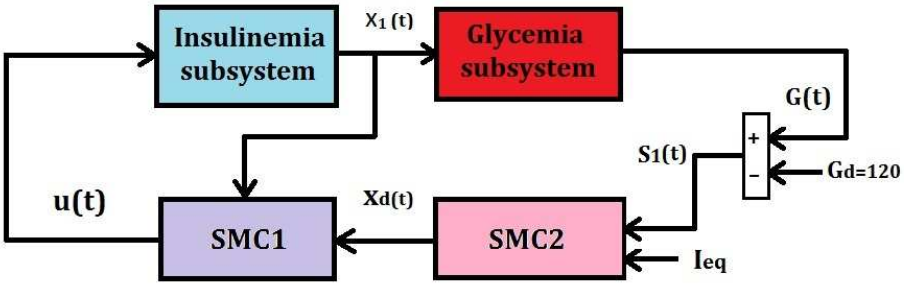

Figure 5.9 A block diagram of the overall SMC controlled system.

From (5.70) and (5.71) yields

$$s_1\dot{s}_1 = s_1(-k_{si}x_d + \theta_1) < 0 \tag{5.73}$$

using the basal plasma insulin defined in (3.36): $I_{eq} = \frac{\theta_1}{K_{si}}$, x_d is designed to verify (5.73) as follows

$$x_d = I_{eq} + k_1 \text{sign}(s_1) \tag{5.74}$$

where $k_1 > 0$. Therefore, the objective of the SMC1 control $u(t)$, as explained earlier, is to reach $s = 0$ and then asymptotically direct $x_1(t)$ to x_d given in (5.74). As x_d is designed via SMC2 above to ensure that (5.73) holds and then to achieve $s_1 = 0$

5.11.1 Positivity of x_d and Choice of k_1

- $s_1 = 0$ i.e. at the equilibrium then $x_d = I_{eq} > 0$
- $s_1 > 0$ or hyperglycemia region then $x_d = (I_{eq} + k_1) > 0$ for any $k_1 > 0$.
- $s_1 < 0$ or hypoglycemia region, to have $x_d > 0$ then $k_1 < I_{eq}$.

As a result, $k_1 < I_{eq}$ is the lower bound to ensure that the desired plasma insulin value is positive. Moreover, the constraint on the gain k given in (5.58) will take this lower bound into account setting $x_d = I_{eq} - k_1$ i.e.

$$0 < k \leq 0.9224 \frac{(I_{eq} - k_1)\lambda_m^2}{b} \tag{5.75}$$

Remark 13. *Taking $k_1 < I_{eq}$ is sufficient to have $x_d > 0$ for any s_1. However, this gain value in times of hyperglycemia ($s_1 >> 0$) yields $x_d = (I_{eq} + k_1) < 2I_{eq}$ which yield a relatively slow convergence of BG to its normal level (see the insulin injections of T1D patients in [58]). Therefore, the switching gain k_1 needs to be adapted according to the switching region to yield a sufficiently high insulin reference value when $G > G_r$ and thus a faster response.*

5.12 Variable Discontinuity Gain k_1

To obtain a sufficiently fast glycemic response, the gain k_1 is chosen to be proportional to the offset $G - G_r$ when $s_1 > 0$ i.e. the switching function is adapted as follows

$$\begin{cases} \text{If} \quad s_1 > 0 \quad \text{then} \quad x_d = I_{eq} + k_o s_1 \\ \text{If} \quad s_1 \leq 0 \quad \text{then} \quad x_d = I_{eq} + k_1 \text{sign}(s_1), \quad k_1 < I_{eq} \end{cases} \tag{5.76}$$

where k_o[U/mg]> 0 is a proportional gain. The gain k_1 is constant and $x_d > 0$ when $s_1 \leq 0$ as explained in section 5.11.1. In this manner $s_1 > 0$ leads to a variable reference value: $x_d(s_1) = I_{eq} + k_o(G - G_r)$ and the insulin sliding surface in this case $s = x_2 + \lambda(x_1 - x_d(s_1))$ is not a line but rather a trajectory as will be shown in the simulation results section. Therefore, if glycemia level is below the desired level $s_1 < 0$ then the desired insulin is less than the basal $x_d = (I_{eq} - k_1) < I_{eq}$ which permits the glycemia to grow due to the endogenous production

(for details see [58]). Moreover, in case $G = G_r$ then the insulin is steered to the basal $x_d = I_{eq}$ to maintain glycemia at that value.

In the following section, the gain k_o is designed such that the reachability condition of the surface s is verified when the new variable reference $x_d(s_1)$ is applied i.e. when $s_1 > 0$.

5.12.1 Reachability of s for $x_d = I_{eq} + k_o s_1$

In the region $s_1 \leq 0$ the desired insulin value x_d is a constant and the previous design analyses of s and k, λ of the first SMC hold. In the case where $s_1 > 0$ then the sliding surface s becomes

$$s = x_2 + \lambda(x_1 - (I_{eq} + k_o s_1)) \tag{5.77}$$

and the reachability condition $s\dot{s} < 0$ with u as described in (5.15) and (5.16) is thus

$$s(-k\text{sign(s)} - \lambda k_o \dot{s}_1) = -(k|s| + \lambda k_o s \dot{s}_1) < 0 \tag{5.78}$$

with $k_o > 0$ the surface s is reachable if $(k|s| + \lambda k_o s \dot{s}_1) > 0$, and the case where $s\dot{s}_1 \geq 0$ directly verifies the reachability condition as k, k_o and λ are positive scalars. Otherwise, the case when $s\dot{s}_1 < 0$ is studied for given λ and k as follows:

- Case1: $\dot{s}_1 > 0, s < 0$: hence from (5.78) $s\dot{s} < 0$ implies

$$k|s| - \lambda k_0 |s| \dot{s}_1 > 0 \tag{5.79}$$

and hence

$$k_o < \frac{k}{\lambda \max|\dot{s}_1|} \tag{5.80}$$

and from (5.70) and $I_{eq} = \frac{\theta_1}{K_{si}}$ then $\dot{s}_1 > 0$ or $\dot{G} > 0$ means that $x_1 < I_{eq}$ and thus $\max(\dot{s}_1) = \lim_{x_1 \to 0} \dot{G} = \theta_1$.

- Case2: $\dot{s}_1 < 0, s > 0$: setting $|\dot{s}_1| = -\dot{s}_1$ in (5.78) leads also to (5.80). However, $\dot{s}_1 < 0$ and (5.70) imply $x_1 > I_{eq}$ and thus $\max|\dot{s}_1|$ depends on the maximum registered plasma insulin level. For instance as presented in [58], the highest plasma insulin among the five clinical data, as interpreted by the model, is $\max(x_1) = 0.01$ U/dL. For this example, (5.70) leads to $\max|\dot{s}_1| = |-0.01 k_{si} + \theta_1|$.

Therefore, $\max(\max|\dot{s}_1|)$ is obtained from case 2 when $\dot{s}_1 < 0$ due to

$$(\max|\dot{s}_1|)\Big|_{(x_1 > I_{eq})} > \theta_1 \geq (\max|\dot{s}_1|)\Big|_{(x_1 < I_{eq})} \tag{5.81}$$

In this manner, denoting $\bar{x}_1 = \max(x_1 > I_{eq})$ then $\max|\dot{s}_1(\bar{x}_1)|$ is used in (5.80) to obtain the lower bound of k_o .

5.12.2 The set M_+

Bearing in mind that the state solution (5.43) and (5.32) are not affected by the choice of x_d and consequently Theorems 5 and 4 hold and the largest PIS M_+ is not affected by the choice of $x_d > 0$.

5.12.3 Is $u \geqslant 0$ in The set M_+

In the case $s_1 > 0$ where the desired insulin is variable $x_d(s_1)$, it can be shown that the previous design of k, λ such that $u(t) \geq 0$ for a constant x_d holds also for $x_d = I_{eq} + k_o s_1$. First of all, the control law in (5.15) has not changed and it is still positive during sliding mode i.e. $s = 0$ implies that $u = u_{eq}$ in (5.48) which is positive in M_+ by simply taking $\lambda < 2\lambda_m$. Secondly, the design conditions in the region $s > 0$ when x_d was a constant (e.g. $x_d = (I_{eq} + k_o s_1)\Big|_{s_1=0}$) are re-verified. As shown in section 5.10.2 the parameters k, λ are designed such that $u \geq 0$ everywhere in $S_+ \setminus S$ or

$$s > u > 0 \equiv -\lambda(x_1 - x_d) > \frac{bk - \lambda_m^2 x_1}{2\lambda_m - \lambda} \tag{5.82}$$

When $x_d = (I_{eq} + k_o s_1)\Big|_{s_1>0}$ then $s > 0$ is equivalent to $x_2 > -\lambda(x_1 - I_{eq}) + \lambda k_o s_1$, thus,

$$s\Big|_{s_1>0} > s\Big|_{s_1=0} > u > 0 \tag{5.83}$$

As a result, the design conditions on k and λ in (5.51) yielding a nonnegative control when $x_d = I_{eq}$ hold also for $x_d = I_{eq} + k_o s_1$. These design conditions ensure $\lambda < 2\lambda_m$ and hence a positive control during sliding in the subset S. The final design conditions given by (5.58), which yielded starting from (5.51) to ensure a positive control in M_{s_-}, hold also since they do not depend on x_d but rather on k and λ. Consequently, $u \geq 0$ everywhere in M_+ with $x_d = I_{eq} + k_o s_1$.

5.13 Numerical Simulation Results

In this section, SMC is designed and applied on five virtual patients whose parameters are given in [58]. The control parameters are designed to fulfill the conditions (5.58) and (5.75)

and (5.80):

$$k = 0.88k_{max},\ k_1 = 0.3I_{eq} \tag{5.84}$$

$$\lambda = 0.9\lambda_{max} > 1.2785\lambda_m,\ k_o = 0.014I_{eq} < k_{o_{max}} \tag{5.85}$$

$k_{max} = (0.9224\frac{x_d\lambda_m^2}{b})$, $\lambda_{max} = \lambda_m + \sqrt{\lambda_m^2 - \frac{bk}{x_d}}$ with $x_d = I_{eq} - k_1$ according to (5.75), $k_{o_{max}} = \frac{k}{\lambda \max|\dot{s}_1(\bar{x}_1)|}$, $\bar{x}_1 = 0.025$ U/dL. As stated in Remark 12, to avoid the chattering phenomenon in the control signal, the signum function for the insulin subsystem is replaced by the sigmoid-like function in (5.69) with $\varepsilon = (1 \times 10^{-4})I_{eq}$.

The first simulation starts with hyperglycemia initial condition $G(0) = 250$ mg/dL and $x_1(0) = 9.7 \times 10^{-4}$U/dL $x_2(0) = 0.1 \times 10^{-4}$ U/(dL.min). The benefit of taking $x_d = I_{eq} + k_o s_1$ is that it is supposed to be larger than if one would take a fixed gain $x_d = I_{eq} + k_1, k_1 < I_{eq}$ as explained in Remark 13. This advantage appears when $s_1 >> 0$, for instance, as illustrated in Fig. 5.10 (a)-(b), at $t = 0$ glycemia offset is $s_1 = 130$ mg/dL and $x_d = 23 \times 10^{-4} > 2I_{eq}$ U/dL knowing that $I_{eq} = 8.04 \times 10^{-4}$ U/dL. The control $u(t)$ is positive the entire time as illustrated in panel (c) of Fig. 5.10. Fig. 5.10 (d) illustrates the phase portrait in the $x_1 - x_2$ plane and how the trajectory slides on the new surface $s(x, x_d(s_1))$. It is good to notice that increasing the gain k_o leads to a faster glycemia response but the resulting trajectory x_d will be faster for the state x_1 to follow as depicted in Fig. 5.11 (a)-(b). As a matter of fact, it is a compromise between glycemia behavior/response time and insulinemia reference tracking.

The second test is performed on patient BE with $G(0) = 70$ mg/dL and $x_2(0) = -0.1 \times 10^{-4}$U/(dL.min) and $x_1(0) = 1.75 \times 10^{-4}$U/dL satisfying (5.40) i.e. on the edge of the the set $M_{s\_}$. In this case where $s_1 < 0$ a constant desired insulinemia $x_d = I_{eq} + k_1 \text{sign}(s_1)$ is applied according to (5.76) and as shown in Fig. 5.12 (a)-(c). As a result the sliding surface is composed of two straight lines depending on x_d as illustrated in Fig. 5.12-(d).

For IF3 patient, the test starts with hypoglycemia $G(0) = 50$ mg/dL and $x_1(0) = 20 \times 10^{-4}$ U/dL, $x_2(0) = 0$ U/(dL.min). In this case the controller administers two different insulin rates based on $x_d(s_1)$, the first is less than the basal injection rate $u = 0.014 < u_b$ U/min. (recall (3.37)) which permits glycemia to augment as a consequence of the endogenous liver production (see (5.70)). Finally, when $G = 120$ mg/dL the injected insulin is the rate that maintains the equilibrium $u = u_b = 0.012$ U/min.

5.14 Conclusion

Positivity analyses of the insulin model presented in [58] was studied in this chapter for the open and closed-loop system. Plasma insulin state is nonnegative in nature, but math-

ematically the second-order model is not positive. For that purpose, the set of points of the second-order model where the plasma insulin is nonnegative was firstly found. It is the largest open-loop PIS that can be defined as the feasible set of initial conditions where the model correctly describes the input-free response of the biological system. Secondly, sliding mode control with constraints of positivity is designed for insulinemia system to regulate the plasma insulin to some desired value. The largest PIS where the plasma insulin variable is nonnegative under SMC was found. Thereafter, the positivity of SMC was ensured everywhere in this set via the design of k and λ. The additional positive input constraint does not reduce the largest closed-loop PIS.

As the plasma insulin is the input state variable to the glycemia subsystem, it was considered as a virtual control variable to regulate glycemia. Thus, the error between blood glucose measurement and its desired constant value was regulated by a second sliding mode controller (SMC2) which is a virtual insulin variable. The virtual controller was designed to be the adequate reference insulin $x_d > 0$ to eliminate glycemia error $s_1 = 0$. The designed virtual controller x_d was used as a desired reference input for SMC1 block. The control effort of SMC1 or $u(t)$ is directed to reach $s = 0$ and then to force $x_1(t) = x_d$. It was shown also that a variable reference trajectory $x_d(s_1,t) > 0$ during hyperglycemia is also a viable solution to yield a relatively faster glycemia response compared to a constant set point. The simulation is made on virtual patients derived from real life clinical data. The simulation results demonstrated the validity and the efficiency of the proposed theoretical results. Positive SMC to regulate glycemia has shown a satisfactory results in terms of following the insulin designed target and regulating glycemia to normal levels without hypoglycemic episodes. The gain of SMC2 is chosen to achieve the trade off between a relatively fast glycemic behavior and avoiding hypoglycemic events. It was noticed that the overall system response was rather slow even though the design parameters of SMC1 were set to their maximum admissible limit to maintain a positive control. This is an expected consequence of designing a positive control instead of applying an unconstrained controller and arbitrarily saturating it to zero or to turning it off whenever it goes negative. Moreover, for this class of systems where a nonnegative control is the only admissible input, even if the output response was rather slow to attain the target, the situation remains under control. In other words, it is always possible to inject a supplementary dose (e.g. a small bolus) to solve the problem. This is actually an important factor as it means that the system is under the admissible control and the risk of hypoglycemia due to overdosing is reduced.

5.15 Perspectives

The following points are worth considering as future work to the presented positive SMC for glycemia regulation of T1D patients:

1. Meal perturbations or the postprandial phase and its influence on the largest closed-loop PIS is to be studied.

2. Positivity analyses for glycemia state variable is to be investigated to find the largest PIS under nonnegative SMC control. In other words, to find by which means the region where $s_1 < 0$ can be reduced for the purpose of lowering the risk of hypoglycemia.

3. Model uncertainties and measurement noise and how they affect the largest PIS and the positivity of the controller.

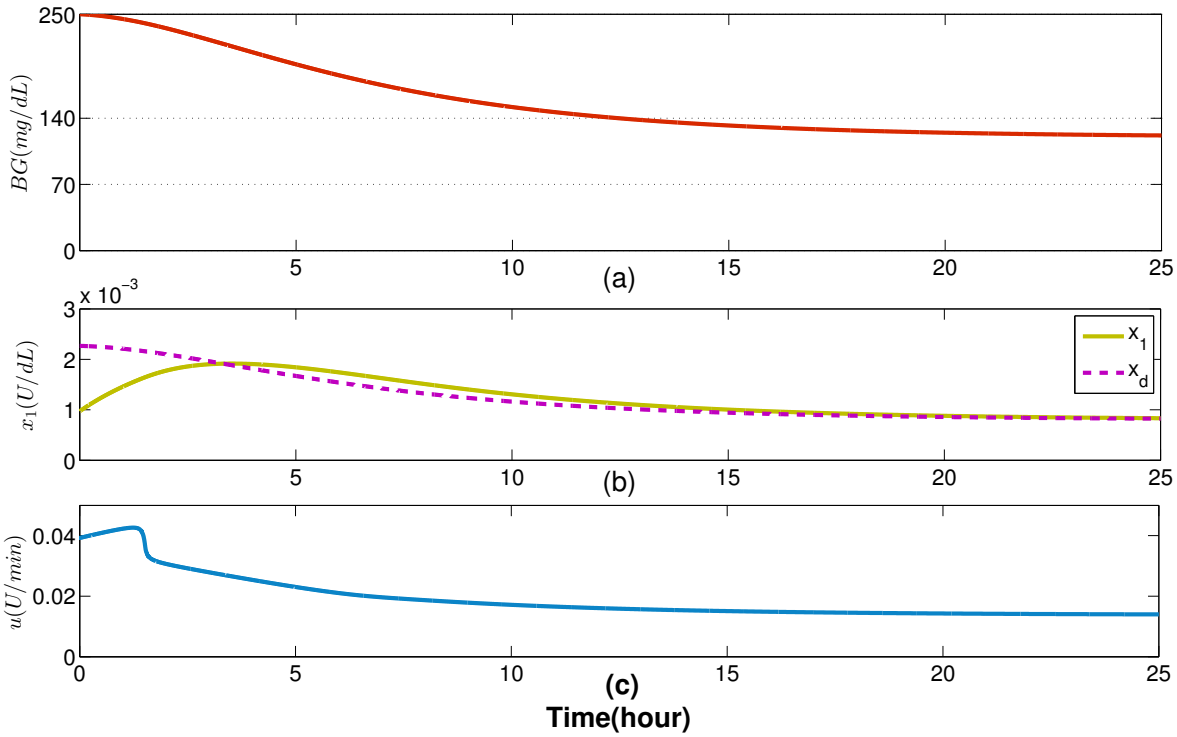

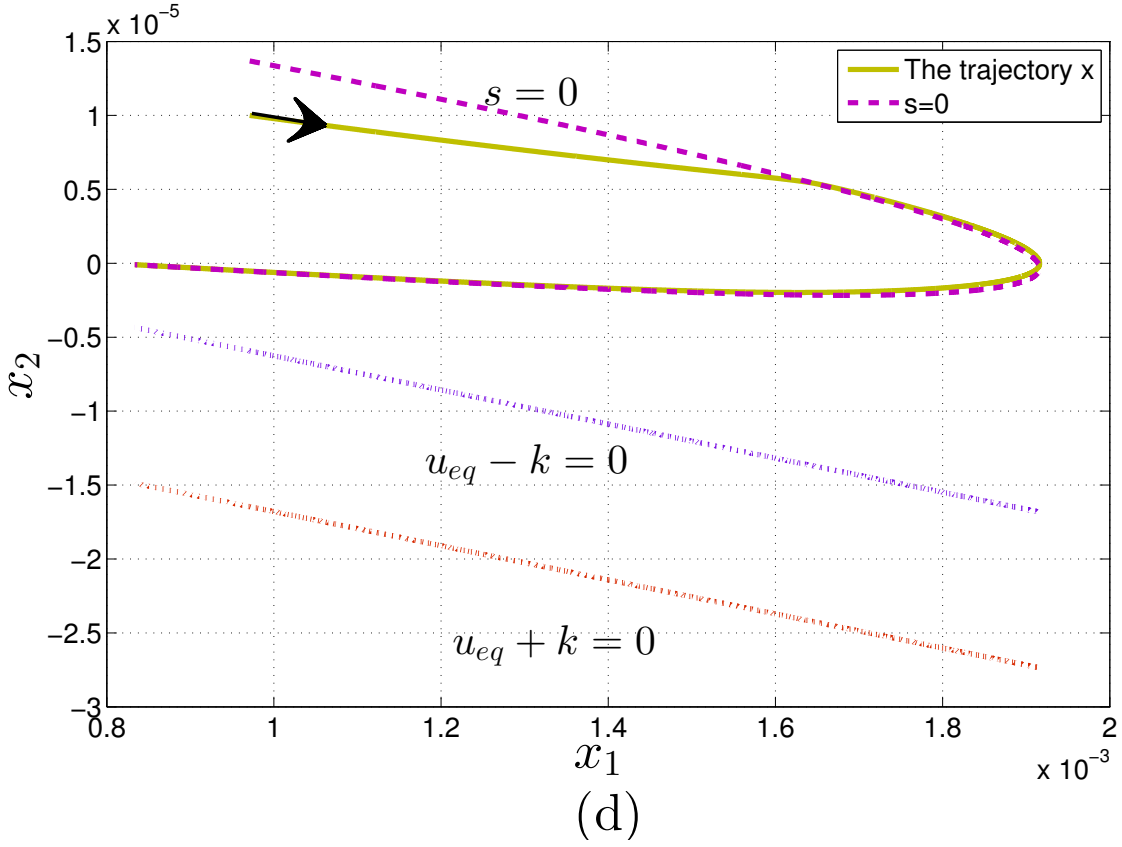

Figure 5.10 Glycemia response of IF2 under SMC, $k_o = 0.014 I_{eq}$. (a): BG behavior. (b): insulinemia versus its desired trajectory $x_1(t)$ and $x_d(t)$. (c): SMC control. (d):phase plane of insulin x_1, x_2 of patient labeled IF2 showing the sliding surface $s = 0$ and the control lines $u = 0$ in $s > 0$ and $s < 0$.

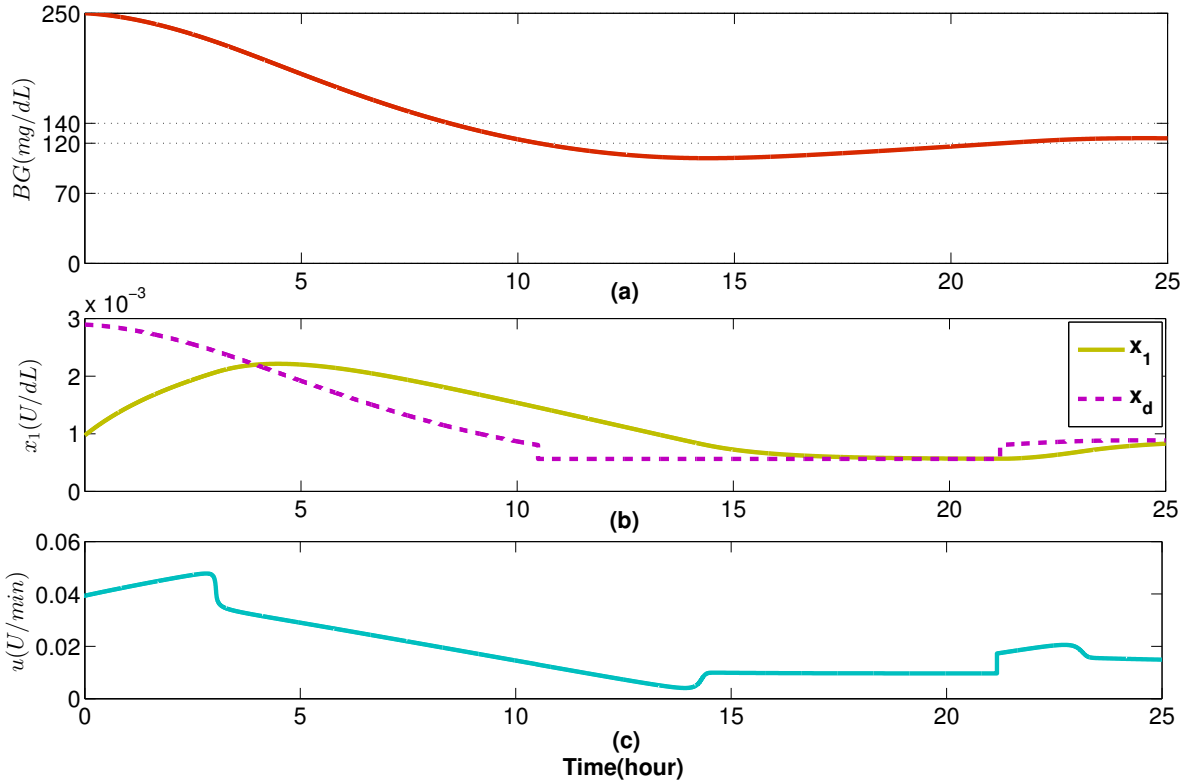

Figure 5.11 Glycemia response of IF2 under SMC, $k_o = 0.02I_{eq}$. (a): BG behavior. (b): insulinemia versus its desired trajectory x_1 and x_d. (c): SMC control.

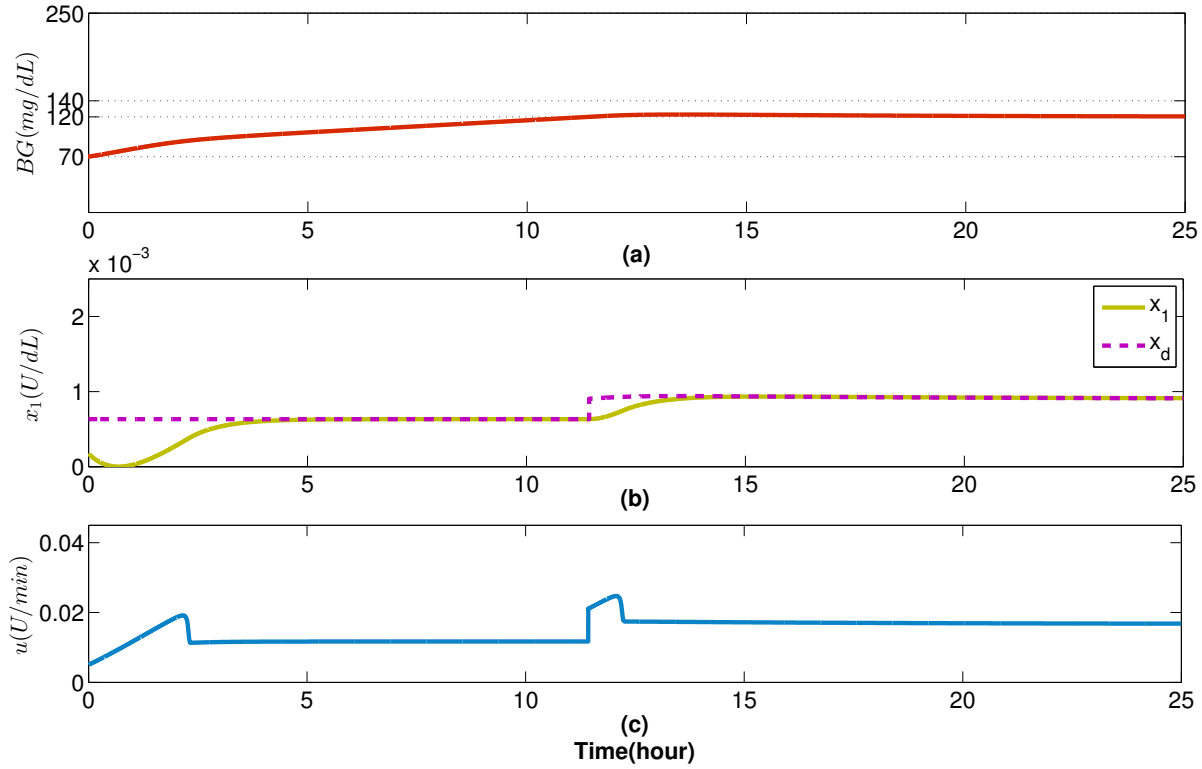

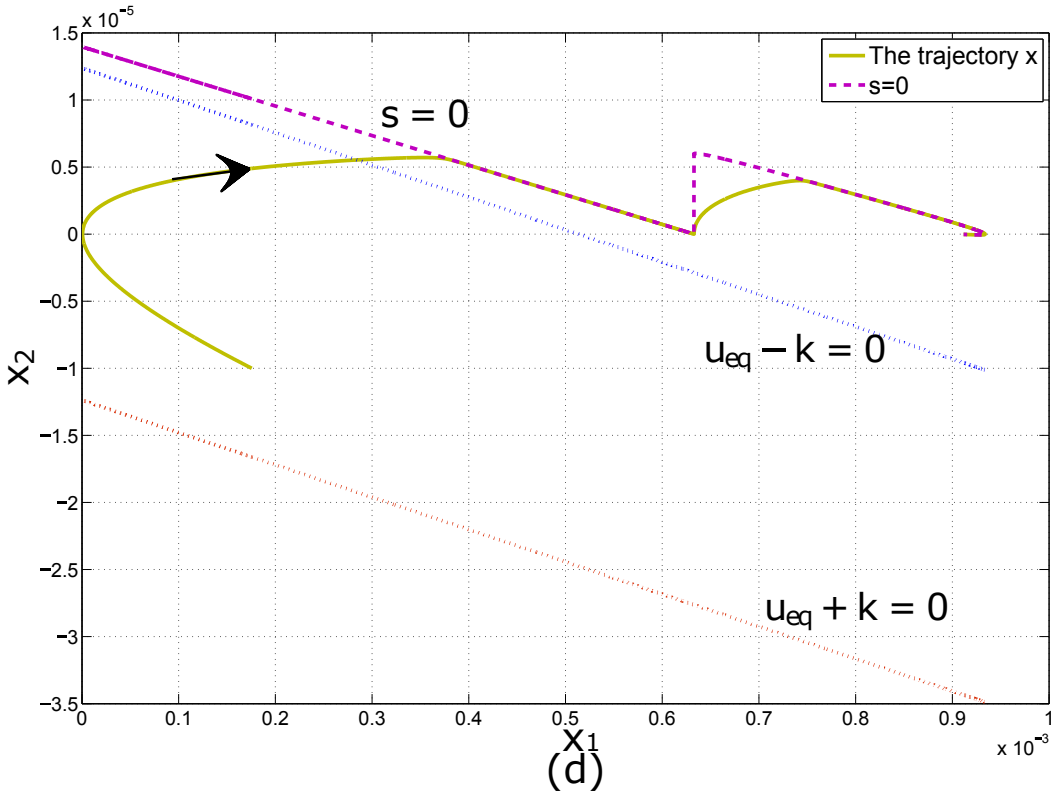

Figure 5.12 Glycemia response of BE under SMC. (a): BG behavior. (b): insulinemia versus its desired trajectory x_1 and x_d. (c): SMC control. (d): Phase plane of insulin x_1, x_2 of patient labeled BE showing the sliding surface $s = 0$ and the trajectory that characterizes $M_{s\_}$.

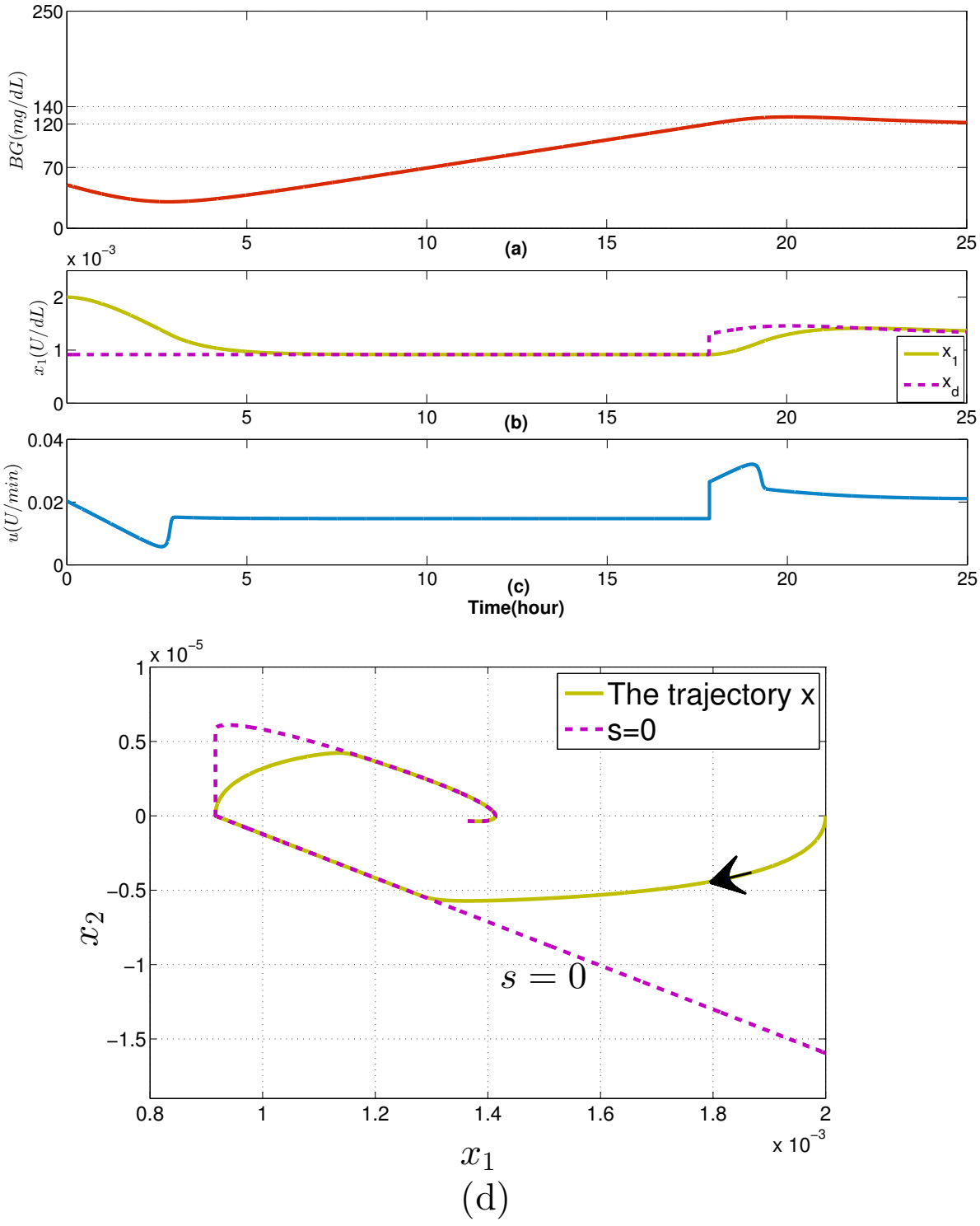

Figure 5.13 Glycemia response of IF3 under SMC. (a): BG behavior. (b): insulinemia versus its desired trajectory x_1 and x_d. (c): SMC control. (d): phase portrait in $x_1 - x_2$ plane.

Chapter 6

Description of Positively Invariant Sets in $\mathbb{R}^3$

6.1 Chapter Introduction in French

Dans ce chapitre, les propriétés d'invariance du modèle glycémique global, telles que la positivité de l'erreur entre la glycémie est son niveau normal est non négative (pour éviter l'hypoglycémie). Dans le chapitre 5, l'analyse de la positivité du sous-système insuline dans les cas boucles ouverte et fermée a été étudiée. Une commande CMG positive dans le plus grand ensemble positivement invariant (EPI) du sous-système d'insuline a été conçue pour réguler la glycémie. Cependant, la positivité de l'erreur de la glycémie (par rapport à l'hypoglycémie) n'a pas été prise en compte dans cette synthèse. En raison de la discontinuité de la loi de commande, concevoir une CMG positive partout dans le plus grand EPI de $\mathbf{R}^3$ tel que l'erreur de la glycémie est non négative est beaucoup plus complexe. Néanmoins, la robustesse de la CMG est encourageante pour mettre le problème en perspective. Dans ce chapitre, la boucle est fermée par une loi de commande continue : un régulateur par retour d'état. La théorie des polyèdres invariants pour les systèmes linéaires continus peut être directement appliquée pour trouver une commande positive par retour d'état. De plus, le régulateur est continu et la structure en boucle fermée qui en résulte est unique. Par conséquent, trouver le plus grand EPI en boucle fermée dans $\mathbf{R}^3$ (pour le système global), sous commande positive, est moins complexe.

Tout d'abord, le plus grand EPI du système en boucle ouverte (où seul un débit basal d'insuline est infusé) est obtenu. Deuxièmement, le plus grand EPI du système en boucle fermée sous la commande positive stabilisante par retour d'état est trouvé. À l'intérieur de cet EPI, la glycémie est régulée sans risque d'hypoglycémie. Le résultat principal du

plus grand EPI en boucles ouverte et fermée est la *prédiction d'hypoglycémie*. Comme montré dans le Chapitre 2, l'hypoglycémie est une complication commune grave pour un DT1. Il s'agit donc d'un problème majeur à résoudre pour la conception du pancréas artificiel. L'hypoglycémie est prédite ici en fonction des conditions initiales du système. La prédiction est établie lorsque les conditions initiales sont en dehors du plus grand EPI en boucle fermée (glycémie <70 mg / dL). Dans ce cas, on vérifie si la condition initiale appartient au EPI de boucle ouverte (sous l'injection basale). Si oui, la boucle est ouverte et le débit basal est injecté. Sinon, une hypoglycémie future est également prévue avec l'injection basale, alors la pompe est arrêtée signalant un épisode hypoglycémique sévère. De cette manière, l'analyse de positivité s'avère très utile pour la régulation de la glycémie et aussi pour la prédiction de l'hypoglycémie et éventuellement la nécessité d'un resucrage.

6.2 Introduction

The problem of finding the largest PIS where glycemia remains *invariant* within or above the desired threshold, is addressed in this chapter. In Chapter 5, positivity analysis of the insulin subsystem in open and closed-loop cases was studied. A positive SMC everywhere in the largest PIS of the insulin subsystem was designed to regulate glycemia. However, positivity of BG error (with respect to hypoglycemia) was not taken into account in the design. Due to the discontinuity of the control law, designing a positive SMC everywhere in the largest PIS in $\mathbb{R}^3$ such that BG error is nonnegative is much more complex. This problem is addressed in this chapter via a simple continuous control law. The loop is closed via a state feedback controller. First of all, the control law is simple and continuous and the resulting closed-loop structure is unique. Therefore, finding the largest closed-loop PIS in $\mathbb{R}^3$ (for the overall system), under positive control, is less complex than that with SMC[1]. Moreover, the theory of invariant polyhedra for continuous linear systems is directly applied to find a positive state feedback controller.

Firstly, the largest PIS of the open-loop system (where only a basal insulin rate is infused) is obtained. Secondly, the largest PIS of the closed-loop system is found under a stabilizing positive state feedback control. Inside the PIS, glycemia is regulated without hypoglycemia risk. The main outcome of the largest open and closed-loop PIS for glycemia system is the *hypoglycemia prediction*. As shown in Chapter 2, hypoglycemia is a serious common complication in T1DM. It is, thus, a major open problem to be solved for the artificial pancreas design. Hypoglycemia is predicted here based on the system initial conditions. The prediction is established when the initial conditions are outside the largest closed-loop PIS

[1] Nevertheless, the robustness of SMC is encouraging to put the problem as a future work.

(BG<70 mg/dL). In this case, the loop is opened to either administrate basal insulin only, or to switch the pump off. If the initial condition belongs to the open-loop (basal) PIS then the loop is opened to inject basal insulin only. Otherwise, if future hypoglycemia is also predicted under basal injection, then the pump is switched off signaling severe hypoglycemia. In this manner, positivity analysis is shown to be very useful for tight glycemia regulation and also for hypoglycemia prediction.

Preliminary results of this chapter are presented in [99]. Open-loop results of this chapter are accepted to be published in [100]. The closed-loop results of this chapter is submitted to be published in Automatica [101].

The theoretical preliminaries given in subsection 5.3.2 will be used in this chapter.

6.3 Positivity Analyses of T1DM Models

In this section internal/external positivity is checked for Magdelaine's linear model, Hovorka's and Dalla Man insulin linear models according to Theorems 1 and 2.

6.3.1 Hovorka and Dalla Man Models

As seen earlier in Sections 3.5.1 and 3.6.1, those models are nonlinear, specifically for glucose subsystems. Thus, the positivity definitions and theorems for linear systems in the preliminary section of Chapter 5 can not be applied on glucose subsystems. Therefore, the positivity of the linear insulin subsystems of both models has been investigated (see Sections 3.5.2, 3.5.3 for Hovorka's model and 3.6.2 for Dalla Man). Both subsystems are positive according to Definition 2 and Theorem 2. For illustration, take Hovorka's insulin model in (3.8) (3.9) and (3.10), that is rewritten as follows:

$$\dot{x}_h = A_h x_h + B_h u(t) \tag{6.1}$$

$$x_h = C_h x_v \tag{6.2}$$

where $x_h = \begin{bmatrix} S_1 & S_2 & I & x_1 & x_2 & x_3 \end{bmatrix}^T$,

$$A_h = \begin{pmatrix} -\frac{1}{t_{max,I}} & 0 & 0 & 0 & 0 & 0 \\ \frac{1}{t_{max,I}} & -\frac{1}{t_{max,I}} & 0 & 0 & 0 & 0 \\ 0 & \frac{1}{V_I.t_{max,I}} & -k_e & 0 & 0 & 0 \\ 0 & 0 & k_{b1} & -k_{a1} & 0 & 0 \\ 0 & 0 & k_{b2} & 0 & -k_{a2} & 0 \\ 0 & 0 & k_{b3} & 0 & 0 & -k_{a3} \end{pmatrix}$$

$B_h = \begin{bmatrix} 1 & 0 & 0 & 0 & 0 & 0 \end{bmatrix}^T$, taking the plasma insulin as output then $C_h = \begin{bmatrix} 0 & 0 & 1 & 0 & 0 & 0 \end{bmatrix}$. According to Definition 3 A_h is Metzler and $B_h \in \mathbb{R}_+^{6\times 1}, C_h \in \mathbb{R}_+^{1\times 6}$, thus Hovorka's insulin subsystem is positive. Similar demonstration can be done to show the positivity of Dalla Man insulin subsystem.

6.3.2 Magdelaine's Model

In this chapter, Magdelaine's model is employed in its second representation (3.23) which seems to be more appropriate due to its compartmental variables as explained in Chapter 3 which has stronger positivity properties as will be explained in the sequel. Another simplified representation is deduced from (3.23), assuming a basal insulin $u(t) = u_b$ is injected:

$$\begin{cases} \begin{pmatrix} \dot{\tilde{x}}_1 \\ \dot{\tilde{x}}_2 \\ \dot{\tilde{x}}_3 \end{pmatrix} = \begin{pmatrix} 0 & -\theta_2 & 0 \\ 0 & -\frac{1}{\theta_3} & \frac{1}{\theta_3} \\ 0 & 0 & -\frac{1}{\theta_3} \end{pmatrix} \begin{pmatrix} \tilde{x}_1 \\ \tilde{x}_2 \\ \tilde{x}_3 \end{pmatrix} + \begin{pmatrix} 0 \\ 0 \\ \frac{1}{\theta_3} \end{pmatrix} \tilde{u} \\ \\ \tilde{y} = C\tilde{x},\ \tilde{x}_o \triangleq \tilde{x}(0). \end{cases} \tag{6.3}$$

via the following change of variables:

$$\tilde{x}_1 = G - G_r, \tag{6.4}$$

$$\tilde{x}_2 = x_{n_1} - u_b, \tag{6.5}$$

$$\tilde{x}_3 = x_{n_2} - u_b, \tag{6.6}$$

$$\tilde{u} = u - u_b \tag{6.7}$$

where $C = \begin{pmatrix} 1 & 0 & 0 \end{pmatrix}$, G_r is the glucose desired reference (e.g. 120 mg/dL), u_b [U/min] is the basal infusion rate in (3.37). Recall that x_{n_1}, x_{n_2} are the plasma and subcutaneous insulin rates respectively.

Remark 14. *The positivity of the new variables $\tilde{x}$ is in the strict sense with respect to their positive reference values and this permits to study the invariance against hypoglycemia for $\tilde{x}_1$. In addition, the conditions for positivity and invariance of the control u is with respect to the basal infusion rate.*

When $u = u_b$ or $\tilde{u} = 0$ the system states are steered to the equilibrium i.e. $\tilde{x}_{eq}$ =($\tilde{x}_1$,0,0) and $\tilde{x}_1$ can settle anywhere. This is biologically true for a T1DM as the basal insulin does not regulate glycemia but it maintains glycemia constant at some value.

Remark 15. *According to Theorem 2, neither the system in its original coordinates nor system* (6.3) *are internally positive as their system matrices are not Metzler. Moreover, according to Theorem 1 they are not externally positive. To show that via Theorem 1, compute the impulse response $h(t)$ of (6.3):*

$$h(t) = \big(\theta_2 + \frac{\theta_2 t}{\theta_3}\big)e^{-\frac{t}{\theta_3}} - \theta_2 \tag{6.8}$$

Thus, the impulse response of the output $\lim_{t\to\infty} h(t) = -\theta_2$ and the system is not externally positive either.

Remark 16. *Although the overall system* (6.3) *is not positive, its insulin subsystem ($\tilde{x}_2, \tilde{x}_3$) is internally positive according to Theorem 2 as the insulin subsystem presented by 2×2 lower right block of matrix A is Metzler, $B \geqslant 0$ and $C \geqslant 0$. According to Corollary 2, $\mathbb{R}^2_+$ for this subsystem is a PIS. Note that although the insulin subsystem is internally positive in the new coordinates* (6.3)*, it is not in the coordinates* (3.17)*. This is just very similar to what is described in Example 1 in subsection 5.3.2.*

Remark 17. *It is good to mention that the insulin subsystem in* (3.23)*, with $u(t) \geqslant 0$, is also positive according to Definition 2 and Theorem 2. This means that insulin subsystem in $\tilde{x}-$coordinates in* (6.3) *is not only positive but also for any $\tilde{x}_2(0) \geqslant -u_b$ and $\tilde{x}_3(0) \geqslant -u_b$ then $\tilde{x}_2(t) \geqslant -u_b, \tilde{x}_3(t) \geqslant -u_b$ for any $\tilde{u}(t) \geqslant -u_b$ and $t \geqslant 0$. In other words, for any $\tilde{u}(t) \geqslant -u_b$, the set $\{\tilde{x} \in \mathbb{R}^3 | \tilde{x}_{2,3} \geqslant -u_b\}$ is a PIS.*

Remark 18. *Internal positivity property is not invariant under the change of state coordinates and this is evident in the change from* (3.17) *to* (6.3) *where the insulin subsystem in* (3.17) *is not positive whereas in* (6.3) *it is positive.*

Remark 16 is interpreted as follows: the set $\Omega(C)$ is not PIS and this motivates the search for the largest PIS of (6.3)in open and closed-loop cases. This is useful to

1. Find the PIS where the system behaves as an externally positive system [2].
2. Ensure that the positivity constraint on glycemia is respected i.e. $\tilde{x}_1(t) \geqslant 0$. In the PIS in $\Omega(C)$ glycemia is restricted to be above or at the desired level G_r in (6.4), thus hypoglycemia is avoided as $G_r \geqslant 70$ mg/dL.

Concerning insulin positivity constraints, as stated in Remark 17, they remain invariant $\tilde{x}_{2,3} \geqslant -u_b$ for any $\tilde{u} \geqslant -u_b$.

[2] or even internally if $C = I_{3\times 3}$

6.4 PIS in $\Omega(C)$

In this section, the largest PIS $\Omega_m := \{\tilde{x}_o \in \Omega(C) | C\tilde{x}(t) \geqslant 0 \forall t \geqslant 0\}$ is found, i.e. the largest set of initial conditions such that state trajectories never cross the plane $C\tilde{x} = 0$. Since each trajectory is unique (does not cross others), the subset of those which are tangent to the plane $C\tilde{x} = 0$ defines a boundary of Ω_m. These trajectories tangent to the plane $C\tilde{x} = 0$ are such that there exists $t^* \geqslant 0$ solution of $C\tilde{x}(t^*) = 0$ and $C\dot{\tilde{x}}(t^*) = 0$ for some initial conditions. These trajectories pass by the line

$$L \triangleq \begin{cases} C\tilde{x} = 0 \\ C\dot{\tilde{x}} = 0 \end{cases} \tag{6.9}$$

L is actually a set of extrema. L is a set of minima for the passing trajectories whose initial condition $\tilde{x}_o \in \Omega(C)$ (or $C\tilde{x}_o \geqslant 0$). The concavity of the trajectory $C\tilde{x}$ is decided by $C\ddot{\tilde{x}}(t^*)$ and from (6.3) $C\ddot{\tilde{x}}_1(t^*) = -\frac{\theta_2}{\theta_3}\tilde{x}_3(t^*)$, hence a minimum occurs if $\tilde{x}_3(t^*) < 0$. Thus, a boundary is given by the set of trajectories whose minimum is zero i.e. the set

$$\tilde{S} \triangleq \{\tilde{x}_o \in \Omega(C) | \min_{t \geqslant 0}(C\tilde{x}(t)) = 0\} \tag{6.10}$$

Theorem 8. *The largest PIS $\Omega_m \subset \Omega(C)$ consists of all points $\tilde{x}_o \in \Omega(C)$ such that:*

1. $\lim_{t\to\infty} C\tilde{x}(\tilde{x}_o, t) \in \Omega(C)$.

2. $\min_{t \geqslant 0} C\tilde{x}(\tilde{x}_o, t) \in \Omega(C)$ *whenever such a minimum exists.*

Proof. Point 1 follows directly from the definition of a PIS. Point 2 follows also from the definition of a PIS that is, the trajectory $\tilde{x}(t) \in \Omega(C)$ for any $t \geqslant 0$. □

6.4.1 Open-loop

The state solution of system (6.3) during the fasting phase with $\tilde{u} = 0$ is:

$$\tilde{x}_1(t) = \tilde{x}_{10} + \theta_2\theta_3 \ (\tilde{x}_{20} + \tilde{x}_{30})(e^{-\frac{t}{\theta_3}} - 1) + \theta_2\tilde{x}_{30}te^{-\frac{t}{\theta_3}}, \tag{6.11}$$

$$\tilde{x}_2(t) = \left(\tilde{x}_{20} + \frac{\tilde{x}_{30}t}{\theta_3}\right)e^{-\frac{t}{\theta_3}}, \tag{6.12}$$

$$\tilde{x}_3(t) = \tilde{x}_{30}e^{-\frac{t}{\theta_3}}. \tag{6.13}$$

The final value of the output BG is $\lim_{t\to\infty} C\tilde{x}(\tilde{x}_o,t) = l\tilde{x}_o$ where $l = \begin{pmatrix} 1 & -\theta_2\theta_3 & -\theta_2\theta_3 \end{pmatrix}$ and the set of points that satisfies the final value condition of Theorem 8 is simply the polyhedron[3] $\Omega(G)$ with

$$G := \begin{pmatrix} C \\ l \end{pmatrix} \tag{6.14}$$

Note that since only the first condition of Theorem 8 is satisfied then $\Omega_m \subset \Omega(G)$. In the next section, it is demonstrated that $\Omega(G)$ is not a PIS and the largest *polyhedral* PIS in $\Omega(G)$ is found. Thereafter, the largest PIS Ω_m is found [100, 101].

6.5 Polyhedral PIS

According to Proposition 1 neither the set $\Omega(C)$ nor the set $\Omega(G)$ are PIS, therefore the largest polyhedral PIS in $\Omega(G)$ is found. It will be useful later in finding Ω_m. The largest polyhedral PIS is sought in a smaller polyhedron $\Omega(G_o) \subset \Omega(G)$ where

$$G_o := \begin{pmatrix} G \\ w \end{pmatrix} \tag{6.15}$$

and $w = (a\ b\ c)$ where a, b and c are unknown constants. The next Theorem states that the largest polyhedral PIS is $\Omega(G^*) := \Omega(G_o|_{w=w^*})$ with $w^* := (1\ -\theta_2\theta_3\ 0)$.

Theorem 9. *The largest polyhedral PIS in* $\Omega(G)$ *for system* (6.3) *with* $\tilde{u} = 0$ *is* $\Omega(G^*)$.

Proof. The set $\Omega(G_o)$ is a PIS according to Proposition1 if the constants a, b, c, are chosen such that $H = G_o A G_o^{-1}$ is Metzler. Thus, choose a, b, c such that H verifies Definition 3:

$$h_{13} = -\frac{\theta_2}{(b-c)} \geqslant 0 \iff b - c < 0 \tag{6.16}$$

$$h_{12} = -\frac{c}{\theta_3(b-c)} \geqslant 0 \text{ and} (6.16) \iff c \geqslant 0 \tag{6.17}$$

$$h_{31} = \frac{(b + a\theta_2\theta_3)^2}{\theta_2\theta_3^2(b-c)} \geqslant 0 \text{ and} (6.16) \iff b = -a\theta_2\theta_3 \tag{6.18}$$

$$h_{32} = -\frac{b^2 + ac\theta_2\theta_3}{\theta_2\theta_3^2(b-c)}, \ (6.18) \iff b \leqslant 0 \tag{6.19}$$

and the remaining off diagonal terms are $h_{21} = h_{12} = 0$. From (6.19) and (6.16) the term h_{32} is nonnegative in either of the following cases:

[3] Recall Definition 5 of a polyhedron

$$\text{Case 1: } a = 0, b = 0, c > 0 \tag{6.20}$$

$$\text{Case 2: } a > 0, b = -a\theta_2\theta_3, c \geqslant 0 \tag{6.21}$$

w satisfying (6.20) or (6.21) renders $\Omega(G_o)$ a PIS and next is to find the largest polyhedral PIS. Denote G_o satisfying case 1 in (6.20) as $G_1 = \begin{pmatrix} C \\ l \\ w_1 \end{pmatrix}$ where $w_1 = (0\,0\,c), c > 0$. For Case 2 denote $G_2 = \begin{pmatrix} C \\ l \\ w_2 \end{pmatrix}$ where $w_2 = (a\ -a\theta_2\theta_3\ c)$ satisfying (6.21).

Firstly, it will be shown that $\tilde{x} \in \Omega(G_1)$ implies $\tilde{x} \in \Omega(G_2)$ or equivalently $\Omega(G_1) \subset \Omega(G_2)$ for $c \geqslant 0$. Secondly, it will be shown that $\Omega(G_2|_{c=0}) \equiv \Omega(G^*)$ is the largest polyhedral PIS.

1. $\Omega(G_1) \subset \Omega(G_2)$ is shown as follows:

   $\tilde{x} \in \Omega(G_1)$ is equivalent to satisfying all of the following inequalities

   $$\tilde{x}_1 \geqslant 0 \tag{6.22}$$

   $$\tilde{x}_1 - \theta_2\theta_3\tilde{x}_2 - \theta_2\theta_3\tilde{x}_3 \geqslant 0 \tag{6.23}$$

   $$c\tilde{x}_3 \geqslant 0 \tag{6.24}$$

   (6.23) yields $\tilde{x}_1 - \theta_2\theta_3\tilde{x}_2 \geqslant \theta_2\theta_3\tilde{x}_3$ and (6.24) implies $\tilde{x}_1 - \theta_2\theta_3\tilde{x}_2 \geqslant 0$ which in turn implies that $a(\tilde{x}_1 - \theta_2\theta_3\tilde{x}_2) + c\tilde{x}_3 \geqslant 0$ for any $a > 0, c \geqslant 0$ or equivalently $w_2\tilde{x} \geqslant 0$. Therefore $\Omega(G_1) \subset \Omega(G_2)$. See Fig. 6.1 for graphical illustration.

2. $\Omega(G_2) \subset \Omega(G^*)$ follows from

   $$\text{If } \tilde{x}_3 \geqslant 0 \text{ then (6.23) implies } \tilde{x}_1 - \theta_2\theta_3\tilde{x}_2 \geqslant 0. \tag{6.25}$$

   $$\text{If } \tilde{x}_3 < 0 \text{ then } w_2\tilde{x} \geqslant 0, c \geqslant 0 \text{ implies } \tilde{x}_1 - \theta_2\theta_3\tilde{x}_2 \geqslant 0. \tag{6.26}$$

   or equivalently $a(\tilde{x}_1 - \theta_2\theta_3\tilde{x}_2) \geqslant 0$ for $a > 0$, therefore $\tilde{x} \in \Omega(G_2)$ implies $\tilde{x} \in \Omega(G^*)$. Thus, $\Omega(G^*)$ is the largest polyhedral PIS as depicted in Fig. 6.2.

□

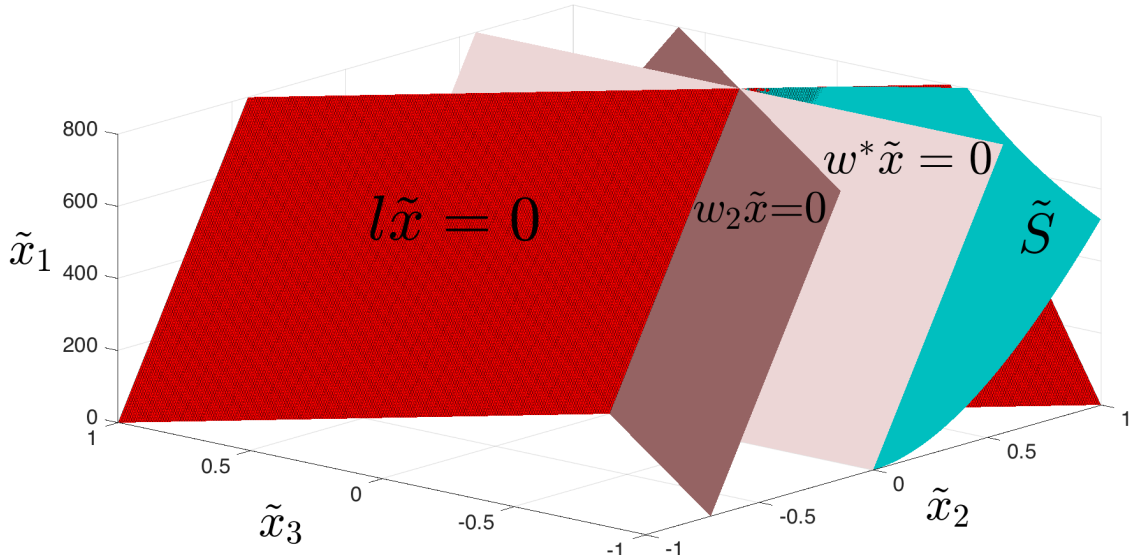

Figure 6.1 The largest polyheral PIS in open-loop using IF2 patient parameters. The largest Polyhedral PIS $\Omega(G^*)$ is with $w = w^*$. The plane $w_2\tilde{x} = 0$ is with $c = 1000$ to characterize $\Omega(G_2)$.

6.6 Non-Polyhedral PIS [99, 100]

Theorem 10. *The largest PIS $\Omega_m \subset \Omega(C)$ following Theorem 8 has a boundary formed by:*

1. $l\tilde{x}_o = 0$ *where* $l = \begin{pmatrix} 1 & -\theta_2\theta_3 & -\theta_2\theta_3 \end{pmatrix}$.

2. $\tilde{S} = \{\tilde{x}_o \in \Omega(C) | \tilde{x}_{30} < 0, \tilde{x}_{20} \geqslant 0, l\tilde{x}_o + \theta_2\theta_3\tilde{x}_{30}e^{\frac{\tilde{x}_{20}}{\tilde{x}_{30}}} = 0\}$.

Proof. The set $\tilde{S}$ as defined in (6.10) is found. The minimum point $\tilde{x}_1(t^*)$ (if any) of (6.11) is found at some critical time t^* such that $\tilde{x}_1(t^*) \geqslant 0$ and $\dot{\tilde{x}}_1(t^*) = 0$. This is achieved by differentiating (6.11) w.r.t. time:

$$\dot{\tilde{x}}_1 = -\theta_2 e^{-\frac{t}{\theta_3}}(\tilde{x}_{20} + \frac{\tilde{x}_{30}t}{\theta_3}) = 0 \tag{6.27}$$

The unique time t^* solution of (6.27) is:

$$t^* = -\frac{\theta_3\tilde{x}_{20}}{\tilde{x}_{30}} \tag{6.28}$$

Note that $t^* \geqslant 0$ in either of the following cases:

- Case 1: $\tilde{x}_{20} \geqslant 0$ and $\tilde{x}_{30} < 0$ or,

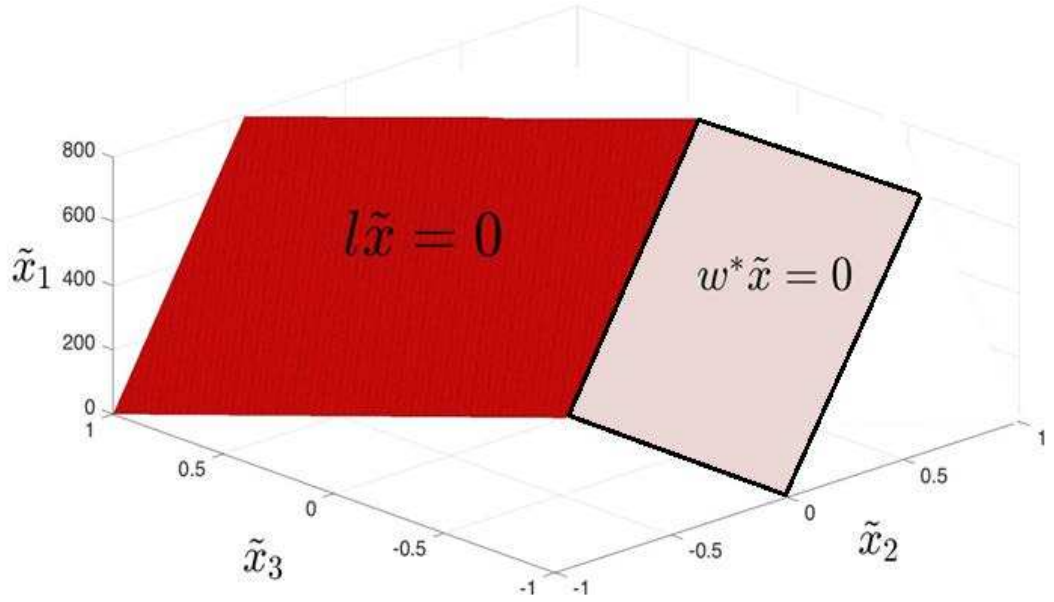

Figure 6.2 $\Omega(G^*)$ the largest open-loop polyhedral PIS, $\theta_2 = 11.6, \theta 3 = 122$ of IF2 patient.

- Case 2: $\tilde{x}_{20} \leq 0$ and $\tilde{x}_{30} > 0$.

Recall that the point $\tilde{x}_1(t^*)$ is a minimum point if $\ddot{\tilde{x}}_1(t^*) > 0$. Computing $\ddot{\tilde{x}}_1(t)$ and substituting $t = t^*$ from (6.28):

$$\ddot{\tilde{x}}_1(t^*) = -\tilde{x}_{30}\frac{\theta_2}{\theta_3}e^{\frac{\tilde{x}_{20}}{\tilde{x}_{30}}} \tag{6.29}$$

If $\tilde{x}_{30} > 0$ (Case 2 above) then $\tilde{x}_1(t^*)$ is a maximum and this case is not of interest as a $\max(\tilde{x}_1) = 0$ implies that $\tilde{x}_o \notin \Omega(C)$. Case 1, the region where $\tilde{x}_1$ admits a minimum, is thus the only case compatible with the positivity of the output.

Substitute (6.28) in (6.11) to get $\tilde{x}_1(t^*)$. Therefore, $\tilde{x}_1(t^*) = 0$ yields $\tilde{x}_o \in \tilde{S}$:

$$\tilde{S} = \{\tilde{x}_o \in \Omega(C) | \tilde{x}_{30} < 0, \tilde{x}_{20} \geqslant 0, l\tilde{x}_o + \theta_2\theta_3\tilde{x}_{30}e^{\frac{\tilde{x}_{20}}{\tilde{x}_{30}}} = 0\} \tag{6.30}$$

The largest PIS $\Omega_m \subset \Omega(C)$ according to Theorem 8 has a boundary formed by

1. $l\tilde{x}_o = 0$ (from $\lim_{t\to\infty} C\tilde{x}(x_o, t) = 0$).
2. $\tilde{S}$.

□

Corollary 3. *From Theorem 8, $\Omega_m \subset \Omega(C)$ is the largest PIS, thus it includes:*

- *all nonnegative final values* $l\tilde{x}_o \geqslant 0$ *or* $\Omega_m \subset \Omega(l)$,

- *all nonnegative minima* $\tilde{x}_1(t^*) \geqslant 0$ *(assuming* $l\tilde{x}_o \geqslant 0$ *is fulfilled) i.e.*

$$\tilde{S}_+ := \{\tilde{x} \in \Omega(G) | \min_{t \geqslant 0}(C\tilde{x}(t)) \geqslant 0\} \tag{6.31}$$

It is good to mention that $\Omega(l)$ *is a PIS according to Proposition 1, consequently* $\tilde{x}(t) \in \tilde{S}_+$ *implies* $x(t) \in \Omega(l) \forall t \geqslant 0$.

As will be shown next, the set Ω_m is actually the union of the largest polyhedral PIS and $\tilde{S}_+$ as illustrated in Fig.6.3.

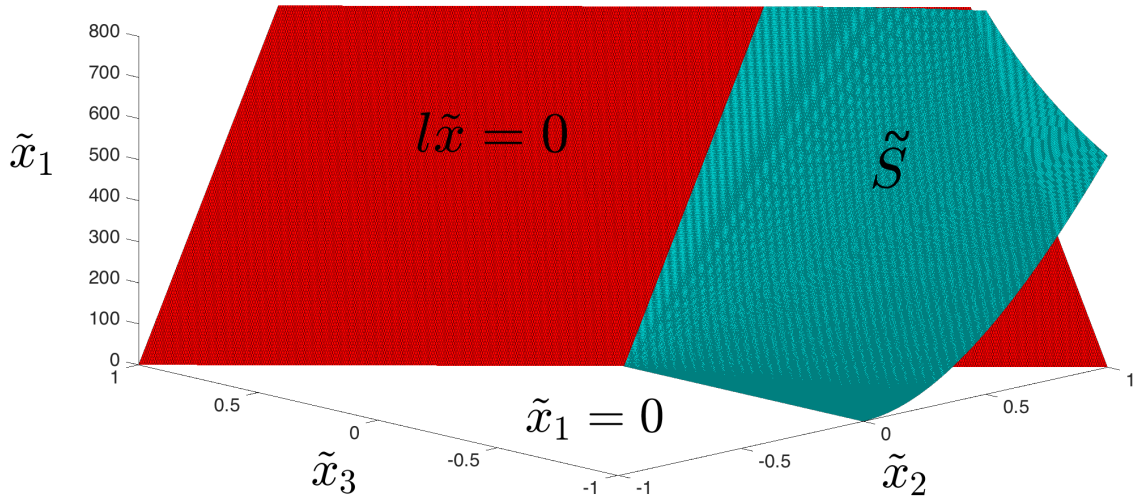

Figure 6.3 Ω_m the open-loop PIS for the glycemia state $\tilde{x}_1(t)$, $\theta_2 = 11.6, \theta_3 = 122$ of IF2 patient.

6.7 The Largest PIS in $\Omega(C)$

Remark 19. *The region outside the largest polyhedral PIS is* $\mathbb{W}_- := \Omega(G) \setminus \Omega(G^*)$ *or equivalently*

$$\mathbb{W}_- := \{\tilde{x}_o \in \Omega(G) | w^* \tilde{x}_o < 0\}. \tag{6.32}$$

Aiming to find the largest PIS in $\Omega(G)$, it is required to find a subset (if any) in $\mathbb{W}_-$ such that $\tilde{x}(t) \in \Omega(G)$ for any $t \geqslant 0$.

Theorem 11. *The largest PIS in $\Omega(G)$ is $\Omega_m = \Omega(G^*) \cup \tilde{S}_+$.*

Proof. According to Theorem 9, the largest polyhedral PIS in $\Omega(G)$ is $\Omega(G^*)$, otherwise if $\tilde{x}(t) \in \Omega(G) \setminus \Omega(G^*)$ then necessarily $\tilde{x}(t) \in \mathbb{W}_-$ according to Remark 19.

$\tilde{x}(t) \in \mathbb{W}_-$ is equivalent to satisfying simultaneously the following inequalities

$$\tilde{x}_1(t) \geqslant 0, \tag{6.33}$$

$$\tilde{x}_1(t) - \theta_2\theta_3(\tilde{x}_2(t) + \tilde{x}_3(t)) \geqslant 0, \tag{6.34}$$

$$\tilde{x}_1(t) - \theta_2\theta_3\tilde{x}_2(t) < 0. \tag{6.35}$$

(6.33) and (6.35) imply that $\tilde{x}_2(t) > 0$, while (6.34) and (6.35) implies that $\tilde{x}_3(t) < 0$. The subset $\mathbb{W}_-$ is thus located in the region $\tilde{x}_2(t) > 0, \tilde{x}_3(t) < 0$ of $\Omega(G)$. $\mathbb{W}_-$ is not a PIS because there exists $t^* \geqslant 0$ such that $\tilde{x}_2(t^*) = 0$ hence $\tilde{x}(t) \notin \mathbb{W}_-$ for $t \geqslant t^*$. Therefore, $\tilde{x}(t) \in \mathbb{W}_-$ only during $0 \leq t < t^*$, t^* is the instant where $\tilde{x}_2(t^*) = 0$ and at which the trajectory leaves $\mathbb{W}_-$. [4]

Thus find the set of trajectories initiated in $\mathbb{W}_-$ that remain in $\Omega(G)$ for all time. As explained before, $\tilde{x}(t) \in \mathbb{W}_-$ implies $\tilde{x}_3(t) < 0$ at any $t \in [0, t^*)$. At $t = t^*$ there are two possibilities either $\tilde{x}_3(t^*) < 0$ or $\tilde{x}_3(t^*) = 0$. The case $\tilde{x}_3(t^*) = \tilde{x}_2(t^*) = 0$ or $\tilde{x}(t^*) = (\tilde{x}_1(t^*), 0, 0) \in \Omega(G^*)$ is in fact an equilibrium point. As for the case $\tilde{x}_3(t^*) < 0$, recall from (6.3) that $\dot{\tilde{x}}_1(t) = -\theta_2\tilde{x}_2(t)$ and $\ddot{\tilde{x}}_1(t) = -\frac{\theta_2}{\theta_3}(\tilde{x}_2(t) + \tilde{x}_3(t))$, then

$$\tilde{x}_2(t^*) = 0,\ \tilde{x}_3(t^*) < 0 \iff C\tilde{x}(t^*) = \min_{t \geqslant 0}(C\tilde{x}(t)) \tag{6.36}$$

Thus, to maintain $\tilde{x}(t) \in \Omega(G)$ it is required that $\min_{t \geqslant 0} C\tilde{x}(t) \geqslant 0$ and hence the set $\tilde{S}_+$. Hence, the only admissible set in $\mathbb{W}_-$ is $\mathbb{W}_- \cap \tilde{S}_+$ [5].

$\tilde{x}_o \in \tilde{S}_+$ implies $\tilde{x}(t) \in \mathbb{W}_-$ for any $0 \leq t < t^*$, thereafter $\tilde{x}(t) \in \Omega(G) \setminus \mathbb{W}_-$ for any $t \geqslant t^*$ or equivalently

$$\tilde{x}(t) \in \tilde{S}_+\ 0 \leq t \leq t^*,\ \ \tilde{x}(t) \in \Omega(G^*)\ t \geqslant t^* \tag{6.37}$$

[4] As inequality (6.34) represent the PIS $\Omega(l)$, thus, the trajectory leaving $\mathbb{W}_-$ means that one or both of the inequalities (6.33) and (6.35) no more hold. Satisfying (6.33) for any $t \geqslant 0$ is the objective, thus, the focus is put on the time t^* at which (6.35) no more holds.

[5] note that $\tilde{S}_+ \not\subset \mathbb{W}_-$ due to $\tilde{x}(t^*) \in \tilde{S}_+$ but $\tilde{x}(t^*) \notin \mathbb{W}_-$.

In words, the trajectory initiated in $\tilde{S}_+$ enters the PIS $\Omega(G^*)$ at $t = t^*$ to remain there[6]. Thus, $\tilde{x}_o \in \tilde{S}_+ \cup \Omega(G^*)$ implies $\tilde{x}(t) \in \tilde{S}_+ \cup \Omega(G^*)$ for any $t \geqslant 0$, hence $\tilde{S}_+ \cup \Omega(G^*)$ is a PIS.

As shown, $\tilde{S}_+$ is the largest admissible set outside the largest polyhedral PIS. Thus, from (6.37) the union $\tilde{S}_+ \cup \Omega(G^*) = \Omega_m$ is the largest PIS in $\Omega(G)$.

$\tilde{S}_+$ as defined in (6.31) for system (6.11)-(6.13) is

$$\tilde{S}_+ = \{\tilde{x}_o \in \Omega(G) | \tilde{x}_{30} < 0, \tilde{x}_{20} \geqslant 0, l\tilde{x}_o + \theta_2\theta_3\tilde{x}_{30}e^{\frac{\tilde{x}_{20}}{\tilde{x}_{30}}} \geqslant 0\} \tag{6.38}$$

□

Recall from Remark 17 that the feasible set of initial conditions in Ω_m is $\tilde{x}_o \in \Omega_m$ such that $\tilde{x}_{20} \geqslant -u_b, \tilde{x}_{30} \geqslant -u_b$.

The set of points where hypoglycemia occurs is

$$\tilde{S}_- := \mathbb{W}_- \setminus (\mathbb{W}_- \cap \tilde{S}_+) \tag{6.39}$$

Remark 20. *The fact that $\tilde{x}_o \in \Omega(G)$ implies that $\lim_{t\to\infty} C\tilde{x}(x_o,t) \geqslant 0$ according to Corollary 3. Therefore, due to the nonnegative initial and final values of $C\tilde{x}(t)$, hypoglycemia events $C\tilde{x}(t) < 0$ are temporary (if any) i.e. the trajectory $C\tilde{x}(t)$ pass by a negative minimum. According to* (6.28)*, the minimum time instant is unique, thus it is a global minimum. Thus, the set of points (initial conditions) which has hypoglycemia nadirs is $\tilde{S}_-$. It is a negative minimum set that will be useful in the following section to predict hypoglycemia.*

The largest PIS of the open-loop case is where glycemia is maintained above or on a pre-specified level (see (6.4)) e.g. a point in the normal range $G_r \in [70, 120]$ mg/dL. In addition, $G_r = 70$ is the least admissible reference value beyond which hypoglycemia $(G < 70)$ zone starts. Checking the offset with hypoglycemia threshold is very useful as it ensures that once glycemia initiated in Ω_m then hypoglycemic risk is avoided. Moreover, the largest PIS of the T1DM model is useful for determining the region where hypoglycemia occurs. As will be shown in the next section, given the initial condition and checking its inclusion in the PIS: $\tilde{x}_o \in \Omega(C) \setminus \Omega_m$ helps predicting that there exists $t > 0$ such that $G(t) < 70$ mg/dL.

[6] As stated earlier, inequality (6.34) is equivalent to $\Omega(l)$ which is a PIS, thus, according to (6.31), $\tilde{x}_o \in \tilde{S}_+ \subset \Omega(l)$ implies that (6.34) holds $\forall t \geqslant 0$.

6.8 Fasting-Hypoglycemia Prediction: Open-loop [100]

Proposition 2. *In the fasting phase and with $\tilde{u} = 0$ and setting $G_r = 70$ mg/dL, hypoglycemia is predicted whenever*

1. $\tilde{x}_o \in \tilde{S}_-$, *or*
2. $\tilde{x}_o \in \Omega(C)$ *but* $\tilde{x}_o \notin \Omega(G)$ *i.e.* $l\tilde{x} < 0$.

Proof. Follows immediately from:

1. $\tilde{x}_o \in \tilde{S}_-$ is the negative minimum region i.e. using (6.28) in (6.11), yields $\tilde{x}_1(t^*, \tilde{x}_o) < 0$.
2. $\tilde{x}_o \in \Omega(C) | l\tilde{x}_o < 0$: negative final value i.e. $\lim_{t\to\infty} \tilde{x}_1(t, \tilde{x}_o) = l\tilde{x}_o < 0$.

□

$\tilde{x}_1(t) < 0$ is equivalent to the fact that $\tilde{x}_o \notin \Omega_m$ and the future hypoglycemic events (in time and value) can be predicted:

- The temporary episodes (point 1 above): the time t^* of event is computed in (6.28) and hypoglycemia value $\tilde{x}_1(t^*)$ is obtained from (6.11).
- Persisting hypoglycemia solving (6.11): hypoglycemia level is predicted from $\lim_{t\to\infty} \tilde{x}_1(t, \tilde{x}_o) = l\tilde{x}_o < 0$. The time at which hypoglycemia starts can be found numerically solving (6.11).

In either of the above cases, the solution is to stop the insulin injection and turn the pump off i.e. $\tilde{u}(t) = -u_b$. The off case is maintained until some finite time $t = t_1 > 0$ after which the trajectory enters the PIS again $\tilde{x}(t_1) \in \Omega_m$ due to the endogenous glucose production. This is explained as follows: when $\tilde{u}(t) = -u_b$ (or $u = 0$) then according to (6.3): $\lim_{t\to t_1} (\tilde{x}_2(t), \tilde{x}_3(t)) = -u_b$, as a result $\tilde{x}_1(t) \geqslant 0 \ \forall t \geqslant t_1$. In the case of a severe predicted hypoglycemic event $\tilde{x}_1(t) << 0$ where turning the pump off is not sufficient then a hypoglycemic alert is signaled and the patient is strongly advised to take some exogenous glucose (CHO).

Assuming that $\tilde{x}_o \in \Omega_m$, the set of equilibrium points of (6.3) is

$$\lim_{t\to\infty} \tilde{x}(t) = (l\tilde{x}_o, 0, 0) \tag{6.40}$$

and the glycemia state can settle anywhere: $\lim_{t\to\infty} \tilde{x}_1 = l\tilde{x}_o \geqslant 0$. Therefore, in the next section glycemia regulation to normal level such that $\tilde{x}_1 = 0$ is established via a stabilizing nonnegative state feedback.

6.9 Closed-loop PIS under a Nonnegative State Feedback

In what follows, the largest closed-loop PIS is found under the following full state feedback control [101]:

$$\tilde{u} = F\tilde{x} \quad , \qquad F = \begin{pmatrix} K_1 & K_2 & K_3 \end{pmatrix} \tag{6.41}$$

The closed-loop system is:

$$\dot{\tilde{x}} = (A+BF)\tilde{x}, \qquad \text{with} \qquad A+BF = \begin{pmatrix} 0 & -\theta_2 & 0 \\ 0 & -\frac{1}{\theta_3} & \frac{1}{\theta_3} \\ \frac{K_1}{\theta_3} & \frac{K_2}{\theta_3} & \frac{K_3-1}{\theta_3} \end{pmatrix} \tag{6.42}$$

First of all, $\Omega(C)$ for the closed-loop system is not a PIS for any F according to Proposition 1.Secondly, the next theorem states that a PIS can not be constructed by adding a second constraint i.e. $\Omega(C)\cap\Omega(w)$ is not a PIS where $w = (a\ b\ c)$ for any real constants a,b,c .

Theorem 12. *$\Omega(C)\cap\Omega(w)$ is not a PIS for any a,b,c and any F.*

Proof. Let $H = \begin{pmatrix} h_1 & h_2 \\ h_3 & h_4 \end{pmatrix}$, $\Omega(C)\cap\Omega(w)$ is PIS according to Proposition1 if H, solution of $\begin{pmatrix} C \\ w \end{pmatrix}(A+BF) = H\begin{pmatrix} C \\ w \end{pmatrix}$, is Metzler or equivalently $h_2 \geqslant 0, h_3 \geqslant 0$ s.t.

$$\begin{pmatrix} 0 & -\theta_2 & 0 \\ \frac{K_1 c}{\theta_3} & -\frac{(b-K_2 c+a\theta_2\theta_3)}{\theta_3} & \frac{(b-c+K_3 c)}{\theta_3} \end{pmatrix} = \begin{pmatrix} h_1+a h_2 & b h_2 & c h_2 \\ h_3+a h_4 & b h_4 & c h_4 \end{pmatrix} \tag{6.43}$$

From the first row it results $b<0$ and $c=0$ and first entry reads $h_2 = -\frac{h_1}{a}$ yielding $a<0$. Taking the last entry of the second row and using the result $c=0$ it leads immediately to $b=0$ which contradicts the previous result of $b<0$ thus a Metzler H does not exist for any a,b,c and any F. □

In practice it is required that $F\tilde{x} \geqslant 0$, therefore the closed-loop PIS for system (6.42) will be found in the following section with stabilizing K_1,K_2,K_3 such that $\tilde{x} \in \Omega(C)\cap\Omega(F)$ for any $t \in \mathbb{R}_+$. The conditions for stability are derived with standard tools in the following subsection.

6.9.1 Stability

Stability conditions of the closed-loop system are investigated via the characteristic equation of $A+BF$:

$$\theta_3^2\lambda^3+\theta_3(2-K_3)\lambda^2+(1-K_2-K_3)\lambda+K_1\theta_2=0 \tag{6.44}$$

According to Routh-Hurwitz stability criterion the coefficients for a cubic polynomial must satisfy:

1. $a_n>0$

$$K_1>0,\quad K_3<2,\quad K_3+K_2<1 \tag{6.45}$$

2. $a_2a_1>a_3a_0$ or:

$$\theta_2\theta_3K_1<(2-K_3)(1-K_2-K_3) \tag{6.46}$$

In what follows, these conditions are used to design F for a stable closed-loop system.

6.10 Positivity and Invariance [101]

In this section, the largest closed-loop PIS $\Omega_{m_F}\subset\{\Omega(C)\cap\Omega(F)\}$ is found for a stabilizing F. The largest closed-loop polyhedral PIS is found which is used to find the largest non-polyhedral PIS.

6.10.1 Polyhedral PIS

The set $\Omega(G_k)$ with $G_k=\begin{pmatrix}1&0&0\\K_1&K_2&K_3\end{pmatrix}$ is not a PIS according to Proposition 1 for any given F. Therefore, a polyhedral PIS is sought in a smaller polyhedron adding a third face to $\Omega(G_k)$ to yield $\Omega(G_e)$ where $G_e=\begin{pmatrix}G_k\\w\end{pmatrix}$, w is as defined earlier after (6.15). According to Proposition 1 $H_e=G_e(A+BF)G_e^{-1}$ has the following off-diagonal terms:

$$H_{12} = \frac{c\theta_2}{\Delta} \tag{6.47}$$

$$H_{13} = -\frac{K_3\theta_2}{\Delta} \tag{6.48}$$

$$H_{21} = \frac{K_2^2 a - K_1K_2(b+c) + K_1K_3(b+a\theta_2\theta_3) - K_1^2 c\theta_2\theta_3}{\theta_3\Delta} \tag{6.49}$$

$$H_{23} = -\frac{K_2^2 + K_1K_3\theta_2\theta_3}{\theta_3\Delta} \tag{6.50}$$

$$H_{31} = -\frac{K_1b^2 - ab(K_2+K_3) - K_3a^2\theta_2\theta_3 + ac(K_2+K_1\theta_2\theta_3)}{\theta_3\Delta} \tag{6.51}$$

$$H_{32} = \frac{b^2 + c\Delta + a\theta_2\theta_3 c}{\theta_3\Delta} \tag{6.52}$$

where $\Delta = K_3b - K_2c$. The off-diagonal entries of the matrix H_e are made nonnegative via a family of stabilizing feedback gain ranges depending on the different choices of the constants a, b and c of w. One of those choices is $w = w^* = \begin{pmatrix} 1 & -\theta_2\theta_3 & 0 \end{pmatrix}$ leading to $G_e = \begin{pmatrix} G_k & w^* \end{pmatrix}^T$, then the following range of stabilizing gain matrix F is obtained such that H_e is Metzler and thus $\Omega(G_e)$ is a PIS:

$$0 < K_1 \leq -\frac{K_2}{\theta_2\theta_3},\ K_2 < 0,\ K_3 \leq -\frac{K_2^2}{K_1\theta_2\theta_3} \tag{6.53}$$

6.10.2 Stability of *F*

Stability conditions of K_2, K_3 in (6.45) and are compatible with invariance conditions of (6.53). For K_1 in (6.53), this range falls in the stable range of (6.46) if

$$-K_2 < (2-K_3)(1-K_2-K_3) \tag{6.54}$$

$$0 < 2(1-K_3) - K_2 - K_3(1-K_2-K_3) \tag{6.55}$$

from (6.53) $K_2 < 0, K_3 < 0$ thus the above inequality holds and thus (6.53) is compatible with stability conditions in (6.45) and (6.46).

It is good to notice that the limit case where $K_2 = -K, K_1 = -\frac{K_2}{\theta_2\theta_3}$, $K_3 = -\frac{K_2^2}{K_1\theta_2\theta_3}$ or $F = F^*$ with

$$F^* \triangleq K(1\ -\theta_2\theta_3\ -\theta_2\theta_3), K > 0 \tag{6.56}$$

leads to $G_e \equiv G^*$. The following theorem presents the largest polyhedral PIS for any F satisfying (6.53).

Theorem 13. *For any F satisfying* (6.53)*, the largest PIS $\Omega(G_e)$ setting $w = w^*$ is obtained with $F = F^*$.*

Proof. The hypothesis is that for any $\tilde{x} \in \mathbb{R}^3$ such that the following inequalities are satisfied:

$$\tilde{x}_1 \geqslant 0, \tag{6.57}$$

$$K_1\tilde{x}_1 + K_2\tilde{x}_2 + K_3\tilde{x}_3 \geqslant 0, \tag{6.58}$$

$$\tilde{x}_1 - \theta_2\theta_3\tilde{x}_2 \geqslant 0. \tag{6.59}$$

implies

$$F^*\tilde{x} \geqslant 0 \equiv \tilde{x}_1 - \theta_2\theta_3(\tilde{x}_2 + \tilde{x}_3) \geqslant 0 \tag{6.60}$$

this statement is demonstrated region by region as follows:

- If $(\tilde{x}_3 + \tilde{x}_2) \leq 0$ then (6.60) is yielded immediately satisfying (6.57) only.
- If $(\tilde{x}_2 + \tilde{x}_3) > 0$ and $\tilde{x}_3 \leq 0$.

  In this region the inequality (6.60) holds directly from (6.57) and (6.59).
- If $(\tilde{x}_2 + \tilde{x}_3) > 0$ and $\tilde{x}_3 > 0$.

  From (6.53) one has $K_3\tilde{x}_3 \leq -\frac{K_2^2}{K_1\theta_2\theta_3}\tilde{x}_3$, $K_1 > 0$, thus form (6.58) the following inequality holds

$$0 \leq \tilde{x}_1 + \frac{K_2}{K_1}\tilde{x}_2 + \frac{K_3}{K_1}\tilde{x}_3 \leq \tilde{x}_1 + \frac{K_2}{K_1}(\tilde{x}_2 - \frac{K_2}{K_1\theta_2\theta_3}\tilde{x}_3) \tag{6.61}$$

  also from (6.53) one has $K_2 < 0$, $K_1 \leq -\frac{K_2}{\theta_2\theta_3}$, multiplying the latter inequality by $\frac{K_2\tilde{x}_3}{K_1^2}$ yields $\frac{K_2}{K_1}(-\frac{K_2}{K_1\theta_2\theta_3})\tilde{x}_3 \leq \frac{K_2}{K_1}\tilde{x}_3$, hence (6.61) becomes:

$$\tilde{x}_1 + \frac{K_2}{K_1}(\tilde{x}_2 - \frac{K_2}{K_1\theta_2\theta_3}\tilde{x}_3) \leq \tilde{x}_1 + \frac{K_2}{K_1}(\tilde{x}_2 + \tilde{x}_3) \tag{6.62}$$

  also from (6.53) one has $\frac{K_2}{K_1} \leq -\theta_2\theta_3$, thus $(\tilde{x}_2 + \tilde{x}_3)\frac{K_2}{K_1} \leq -\theta_2\theta_3(\tilde{x}_2 + \tilde{x}_3)$, hence:

$$0 \leq \tilde{x}_1 + \frac{K_2}{K_1}\tilde{x}_2 + \frac{K_2}{K_1}\tilde{x}_3 \leq \tilde{x}_1 - \theta_2\theta_3(\tilde{x}_2 + \tilde{x}_3). \tag{6.63}$$

Therefore, for any F satisfying (6.53) then $\tilde{x} \in \Omega(G_e)$ implies $\tilde{x} \in \Omega(G^*)$ or the largest PIS is obtained with $F = F^*$. Moreover, as $F^* \equiv Kl$, then this result holds also for any $K > 0$. □

In the next section, the procedure followed to find the non-polyhedral PIS of the open-loop is applied to find the surface that characterizes the closed-loop non-polyhedral PIS.

Remark 21. *The first condition of Theorem 8 is guaranteed for the closed-loop system as glycemia error is driven asymptotically to zero and the origin is the new stable equilibrium.*

Remark 22. *Note that $\Omega(F^*) \equiv \Omega(l)$ with l as defined earlier, moreover, this set is a PIS according to Proposition 1. The set denoted as $\Omega(G)$ defined in* (6.14) *will be used to label the closed-loop positive input/output set as:*

$$\Omega(C) \cap \Omega(F^*) \equiv \Omega(G) \tag{6.64}$$

The remaining non- investigated region is $\tilde{x} \in \Omega(G) \setminus \Omega(G^*)$ which implies $\tilde{x} \in \mathbb{W}_-$, where $\mathbb{W}_-$ is as defined in (6.32).

Similarly to what has been done for the open-loop system, the largest closed-loop PIS in $\Omega(G)$ is the union between the largest polyhedral PIS and the largest set in $\mathbb{W}_-$ whose trajectories remain in $\Omega(G)$. Firstly, the non-polyhedral set $\tilde{S} \subset \Omega(G)$ will be computed. Later, it will be shown that, the largest closed-loop PIS is again $\Omega(G^*) \cup \tilde{S}_+$, where $\tilde{S}_+$ is as defined in (6.31) but for the closed-loop system.

Remark 23. *Recall that the feasible set of insulin states is such that $\tilde{x}_{2,3}(t) \geqslant -u_b$. Thus the admissible set of initial conditions $\tilde{x}_o \in \Omega(G^*)$ (respectively in any set in $\Omega(G)$) is such that $\tilde{x}_{20} \geqslant -u_b, \tilde{x}_{30} \geqslant -u_b$. According to Remark 17, $\tilde{x}_{2,3}(t) \geqslant -u_b$ for any $\tilde{u}(t) \geqslant -u_b$, $t \geqslant 0$. according to Remark 22 the set $\Omega(F^*)$ is a PIS and thus $\tilde{u}(t) \geqslant 0$ for any $t \geqslant 0$. Thus, if $\tilde{x}_{20} \geqslant -u_b$,$\tilde{x}_{30} \geqslant -u_b$ then $\tilde{x}_{2,3}(t) \geqslant -u_b$ for any $t \geqslant 0$.*

In what follows consider $\tilde{x}_o \in \Omega(G)$ such that $\tilde{x}_{20} \geqslant -u_b$ and $\tilde{x}_{30} \geqslant -u_b$.

6.11 Non-Polyhedral PIS

In this Section, it is shown that the largest PIS in $\Omega(G)$ is bounded by $\tilde{S}$. The set $\tilde{S}$ is characterized for the closed-loop system such that $\tilde{S} \subset \Omega(G)$. Consider the stable positive state feedback control found in Theorem 13, $F^* = K\begin{pmatrix} \frac{1}{\theta_2} & -\theta_3 & -\theta_3 \end{pmatrix}$ with $K > 0$ for the system (6.3) yielding closed-loop eigenvalues $\lambda_{1,2} = -\frac{1}{\theta_3}$ and $\lambda_3 = -K$. The resulting state solution with $\tilde{x}_o = (\tilde{x}_{10}\ \tilde{x}_{20}\ \tilde{x}_{30})^T$ is:

$$\tilde{x}_1(t) = \frac{1}{\tilde{K}^2}\Big(\tilde{x}_{10}\Big[(K^2\theta_3 t + K^2\theta_3^2 - 2K\theta_3 - Kt)e^{-\frac{t}{\theta_3}} + e^{-Kt}\Big] + \theta_2\theta_3\tilde{x}_{20}\Big[(1 + Kt - K^2\theta_3 t)e^{-\frac{t}{\theta_3}} - e^{-Kt}\Big]$$

$$+\tilde{x}_{30}\Big[(t\theta_2+\theta_2\theta_3-K\theta_2\theta_3 t)e^{-\frac{t}{\theta_3}}-\theta_2\theta_3 e^{-Kt}\Big]\Big) \tag{6.65}$$

$$\tilde{x}_2(t)=\frac{1}{\tilde{K}^2}\Big(\frac{K\tilde{x}_{10}}{\theta_2\theta_3}\Big[(K\theta_3 t-t-\theta_3)e^{-\frac{t}{\theta_3}}+\theta_3 e^{-Kt}\Big]+\tilde{x}_{20}\Big[(1+Kt-K^2\theta_3 t-K\theta_3+K^2\theta_3^2)e^{-\frac{t}{\theta_3}}-K\theta_3 e^{-Kt}\Big]$$

$$+\frac{\tilde{x}_{30}}{\theta_3}\Big[(t-K\theta_3 t+K\theta_3^2)e^{-\frac{t}{\theta_3}}-K\theta_3^2 e^{-Kt}\Big]\Big) \tag{6.66}$$

$$\tilde{x}_3(t)=\frac{1}{\tilde{K}}\Big(K[e^{-Kt}-e^{-\frac{t}{\theta_3}}][-\frac{\tilde{x}_{10}}{\theta_2}+\theta_3\tilde{x}_{20}]+\tilde{x}_{30}[K\theta_3 e^{-Kt}-e^{-\frac{t}{\theta_3}}]\Big) \tag{6.67}$$

where

$$\tilde{K}=K\theta_3-1 \tag{6.68}$$

6.11.1 Critical time t^*

The critical time t^* such that $\tilde{x}_1(t^*)=0$ is found by solving $\dot{\tilde{x}}_1(t^*)=-\theta_2\tilde{x}_2(t^*)=0$. Multiplying $\tilde{x}_2(t^*)=0$ by $(e^{\frac{t}{\theta_3}}\tilde{K}^2\theta_2\theta_3)$ and using (6.68) yields:

$$K\tilde{x}_{10}\Big[\Big(t^*\tilde{K}-\theta_3\Big)+\theta_3 e^{-\frac{\tilde{K}t^*}{\theta_3}}\Big]+\theta_2\theta_3\tilde{x}_{20}\Big[\Big(1+Kt^*(-\tilde{K})-K\theta_3+K^2\theta_3^2\Big)-K\theta_3 e^{-\frac{\tilde{K}t^*}{\theta_3}}\Big]$$

$$+\theta_2\tilde{x}_{30}\Big[\Big(t^*(-\tilde{K})+K\theta_3^2\Big)-K\theta_3^2 e^{-\frac{\tilde{K}t^*}{\theta_3}}\Big]=0 \tag{6.69}$$

rearranging

$$-t^*\tilde{K}\Big[-K\tilde{x}_{10}+\theta_2\theta_3 K\tilde{x}_{20}+\theta_2\tilde{x}_{30}\Big]=K\theta_3 e^{-\frac{\tilde{K}t^*}{\theta_3}}\Big[-x_{10}+\theta_2\theta_3(\tilde{x}_{20}+\tilde{x}_{30})\Big]$$

$$+K\theta_3\tilde{x}_{10}-\theta_2\theta_3\tilde{x}_{20}\Big(1+K^2\theta_3^2-K\theta_3\Big)-\theta_2\theta_3^2 K\tilde{x}_{30} \tag{6.70}$$

and thus

$$t^*=\frac{K\theta_3 e^{\frac{(-\tilde{K})t^*}{\theta_3}}\Big[-x_{10}+\theta_2\theta_3(\tilde{x}_{20}+\tilde{x}_{30})\Big]+K\theta_3\Big[\tilde{x}_{10}+\theta_2\theta_3(\tilde{x}_{20}-\tilde{x}_{30})\Big]-\theta_2\theta_3(1+K^2\theta_3^2)\tilde{x}_{20}}{(-\tilde{K})\Big[-K\tilde{x}_{10}+\theta_2\theta_3 K\tilde{x}_{20}+\theta_2\tilde{x}_{30}\Big]} \tag{6.71}$$

using $K\theta_3(\theta_2\theta_3\tilde{x}_{20})=-K\theta_3(\theta_2\theta_3\tilde{x}_{20})+2K\theta_3(\theta_2\theta_3\tilde{x}_{20})$ and rearranging

$$t^*=\frac{K\theta_3 e^{\frac{(-\tilde{K})t^*}{\theta_3}}\Big[-x_{10}+\theta_2\theta_3(\tilde{x}_{20}+\tilde{x}_{30})\Big]+K\theta_3\Big[\tilde{x}_{10}-\theta_2\theta_3(\tilde{x}_{20}+\tilde{x}_{30})\Big]-\theta_2\theta_3(1+K^2\theta_3^2)\tilde{x}_{20}+2K\theta_3(\theta_2\theta_3\tilde{x}_{20})}{(-\tilde{K})\Big[-K\tilde{x}_{10}+\theta_2\theta_3 K\tilde{x}_{20}+\theta_2\tilde{x}_{30}\Big]} \tag{6.72}$$

simplifying

$$t^* = \frac{K\theta_3 e^{\frac{(-\tilde{K})t^*}{\theta_3}}\Big[-x_{10}+\theta_2\theta_3(\tilde{x}_{20}+\tilde{x}_{30})\Big]+K\theta_3\Big[\tilde{x}_{10}-\theta_2\theta_3(\tilde{x}_{20}+\tilde{x}_{30})\Big]-\theta_2\theta_3\tilde{K}^2\tilde{x}_{20}}{(-\tilde{K})\Big[-K\tilde{x}_{10}+\theta_2\theta_3K\tilde{x}_{20}+\theta_2\tilde{x}_{30}\Big]} \tag{6.73}$$

Let

$$q_1(\tilde{x}_o) := -K\tilde{x}_{10}+\theta_2\theta_3K\tilde{x}_{20}+\theta_2\tilde{x}_{30} \tag{6.74}$$

and recall that

$$l\tilde{x}_o = \tilde{x}_{10}-\theta_2\theta_3(\tilde{x}_{20}+\tilde{x}_{30}). \tag{6.75}$$

Substituting $q_1(\tilde{x}_o)$ and $l\tilde{x}_o$ in (6.73) and rearranging terms yields

$$t^* = \frac{K\theta_3 l\tilde{x}_o(1-e^{-\frac{\tilde{K}t^*}{\theta_3}})-\tilde{K}^2\tilde{x}_{20}\theta_2\theta_3}{(-\tilde{K})q_1(\tilde{x}_o)} \tag{6.76}$$

To solve for $t^* \geqslant 0$, use also $\min_{t\geqslant 0}(C\tilde{x}(t)) = \tilde{x}_1(t^*) = 0$. Thus, equating (6.65) to zero, rearranging, multiplying by $e^{\frac{t}{\theta_3}}$ and using (6.68) results in:

$$-t^*\tilde{K}[-K\tilde{x}_{10}+\theta_2\theta_3K\tilde{x}_{20}+\theta_2\tilde{x}_{30}]+\tilde{x}_{10}(K^2\theta_3^2-2K\theta_3)+\theta_2\theta_3(\tilde{x}_{20}+\tilde{x}_{30}) = e^{-\frac{\tilde{K}}{\theta_3}t^*}[-\tilde{x}_{10}+\theta_2\theta_3(\tilde{x}_{20}+\tilde{x}_{30})]. \tag{6.77}$$

Adding and subtracting $\tilde{x}_{10}$ to the left hand side of the above equation and using (6.74) and (6.75) yields:

$$-t^*\tilde{K}q_1(\tilde{x}_o)+\tilde{x}_{10}\tilde{K}^2 = l\tilde{x}_o(1-e^{-\frac{\tilde{K}}{\theta_3}t^*}). \tag{6.78}$$

The above equation yields:

$$t^* = \frac{l\tilde{x}_o(1-e^{-\frac{\tilde{K}}{\theta_3}t^*})-\tilde{x}_{10}\tilde{K}^2}{(-\tilde{K})q_1(\tilde{x}_o)} \tag{6.79}$$

Now to solve for $t^* \geqslant 0$, first equate (6.76) and (6.79):

$$l\tilde{x}_o(1-e^{-\frac{\tilde{K}}{\theta_3}t^*})-\tilde{x}_{10}\tilde{K}^2 = K\theta_3 l\tilde{x}_o(1-e^{\frac{(-\tilde{K})t^*}{\theta_3}})-\tilde{K}^2\tilde{x}_{20}\theta_2\theta_3 \tag{6.80}$$

which is simplified to

$$-\tilde{K}l\tilde{x}_o(1-e^{-\frac{\tilde{K}}{\theta_3}t^*}) = \tilde{K}^2[\tilde{x}_{10}-\tilde{x}_{20}\theta_2\theta_3]. \tag{6.81}$$

Recall that $w^*\tilde{x}_o = \tilde{x}_{10} - \tilde{x}_{20}\theta_2\theta_3$, thus

$$e^{-\frac{\tilde{K}}{\theta_3}t^*} = 1 + \frac{\tilde{K}w^*\tilde{x}_o}{l\tilde{x}_o}. \tag{6.82}$$

Take the natural logarithm for both sides:

$$-\frac{\tilde{K}}{\theta_3}t^* = \ln(1 + \frac{\tilde{K}w^*\tilde{x}_o}{l\tilde{x}_o}) \tag{6.83}$$

which is solved in t^* as

$$t^* = -\frac{\theta_3}{\tilde{K}}\ln(1 + \frac{\tilde{K}w^*\tilde{x}_o}{l\tilde{x}_o}) \tag{6.84}$$

For a defined natural logarithm solution the argument must satisfy $(1 + \frac{\tilde{K}w^*\tilde{x}_o}{l\tilde{x}_o}) > 0$, and according to Remark22 $l\tilde{x}_o \geqslant 0$, thus

$$\tilde{K}w^*\tilde{x}_o > -l\tilde{x}_o \tag{6.85}$$

For t^* to be positive in (6.84), two cases are considered:

- $\tilde{K} > 0 \equiv K > \frac{1}{\theta_3}$ implies $\ln(1 + \frac{\tilde{K}w^*\tilde{x}_o}{l\tilde{x}_o}) \leq 0$ or the argument of natural logarithm satisfies $(0 < (1 + \frac{\tilde{K}w^*\tilde{x}_o}{l\tilde{x}_o}) \leq 1)$ yielding

$$-l\tilde{x}_o < \tilde{K}w^*\tilde{x}_o \leq 0, \tag{6.86}$$

  and

$$\tilde{K}w^*\tilde{x}_o \leq 0 \iff w^*\tilde{x}_o \leq 0 \tag{6.87}$$

- $\tilde{K} < 0 \equiv K < \frac{1}{\theta_3}$ implies $\ln(1 + \frac{\tilde{K}w^*\tilde{x}_o}{l\tilde{x}_o}) \geqslant 0$ or $(1 + \frac{\tilde{K}w^*\tilde{x}_o}{l\tilde{x}_o}) \geqslant 1$ that is

$$\tilde{K}w^*\tilde{x}_o \geqslant 0 \iff w^*\tilde{x}_o \leq 0 \tag{6.88}$$

The minimum condition $C\ddot{\tilde{x}}(t^*) > 0$ is presented in the next section to find the surface $\tilde{S} \subset \Omega(G)$ and to identify the closed-loop set of nonnegative minimum $\tilde{S}_+$ defined earlier.

6.11.2 Minimum Condition $\ddot{\tilde{x}}_1 \geqslant 0$

Assuming that the time $t^* \geqslant 0$ exists, then, as stated earlier the point $\tilde{x}_1(t^*) = 0, \dot{\tilde{x}}_1(t^*) = 0$ is a minimum if $\ddot{\tilde{x}}_1(t^*) > 0$ or equivalently:

$$\tilde{x}_3(t^*) < 0 \tag{6.89}$$

from (6.67)

$$\Big(K(e^{-Kt^*}-e^{-\frac{t^*}{\theta_3}})[-\frac{\tilde{x}_{10}}{\theta_2}+\theta_3\tilde{x}_{20}]+\tilde{x}_{30}(K\theta_3e^{-Kt^*}-e^{-\frac{t^*}{\theta_3}})\Big)<0 \tag{6.90}$$

multiplying by $\theta_2 e^{\frac{t^*}{\theta_3}}$ and rearranging

$$Ke^{-\frac{\tilde{K}t^*}{\theta_3}}\Big[-\tilde{x}_{10}+\theta_2\theta_3(\tilde{x}_{20}+\tilde{x}_{30})\Big]-\Big[-K\tilde{x}_{10}+\theta_2\theta_3K\tilde{x}_{20}+\theta_2\tilde{x}_{30}\Big]<0 \tag{6.91}$$

and substituting (6.74) and (6.75) in the above inequality yields

$$-Kl\tilde{x}_oe^{-\frac{\tilde{K}t^*}{\theta_3}}-q_1(\tilde{x}_o)<0 \tag{6.92}$$

substituting (6.82) in the above equation yields the condition for a minimum point as follows

$$q_1(\tilde{x}_o)>-Kl\tilde{x}_o(1+\frac{\tilde{K}w^*\tilde{x}_o}{l\tilde{x}_o}) \tag{6.93}$$

The region of minimum is thus defined as the set that verifies (6.86) (or (6.88) depending on the choice of K) and (6.93):

- From (6.86) where $\tilde{K}>0\equiv K>\frac{1}{\theta_3}$ yields the following minimum region

$$\mathbb{Q}_1:=\Big\{\tilde{x}_o\in\Omega(G)\Big|\ 0\geqslant\tilde{K}w^*\tilde{x}_o>-l\tilde{x}_o,\ q_1(\tilde{x}_o)>-Kl\tilde{x}_o(1+\frac{\tilde{K}w^*\tilde{x}_o}{l\tilde{x}_o})\Big\},\quad \tilde{K}>0 \tag{6.94}$$

- From (6.88) the following minimum region is obtained

$$\mathbb{Q}_2:=\Big\{\tilde{x}_o\in\Omega(G)\Big|\ \tilde{K}w^*\tilde{x}_o\geqslant 0,\ q_1(\tilde{x}_o)>-Kl\tilde{x}_o(1+\frac{\tilde{K}w^*\tilde{x}_o}{l\tilde{x}_o})\Big\},\quad \tilde{K}<0 \tag{6.95}$$

6.11.3 The Closed-loop Surface $\tilde{S}$

The set $\tilde{S}$ as defined (6.10) for the closed-loop system is found in this subsection. Substitute (6.84) in (6.65) to get $\tilde{x}_1(t^*)=0$ which yields $\tilde{x}_o\in\tilde{S}$ in the regions $\mathbb{Q}_1$ (or in $\mathbb{Q}_2$ respectively depending on the choice of $\tilde{K}$):

$$\tilde{S}=\Big\{\tilde{x}_o\in\mathbb{Q}_1\Big|\ \tilde{K}\Big(K\tilde{x}_{10}-\theta_2\tilde{x}_{20}\Big)=-q_1(\tilde{x}_o)\ln\Big(1+\frac{\tilde{K}w^*\tilde{x}_o}{l\tilde{x}_o}\Big)\Big\},\ \text{if } \tilde{K}>0 \tag{6.96}$$

6.12 Largest Closed-loop PIS [101]

The largest closed-loop PIS is characterized in the following theorem.

Theorem 14. *The largest closed-loop PIS in $\Omega(G)$ is $\Omega_{m_F} = \Omega(G^*) \cup \tilde{S}_+$.*

Proof. The final value of $\tilde{x}(t)$ is in $\Omega(G)$, bearing in mind that the closed-loop system equilibrium is the origin. The additional constraint or $\Omega(F^*)$ already represents a PIS as stated earlier in Remark 22 i.e. $\tilde{x}_o \in \Omega(G)$ implies $\tilde{x}(t) \in \Omega(l)$. What remains is thus to ensure $C\tilde{x}(t) \geqslant 0$ for any $t \geqslant 0$ in the set $\Omega(G)$. According to Theorem13 the largest polyhedral PIS is $\Omega(G^*)$ and if $\tilde{x} \in \Omega(G) \setminus \Omega(G^*)$ then necessarily $\tilde{x}(t) \in \mathbb{W}_-$. From this point, the reader is referred to the proof of Theorem 11 to show that $\tilde{S}_+ \cup \Omega(G^*)$ is the largest closed-loop PIS[7]. The Surface $\tilde{S}$ in (6.96), together with the planes $C\tilde{x} = 0$ and $l\tilde{x} = 0$, they form the boundary of the largest closed-loop PIS. □

As $\tilde{S}$ is found for the limit case $\tilde{x}_1(t^*) = 0$, to find the set $\tilde{S}_+$, given the initial condition ($\tilde{x}_o \in \mathbb{W}_-$) solve (6.84) to find $\tilde{x}_1(t^*) \geqslant 0$ and not only $\tilde{x}_1(t^*) = 0$. In this case, a solution of (6.84) can be found numerically as presented in the following section.

6.12.1 Finding $\tilde{S}_+$ using Lambert Function

A way to solve (6.84) is using Lambert W-function which characterizes the solutions $y = W(z)$ for $ye^y = z$, for any complex number z. Real solutions $W(z)$ are only obtained in the real range $z \geqslant -e^{-1}$ [102]. Equation (6.84) is rewritten to look like $ye^y = z$. Rearrange and multiply both sides of (6.76) by $\frac{e^{\frac{\tilde{K}t^*}{\theta_3}}}{\theta_3}$:

$$e^{\frac{\tilde{K}t^*}{\theta_3}} \left(\frac{\tilde{K}t^*}{\theta_3} + \frac{Kl\tilde{x}_o - \tilde{K}^2\theta_2\tilde{x}_{20}}{q_1(\tilde{x}_o)} \right) = \frac{Kl\tilde{x}_o}{q_1(\tilde{x}_o)} \tag{6.97}$$

denote $q_2(\tilde{x}_o) = \frac{Kl\tilde{x}_o - \tilde{K}^2\theta_2\tilde{x}_{20}}{q_1(\tilde{x}_o)}$ multiply both sides by $e^{q_2(\tilde{x}_o)}$ yields

$$e^{\frac{\tilde{K}t^*}{\theta_3} + q_2(\tilde{x}_o)} \left(\frac{\tilde{K}t^*}{\theta_3} + q_2(\tilde{x}_o) \right) = e^{q_2(\tilde{x}_o)} \frac{Kl\tilde{x}_o}{q_1(\tilde{x}_o)} \tag{6.98}$$

the above equation matches the form $ye^y = z$, thus the solution $y = W(z)$

$$\frac{\tilde{K}t^*}{\theta_3} + q_2(\tilde{x}_o) = W\left(e^{q_2(\tilde{x}_o)} \frac{Kl\tilde{x}_o}{q_1(\tilde{x}_o)} \right) \tag{6.99}$$

[7] $\tilde{S}_+$ is as defined in (6.31)

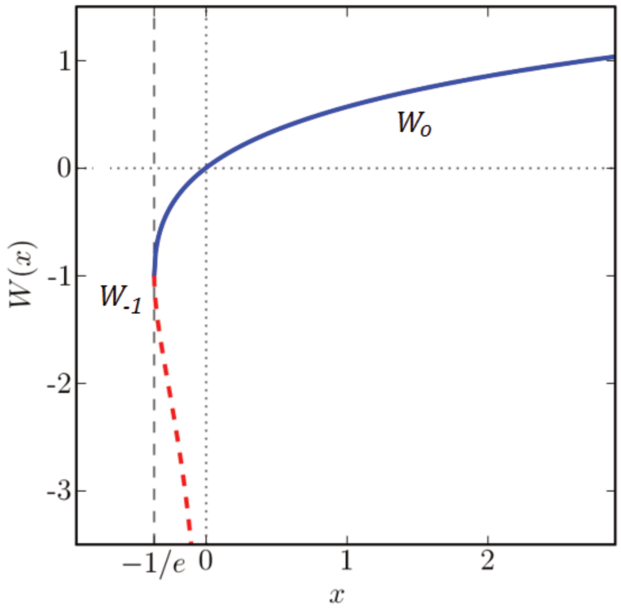

Figure 6.4 Lambert W-function and its two branches.

and thus

$$t^* = \frac{\theta_3}{\tilde{K}}\left(W\left(e^{q_2(\tilde{x}_o)}\frac{Kl\tilde{x}_o}{q_1(\tilde{x}_o)}\right) - q_2(\tilde{x}_o)\right) \tag{6.100}$$

A W-function is a multivalued function, it has two branches: the negative branch W_{-1} for $-e^{-1} \leq z < 0$ and the principal branch W_o for $-e^{-1} \leq z < \infty$ which connect at $-e^{-1}$. It means that in the interval $-e^{-1} < z < 0$ the equation $W(z)e^{W(z)} = z$ has two solutions as depicted in Fig. 6.4. Various numerical approximations are provided in the literature to compute the W-function [102] that are available in many computer packages like *Mathematica* and *MATLAB*.

Once $t^* \geqslant 0$ is calculated via (6.100), and using (6.65) compute $\tilde{x}(t^*)$ to find out whether $\tilde{x}(t^*) \in \tilde{S}_+ \subset \Omega_{m_F}$ or not to predict for hypoglycemia.

As will be shown in §6.14, if hypoglycemia is predicted in both open and also closed-loop whenever $\tilde{x}_o \in \tilde{S}_-$. As detailed in §6.8, if hypoglycemia is predicted in open-loop (continuous basal injection $\tilde{u} = 0$), then pump-off state is activated and insulin injection is seized i.e. $\tilde{u} = -u_b$. Hypoglycemia may also occur even when the pump is off due to insulin overdosing, physical activity, stress or sickness.

6.13 Pump-off hypoglycemia Prediction $\tilde{u} = -u_b$

In this section, pump off state $\tilde{u} = -u_b$ ($u = 0$) for system (6.3) is studied to predict off-state hypoglycemia episodes. High hypoglycemia risk is signaled in this case and the patient must take exogenous glucose to avoid the future hypoglycemic episode. This important step will complete the general hypoglycemia prediction algorithm in § 6.14.

Setting $\tilde{u} = -u_b$ ($u = 0$ pump-off condition) in (6.3) yields the following solution with the set of initial conditions $(\tilde{x}_{10}, \tilde{x}_{20}, \tilde{x}_{30})$:

$$\tilde{x}_1(t) = \tilde{x}_{10} + \theta_2\theta_3(\tilde{x}_{20} + \tilde{x}_{30} + 2u_b)(e^{-\frac{t}{\theta_3}} - 1) + \theta_2(\tilde{x}_{30} + u_b)te^{-\frac{t}{\theta_3}} + \theta_2 u_b t \tag{6.101}$$

$$\tilde{x}_2(t) = \left(\tilde{x}_{20} + u_b + \frac{(\tilde{x}_{30} + ub)t}{\theta_3}\right)e^{-\frac{t}{\theta_3}} - u_b, \tag{6.102}$$

$$\tilde{x}_3(t) = (\tilde{x}_{30} + u_b)e^{-\frac{t}{\theta_3}} - u_b. \tag{6.103}$$

To predict pump-off hypoglycemia, the decreasing rate of change condition ($\dot{\tilde{x}}_1(t) < 0$) is studied to find the time instant t^* at which $\dot{\tilde{x}}_1(t^*) = 0$.

Note that glycemia will diverge if zero insulin injection is maintained (see (6.101)) due to endogenous glucose production. Thus any pump-off hypoglycemia event will be temporary having hypoglycemic nadir $\tilde{x}_1(t^*) < 0$. Therefore, the focus will be again on the minimum conditions of glycemia $\min_{t \geqslant 0}(C\tilde{x}(t))$.

6.13.1 Critical time

As explained earlier, the time instant t^* such that $C\tilde{x}(t^*) = \min_{t \geqslant 0}(C\tilde{x}(t))$ is the solution of $\dot{\tilde{x}}_1(t^*) = 0$:

$$t^* = \frac{\theta_3}{\tilde{x}_{30} + u_b}[u_b e^{\frac{t^*}{\theta_3}} - (\tilde{x}_{20} + u_b)] \tag{6.104}$$

The point $\dot{\tilde{x}}_1(t^*) = 0$ is a minimum if $\ddot{\tilde{x}}_1(t^*) > 0$ and thus $\tilde{x}_3(t^*) < 0$ equivalently:

$$\tilde{x}_{30} < -u_b(1 - e^{\frac{t^*}{\theta_3}}) \implies \tilde{x}_{30} < 0 \tag{6.105}$$

The time instant t^* can be calculated using Lambert W-function, thus rearranging (6.104) to become

$$t^* = -\theta_3\Big(\frac{\tilde{x}_{20} + u_b}{\tilde{x}_{30} + u_b} + W\big(-\frac{u_b e^{-\frac{\tilde{x}_{20}+u_b}{\tilde{x}_{30}+u_b}}}{\tilde{x}_{30} + u_b}\big)\Big) \tag{6.106}$$

In this manner, hypoglycemia episodes can be predicted given the initial conditions and using (6.104) in (6.101). It is good to mention that the system, in this case, does not have any equilibrium due to the divergence of glycemia (continuous endogenous glucose production versus zero insulin injection see (6.101)).

In the following section, a general algorithm of hypoglycemia prediction for open and closed-loop system is presented.

6.14 Fasting-Hypoglycemia Prediction: a General algorithm

The PIS of open and closed-loop systems can be used to detect and predict future hypoglycemic episodes given the initial condition $\tilde{x}_o$ apply the following procedure:

1. If $\tilde{x}_o \notin \Omega_{m_f}$ ($\tilde{x}_o \in \tilde{S}_-$), then check whether $\tilde{x}_o \in \Omega_m$ if yes then set $K = 0$ and apply the basal control to stabilize glycemia to some equilibrium according to (6.11)-(6.13). Once the system is at rest at some $t = t_1$, then $\tilde{x}(t_1) \in \Omega_{m_f}$ then turn on the state feedback control $\tilde{u} = F^* \tilde{x}$ to steer glycemia to its reference.

2. Otherwise

   Proposition 3. *If $\tilde{x}_o \notin \Omega_m$ then the following Hypoglycemia alert algorithm is applied:*

   (a) Solve (6.104) *in t^* (if any).*

   (b) Check for a minimum by evaluating t^* in (6.103).

   (c) If $\tilde{x}_3(t^*) < 0$ then check whether $\tilde{x}_1(t^*) < 0$.

   During hypoglycemia alert ($\tilde{u} = -u_b$) the patient is strongly advised to take some carbohydrates.

   $\tilde{u} = -u_b$ (pump is off) is maintained until the state trajectory enters one of the PIS Ω_m, Ω_{m_f}.

In the next section, the largest polyhedral PIS of the overall system including the plasma and the subcutaneous insulin rates $\tilde{x}_2$ and $\tilde{x}_3$ respectively is found. In this case the output matrix becomes $C = I_{3\times 3}$. The PIS is firstly characterized in open-loop case $\tilde{u}(t) = 0$ and then for the closed-loop system such that $\tilde{u}(t) = F^* \tilde{x}(t) \geqslant 0$.

6.15 The Polyhedral PIS in $\mathbb{R}^3_+$: $C = I_{3\times 3}$

So far, the feasible invariant set is formed considering a single output: glycemia concentration $C\tilde{x} \geqslant 0$, $C = (1\,0\,0)$. In this section, the problem is to find the positivity and invariance of all states: glycemia and insulin considering $C = I_{3\times 3}$. The largest PIS is found in $\Omega(C)$ or in $\mathbb{R}^3_+$. According to (6.5) and (6.6), insulin states are constrained to the basal level i.e. $\tilde{x}_2(t) \geqslant 0, \tilde{x}_3(t) \geqslant 0$. For this purpose, define $Q = \begin{pmatrix} 0 & 1 & 0 \\ 0 & 0 & 1 \\ & l & \end{pmatrix}$. It will be shown in the following subsections that $\Omega(Q)$ is the largest polyhedral PIS in $\Omega(C)$ (or in $\mathbb{R}^3_+$). According to Definition 5, $\Omega(Q)$ implies $l\tilde{x} \geqslant 0$. The latter inequality, in open-loop case, ensures a nonnegative final values for $\tilde{x}_1(t)$ as show in § 6.4.1. In closed-loop $\tilde{u} = F^*\tilde{x}$, recall that $F^* = Kl$, $K > 0$, thus $\Omega(Q)$ guarantees the positivity of the control.

6.15.1 Open-loop $\tilde{u} = 0$

The following proposition is applied for system (6.3) with $C = I_{3\times 3}$ and $\tilde{u} = 0$.

Proposition 4. *The set $\Omega(Q)$ is the largest polyhedral PIS in $\Omega(C)$ (or in $\mathbb{R}^3_+$).*

Proof. According to Proposition 1, $\Omega(Q)$ is PIS with a unique Metzler matrix H:

$$H = \begin{pmatrix} -\frac{1}{\theta_3} & \frac{1}{\theta_3} & 0 \\ 0 & -\frac{1}{\theta_3} & 0 \\ 0 & 0 & 0 \end{pmatrix} \tag{6.107}$$

Thus, $\tilde{x} \in \Omega(Q)$ implies $\tilde{x}_2(t) \geqslant 0, \tilde{x}_3(t) \geqslant 0$ and $\tilde{x}_1 \geqslant \theta_2\theta_3(\tilde{x}_2 + \tilde{x}_3)$ for any $t \geqslant 0$. Satisfying these inequalities simultaneously implies $\tilde{x}_1(t) \geqslant 0$ for any $t \geqslant 0$. □

6.15.2 Closed-loop $\tilde{u}(t) = F^*\tilde{x}(t) \geqslant 0$

The following proposition is applied for system (6.3) with $C = I_{3\times 3}$ and $\tilde{u} = F^*\tilde{x}$.

Proposition 5. *The set $\Omega(Q)$ is the largest closed-loop polyhedral PIS in $\Omega(C)$ (or in $\mathbb{R}^3_+$).*

Proof. The proof follows from applying Proposition 1 on system (6.3) with $\tilde{u}(t) = F^*\tilde{x}(t)$ with the following unique Metzler matrix H

$$H = \begin{pmatrix} -\frac{1}{\theta_3} & \frac{1}{\theta_3} & 0 \\ 0 & -\frac{1}{\theta_3} & \frac{1}{\theta_3} \\ 0 & 0 & -K\theta_2 \end{pmatrix} \tag{6.108}$$

Thus, $\tilde{x} \in \Omega(Q)$ implies $\tilde{x}_2(t) \geqslant 0, \tilde{x}_3(t) \geqslant 0$ and $\tilde{x}_1 \geqslant \theta_2\theta_3(\tilde{x}_2 + \tilde{x}_3)$ for any $t \geqslant 0$. Satisfying these inequalities simultaneously implies $\tilde{x}_1(t) \geqslant 0$ for any $t \geqslant 0$. □

The state/input positivity is ensured in the largest polyhedral PIS $\Omega(G)$ of the closed-loop system.

In the following section, some numerical simulation results are presented to demonstrate the performance of the positive state feedback controller.

6.16 Numerical Results

Firstly, the positive controller performance is tested on the nominal system during fasting phase and then under meal perturbations on Magdelaine's Simulator or Simulator 1. Secondly, non-nominal test is conducted testing the controller on Uva/Padova simulator on 10 adults under measurement noise. Thereafter, a second non-nominal case study is performed on Simulator 1 to see the influence of the uncertainty of the intra patient parameters on the positivity constraints of the controller and BG error.

6.16.1 Fasting phase

The state feedback gain is designed as $K = 0.05$ in (6.56) setting BG reference in (6.4) at $G_r = 110$ mg/dL. The design is tested during fasting phase on five T1DM virtual subjects labeled as IF2, IF3, IF9, LR and BE. The virtual patient parameters are as given [58]. The state variables are considered available for the controller. BG behavior is as illustrated in Fig. 6.5. The state trajectory of IF2 case is shown in Fig. 6.7 in $\tilde{x}$ coordinates. $\tilde{u}(0) = 0.611$U/min. and the trajectory remains above the blue plane in Fig. 6.7 and then it slides on it i.e. $\tilde{u}(t) \geqslant 0$.

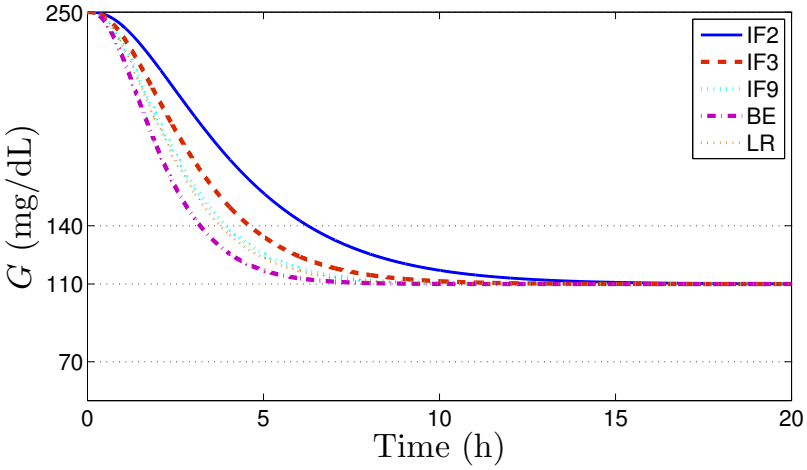

Figure 6.5 Closed-loop response of glycemia for five virtual patients with $\tilde{x}_o = (140, 0, 0)$.

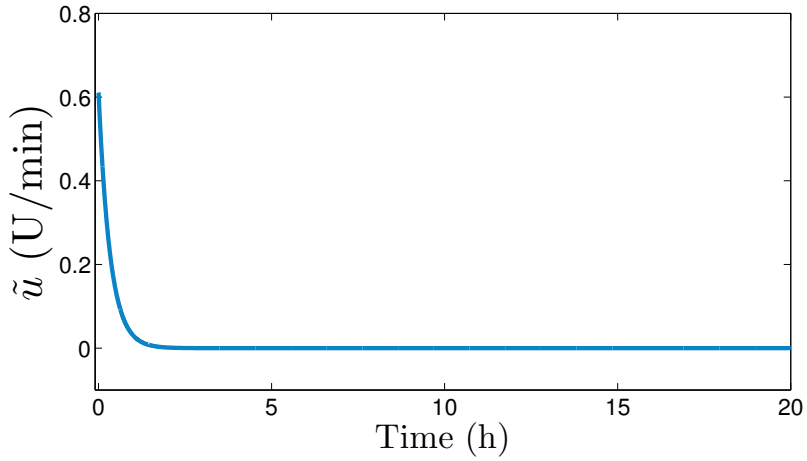

Figure 6.6 The control $\tilde{u}(t)$ for IF2 patient.

In the following subsection, *in silico* trials under meal perturbations are considered.

6.16.2 Including meals

A Luenberger observer is firstly designed to estimate the insulin states $\tilde{x}_2, \tilde{x}_3$ for the state feedback controller:

$$\dot{\hat{\tilde{x}}} = A\hat{x} + B\tilde{u}(t) + LC(\tilde{x} - \hat{\tilde{x}}) \tag{6.109}$$

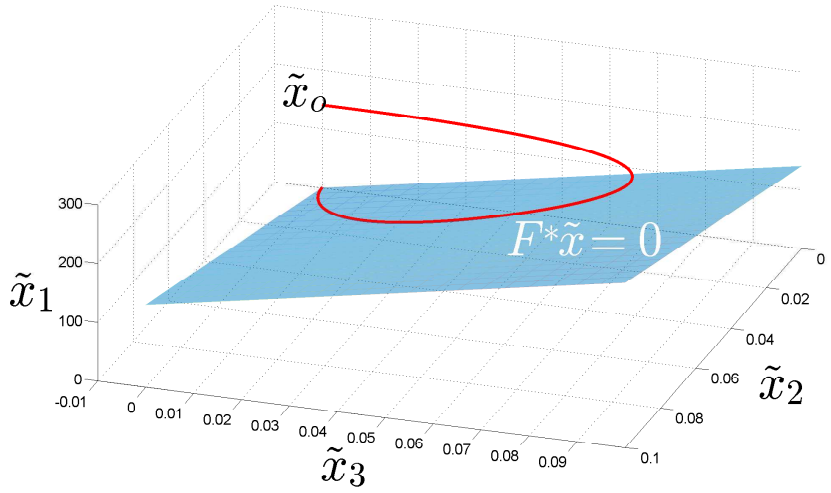

Figure 6.7 A trajectory plot in phase portrait for IF2 with $\tilde{x}(0) = (140, 0, 0)$, the blue plane represents $F^*\tilde{x} = 0$ with $K = 0.05$.

based on the BG output measurement i.e. $C = (1\,0\,0)$. L is the observer gain matrix designed using pole placement method with the following poles $\lambda_L = -(10K \ \frac{1}{\theta_3} \ \frac{1}{\theta_3})$ that yielded a relatively fast convergence as shown in Fig. 6.8.

Nominal test The test is conducted on two patients tagged as BE and LR applying the meal scenario of the clinical diary in [58]. The reference value is set to $G_r = 120$ mg/dL and the results are compared to the patient manual open-loop injections. The BG behavior and the closed-loop injections are illustrated in Fig. 6.9 and 6.10. As shown, hypoglycemia is completely prevented throughout the simulation. In BE case, the estimation error illustrated in Fig. 6.8 at the beginning of the simulation led the controller to slightly cross the basal rate for a while i.e. $-u_b < \tilde{u} < 0$, i.e. $\min(\tilde{u}) = -0.0083 > -u_b$. Other than that, the controller remains positive for the remaining simulation time. In LR case (Fig. 6.10), no estimation error is considered here where $\hat{\tilde{x}}_{2,3}(0) = \tilde{x}_{2,3}(0)$.

Although parameters uncertainties are not taken into account in the design of the positive control and its largest PIS, a robustness test is also conducted in the following trials.

Non-nominal test

1. **Uva/Padova trial** This *in silico* trial comprises a fasting period of around 30 hours followed by normal 36 hours meal scenario of subsection 4.14.2. The controller is tested on ten virtual T1DM adults in noisy environment using Dexcom 70 CGM sensor and a generic insulin pump. For robustness against measurement noise, the trial is

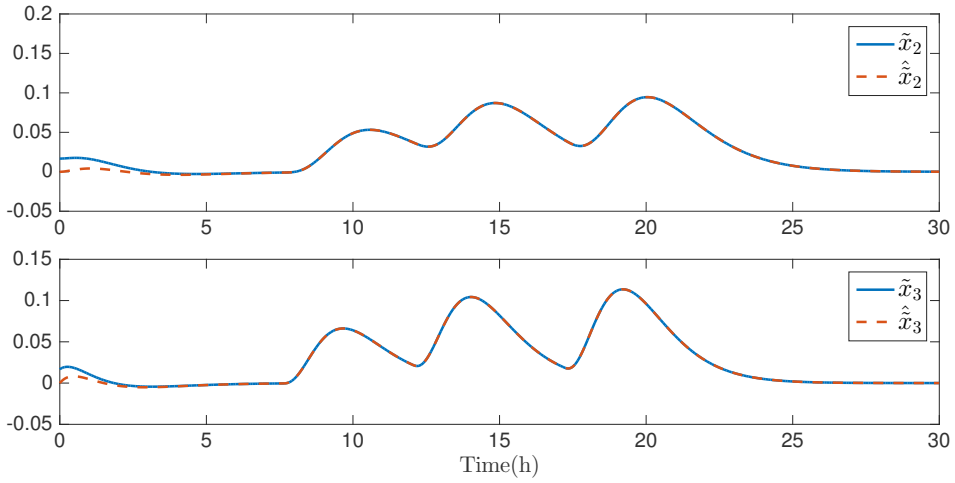

Figure 6.8 Observer behavior: insulin states and their estimation in closed-loop $K = 0.03$.

repeated 5 times per subject with different simulated sensor noises. $G_r = 120$ mg/dL and the controller is tuned setting $K = 0.005$. The control parameters θ_i, $i = 1,2,3$ are identified here on Uva/Padova simulator by the developer of Simulator 1. He used data fitting to identify the parameters of the linear model of Simulator 1 on the open-loop BG profile of each adult of Uva/Padova under some meal scenario. For instance, open-loop data fitting for adult 7 yielded $\theta_i = 0.8, 40, 80, u_b = \frac{\theta_1}{\theta_2}$. The mean BG of the 10 adults $\times$ 5 runs is illustrated in Fig. 6.11.

The Control Variability Grid Analysis (CVGA) points is depicted in Fig. 6.12. CVGA results represent per-subject glucose extremes as computed by the Uva/Padova simulator. In this plot, each point is plotted with an x-coordinate and y-coordinate equal to the per-subject minimum and maximum BG values over the observation period, respectively. As illustrated in Fig. 6.12, hypoglycemia is avoided during the 50 simulations and a satisfactory postprandial behavior is achieved. Moreover, a good robustness level is achieved applying the same design on different patients. The positivity of the control $\tilde{u}$ is not guarantied as illustrated in Fig. 6.13. This is not surprising as the the positive controller is designed for the nominal system and the parameters uncertainty and measurement noise were not taken into account in the design. However, it was noticed that the overall control remained positive i.e. $u(t) = \tilde{u} + u_b, u(t) \geqslant 0$ as illustrated in the case of Fig. 6.13. [8]

[8]The minimum estimated basal rate of the ten adults of Uva/Padova simulator $u_b = 0.0158$ U/min for adult9.

2. **Simulator 1** Another robustness test is performed on Simulator 1 to explore the controller performance under an intra-patient parameters uncertainty[9]. Assume that the insulin sensitivity factor θ_2 and insulin time constant θ_3 are underestimated by 30% i.e. $\hat{\theta}_{2,3} = 0.7\theta_{2,3}$. The controller (and the observer respectively) are based on the uncertain parameters: $F^* = (\frac{1}{\hat{\theta}_2} - \hat{\theta}_3 - \hat{\theta}_3)$. The resulting BG behavior of patient BE is illustrated in Fig. 6.14. As shown, the positivity of controller in the uncertain case is no more guaranteed and it hits the negative lower limit[10] $\tilde{u}(t) = -u_b$ several times. Moreover, hypoglycemia threshold is slightly crossed.

From these results, it is shown that a good robustness level is achieved. Yet, positivity and invariance properties of the input/output of the closed-loop system are affected by parameters uncertainties and also by measurement noise. For these reasons, positivity and invariance of the closed-loop system considering parameters uncertainty is envisioned as a perspective of this work.

6.17 Conclusion

The main results of this chapter are summarized in the following points:

- The first characterization of the largest PIS of glycemia dynamical system under fixed basal insulin input.
- The major outcome of this PIS is that any initial condition outside this set signals future hypoglycemia episode.
- This basal PIS outcome is general: basal injection is essential for glycemia regulation in both open and closed-loop. Glycemia dynamics under basal control is found in nocturnal time, pre-prandial and follows the postprandial bolus.
- This hypoglycemia prediction holds from any initial condition independently from the previous control that was applied to the system.

The system in open-loop is critically stable of one pole at the origin and two repeated negative poles. In other words, under basal injection ($\tilde{u} = 0$) glycemia state can settle anywhere. To regulate glycemia to normal level, state feedback control is designed.

[9] without any observer estimation error $\hat{\tilde{x}}_{2,3}(0) = \tilde{x}_{2,3}(0)$.

[10] Recall that the lower negative bound for $\tilde{u}(t)$ is $-u_b$ which corresponds to the zero limit of the overall insulin injection: $u(t) = (\tilde{u}(t) + u_b) \geqslant 0$.

- First positive state feedback control is designed to regulate glycemia. This is due to the fact that glycemia regulation is a positive control problem, namely, once insulin is injected it can not be taken back.
- The controller is designed such that glycemia remains invariant above or within the desired set point.
- In the resulting largest PIS, tight glycemia regulation is achieved and thus hypoglycemia is prevented.
- A general hypoglycemia prediction algorithm is implemented benefiting from the largest open and closed-loop PIS.
- Hypoglycemia prediction permits to decide in advance whether to keep the current control strategy, to turn to basal or to switch the pump off completely.
- The numerical simulations demonstrated the invariance properties of the state/input solutions.
- Hypoglycemia, the major challenge and open problem for AP studies, is avoided.
- Uncertainty of system parameters affects the observer and the overall control especially in respecting positivity constraints.

6.18 Perspectives

Input/output positivity constraints have been treated in this chapter for the nominal system. Parameters uncertainties and measurement noise were not taken into account in the design of positive controller and the resulting largest PIS. Positivity analysis under these circumstances is considered as a perspective. The future work of this chapter results are summarized as follows:

- To consider the bounds of the parameter uncertainties in the design of the positive controller and the characterization of the largest PIS.
- To take the worst case scenario of the parameters uncertainties in the hypoglycemia prediction algorithm.
- To implement and realize the positive closed-loop control algorithm incorporating the hypoglycemia prediction algorithm and test the resulting artificial pancreas *in silico*.

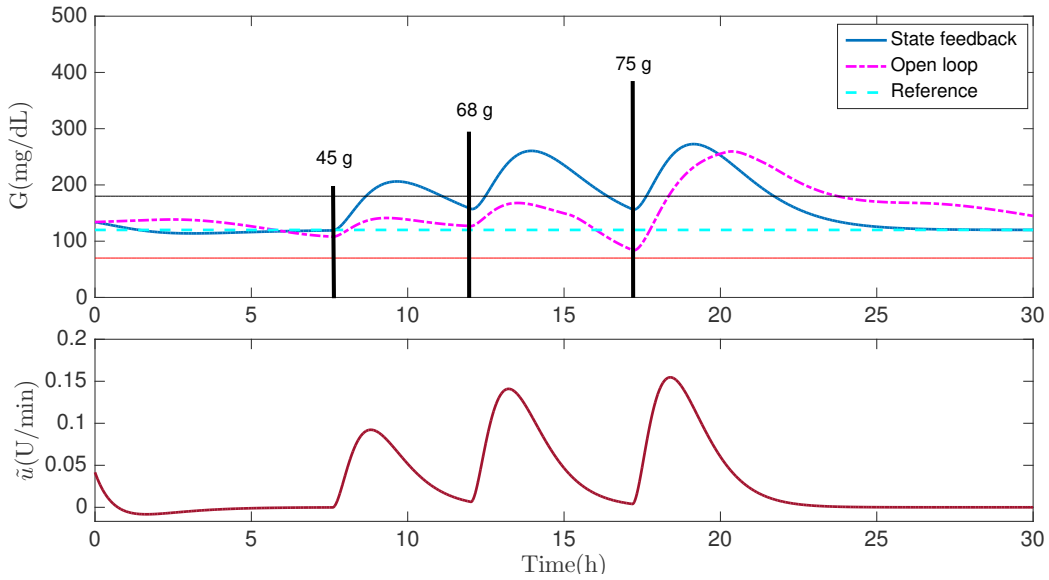

Figure 6.9 BG behavior of BE patient under state feedback control with $K = 0.03$.

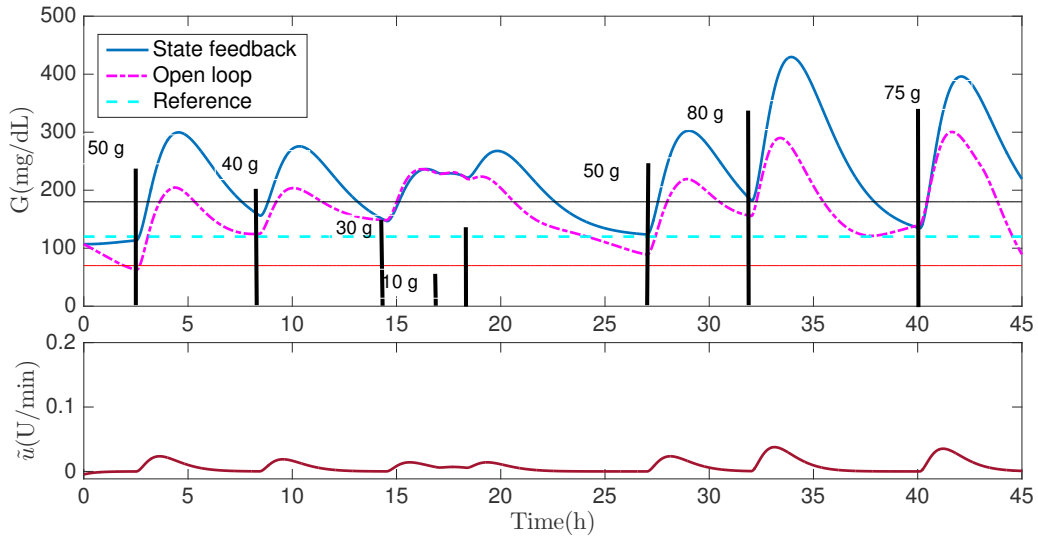

Figure 6.10 BG behavior of LR patient under state feedback control with $K = 0.03$.

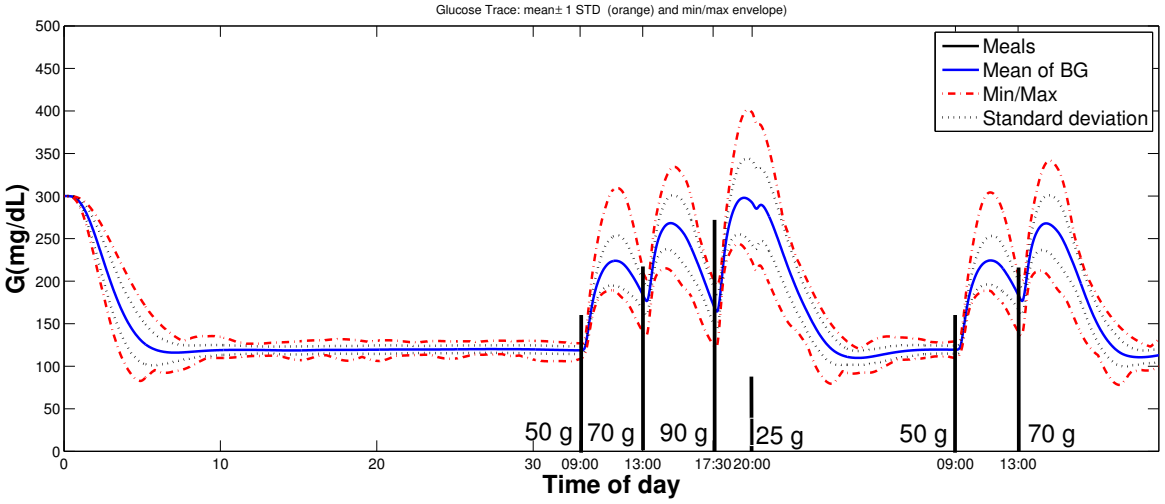

Figure 6.11 BG behavior of 10 adults under 5 runs with $K = 0.005$.

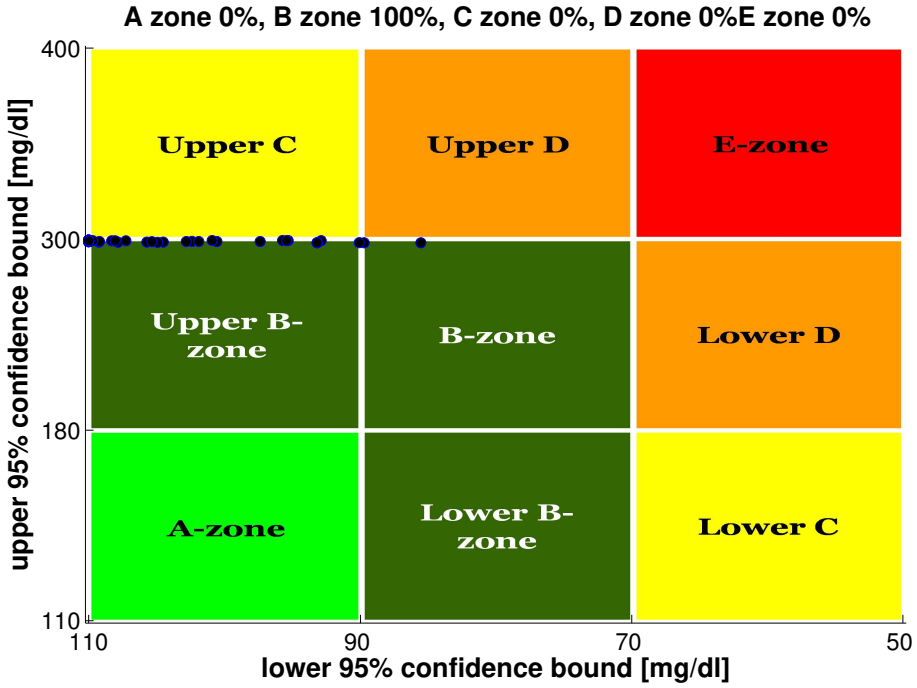

Figure 6.12 Control Variability Grid Analysis (CVGA) plot of Uva/Padova (10 adults $\times$ 5 runs) simulations.

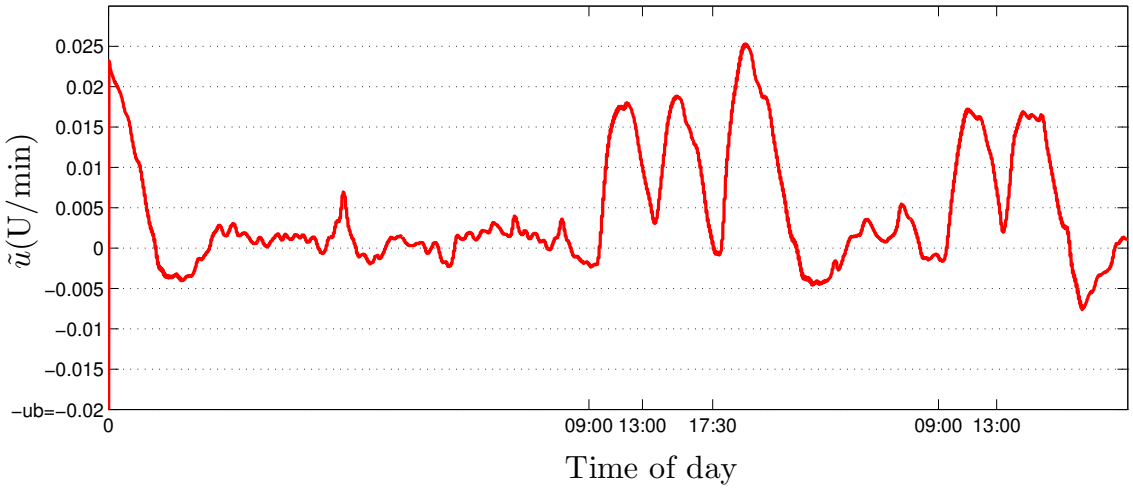

Figure 6.13 The state feedback insulin infusion rates of adult7 of Uva/Padova simulator: a one sample of the (10 adults $\times$ 5 runs) simulations.

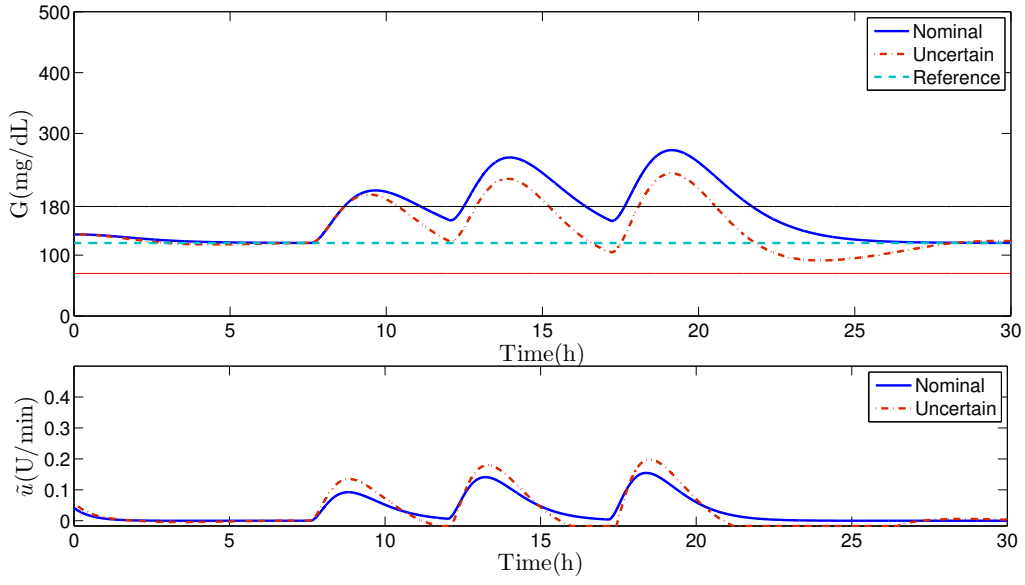

Figure 6.14 BG behavior of BE patient (Simulator 1): nominal system versus uncertain parameters. $K = 0.03, \hat{\theta}_{2,3} = 70\%\theta_{2,3}$ $\tilde{u}$ lower bound is $-u_b = -0.0167$.

Chapter 7

Conclusions and Perspectives

7.1 General Conclusion and Perspectives in French

Avant de passer à l'évaluation des algorithmes de commande, un facteur important est discuté, qui est la modélisation mathématique du système de DT1. D'après le bref aperçu des principaux modèles de la littérature PA, les points suivants sont conclus :

- Les modèles historiques largement utilisés comme Bergman ont des points d'équilibre non naturels qui ne sont pas compatibles avec le comportement glycémique de DT1 dans la vie réelle.
- Ces équilibres non naturels impliquent un ensemble d'insuline basale qui mantient la glycémie constante. Alors qu'un patient DT1 a un niveau d'insuline basale unique qui stabilise glycemié à n'importe quelle valeur.
- Une bonne description mathématique de la dynamique glycémie-insulinémie d'un DT1 est requise pour tout algorithme de commande pour la validation *in silico* et parfois dans sa conception comme modèle interne.
- Une mauvaise réponse en boucle fermée est donc attendue lorsque toute conception d'algorithme de commande (ou simulation) est basée sur un mauvais modèle mathématique.

Pour ces raisons, le modèle employé dans cette thèse est le modèle de DT1 à long terme récemment développé. Ce modèle a montré une bonne description de la dynamique glycémie-insulinémie de DT1.

La commande sans modèle (CSM) est conçu pour la régulation de la glycémie pour la première fois.

Résumé des résultats de CSM et conclusions principales

- iP est d'abord testée en utilisant une trajectoire de référence variable.
- L'hyperglycémie est réduite par la commande impulsive en forme de bolus résultant d'une réaction rapide aux repas. Cependant, un bon compromis de performance basal-postprandial par sujet ne peut être cédé en utilisant une conception fixe.
- Les résultats *in silico* ont montré une meilleure régulation de la glycémie postprandiale avec une iPID de référence constante par rapport au iP avec référence variable et par rapport au PID classique.
- Une solution, utilisée dans la littérature de PA, pour éviter le "windup" du term intégra,l consiste à remplacer le terme intégral par le débit basal spécifique du sujet, c'est-à-dire PD + débit basal.
- iPD + débit basal a été comparé à PD + débit basal. Le régulateur intelligent a détecté les repas et a réagi plus rapidement à ces perturbations par rapport à un PD classique.

CSM a montré un bon niveau de robustesse. Le système est considéré comme une boîte noire et les paramètres du CSM sont réglés empiriquement sur la base des mesures d'entrée/sortie. En ce qui concerne la performance, les questions suivantes ont été soulevées :

1. Les contraintes du système ne sont pas prises en compte dans la conception, à savoir le seuil d'hypoglycémie et la positivité du contrôleur. Le régulateur a été saturé à zéro qui est la limite inférieure admissible.
2. Lorsque le régulateur est saturé à zéro, la boucle est cassée et la glycémie n'est plus sous contrôle iPID.
3. Pour les systèmes sous contraintes d'actionneur, le problème de saturation du term intégral est un défaut connu pour les régulateurs de type PID.
4. L'évitement de l'hypoglycémie n'est pas assurée.

Ainsi, le maintien d'une contrôle glycémique "serrée", en particulier pendant la phase post-prandiale, n'est pas une tâche facile pour cet iPID entièrement automatique.

En dehors de l'application spécifique de la glycémie, la stabilité en boucle fermée, en particulier pour le régulateur iP, est non seulement liée à la première dynamique d'erreur résultant de la commande constituent le modèle ultra-locale. Il a été montré, par un exemple, qu'un système ne peut pas être stabilisé inconditionnellement par une commande iP.

Les résultats principaux de la conception du CMG dans ce travail sont :

- L'existence d'un CMG positif pour la régulation de la glycémie a été montrée ici pour la première fois.
- Au meilleur de la connaissance de l'auteur, CMG positif n'a pas été considéré précédemment dans l'histoire des études du PA.
- Le plus grand EPI où la variable d'insuline plasmatique est non négative sous CMG a été trouvé.
- La positivité du GMC a été assurée partout dans cet ensemble via les paramètres de conception. Ainsi, les contraintes d'entrée / d'état, du système d'insuline du second ordre, sont respectées.
- La contrainte CMG positive supplémentaire ne réduisait pas le plus grand EPI en boucle fermée.

Le futur CMG positif

- Le CMG positif conçu est une preuve de concept et la conception peut être étendue pour inclure la contrainte d'hypoglycémie.
- Les incertitudes des paramètres et les perturbations des repas seront prises en compte dans la conception du CMG positif.

Le problème de trouver le plus grand EPI où la glycémie reste *invariant*, dans ou au-dessus du seuil souhaité, a également été considéré dans ce travail. La boucle est fermée par l'intermédiaire d'un régulateur par retour d'état positif.

Prestations de la conception de la commande par retour d'état positive contre le CMG positif

- La loi de commande est simple et continue et la structure en boucle fermée qui en résulte est unique.
- Donc, trouver le plus grand PIS en boucle fermée (pour le système global), sous commande positive, est moins complexe que celui avec CMG.

Les mérites de cette commande par retour d'état positive sont :

- La contrainte des injections d'insuline (comme entrée positive) dans la conception de la commande par retour d'etat n'a pas été considérée précédemment dans les études du PA.
- En comparaison avec le courant dominant des algorithmes de commande de PA, le retour d'état positif conçu rassemble la simplicité de conception en prenant des contraintes du système en compte.
- Dans le plus grand EPI en boucle fermée, un contrôle "serré" de la glycémie est atteint et l'hypoglycémie est totalement évitée.
- Un autre résultat important du plus grand EPI de la glycémie du système en boucle ouverte et fermée est la prédiction de l'hypoglycémie. Une solution pour éviter la barrière potentiellement mortelle au traitement diabétique optimal.

L'analyse de positivité s'avère très utile pour la régulation étroite de la glycémie et aussi pour la prédiction de l'hypoglycémie.

Perspectives de la commande positive par retour de l'état

- Considérer les incertitudes des paramètres intra-patient dans la conception de la commande.
- Prendre le pire scénario des incertitudes des paramètres dans l'algorithme de prédiction de l'hypoglycémie.
- Implémenter et réaliser l'algorithme de commande en boucle fermée incorporant l'algorithme de prédiction d'hypoglycémie et tester le pancréas artificiel résultant *in silico*.

7.2 General Conclusion and Perspectives

Before going through closed-loop control assessment, an important factor is highlighted, that is mathematical modeling of T1DM system. From the the brief overview of the main models in the AP literature, the following points are concluded:

- The widely used historical models like Bergman have non-natural equilibria that are not consistent with T1DM glycemic behavior in real life.

- Those non-natural equilibria imply a *set* of basal insulin that maintains BG constant. Whereas a T1DM patient has a unique basal insulin level that stabilizes BG at any value.
- A good mathematical description of glycemia-insulinemia dynamics for a T1DM is required for any controller for the *in silico* validation and sometimes in its design as internal model.
- A poor closed-loop response is thus expected when any control algorithm design (or simulation) is based on a poor mathematical model.

For theses reasons, the employed model in this thesis is the recently developed long-term T1DM model. This model has shown a good description of glycemia-insulinema dynamics of T1DM.

MFC is designed for glycemia regulation for the first time. In opposition to previous PID studies, the control algorithm developed here is fully automated without any feed-forward or supplementary insulin doses.

MFC results summary and main conclusions

- iP is firstly tested employing a variable reference trajectory.
- Hyperglycemia is reduced via the resulting bolus-shaped impulsive control of fast reaction to meals. However, a good, per-subject, fasting-postprandial performance compromise can not be yielded using fixed design.
- *In silico* results showed a better postprandial glycemia regulation with constant reference iPID and over iP with variable reference and over classic PID.
- One solution, used in the literature of AP, to avoid the integral windup is to replace the integral term by the subject's specific basal rate, i.e. PD+basal.
- iPD+basal was compared to PD+basal. The intelligent controller detected meals and reacted faster to theses perturbations as compared to a classic PD without neglecting safety.

iPID combines the classic PID nice properties with new adaptive features. MFC showed a good robustness level. The system is considered as a black box and MFC parameters are tuned empirically based on the input/output measurements. Regarding the performance, the following issues were raised:

1. System constraints are not taken into account in the design, namely, hypoglycemia threshold and the positivity of the controller. The controller was saturated to zero which is the lower admissible bound.

2. When the controller saturates to zero, the loop is broken and glycemia is not under iPID control.

3. For systems under actuator constraints, the integral windup is known defect for PID-like controllers.

4. Hypoglycemia avoidance is not ensured.

Thus, maintaining a tight BG control, especially during postprandial phase, is not an easy task for this fully automatic iPID. Aside from the specific glycemia application, closed-loop stability, specifically for iP controller, is not simply related to the first order error dynamics resulting form the ultra-local model. It was shown, via an example, that a system can not be unconditionally stabilized by an iP control.

The main outcomes of SMC design in this work

- The existence of a positive SMC for glycemia regulation was shown without the need of a saturation.

- To the best of the author knowledge, positive SMC has not been considered previously in the history of AP studies.

- The largest PIS where the plasma insulin variable is nonnegative under SMC was found.

- The positivity of SMC was ensured everywhere in this set via the design parameters. Thus, input/state constraints, of the second order insulin system, are respected.

- The additional positive SMC constraint does not reduce the largest closed-loop PIS.

The future positive SMC

- The designed positive SMC is a proof of concept and the design can be extended to include hypoglycemia constraint.

- Parameter uncertainties and meal perturbations are to be considered in the design of positive SMC.

The problem of finding the largest PIS where glycemia remains *invariant* within or above the desired threshold was also considered in this work. The loop is closed via a positive state feedback controller.

Positive state feedback design benefits over positive SMC design

- The control law is simple and continuous and the resulting closed-loop structure is unique.
- Therefore, finding the largest closed-loop PIS in $\mathbb{R}^3$ (for the overall system), under positive control, is less complex than that with SMC.

The merits of this state feedback are:

- The constraint of insulin injections (as positive input) in the design of state feedback controller has not been considered previously in AP studies.
- In comparison to the mainstream of AP controllers, the designed positive state feedback gathers the simplicity of the design taking system constraints into account.
- In the largest closed-loop PIS, tight glycemia control is achieved where hypoglycemia is prevented.
- Another important outcome of the largest open and closed-loop PIS for glycemia system is the hypoglycemia prediction. A solution to avoid the life-threatening barrier to the optimal diabetic treatment.

Positivity analysis is shown to be very useful for tight glycemia regulation and also for hypoglycemia prediction.

Perspectives of the positive state feedback

- To consider the the intra-patient parameter uncertainties in the design of the positive controller.
- To take the worst case scenario of the parameters uncertainties in the hypoglycemia prediction algorithm.
- To implement and realize the positive closed-loop control algorithm incorporating the hypoglycemia prediction algorithm and test the resulting artificial pancreas *in silico*.

Résumé de la thèse

Le problème de la régulation de la glycémie du diabète de type 1 (DT1) est étudié dans ce travail. Le DT1 est une maladie auto-immune et chronique qui touche environ 25 millions d'individus dans le monde. Un patient diabétique souffre d'un manque absolu d'insuline due à la destruction auto-immune des cellules *beta* du pancréas. L'insuline stimule l'absorption de glucose dans le sang par les cellules et les muscles. Sans insuline stimulant l'absorption du glucose, la glycémie reste dans la circulation sanguine et conduit à l'hyperglycémie, état défini par une glycémie supérieure à 180 mg/dL. Pour survivre, l'injection exogène d'insuline est la seule solution pour réguler la glycémie. La maladie était fatale avant la découverte de l'insuline en 1921.

Le traitement actuel nécessite des injections programmées. Il s'agit, soit de multiples injections quotidiennes d'insuline, soit d'une perfusion d'insuline sous-cutanée continue (PCSI) délivrée par une pompe. Tout en calculant les doses d'insuline, le patient doit considérer beaucoup de facteurs comme la quantité de glucide dans chaque repas et les activités physiques. Un mauvais traitement cause des complications à long terme comme l'insuffisance rénale et les complications vasculaires périphériques. En conséquence, l'injection automatique d'insuline a reçu un grand intérêt notamment avec le développement rapide de la technologie des capteurs de glycémie et des pompes à insuline. Depuis plus de 50 ans, l'idée de développer un dispositif de Pancréatique Artificiel (PA) a été envisagée. Le cœur du dispositif est l'algorithme de commande qui ferme la boucle entre les mesures de glucose sanguin et les injections d'insuline d'un patient diabétique.

En général, le but de toute recherche sur le PA est de concevoir un algorithme de commande adaptable à la sensibilité à l'insuline du patient et suffisamment robuste pour traiter les dynamiques non modélisées, les incertitudes et le bruit de mesure. Un facteur important qui affecte la performance des algorithmes de commande est de parvenir à un compromis entre la réduction de l'hyperglycémie et l'évitement de l'hypoglycémie. De plus, la positivité de l'infusion d'insuline doit être prise en compte dans la conception du réglateur. De même, toutes les concentrations d'insuline ou de glucose sont des variables d'état positives.

Le courant dominant des algorithmes de commande utilisés précédemment dans différents tests cliniques est le régulateur Proportionel-Intégral-Dérivativé (PID) et la commande prédictive (CP). CP est populaire dans ce domaine car il gère les contraintes du système dans sa conception. L'inconvénient principal de la CP est son lourd processus d'optimisation. Le PID a également été fréquemment testé car il a été observé qu'il imitait le comportement des cellules *beta* déficientes dans le pancréas. En outre, sa conception ne nécessite pas un modèle précis du système.

Dans ce travail, deux types de commandes sont utilisés : les commandes basées sur des modèles et les commandes non-basées sur des modèles. Pour évaluer leur efficacité, les deux types sont testés *in silico* sur deux simulateurs de DT1. Le premier simulateur est un modèle à long terme développé au LS2N et qui est déduit à partir des données cliniques de sujets DT1. Le deuxième est le simulateur Uva / Padova qui est approuvé par le Food and Drugs Administration (FDA). Tous les régulateurs conçus et testés ci-après sont entièrement automatiques sans annonces de repas ni des doses supplémentaires d'insuline.

Dans ce travail, la commande sans modèle (CSM) est utilisée pour la première fois pour la régulation de la glycémie. Les dynamiques et les perturbations inconnues sont estimées en ligne grâce à la connaissance unique des mesures d'entrée / sortie. L'estimation est utilisée dans la loi de commande pour compenser les perturbations et la boucle est fermée *via* un régulateur PID simple. La CSM avec un PID dans la boucle est appelé PID intelligent (iPID). Elle offre les fonctions simples d'un contrôle PID dans le cadre d'une conception sans modèle. Contrairement aux études PID précédentes, le iPID est entièrement automatique sans aucune dose d'insuline supplémentaire. On montre tout d'abord qu'un système du second ordre ne peut pas être stabilisé de manière inconditionnelle par un régulateur iP. On teste d'abord le régulateur proportionnel intelligent (iP) en utilisant une trajectoire de référence variable pour contourner le mauvais comportement postprandial de la référence constante iP. La référence variable produit un débit impulsif en réaction rapide aux repas qui réduit l'hyperglycémie postprandiale dans le cas du régulateur iP. Pour améliorer encore la réponse postprandiale, des termes supplémentaires de boucle fermée sont ajoutés et un PID intelligent (iPID) est conçu en utilisant une référence de glycémie constante. Les résultats *in silico* de la comparaison ont montré une meilleure régulation de la glycémie postprandiale pour le iPID avec une référence constante contre le iP avec une référence variable. Le régulateur iPID est également comparé à un PID classique. Les résultats ont montré que la réponse postprandiale a été améliorée avec le régulateur iPID réduisant les excursions hyperglycémiques avec des événements hypoglycémiques minimes. De plus, le iPID imitait mieux le comportement postprandial naturel des cellules *beta* du pancréas qu'un PID avec une réponse plus rapide. La CSM a montré un bon niveau de robustesse. Le système est considéré comme une boîte

noire, et les paramètres de la commande CSM sont réglés de manière empirique en se fondant sur les mesures d'entrée / sortie.

Un autre algorithme de commande robuste est conçu et testé dans cette thèse : la commande par modes glissants (CMG). Notre contribution essentielle est la démonstration de l'existence d'un régulateur rigoureusement positif apte à assurer la positivité des variables d'état, en particulier l'insuline de plasma. Un régulateur CMG *positif* est conçu pour la première fois pour la régulation de la glycémie. La commande est positive partout dans le plus grand ensemble positivement invariant (EPI) du sous-système d'insuline dans le plasma. Deux CMG sont calculées ; le deuxième bloc CGM2 utilise l'erreur de glycémie (par rapport au niveau souhaité) pour concevoir la trajectoire d'insuline souhaitée. Ensuite, l'état d'insuline dans le plasma est forcé de suivre la référence via la commande CMG1. La variable de commutation de CMG1 est un polynôme de premier ordre de l'erreur d'insuline. La commande par modes glissants CMG1 garantit le suivi des références d'insuline. La trajectoire d'insuline souhaitée résultante est l'entrée de commande virtuelle requise du système glycémique pour éliminer l'erreur de glycémie. L'erreur de glycémie est la variable de commutation de CMG2. La glycémie est pilotée vers le point de consigne normal pendant le mode de glissement de CMG2. L'essai *in silico* est effectué pour valider les résultats théoriques sur le système nominal pendant la phase de jeûne. La robustesse de la commande CMG par rapport aux changements de paramètres, aux perturbations des repas et au bruit des capteurs est considérée comme une perspective. En raison de la discontinuité de la loi de commande, la conception d'une commande CMG positive partout dans le plus grand EPI dans R^3 telle que la glycémie reste dans le niveau souhaité est beaucoup plus complexe. La commande CMG positive est une preuve de concept et la conception peut être étendue pour inclure la contrainte d'hypoglycémie. En d'autres termes, le futur problème peut être de concevoir une commande CMG positive dans le plus grand EPI où la glycémie est supérieure au seuil hypoglycémique (Glycémie >70 mg/dL).

Le problème de trouver le plus grand EPI où la glycémie reste *invariant* dans ou au-dessus du seuil souhaité, est adressé *via* une loi de commande simple et continue. Il s'agit de concevoir une commande positive qui prend la contrainte d'hypoglycémie en compte et établit un contrôle "serré" de la glycémie. La boucle est fermée via un régulateur *positif* par retour d'état. Tout d'abord, la loi de commande est simple et continue. Le retour d'état qui en résulte est unique. Par conséquent, trouver le plus grand EPI en boucle fermée en $\mathbf{R}^3$ (pour le système global), sous commande positive, est moins complexe que celui avec CMG. De plus, la théorie des polyèdres invariants pour les systèmes linéaires continus est appliquée directement pour trouver un régulateur positif par retour d'état. Le plus grand EPI du système en boucle ouverte (où seul un débit basal d'insuline est infusé) est d'abord calculé. En second

lieu, on détermine le plus grand EPI du système en boucle fermée sous une commande par retour d'état positif et stabilisant. À l'intérieur de cet EPI, la glycémie est régulée au niveau désiré sans risque d'hypoglycémie puisque les variables d'état sont garanties positives.

Le résultat principal des plus grands EPI en boucle ouverte et fermée est la *prédiction de l'hypoglycemie*. Une solution alternative de resucrage permettra d'éviter la barrière de l'hypoglycémie dans le traitement diabétique optimal. L'hypoglycémie est prédite ici en fonction des conditions initiales du système. La prédiction est établie lorsque les conditions initiales sont en dehors du plus grand EPI en boucle fermée (Glycémie <70 mg / dL). Dans ce cas, la boucle est ouverte soit pour administrer l'insuline basale seulement, soit pour arrêter totalement la pompe. Si la condition initiale appartient au EPI en boucle ouverte (seulement sous injection du débit basal), la boucle est ouverte pour injecter l'insuline basale uniquement. Sinon, si une hypoglycémie future est également prédite sous injection basale, alors la pompe est arrêtée signalant une hypoglycémie sévère. De cette manière, l'analyse de positivité s'avère très utile pour une régulation stricte de la glycémie et aussi pour la prédiction de l'hypoglycémie.

References

[1] W. S. Haubrich. *Medical Meanings: A Glossary of Word Origins*. American College of Physicians, 2003.

[2] J. M. Berg, J. L. Tymoczko, and L. Stryer. *Biochemistry*. 5th edition, Section 30.2, W.H. Freeman, New York, 2002.

[3] M. Stumvoll. Glucose Production by the Human Kidney–its Importance Has Been Underestimated. *Nephrology Dialysis Transplantation*, 13(12):2996–2999, 1998.

[4] G. Mithieux and A. Gautier-Stein. Intestinal Glucose Metabolism Revisited . *Diabetes Research and Clinical Practice*, 105(3):295 – 301, 2014.

[5] L. Szablewski. *Glucose Homeostasis-mechanism and Defects*. INTECH Open Access Publisher, 2011.

[6] S. M. Gray, R. I. Meijer, and E. J. Barrett. Insulin Regulates Brain Function, But How Does It Get There? *Diabetes*, 63(12):3992–3997, 2014.

[7] Y. Minokoshi, C. R. Kahn, and B. B. Kahn. Tissue-specific Ablation of the GLUT4 Glucose Transporter or the Insulin Receptor Challenges Assumptions About Insulin Action and Glucose Homeostasis. *Journal of Biological Chemistry*, 278(36):33609–33612, 2003.

[8] A. Caumo and L. Luzi. First-phase Insulin Secretion: Does it Exist in Real Life? Considerations on Shape and function. *American Journal of Physiology-Endocrinology And Metabolism*, 287(3):E371–E385, 2004.

[9] M. K. Cavaghan. The Beta Cell and First-phase Insulin Secretion. *Medscape Diabetes Endocrinol*, 6(2), 2004.

[10] T. Taylor. Pancreas Anatomy, October 2012. [online article, visited 19-04-2016] http://www.innerbody.com/image/endo03.html.

[11] M. A. Pfeifer, J. B. Halter, and D. Porte. Insulin Secretion in Diabetes Mellitus. *The American Journal of Medicine*, 70(3):579 – 588, 1981.

[12] M. A. Atkinson. The Pathogenesis and Natural History of Type 1 Diabetes. *Cold Spring Harbor Perspectives in Medicine*, 2(11):a007641, 2012.

[13] R. J. McCrimmon and R. S. Sherwin. Hypoglycemia in Type 1 Diabetes. *Diabetes*, 59(10):2333–2339, 2010.

[14] R. Couch et al. Diabetes Education for Children with Type 1 Diabetes Mellitus and Their Families. 2008.

[15] E. Bhatia and A. Aggarwal. Insulin Therapy for Patients with Type 1 Diabetes. *Journal-Association of Physicians of India*, 55(L):29, 2007.

[16] B. D. Saboo and P. A. Talaviya. Continuous Subcutaneous Insulin Infusion: Practical Issues. *Indian Journal of Endocrinology and Metabolism*, 16(Suppl 2):S259, 2012.

[17] P. R. Dijk et al. Intraperitoneal Insulin Infusion: Treatment Option for Type 1 Diabetes Resulting in Beneficial Endocrine Effects Beyond Glycaemia. *Clinical endocrinology*, 81(4):488–497, 2014.

[18] L. M. Huyett et al. Design and Evaluation of a Robust PID Controller for a Fully Implantable Artificial Pancreas. *Industrial & Engineering Chemistry Research*, 54(42):10311–10321, 2015.

[19] S. J. Logtenberg et al. Improved Glycemic Control With Intraperitoneal Versus Subcutaneous Insulin in Type 1 Diabetes. *Diabetes Care*, 32(8):1372–1377, 2009.

[20] San Francisco Diabetes Teaching Center at the University of California. Calculating Insulin Dose. [online article, visited on 2016-04-27] Diabetes Education Online, http://www.dtc.ucf.edu.

[21] J. Walsh, R. Roberts, and T. Bailey. Guidelines for Insulin Dosing in Continuous Subcutaneous Insulin Infusion Using New Formulas from a Retrospective study of Individuals with Optimal Glucose Levels. *Journal of Diabetes Science and Technology*, 4(5):1174–1181, 2010.

[22] E. Cobry et al. Timing of Meal Insulin Boluses to Achieve Optimal Postprandial Glycemic Control in Patients with Type 1 Diabetes. *Diabetes Technology & Therapeutics*, 12(3):173–177, 2010.

[23] C. Toffanin et al. Dynamic Insulin on Board: Incorporation of Circadian Insulin Sensitivity Variation. *Journal of Diabetes Science and Technology*, 7(4):928–940, 2013.

[24] J. Walsh, R. Roberts, and L. Heinemann. Confusion Regarding Duration of Insulin Action A Potential Source for Major Insulin Dose Errors by Bolus Calculators. *Journal of diabetes science and technology*, 8(1):170–178, 2014.

[25] V. Iacovacci et al. The Bioartificial Pancreas (BAP): Biological, Chemical and Engineering Challenges . *Biochemical Pharmacology*, 100:12 – 27, 2016.

[26] P. A. Halban et al. Gene and Cell-Replacement Therapy in the Treatment of Type 1 Diabetes: How High Must the Standards Be Set? *Diabetes*, 50(10):2181–2191, 2001.

[27] P. C. Nett, H. W. Sollinger, and T. Alam. Hepatic Insulin Gene Therapy in Insulin-Dependent Diabetes Mellitus. *American Journal of transplantation*, 3(10):1197–1203, 2003.

[28] P. Keith-Hynes et al. The Diabetes Assistant: A Smartphone-Based System for Real-time Control of Blood Glucose. *Electronics*, 3(4):609–623, 2014.

[29] F. J. Doyle et al. Closed-Loop Artificial Pancreas Systems: Engineering the Algorithms. *Diabetes Care*, 37(5):1191–1197, 2014.

[30] A. H. Kadish. Automation Control of Blood Sugar a Servomechanism for Glucose Monitoring and Control. *ASAIO Journal*, 9(1):363–367, 1963.

[31] W. L. Clarke et al. Closed-loop Artificial Pancreas Using Subcutaneous Glucose Sensing and Insulin Delivery and a Model Predictive Control Algorithm: the Virginia Experience. *Journal of Diabetes Science and Technology*, 3(5):1031–1038, 2009.

[32] I. Pagkalos et al. A Vhdl Implementation of the Biostator II Glucose Control Algorithm for Critical Care. In *Biomedical Circuits and Systems Conference (BioCAS), 2011 IEEE*, pages 94–97. IEEE, 2011.

[33] F. Chee et al. Expert PID Control System for Blood Glucose Control in Critically Ill Patients. *Information Technology in Biomedicine, IEEE Transactions on*, 7(4):419–425, 2003.

[34] G. M. Steil, A. E. Panteleon, and K. Rebrin. Closed-loop Insulin Delivery—the Path to Physiological Glucose Control. *Advanced drug delivery reviews*, 56(2):125–144, 2004.

[35] G. M. Steil et al. Feasibility of Automating Insulin Delivery for the Treatment of Type 1 Diabetes. *Diabetes*, 55(12):3344–3350, 2006.

[36] S. A. Weinzimer et al. Fully Automated Closed-loop Insulin Delivery versus Semiautomated Hybrid control in Pediatric Patients with Type 1 Diabetes Using an Artificial Pancreas. *Diabetes Care*, 31(5):934–939, 2008.

[37] G. M. Steil et al. The Effect of Insulin Feedback on Closed Loop Glucose Control. *The Journal of Clinical Endocrinology & Metabolism*, 96(5):1402–1408, 2011.

[38] J. L. Ruiz et al. Effect of Insulin Feedback on Closed-Loop Glucose Control: A Crossover Study. *Journal of diabetes science and technology*, 6(5):1123–1130, 2012.

[39] M. Loutseiko et al. Closed-loop Insulin delivery Utilizing Pole Placement to Compensate for Delays in subcutaneous insulin delivery. *Journal of Diabetes Science and Technology*, 5(6):1342–1351, 2011.

[40] J. L. Sherr et al. Reduced Hypoglycemia and Increased Time in Target Using Closed-loop Insulin Delivery During Nights with or without antecedent Afternoon Exercise in Type 1 Diabetes. *Diabetes Care*, 36(10):2909–2914, 2013.

[41] S. Laxminarayan et al. Use of a Food and Drug Administration-Approved Type 1 Diabetes Mellitus Simulator to Evaluate and Optimize a Proportional-Integral-Derivative Controller. *Journal of Diabetes Science and Technology*, 6(6):1401–1412, 2012.

[42] Z. Trajanoski, W. Regittnig, and P. Wach. Simulation Studies on Neural predictive Control of Glucose Using the Subcutaneous Route. *Computer Methods and Programs in Biomedicine*, 56(2):133–139, 1998.

[43] R. S. Parker, F. J. Doyle III, and N. A. Peppas. A Model-based Algorithm for Blood Glucose Control in type I Diabetic Patients. *Biomedical Engineering, IEEE Transactions on*, 46(2):148–157, 1999.

[44] R. Hovorka et al. Nonlinear Model Predictive Control of Glucose Concentration in Subjects with Type 1 Diabetes. *Physiological measurement*, 25(4):905, 2004.

[45] R. Hovorka et al. Partitioning Glucose Distribution/transport, Disposal, and Endogenous Production During IVGTT. *American Journal of Physiology-Endocrinology and Metabolism*, 282(5):E992–E1007, 2002.

[46] L. Magni et al. Model Predictive Control of Type 1 Diabetes: An In silico Trial. *Journal of Diabetes Science and Technology*, 1(6):804–812, 2007.

[47] E. Dassau et al. Implications of Meal Library & Meal Detection to Glycemic Control of Type 1 Diabetes Mellitus Through MPC control. *Energy (KJ)*, 1516:35, 2008.

[48] H. Lee et al. A Closed-loop Artificial Pancreas Using Model Predictive Control and a Sliding Meal Size Estimator. *Journal of diabetes science and technology*, 3(5):1082–1090, 2009.

[49] S. Arnolds et al. How Pharmacokinetic and Pharmacodynamic Principles Pave The Way for Optimal Basal Insulin Therapy in Type 2 Diabetes. *International Journal of Clinical Practice*, 64(10):1415–1424, 2010.

[50] B. P. Kovatchev et al. In silico Model and Computer Simulation Environment Approximating the Human Glucose/Insulin Utilization. *Food and Drug Administration Master File MAF*, 1521, 2008.

[51] B. P. Kovatchev et al. Feasibility of Outpatient Fully Integrated Closed-loop Control First Studies of Wearable Artificial Pancreas. *Diabetes Care*, 36(7):1851–1858, 2013.

[52] S. J. Russell et al. Outpatient Glycemic Control with a Bionic Pancreas in Type 1 Diabetes. *New England Journal of Medicine*, 371(4):313–325, 2014.

[53] P. Kaveh and Y. B. Shtessel. Blood glucose regulation using higher-order sliding mode control. *International Journal of Robust and Nonlinear Control*, 18(4-5):557–569, 2008.

[54] A. Abu-Rmileh and W. Garcia-Gabin. Wiener sliding-mode control for artificial pancreas: A new nonlinear approach to glucose regulation. *Computer Methods and Programs in Biomedicine*, 107(2):327–340, 2012.

[55] Ana Gabriela Gallardo Hernández et al. High-order sliding-mode control for blood glucose: Practical relative degree approach. *Control Engineering Practice*, 21(5):747–758, 2013.

[56] N. T. Parsa, A. R. Vali, and R. Ghasemi. Back Stepping Sliding Mode Control of Blood Glucose for Type I Diabetes. *World Academy of Science, Engineering and Technology, International Journal of Medical, Health, Biomedical, Bioengineering and Pharmaceutical Engineering*, 8(11):779–783, 2014.

[57] J. T. Sorensen. *A Physiologic Model of Glucose Metabolism in Man and its Use to Design and Assess Improved Insulin Therapies for Diabetes*. PhD thesis, Massachusetts Institute of Technology, 1985.

[58] N. Magdelaine et al. A Long-term Model of the Glucose-Insulin Dynamics of Type 1 Diabetes. *IEEE Transactions on Biomedical Engineering*, 62(6):1546–1552, May 2015.

[59] G. C. Goodwin et al. A Fundamental Control Limitation for Linear Positive Systems with Application to Type 1 Diabetes Treatment. *Automatica*, 55:73–77, 2015.

[60] H. Zakeri and S. Ozgoli. A Polynomial Modeling and State Feedback Control of Blood Glucose Regulatory in Diabetic Patients. In *Intelligent and Advanced Systems (ICIAS), 2012 4th International Conference on*, volume 1, pages 388–392. IEEE, 2012.

[61] A. Hariri and L. Y. Wang. Observer-based state feedback for enhanced insulin control of type 'i'diabetic patients. *The Open Biomedical Engineering Journal*, 5:98, 2011.

[62] G. M. Steil. Algorithms for a Closed-loop Artificial Pancreas: the Case for Proportional-Integral-Derivative Control. *Journal of Diabetes Science and Technology*, 7(6):1621–1631, 2013.

[63] M. Fliess and C. Join. Model-free Control. *International Journal of Control*, 86(12):2228–2252, 2013.

[64] J. B. Bassingthwaighte et al. Compartmental Modeling in the Analysis of Biological Systems. *Computational Toxicology: Volume I*, pages 391–438, 2012.

[65] M. Blomhøj, T. H. Kjeldsen, and J. Ottesen. Compartment Models (Notes). *Latest version available at: http://www4.ncsu.edu/ msolufse/Compartmentmodels.pdf*, 2014.

[66] M. Loutseiko et al. Closed-loop Insulin Delivery Utilizing Pole Placement to Compensate for Delays in Subcutaneous Insulin Delivery. *Journal of Diabetes Science and Technology*, 5(6):1342–1351, 2011.

[67] V. W. Bolie. Coefficients of Normal Blood Glucose Regulation. *Journal of Applied Physiology*, 16(5):783–788, 1961.

[68] R. N. Bergman, L. S. Phillips, and C. Cobelli. Physiologic Evaluation of Factors Controlling Glucose Tolerance in Man: Measurement of Insulin Sensitivity and Beta-cell Glucose Sensitivity from the Response to Intravenous Glucose. *Journal of Clinical Investigation*, 68(6):1456, 1981.

[69] A. De Gaetano and O. Arino. Mathematical Modeling of the Intravenous Glucose Tolerance Test. *Journal of Mathematical Biology*, 40(2):136–168, 2000.

[70] D. Boiroux et al. Optimal Insulin Administration for People with Type 1 Diabetes. *IFAC Proceedings Volumes*, 43(5):248–253, 2010.

[71] C. Dalla Man, R. A. Rizza, and C. Cobelli. Meal Simulation Model of the Glucose-Insulin System. *IEEE Transactions on Biomedical Engineering*, 54(10):1740–1749, Oct 2007.

[72] C. Dalla Man et al. GIM, Simulation Software of Meal Glucose—insulin Model. *Journal of Diabetes Science and Technology*, 1(3):323–330, 2007.

[73] C. Cobelli, E. Renard, and B. Kovatchev. Artificial Pancreas: Past, Present, Future. *Diabetes*, 60(11):2672–2682, 2011.

[74] A. Mohn et al. Insulinothérapie fonctionnelle: un modèle d'approche éducative pour les patients ayant un diabète de type 1. *Médecine des Maladies Métaboliques*, 6(6):469–476, 2012.

[75] M. Fliess and C. Join. Model-free Control and Intelligent PID controllers: Towards a Possible Trivialization of Nonlinear Control? *IFAC Proceedings Volumes*, 42(10):1531–1550, 2009.

[76] M. Fliess and C. Join. Intelligent pid controllers. In *16th Mediterrean Conference on Control and Automation*, 2008.

[77] M. Fliess, C. Join, and H. Sira-Ramirez. Complex continuous Nonlinear Systems: Their Black Box Identification and Their Control. *IFAC Proceedings Volumes*, 39(1):416–421, 2006.

[78] M. Voicu. *Advances in Automatic Control*, volume 754. Springer Science & Business Media, 2012.

[79] J. R. Partington and C. Bonnet. H$^\infty$ and {BIBO} Stabilization of Delay Systems of Neutral Type . *Systems & Control Letters*, 52(3–4):283 – 288, 2004.

[80] H. Mounier. Personal Communication, University of Paris-Sud, France, 2017.

[81] C. Bonnet. Personal Communication, INRIA, Paris, France, 2017.

[82] T. Vyhlidal. Quasi-Polynomial Mapping Based Rootfinder. http://www.cak.fs.cvut.cz/algorithms/qpmr, 2008. [Online; accessed 24-May-2017].

[83] S. Choi et al. Model-free Control of Automotive Engine and Brake for Stop-and-Go Scenarios. In *European Control Conference (ECC)*, pages 3622–3627, 2009.

[84] T. MohammadRidha et al. A Variable Reference Trajectory for Model-free Glycemia Regulation. In *SIAM CT15*, Paris, France, 2015.

[85] G. Marchetti et al. An Improved PID Switching Control Strategy for Type 1 Diabetes. *IEEE TBME*, 55(3):857–865, 2008.

[86] H. W. Rodbard et al. American Association of Clinical Endocrinologists Medical Guidelines for Clinical Practice for the Management of Diabetes Mellitus. *Endocrine practice*, 13:1–68, 2007.

[87] T. MohammadRidha et al. Model Free iPID Control for Glycemia Regulation of Type-1 Diabetes. *Accepted in IEEE Transactions on Biomedical Engineering*, April, 2017.

[88] T. MohammadRidha and C. H. Moog. Model Free Control for Type-1 Diabetes: A Fasting-Phase Study. In *9th IFAC Symposium on Biological and Medical Systems*, Berlin, Germany, August 2015.

[89] F. Cameron et al. A Closed-loop Artificial Pancreas Based on Risk Management. *Journal of Diabetes Science and Technology*, 5(2):368–379, 2011.

[90] I. Ben Abbes et al. A Closed-Loop Artificial Pancreas Using a Proportional Integral Derivative with Double Phase Lead Controller Based on a New Nonlinear Model of Glucose Metabolism. *Journal of Diabetes Science and Technology*, 7(3):699–707, 2013.

[91] F. J. Service. Glucose Variability. *Diabetes*, 62(5):1398, 2013.

[92] K. Menani et al. Positive Sliding Mode Control for Glycemia Regulation. *International Journal of Systems Science*, July, 2017.

[93] F. Blanchini. Survey Paper: Set Invariance in Control. *Automatica (Journal of IFAC)*, 35(11):1747–1767, 1999.

[94] L. Farina and S. Rinaldi. *Positive Linear Systems: Theory and Applications*, volume 50. John Wiley & Sons, 2011.

[95] E. B. Castelan and J. C. Hennet. On Invariant Polyhedra of Continuous-time Linear Systems. *IEEE Transactions on Automatic Control*, 38(11):1680–85, 1993.

[96] G. Monsees. *Discrete-time Sliding Mode Control*. TU Delft, Delft University of Technology, 2002.

[97] A. Vignoni. Invariance and Sliding Modes. Application to Coordination of Multi-agent Systems, Bioprocesses Estimation, and Control in Living Cells. Master's thesis, Universitat Politècnica de València, València, 2014.

[98] C. Edwards and S. Spurgeon. *Sliding Mode Control: Theory and Applications*. CRC Press, 1998.

[99] Taghreed MohammadRidha et al. Description of the Positively Invariant Sets of a Type 1 Diabetic Patient Model. *The 17th CLCA Latin American Conference of Automatic Control*, 2016.

[100] T. MohammadRidha et al. Toward Hypoglycemia Prediction and Avoidance for Type 1 Diabetic Patients. *56th IEEE Conference on Decision and Control*, accepted, July, 2017.

[101] T. MohammadRidha et al. Positively Invariant Sets of a T1DM Model: Hypoglycemia Prediction and Avoidance. *Automatica*, submitted, July, 2017.

[102] D. A. Barry et al. Analytical Approximations for Real Values of the Lambert W-function. *Mathematics and Computers in Simulation*, 53(1):95–103, 2000.

[103] F. Zaccardi et al. Group of Signs: A New Method to Evaluate Glycemic Variability. *Journal of Diabetes Science and Technology*, 2(6):1061–1065, 2008.

[104] C. R. Marling et al. Characterizing Blood Glucose Variability Using New Metrics with Continuous glucose monitoring data. *Journal of Diabetes Science and Technology*, 5(4):871–878, 2011.

[105] G.D. Molnar et al. Mean Amplitude of Glycemic Excursions, a Measure of Diabetic Instability. *Diabetes*, 19(9):644–655, 1970.

[106] J. C. Segen. *The Dictionary of Modern Medicine*. CRC Press, 1992.

[107] F. Bertuzzi et al. Brittle Type 1 Diabetes Mellitus. *Current Medicinal Chemistry*, 14(16):1739–1744, 2007.

Appendix A

A.1 On the estimated derivative $\dot{y}_e(t)$

A.1.1 Algebraic Derivative Estimator

To estimate the derivative of a signal $y(t)$ using the algebraic derivative estimator (see[83] and the references therein), start from Taylor series:

$$y(t) = \Sigma_{i=0}^{N} \frac{y(0)^{(i)} t^i}{i!} \tag{A.1}$$

To estimate the first derivative set $N = 1$:

$$y(t) = y(0) + \dot{y}(0)t \tag{A.2}$$

Take Laplace for above knowing that $y(0), \dot{y}(0)$ are constants yields:

$$sY(s) = y(0) + \frac{\dot{y}(0)}{s} \tag{A.3}$$

Remark 24. *Note that at this stage,* (A.3) *is also obtained if* $F_e = \dot{y}(t)$ *in*(4.26) *(setting* $u(t) = 0$*) and taking Laplace to the result. In this case,* F_e *in* (4.27) *is equivalent to* $\dot{y}(0)$ *in* (A.3) $F_e = \dot{y}(0)$*, thus* F_e *will estimate* $\dot{y}(t)$*.*

Differentiate both sides of (A.3) w.r.t. s:

$$Y(s) + \frac{sdY(s)}{ds} = -\frac{\dot{y}(0)}{s^2} \tag{A.4}$$

To filter out, multiply both sides by s^{-2}:

$$\frac{Y(s)}{s^2} + \frac{dY(s)}{sds} = -\frac{\dot{y}(0)}{s^4} \tag{A.5}$$

To take Laplace inverse using the following:

$$\mathscr{L}^{-1}\{F(s)G(s)\} = \int_0^t f(t-\tau)g(\tau)\mathrm{d}\tau \tag{A.6}$$

$$\mathscr{L}^{-1}\{\frac{d^iF(s)}{ds^i}\} = (-t)^i f(t) \tag{A.7}$$

then we have the derivative in the time interval $\tau \in [0,\ T]$:

$$\dot{y}(0) = -\frac{6}{T^3}\int_0^T (T-2\tau)y(\tau)\mathrm{d}\tau \tag{A.8}$$

To estimate the derivative at the instant t, shift the argument of the function $y(\tau)$ by $y(t+\tau)$ (if $y(T)$ by $y(t+T)$) for a sliding time window estimation of $\dot{y}(t)$

$$\dot{y}_e(t) = -\frac{6}{T^3}\int_0^T (T-2\tau)y(t+\tau)\mathrm{d}\tau \tag{A.9}$$

The above equation allows to estimate the derivative in the interval $[t\ t+T]$ as $\tau \in [0\ T]$. To make the estimation causal, invert the time intervals i.e. T to $-T$ and τ to $-\tau$. First change T to $-T$ in (A.9):

$$\dot{y}_e(t) = -\frac{6}{(-T)^3}\int_0^{-T} (-T-2\tau)y(t+\tau)\mathrm{d}\tau \tag{A.10}$$

or

$$\dot{y}_e(t) = -\frac{6}{T^3}\int_{-T}^0 (-T-2\tau)y(t+\tau)\mathrm{d}\tau \tag{A.11}$$

now, change of variable τ to $-\tau$ denote $\sigma = -\tau$, $\mathrm{d}\tau = -\mathrm{d}\sigma$, $\tau = 0, -T$ implies $\sigma = 0, T$:

$$\dot{y}_e(t) = \frac{6}{T^3}\int_T^0 (-T+2\sigma)y(t-\sigma)\mathrm{d}\sigma \tag{A.12}$$

or

$$\dot{y}_e(t) = \frac{6}{T^3}\int_0^T (T-2\sigma)y(t-\sigma)\mathrm{d}\sigma \tag{A.13}$$

To change the integration limits from $[0\ T]$ to $[t-T\ t]$ using the following change of variables $\sigma = t-\tau$, $\mathrm{d}\sigma = -\mathrm{d}\tau$ and $\tau = 0, T \implies \sigma = t, t-T$ and hence:

$$\dot{y}_e(t) = \frac{6}{T^3}\int_{t-T}^t (T-2t+2\sigma)y(\sigma)\mathrm{d}\sigma \tag{A.14}$$

$\dot{y}_e(t)$ is equivalent to F_e in (4.37) with $u(t) = 0$, thus this result is used to compare the two estimators equations: eq. (A.14) and the estimator equation in section 3.4.1 in [63] with $u(t) = 0$.

Example

(A.14) is used to estimate the derivative of the following function:

$$y(t) = t \tag{A.15}$$

$$\dot{y}_e(t) = \frac{6}{T^3}\int_{t-T}^{t}(T - 2t + 2\sigma)\,\sigma\,\mathrm{d}\sigma \tag{A.16}$$

$$F_e = \dot{y}_e(t) = \dot{y}(t) = 1 \tag{A.17}$$

whereas the first formula of the estimator equation in section 3.4.1 of [63] (F_e is denoted ϕ in the reference) is as follows (with $u(t) = 0$) :

$$F_e = \dot{y}_e(t) = -\frac{6}{T^3}\int_{t-T}^{t}(T - 2\tau)y(\tau)d\tau \tag{A.18}$$

with $y(t) = t$ yields

$$\dot{y}_e = \frac{(7T^2 - 18Tt + 12t^2)}{T^2} \neq \dot{y}(t) \tag{A.19}$$

Consequently F_e in (4.37) gives the correct expected estimation.

Remark 25. *It is suggested to take a small estimation time window T in [63] for a better estimation in* (4.37)*, this can be seen assuming again that $F_e = \dot{y}_e$ and take for instance*

$$y_1(t) = t^2,\ y_2(t) = t^3 \tag{A.20}$$

then (4.37) *($u(t) = 0$) yields:*

$$\dot{y}_{1_e} = 2\big(t - \frac{T}{2}\big),\ \dot{y}_{2_e} = 3\big(t - \frac{T}{2}\big)^2 + \frac{3T^2}{20} \tag{A.21}$$

thus the smaller the T the closer the result to $\dot{y}(t)$.

A.2 The delay on $u(t)$

It was shown in Remark24 of A.1 that the first term of the integral of (4.37) is equivalent to $\dot{y}(t)$, and according to (4.6) $F_e = \dot{y}(t) - \alpha u(t-h)$, thus the second part of the integral of (4.37) is equivalent to $u(t-h)$. Hence, the following buffer extracted from (4.37) (with

$y(t) = 0$) is supposed to maintain the signal $f(t)$ unchanged like a buffer:

$$\tilde{f}(t) = \frac{6}{T^3} \int_{t-T}^{t} (t-\sigma)(T-t+\sigma) f(\sigma) \mathrm{d}\sigma \tag{A.22}$$

This buffer outputs the same input signal but delayed by $\frac{T}{2}$, *i.e.* $\tilde{f}(t) = f(t - \frac{T}{2})$. This function is used and compared to the ordinary transport delay function of delay h on numerical examples below. If T is small enough, both passes the signal delayed by $h = \frac{T}{2}$. Initial conditions for the following examples are set to zero: $f(t) = 0 \quad \forall t < 0$ with $h = 0.5$.

A.2.1 example 1

A unit step function:

$$f(t) = 1 \quad \forall t \geq 0 \tag{A.23}$$

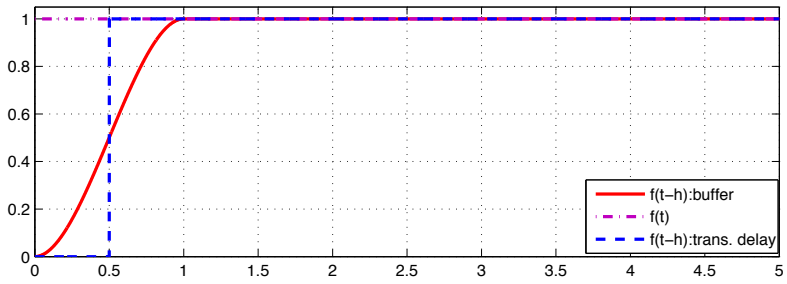

Figure A.1 Unit step function $f(t)$ in dotted red curve and its delay using the integral buffer in red solid curve versus the transport delay $f(t-h)$ in dotted blue curve.

A.2.2 example 2

A sinusoidal function

$$f(t) = sin(3t) \tag{A.24}$$

A.2.3 Influence of the integration horizon T

It is noticed in the latter example that the time window of this buffer should respect Nyquist rate condition:

$$f_b \geq 2 f_m$$

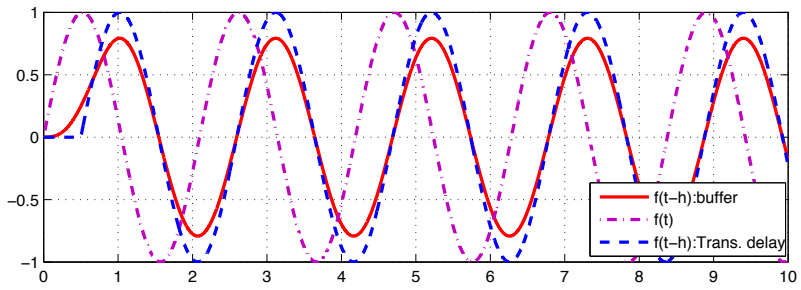

Figure A.2 Sinusoid function in dotted red and its delay using the integral buffer in solid red versus the transport delay in dotted blue.

i.e. in order to capture all signal information, the buffering rate f_b should be at least as twice as faster as the highest frequency of the transmitted signal f_m.

In (A.24) $f_m = 3$ while $f_b = \frac{1}{T} = 1$ which resulted in difference of amplitude in the transmitted signal as illustrated in Fig. A.2.

For instance, the following signal whose highest frequency is $f_m = 3$ Hz or $T_m = 0.33sec.$ is illustrated in Fig. A.3 with its two delayed versions taking $T_b = T = 2 > T_m$.

$$f(t) = \tanh(t) + e^{-0.5t} sin(3t) \tag{A.25}$$

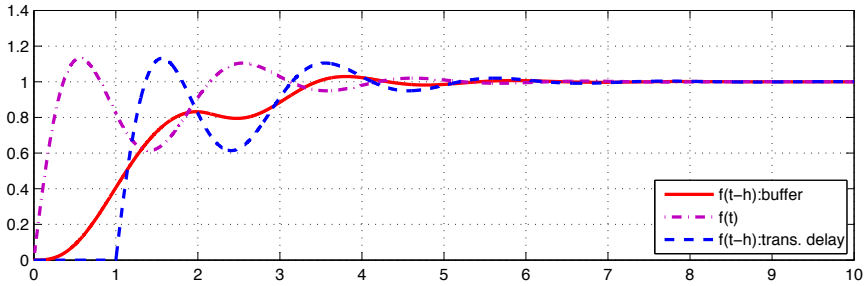

Figure A.3 $f(t)$ and $f(t-h)$ using the integral buffer versus the transport delay $T = 2sec.$

While for $T = 0.3sec.$ the buffer produces a nice approximation of $f(t-h)$ as illustrated in Fig. A.4.

Therefore, the estimation frequency should be at least as high as twice the highest frequency component of the input signal.

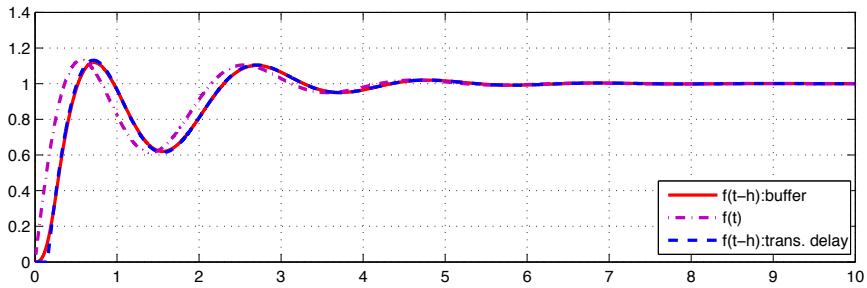

Figure A.4 $f(t)$ and $f(t-h)$ using the integral buffer versus the transport delay setting $T = 0.3sec$.

A.3 iP Results with noise

The modeling error (e.g. unmodeled dynamics, CGM measurement noise) due to the identification process is considered as noise and added to the mathematical model output as illustrated in Fig. A.5 and see, for instant, Fig. A.6 for IF2 noise. IF2, IF3 and BE results are illustrated in Figures A.7, A.8 and A.9 respectively.

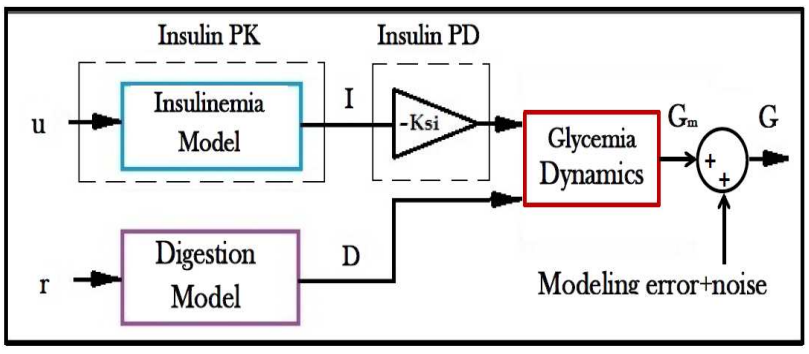

Figure A.5 A block diagram of a T1D glucose-insulin dynamics. with modeling error on the output

.

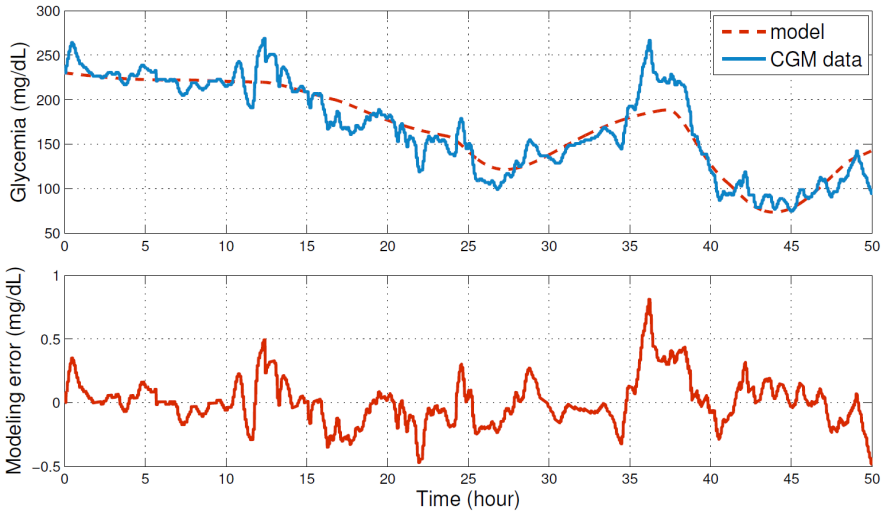

Figure A.6 IF2 BG response. (a) Open-loop CGM data and BG model output as in (3.17) (b) modeling error [58] (0.0056 ± 0.18).

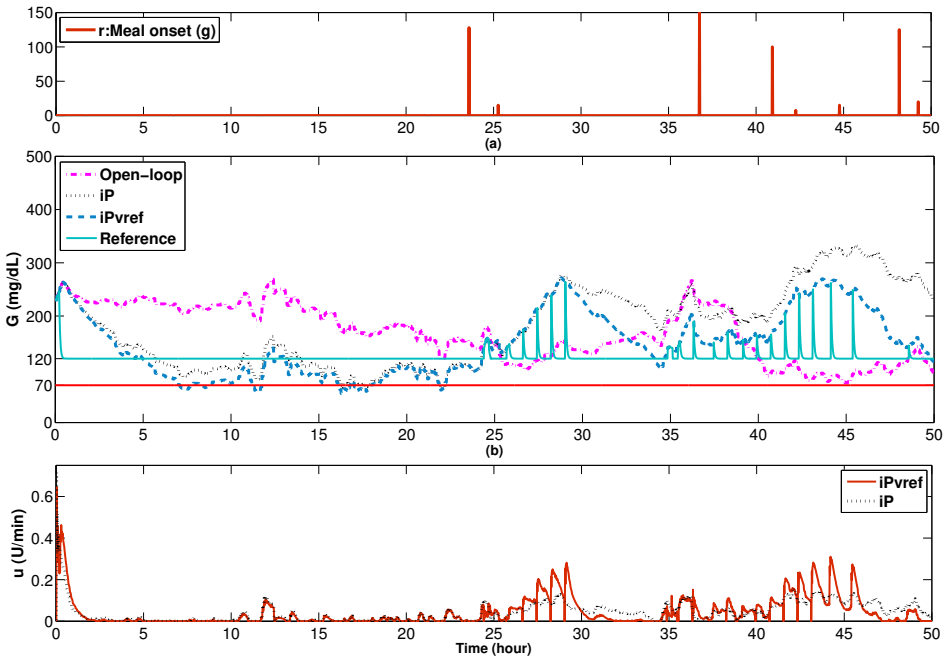

Figure A.7 IF2 BG response with noise under iP with $-\alpha = 180$ and iPvref $-\alpha = 198$. (a) Meal intake (b) BG response (c) iP and iPvref control rates

.

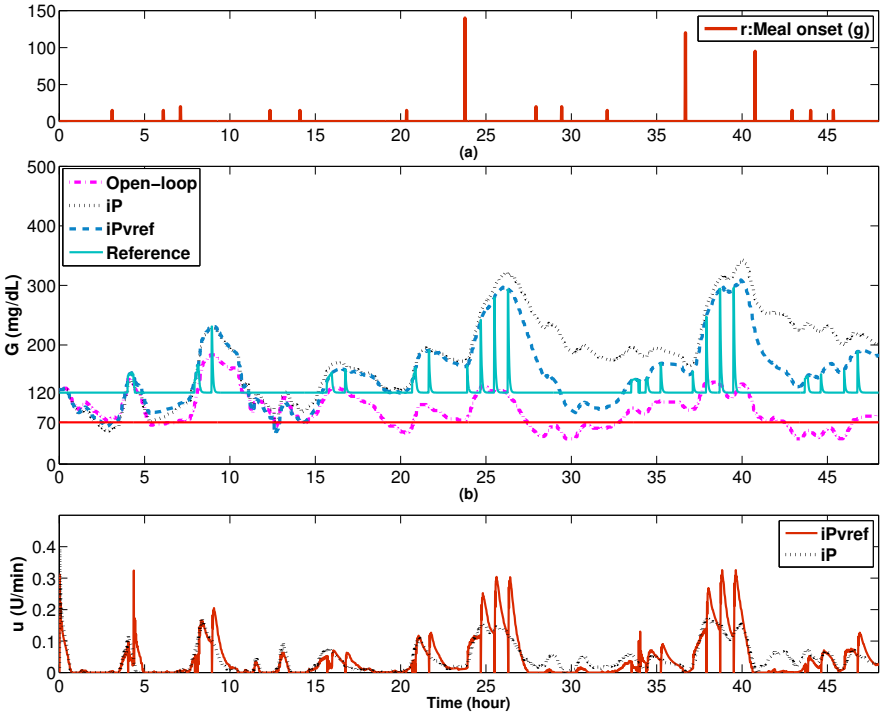

Figure A.8 IF3 BG response with noise under iP with $-\alpha = 176$ and iPvref $-\alpha = 223$. (a) Meal intake (b) BG response (c) iP and iPvref control rates

.

A.4 Luenberger Observer Design

The observer model to estimate $\dot{y}(t)$ of a signal $y(t)$ is designed as follows:

$$\dot{\hat{x}} = A\hat{x} + L(y - C\hat{x}) \tag{A.26}$$

$$\hat{y} = C\hat{x} \tag{A.27}$$

Where $\hat{x} = \begin{bmatrix} \hat{x}_1 \\ \hat{x}_2 \end{bmatrix}$, $A = \begin{bmatrix} 0 & 1 \\ 0 & 0 \end{bmatrix}$, $C = \begin{bmatrix} 1 & 0 \end{bmatrix}$ with the estimated derivative $\hat{x}_2 = \dot{y}$. Pole placement is used to design L such that the characteristic polynomial of the observer $A - LC$ is $(s + \frac{1}{T_o})^2$ and hence: $L = \begin{bmatrix} \frac{2}{T_o} \\ \frac{1}{T_o^2} \end{bmatrix}$. with $T_o = 0.15$ for a fast convergence and to obtain a high gain observer.

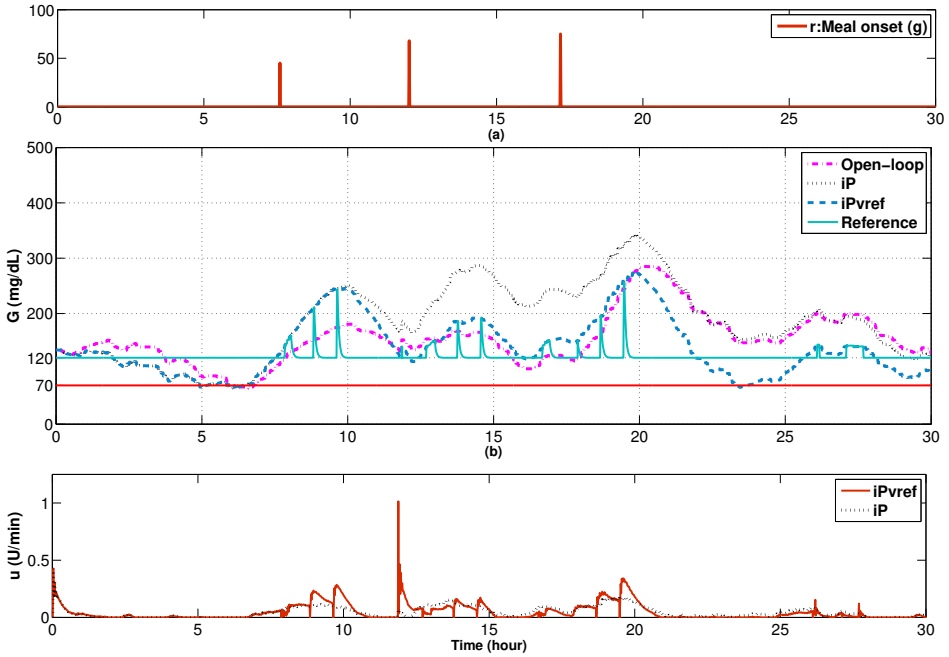

Figure A.9 IF3 BG response with noise under iP with $-\alpha = 175$ and iPvref $-\alpha = 175$. (a) Meal intake (b) BG response (c) iP and iPvref control rates

.

A.5 MAGE and Diabetic Stability

Glycemic variability is an important parameter to solve potential clinical problems in diabetic patients [103]. It generates oxidative stress and potentially contributes to long term complications like the development of macro- and microvascular complications [103, 104]. Mean Amplitude of Glycemic Excursion (MAGE) is a well-known index characterizing glycemic variability proposed by [105]. Three ranges of MAGE divide subjects into normal between (22 to 60 mg/dL), stable diabetes (67 to 82 mg/dL) and unstable diabetes with the largest MAGE range (119 to 200 mg/dL) [105]. In unstable or *brittle diabetes* BG fluctuates widely with unpredictable rapid oscillations from hypoglycemia to hyperglycemia [106]. Brittle diabetes are difficult to treat and have a poor quality of life due to frequent acute events leading to hospital admissions [107].

24-hours MAGE values calculated for each of the five subjects for the basal-bolus FIT therapy are as follows: MAGE=[82, 55, 97, 207, 161] for IF2, IF3, BE, IF9 and LR subjects respectively. IF2, IF3 and BE respond smoothly to insulin infusion producing a stable behavior. Whereas, IF9 and LR are unstable with different instability degrees. MAGE index provides a criterion with which brittle patients can be classified before any control design tests due to their particular unpredictable BG behavior.

UNIVERSITE BRETAGNE LOIRE

CENTRALE NANTES

Thèse de Doctorat

Taghreed MOHAMMADRIDHA

La Régulation Automatique de la Glycémie du Diabète de Type I
Automatic Glycemia Regulation of Type I Diabetes

Résumé

Cette thèse étudie le contrôle en boucle fermée pour la régulation de la glycémie du diabète de type 1 (DT1). Deux catégories principales de commande sont conçues: l'une est basée sur un modèle et l'autre non. Pour tester leur efficacité, les deux types sont testés *in silico* sur deux simulateurs de DT1. Le premier est un modèle à long terme qui est dérivé des données cliniques des sujets de DT1 et le second est le simulateur Uva/Padova. Tout d'abord, la commande sans modèle (CSM) est conçue. Après avoir montré qu'un régulateur proportionnel intelligent (iP) à référence constante peut être mis en défaut sur un simple second ordre, nous avons conçu un régulateur iP à référence variable. Une solution alternative est un régulateur proportionnel-intégral-dérivé intelligent (iPID) à référence constante. Une meilleure performance globale est obtenue avec iPID par rapport à iP et par rapport à un PID classique. Deuxièmement, une commande par modes glissants (CMG) garantie positive est conçue pour la première fois pour la régulation de la glycémie. La conception de cette commande est basée sur un modèle. La commande CMG est choisie pour la régulation de la glycémie en raison de ses propriétés de robustesse bien connues. Cependant, notre contribution majeure est l'assurance d'une commande rigoureusement positive. La commande CMG est conçue pour être positive partout dans un ensemble invariant du sous-système d'insulinémie du plasma. Enfin, un régulateur positif par retour d'état est calculé pour la première fois pour la régulation de la glycémie. Le plus grand ensemble positif invariant (EPI) est trouvé. Non seulement la positivité de la commande est révisée, mais plutôt un contrôle glycémique serré est atteint. Lorsque l'état initial du système appartient à l'EPI, l'hypoglycémie est évitée. Dans le cas contraire, l'hypoglycémie future est prédite pour tout état initial en dehors de l'EPI.

Mots clés
Diabète de type I, régulation de la glycémie, Commande positive, prédiction de l'hypoglycémie, Ensemble invariant, Insulin on board, Commande par modes glissants, Commande sans modèle.

Abstract

This thesis investigates closed-loop control for glycemia regulation of Type1 Diabetes Mellitus (T1DM). Two main controller categories are designed: non-model-based and model-based. To test their efficiency, both types are tested *in silico* on two T1DM simulators.
The first is a long-term model that is derived from clinical data of T1DM subjects and the second is the Uva/Padova simulator. Firstly, Model-free Control (MFC) is designed: a variable reference intelligent Proportional (iP) control and a constant reference intelligent Proportional-Integral-Derivative (iPID). Better overall performance is yielded with iPID over iP and over a classic PID. Secondly, a positive Sliding Mode Control SMC is designed for the first time for glycemia regulation. The model-based controller is chosen for glycemia regulation due to its well-known robustness properties. More importantly, our main contribution is that SMC is designed to be positive everywhere in the positively invariant set for the plasma insulin subsystem.
Finally, a positive state feedback controller is designed for the first time to regulate glycemia. The largest Positively Invariant Set (PIS) is found. Not only control positivity is respected but rather a tight glycemic control is achieved. When the system initial condition belongs to the PIS, hypoglycemia is prevented, otherwise future hypoglycemia is predicted for any initial condition outside the PIS.

Key Words
Type I Diabetes, Glycemia Regulation, Positive Control, Hypoglycemia prediction, Positively invariant set, Insulin on board, Sliding mode control, Model-free control.